CHARACTERISTICS OF HURRICANE LILI'S INTENSITY CHANGES

A Thesis

Submitted to the Graduate Faculty of the
Louisiana State University and
Agricultural and Mechanical College
In partial fulfillment of the
Requirements for the degree of
Master of Natural Sciences

in

The Interdepartmental Program in Natural Sciences

by
Adele Marie Babin
B.S. Louisiana State University, 1995
December 2004

DEDICATION

       I dedicate this research first and foremost to my mother Jane Alice Head Babin who passed before its completion, but her encouragement and inspiration motivated me onward.

I also wish to dedicate the manuscript to my immediate family members:

Father- Alfred Mark Babin

Sister- Christa Babin Marshall, and husband Robert Andrew Marshall

Brother- Dane Mark Babin, and wife Rachel Gros Babin

and

Grandmother: Mabel Babin Clement.

ACKNOWLEDGEMENTS

TABLE OF CONTENTS

ABSTRACT

Rapid intensity changes of Hurricane Lili in the Gulf of Mexico (GOM) were studied in three distinct ways: climatology, satellite remote sensing, and surface meteorological and oceanographic measurements. Each research methodology provided insight about Hurricane Lili's intensity behavior.

A climatology of rapid and explosive intensifications of hurricanes was developed using minimum central pressure observations for the Atlantic tropical cyclone record. Results showed these events were frequent, especially in the GOM. The majority of intensification events occurred $\leq$ 24 h before landfall, with a third to one-half $\leq$ 12 h. Lili emerged anomalous as the only hurricane to weaken at a greater rate (+17 hPa over 6 h or +2.83 hPa h^{-1}) than its rapid intensification event rate (-13 hPa over 6 h or -2.16 hPa h^{-1}).

GOES-8 satellite water vapor brightness temperature data were investigated using a -24 °C vapor front to delineate a dry air mass west of Lili. Drier air was shown to affect Lili during a rapid weakening phase after the two features were less than 250 km mean or 215 km minimum distance apart. These critical distances are offered as a criterion for a relationship between tropical cyclone weakening and dry air advection. During the time periods where Lili was intensifying or maintaining intensity, this vapor front exhibited more complex signatures of definitive breaks, shape changes, and protrusions. During the rapid weakening phase and when the two features were the greatest distance apart, the vapor front resembled a smooth, strong boundary line. The dry air mass was shown to have the greatest effect upon Lili after the rapid intensification phases.

SST and heat flux calculations illustrated that oceanic contributions to hurricane intensity were more significant during rapid intensification periods. Ocean heat content directly under the center was more vital as seen in Lili's second rapid intensification phase occurring directly over the GOM Loop Current. Although Tropical Storm Isidore cooled surface water temperatures by around 1 °C, pre-Isidore water temperature levels were shown to increase latent heat flux values by > 100 W m^{-2} ($+ 40\%$) over observed values during Lili's weakening phase.

CHAPTER 1. INTRODUCTION

1. Introduction

Rapid intensity changes are of specific interest in tropical cyclone research because intensity forecasting is substantially poorer than track forecasting. Hurricane Lili (2002) was a recent example of a tropical cyclone in the Atlantic basin which exhibited both rapid intensification and rapid weakening. At the time, Lili's intensity changes within the Gulf of Mexico seemed distinctive. Therefore this research was undertaken to investigate the mechanisms of Lili's intensity changes.

First, several definitions of rapid and explosive intensification were used to create a minimum central pressure climatology. This was prepared to add perspective on the frequency of rapid intensity changes throughout Atlantic tropical cyclone historical activity. Additionally, patterns of tropical cyclone decay after rapid intensification were investigated to assess the frequency for comparison to Lili.

After gaining some perspective on the general frequency of intensity changes, the mechanisms of Lili's intensity changes were studied. Several typical mechanisms attributed to rapid intensity changes are internal eyewall dynamics, upper-level shearing, dry air entrainment, and relatively cooler (decay) or warmer (intensification) ocean temperatures. Here, the latter two mechanisms were studied using readily available thermal infrared imagery and surface observations at ocean buoy locations. The GOES-8 satellite water vapor study investigated a relationship between a dry air mass and Lili's intensity changes. Air-sea interactions were assessed using heat flux calculations from surface meteorological and oceanographic data at National Data Buoy Center (NDBC) Gulf of Mexico locations. Also, sea-surface temperatures (SST) were compared before and after Tropical Storm Isidore to see if this storm, which occurred a week prior to Lili, had any effect on the atmospheric and oceanic conditions for Lili.

2. Background Information

a. Hurricane Lili

This study focused on Lili's intensity changes which occurred in the Gulf of Mexico (Figure 1). However, a synoptic history of Hurricane Lili is presented for reader familiarization. Lili formed into a tropical depression on 21 September 2002 from a wave off the African coast. Lili reached tropical storm status on 23 September and decayed down to a wave due to wind shear. After producing a large amount of rainfall over Jamaica for 4 days, Lili became a hurricane on 30 September in the western Caribbean Sea, while passing over the Cayman Islands. Lili made landfall as a category 2 hurricane on 1 October on the extreme western tip of Cuba. After emerging from Cuba, Lili began strengthening and had 2 rapid intensification (RI) periods. While still over water, Lili weakened more rapidly than it intensified. Then, Lili accelerated forward speed and made landfall west of Intracoastal City, Louisiana on 3 October. Maximum sustained winds at landfall were 41 m s^{-1} at category 1 status.

Lili's peak intensity was 64 m s^{-1} (category 4 status) on 0000 UTC 3 October 2002 while in the north-central Gulf. Peak intensity was based upon a 700-hPa flight-level wind speed of 73 m s^{-1} and 938 hPa minimum central pressure. This wind speed extrapolated down to a surface wind speed of 66 m s^{-1}. NDBC buoy 42001 measured a 51 m s^{-1} wind speed with a 67 m s^{-1} gust, which both were the highest ever recorded at an NDBC buoy up to that point. The rapid intensification and rapid weakening events of Lili were not predicted by model guidance and were not forecasted in the advisories either (Pasch et al. 2004). More detailed information on Lili can be found in Pasch et al. (2004).

b. Tropical Storm Isidore

A brief description of Hurricane Isidore is also included because it traversed the Gulf of Mexico one week prior to Lili. Although Isidore reached hurricane strength, it is referred to

Tropical Storm Isidore in this research because that is the intensity it held when traveling over the same areas as Lili would the next week. Isidore developed from a tropical wave off the west coast of Africa on 9 September 2002. Tropical depression status was issued on 14 September and it strengthened to a hurricane on 20 September after fluctuations between tropical wave, storm, and depression status. Isidore remained over Cuba for 12 h and dumped copious amounts of rain. Isidore re-strengthened and made landfall on the Yucatan Peninsula, Mexico, at maximum intensity (56 m s^{-1}) on 22 September. Isidore remained stationary, decreased to tropical storm status, and never regained its inner core of strong winds. Isidore traversed the Gulf of Mexico as a tropical storm and made landfall west of Grand Isle, Louisiana at 0600 UTC 26 September. More information can be found in Pasch et al. (2004).
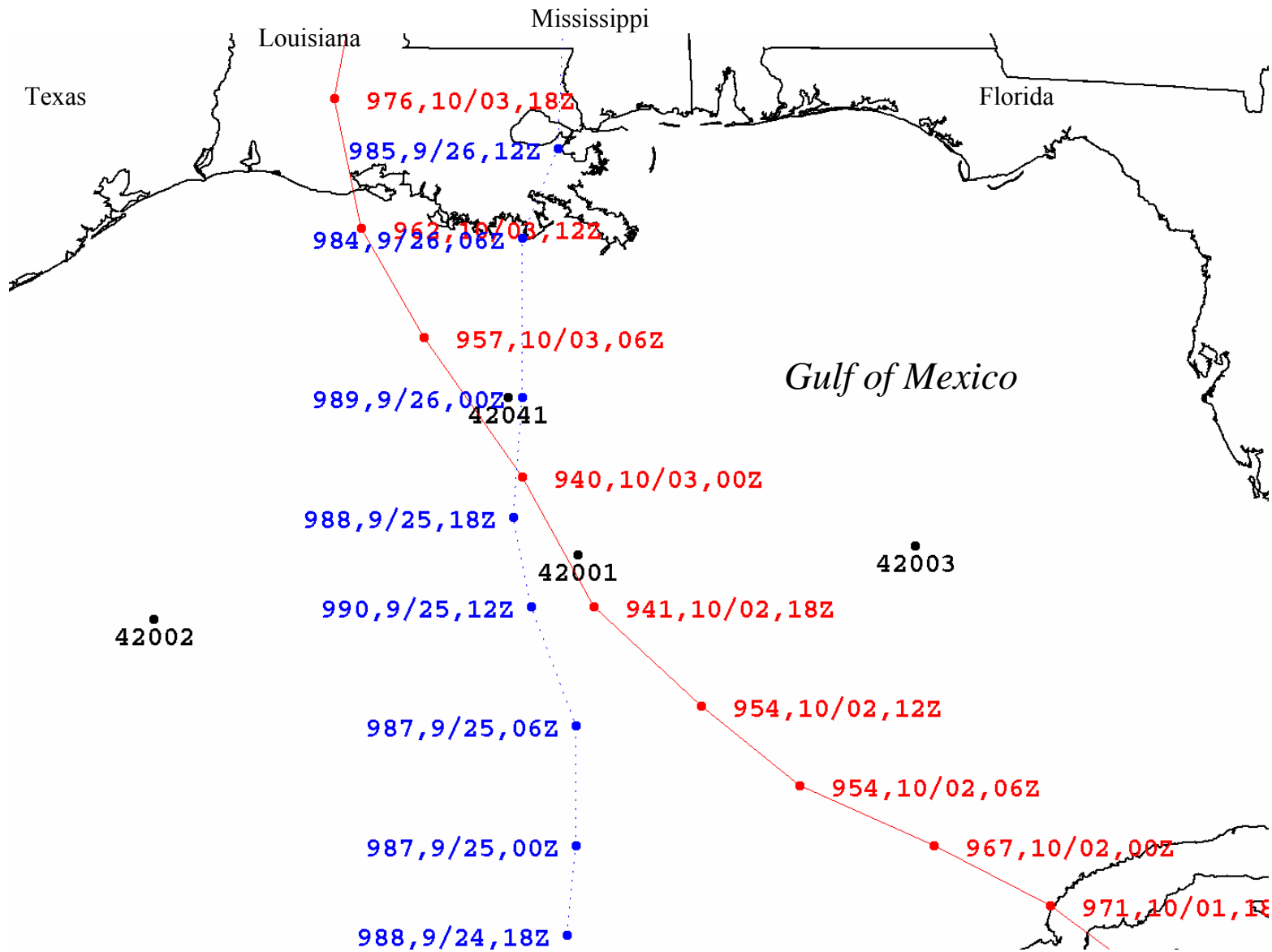
Figure 1. Plane view of the study area with NDBC buoys (black dots), Tropical Storm Isidore's path (blue dotted), and Hurricane Lili's path (red solid) overlain. Minimum central pressure (hPa), date, and time (UTC or Z) are next to the NHC 6-h best track.

CHAPTER 2. A CLIMATOLOGY OF RAPID AND EXPLOSIVE PRESSURE CHANGES IN HURRICANES

1. Introduction

Hurricane Lili was a recent example of a tropical cyclone in the Atlantic basin which exhibited both rapid intensification and rapid weakening. At the time, Lili's intensity changes seemed distinctive. Lili underwent two rapid intensification periods in the Gulf of Mexico (GOM) which caused the storm to increase to a category 4 hurricane. Then Lili rapidly weakened to a category 1 before landfall on the Louisiana coast. The question arose whether Lili's intensity behavior was anomalous. To answer this question, pressure change events were studied over the length of record for Atlantic basin tropical cyclones. A more detailed analysis of Gulf of Mexico events is included here. Objectives for this section are:

1. development of a pressure climatology for rapid and explosive deepening events,

2. investigation of the Saffir-Simpson category changes which accompany these intensifications,

3. quantification of storms that underwent a rapid weakening after rapid intensification for comparison to Lili.

2. Literature Review

Accurate predictions of tropical cyclone intensity change still allude forecasters (Lawrence et al 1998). Despite advances in technology and computing, intensity forecasts have not improved much in recent decades (Elsberry et al. 1992; Marks and Shay 1998). Along their paths, hurricanes move in and out of environments that are either conducive or inhibitive to intensity strengthening. Titley and Elsberry (2000) found most major hurricanes undergo at least one rapid intensification event. Also, these rapid intensity changes as a whole are not predicted

well because 5% of 24-h forecasts have wind speed errors exceeding 20 m s^{-1} (Titley and Elsberry 2000). Hurricane intensity research has been spurred on by a predicted increase in tropical activity and the number of major hurricanes from 1990 through the current decade for the Atlantic basin (Gray 1990) as a result of climatic variability. Rapid intensification events have been studied on individual storm basis using satellite data, in-situ measurements, and model outputs for Hurricane Camille (Shenk and Rodgers 1978), Super Typhoon Flo (Titley and Elsberry 2000), Typhoon Herb (Chen et al. 2001), and Hurricane Opal (Rodgers et al. 1998; Bosart et al. 2000; Hong et al. 2000; Shay et al. 2000).

Holliday and Thompson (1979) studied climatological characteristics of rapidly deepening typhoons in the Pacific and determined central pressure to be the critical observation when evaluating intensification beyond a normal increase. They defined rapid deepening as a $\geq$ 42 mb decrease over 24 h, or 1.75 mb h^{-1}. Additionally, Jordan (1961) examined typhoons with central pressures of < 900 mb and found that each had declines in pressure of > 2.4 mb h^{-1} for at least 12 h. The National Hurricane Center/Tropical Prediction Center (NHC/TPC) Glossary of Terms (available at http://www.nhc.noaa.gov/aboutgloss.shtml) defines rapid deepening as a decrease in the minimum sea-level pressure of a tropical cyclone of 1.75 mb h^{-1} or 42 mb for 24 h. The same source also outlines explosive deepening as a decrease in the minimum sea-level pressure of a tropical cyclone of 2.5 mb h^{-1} for at least 12 h or 5 mb h^{-1} for at least 6 h. The NHC utilizes the criterion from both the Holliday and Thompson (1979) and Jordan (1961) studies even though these were based on Pacific storms. Dodge et al. (1999) showed the Pacific basin generates a higher frequency of tropical cyclones which deepen to lower pressures and therefore provide more definitive empirical characteristics.

Frederick (2003) compared Lili's rapid intensification and subsequent weakening to Atlantic basin historical hurricanes. He found the dual process of rapid intensification and rapid decay occurred 11 other times since 1851. According to Frederick (2003), Lili's intensification rate of 35 kt (18 m s^{-1}) over 24 h ranked it in the 11th percentile, while Lili's rapid decay rate of 40 kt (21 m s^{-1}) over 24 h ranked in the 1st percentile of 769 hurricanes. Frederick (2003) used maximum sustained wind speed rather than the minimum central pressure climatology presented here. Emanuel (2000) performed a statistical analysis of hurricane intensity over both the Pacific and Atlantic basins. Emanuel (2000) found average intensification rates of 12 m s^{-1} and average decay rates of 8 m s^{-1}. However, for storms which reached a sharp peak in intensity, the decay was roughly two-thirds of the prior intensification (Emanuel 2000). Rogers and Davis (1993) found that stronger storms fill more rapidly.

3. Data and Methods

The National Hurricane Center's (NHC) best track dataset (HURDAT) contains measurements of center location, wind speed, and pressure every 6 h. This dataset can be obtained at http://www.nhc.noaa.gov/pastall.shtml and follows Jarvinen et al. (1984). Neumann et al. (1993) advised that reliable observations begin in 1944, with the onset of aircraft reconnaissance. HURDAT wind speeds were collected under differing observational techniques resulting in an overestimation bias from 1944 to 1969 at 5 m s^{-1} for categories 4 and 5 and 2.5 m s^{-1} for weaker intensities (Landsea 1993). Although consistent minimum central pressure observations are available only since 1979, central pressure was used in this study rather than wind speed due to the known wind bias and because the NHC definitions and literature climatologies (Holliday and Thompson 1979; Jordan 1961) base their criterion upon pressure.

Since pressure measurements are every 6 h, there is an assumption of linear pressure change though a more complicated pattern in the pressure could have occurred. A pressure difference was calculated between each 6-h HURDAT observation for every Atlantic basin tropical cyclone from 1944 through 2002. For the 12-h pressure change, the sum of the 6-h pressure differences was calculated. The 24-h difference value was constructed in a similar manner. Data were not interpolated because the primary criterion factor was a rate of change and inferred data over 6 h would not lend satisfactory confidence for this study. Storms prior to 1979 are included if the pressure data were consistent for short periods of time. Conversely, a rapid or explosive event could have occurred prior to 1979, but not be included here if measurements did not match the temporal criterion of 6, 12, or 24 h. Four pressure climatology types were created using the NHC criterion of rapid and explosive deepening. Although the NHC criterion and the HURDAT database denote pressure in mb, pressure will be presented in hPa (1 mb = 1 hPa) for consistency with other sections of this document. The first rapid deepening type events (RD1) are defined by a decrease of ≥ 1.75 hPa h^{-1} based upon a 6-h pressure difference. Rapid deepening 2 events (RD2) occur with a ≥ 42 hPa decrease over 24 h and were based upon a 24-h pressure difference. Explosive deepening 1 events (ED1) consist of a ≥ 30 hPa decrease over 6 h (or $\geq$ -5 hPa h^{-1}) based upon a 6-h pressure difference. Explosive deepening 2 events (ED2) are determined by a ≥ 30 hPa decrease over 12 h (or -2.5 hPa h^{-1}) based upon a 12-h pressure difference. The calculated 6, 12, and 24-h pressure differences were then sorted in descending order to categorize, quantify, and rank the events by type over the entire Atlantic basin and the Gulf of Mexico (GOM). A cyclone storm count was also performed as several individual storms had numerous events. Storm here relates to a tropical cyclone at any categorization whether tropical storm or hurricane.

Table 1. Saffir-Simpson damage potential scale (after Simpson and Riehl 1981).

Category	Minimum Central Pressure (mb) or (hPa)	Maximum Wind Speed (kt)	(mph)	Damage Level
1	> 980	64-82	74-95	Minimal
2	965-979	83-95	96-110	Moderate
3	945-964	96-113	111-130	Extensive
4	920-944	114-135	131-155	Extreme
5	< 920	>135	> 155	Catastrophic

Next, RD1, RD2, ED1, and ED2 events were examined by category on the Saffir-Simpson scale for category change or persistence in the same category. Although central pressures defined the actual rapid and explosive events database, wind speeds were used in the category change analysis to match results of the NHC individual storm reports. For familiarization, the Saffir-Simpson category scale is given in Table 1. Note that the overestimation of wind speeds mentioned previously (Landsea 1993) would have had an effect on the storms included prior to 1979.

Pressure observations 24 h prior, and 24 h after, each GOM RD1 event were studied for those matching or exceeding Lili's rank of 12 (13 hPa over 6 h or 2.16 hPa h^{-1}). This analysis was initiated to determine if Lili's rapid decay within 24 h after rapid intensification was anomalous.

Table 2. Rapid and explosive deepening events categorized by the four pressure climatology types with storm count and event count for both the full Atlantic basin and GOM areas.

	Full		GOM	
	Storm Count	Event Count	Storm Count	Event Count
RD1 1.75 hPa h^{-1}	74	137	20	27
RD2 1.75 hPa h^{-1} for 24 h	23	54	5	8
ED1 5 hPa h^{-1} drop for at least 6 h	2	2	1	1
ED2 2.5 hPa h^{-1} drop for 12 h	11	19	5	7

4. Results

a. Pressure Climatology by Type

Both rapid deepening types were numerous and the longer time criterion pressure drop of ED2 was also frequent. Table 2 summarizes the number of storms and events for each pressure climatology type which are grouped by full Atlantic basin and GOM areas respectively. One would expect from the designed nomenclature that rapid intensification would occur more frequently than the explosive, which is the case. RD1 contained the most events over the Atlantic basin tallying 137, with 27 located in the GOM. These events were spread over 74 storms basin wide, 37 of which had at least two events satisfying the RD1 criterion. The 27 GOM RD1 events occurred during 20 storms where 5 storms met the RD1 criterion more than once. Hurricane Allen (1980) had the most occurrences for one storm, totaling 7 RD1 events

10

over the entire basin with 2 located in the GOM region. Hurricane Beulah (1967) had the largest

drop in pressure of the RD1 type at 38 hPa over 6 h.

RD2 events occurred 54 times over the entire basin, and 8 of these were located in the

GOM. RD2 events took place in 23 storms basin wide and only 5 occurred in the GOM. Again,

there were storms which had more than one RD2 event, 15 for the full basin and 2 when

narrowed spatially to the GOM. For RD2 events, Hurricane Gilbert (1988) produced the top two

events: a 71 hPa pressure decrease over 24 h and a 72 hPa pressure decrease over 24 h.

Hurricane Mitch (2001) met the RD2 criterion 5 times in the entire basin, while Hurricane Hilda

(1964) had the most RD2 events in the GOM (3 events).

Simpson and Riehl (1981) delineated between oscillations of intensity changes versus

more long-term intensity changes. The separate rapid deepening categories could be interpreted

as a threshold of this delineation since RD2 storm counts were less than RD1 counts as a result

of the time persistence factor. RD1 events occurred over short 6 h time periods, whereas the

RD2 events involved a sliding temporal scale. Storms with subsequent RD2 events exhibited a

pattern of long term intensity change. Take for example Hurricane Andrew (1992) which had

four RD2 events over the basin. The first RD2 event was a 43 hPa decrease on 0000 UTC 23

August 1992. The next RD2 decrease was 53 hPa and ended at 0600 UTC 23 August 1992, then

a 61 hPa decrease at 1200 UTC, and finally a 59 hPa decrease at 1800 UTC. As observed, the

decreases built upon one another over a sliding 24 h time scale. The RD1 6-hourly decreases of

1.75 hPa h^{-1} occurred from 22 August 1992 - 23 August 1992. RD1 events can be isolated

instances until the intensification persists long enough to classify it into an RD2 event.

Explosive events were fewer in number because the pressure decrease must be a greater

to satisfy ≥ 30 hPa over 6 or 12 h. ED1 was a very rare event demonstrated by only 2 events

across the entire basin, each one in a separate storm. Hurricane Gloria's (1985) ED1 event should be discounted because it occurred within a tropical storm wind categorization (Table 2), very far north in the basin (55 °N and 30 °W), and after extratropical transition (Hart and Evans 2001). The other ED1 storm and event deepened in the southwestern GOM (Hurricane Beulah 1967) and was the largest ED1 event observed with a 38 hPa pressure fall over 6 h. This also was the top rank for the RD1 type. ED2 events numbered 19 for the basin and 7 for the GOM. ED2 events were more common than ED1 events because the pressure change occurred over a longer period of time. When narrowed spatially, the GOM ED2 breakdown included 5 of the Atlantic basin storms. Multiple ED2 events occurred in 4 storms for the full basin with 2 of those in the GOM. Hurricane Allen (1980) had the most ED2 events over the entire basin with 5. However, Hurricane Opal (1995) and Hurricane Allen (1980) each had 2 ED2 events in the GOM.

Timing of these rapid and explosive intensifications within the storm life cycle was also examined. To investigate GOM events more closely since Lili's events occurred there, one rapid type (RD1) and one explosive type (ED2) were chosen as a sample of the entire dataset because each contained the highest number of events (Table 3). Figures 2-8 provide a visual representation of GOM RD1 and ED2 event timing through a storm's life cycle until landfall. No conclusive pattern emerged as to the timing of RD1 and ED2 events since storm inception. Hurricane Celia (1970) was the fastest storm to have a RD1 event in the GOM, just 48 h after formation. Hurricane Inez (1966) contained the RD1 event farthest into life cycle at 372 h. Inez was a long-lived storm (> 21 days) and had 3 different landfalls (Cuba, the Bahamas, and Mexico). Average timing of a GOM RD1 event was 165 h after storm formation, or almost 7 days. The GOM ED2 events developed later in a storm's life span averaging 177 h, just over 7

Table 3. GOM RD1 and ED2 events ranked in order of largest decrease. This is the companion listing to Figures 2-8.

GOM RD1 Rank	Storm Name	Ending Date and Time	Wind (kt)	Pressure (hPa)	Pressure Difference over 6 h	ED1 or ED2 type
						explosive type1 ***
1	BEULAH	9/19/67 1800	135	923	-38	explosive type 2- rank 3
2	ALLEN	8/9/80 0000	145	912	-28	explosive type 2- rank 1
3	CELIA	8/3/70 1800	110	945	-26	explosive type 2- rank 2
4	CELIA	8/2/70 0000	100	965	-25	
5	HILDA	10/1/64 0600	110	955	-22	
6	BRET	8/22/99 0000	120	954	-21	
7	ALLEN	8/8/80 1800	130	940	-20	
8a	ANITA	9/1/77 1800	110	945	-18	
8b	OPAL	10/4/95 0600	110	935	-18	explosive type 2- rank 7
9	CELIA	8/3/70 1200	90	971	-17	
10	OPAL	10/4/95 1200	130	919	-16	explosive type 2- rank 4
11a	CAROLINE	8/31/75 0000	100	973	-14	
11b	ANITA	9/2/77 0000	140	931	-14	explosive type 2- rank 5
11c	BARRY	8/5/01 1200	50	990	-14	
12a	INEZ	10/7/66 0000	105	961	-13	
12b	FLORENCE	9/9/88 1800	65	985	-13	
12c	LILI	10/1/02 0600	100	954	-13	
12d	LILI	10/1/02 1800	120	941	-13	
13a	BETSY	9/10/65 0000	135	941	-12	
13b	CARMEN	9/6/74 0600	70	971	-12	

(table continued)

GOM RD1 Rank	Storm Name	Ending Date and Time	Wind (kt)	Pressure (hPa)	Pressure Difference over 6 h	ED1 or ED2 type
13c	ELOISE	9/23/75 0000	95	968	-12	
13d	FREDERIC	9/11/79 1800	95	968	-12	
13e	KATE	11/20/85 1200	105	956	-12	
13f	OPAL	10/4/95 0000	100	953	-12	
14a	ELLA	9/12/70 0000	85	973	-11	
14b	JOSEPHINE	10/7/96 1200	60	981	-11	
14c	ISIDORE	9/22/02 600	110	936	-11	

***only GOM explosive type 1 event

GOM ED2 Rank	Storm Name	Ending Date and Time	Wind (kt)	Pressure (hPa)	Pressure Difference over 12 h
1	ALLEN	8/9/80 0000	145	912	-48
2	CELIA	8/3/70 1800	110	945	-43
3	BEULAH	9/20/67 0000	140	923	-38
4	OPAL	10/4/95 1200	130	919	-34
5	ANITA	9/2/77 0000	140	931	-32
6	ALLEN**	8/9/80 0600	155	909	-31
7	OPAL	10/4/95 0600	110	935	-30

**only event not in RD1 because did not meet shorter 6-h time criterion

Figure 2. GOM RD1 events ranked 1-5 shown by time from storm inception through landfall with the actual location of 6-h pressure events labeled.

Gulf of Mexico RD1 Events
Ranks 6-8

Figure 3. GOM RD1 events ranked 6-8 shown by time from storm inception through landfall with the actual location of 6-h pressure events labeled. For ranks with more than one event, the letter is assigned by date order.
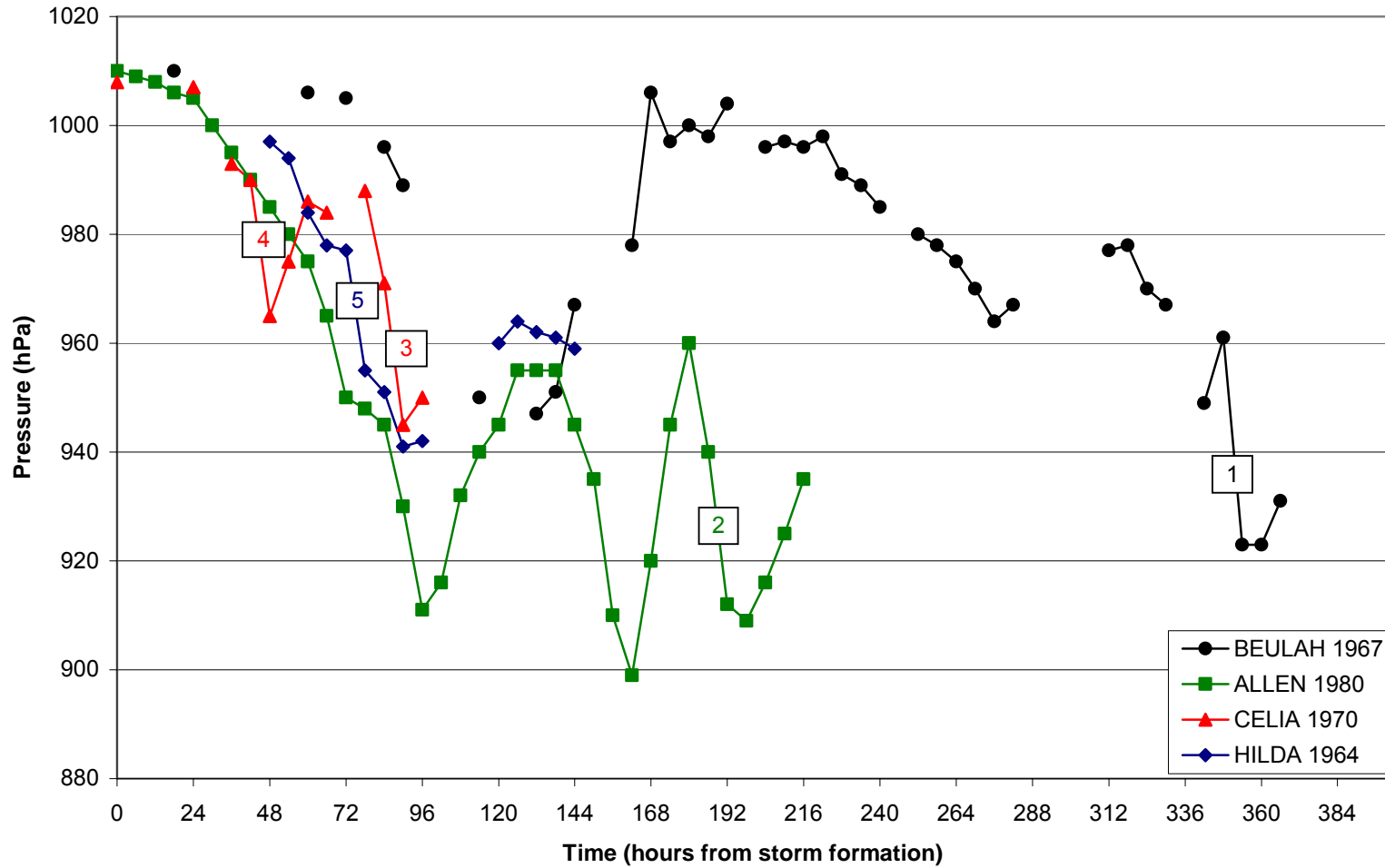
16

Gulf of Mexico RD1 Events
Ranks 9-11

Figure 4. GOM RD1 events ranked 9-11 shown by time from storm inception through landfall with the actual location of 6-h pressure events labeled. For ranks with more than one event, the letter is assigned by date order.

Gulf of Mexico RD1 Events
Rank 12

Figure 5. GOM RD1 events ranked 12a-d shown by time from storm inception through landfall with the actual location of 6-h pressure events labeled. For ranks with more than one event, the letter is assigned by date order.
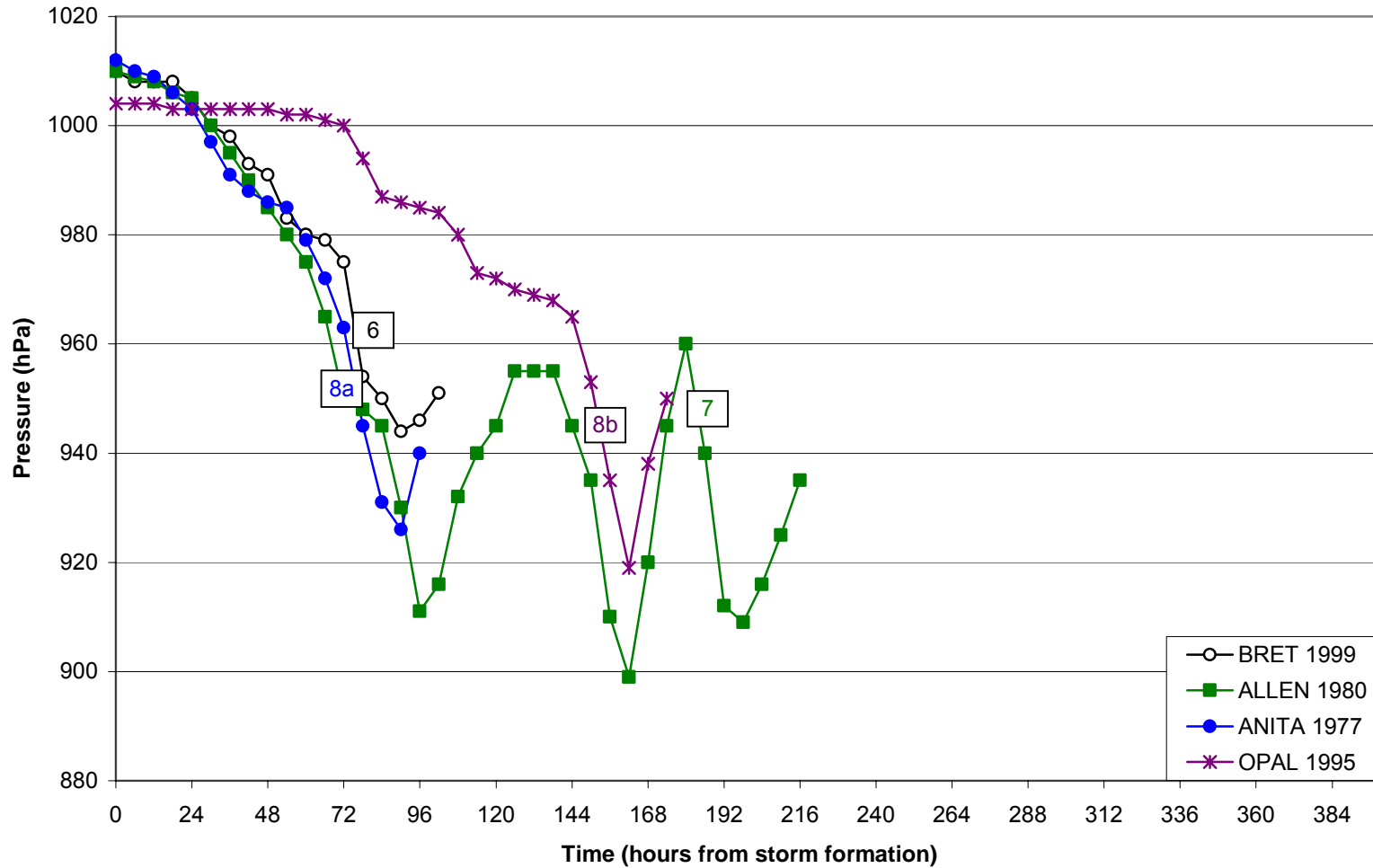
18

Figure 6. GOM RD1 events ranked 13a-f shown by time from storm inception through landfall with the actual location of 6-h pressure events labeled. For ranks with more than one event, the letter is assigned by date order.
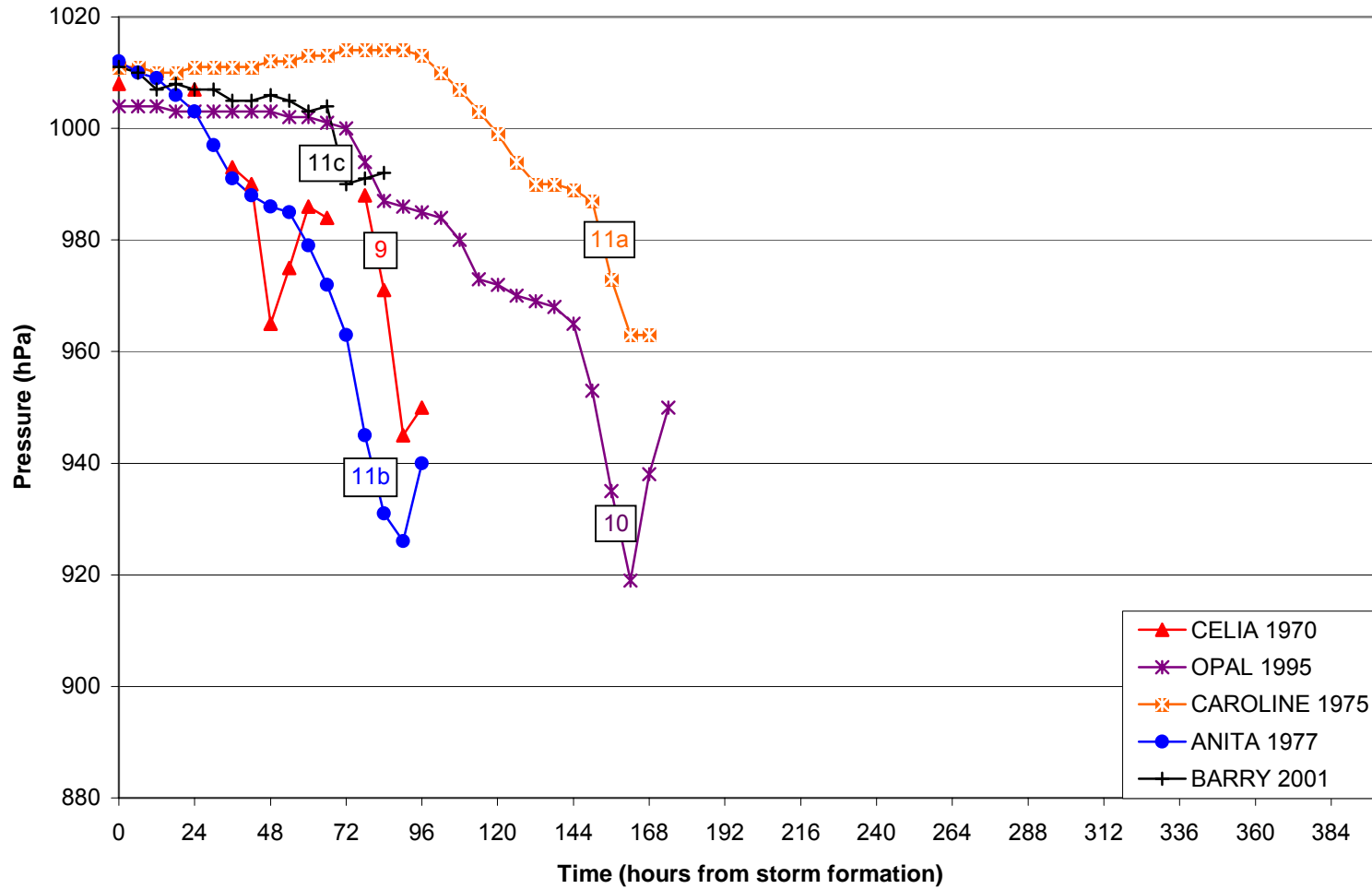
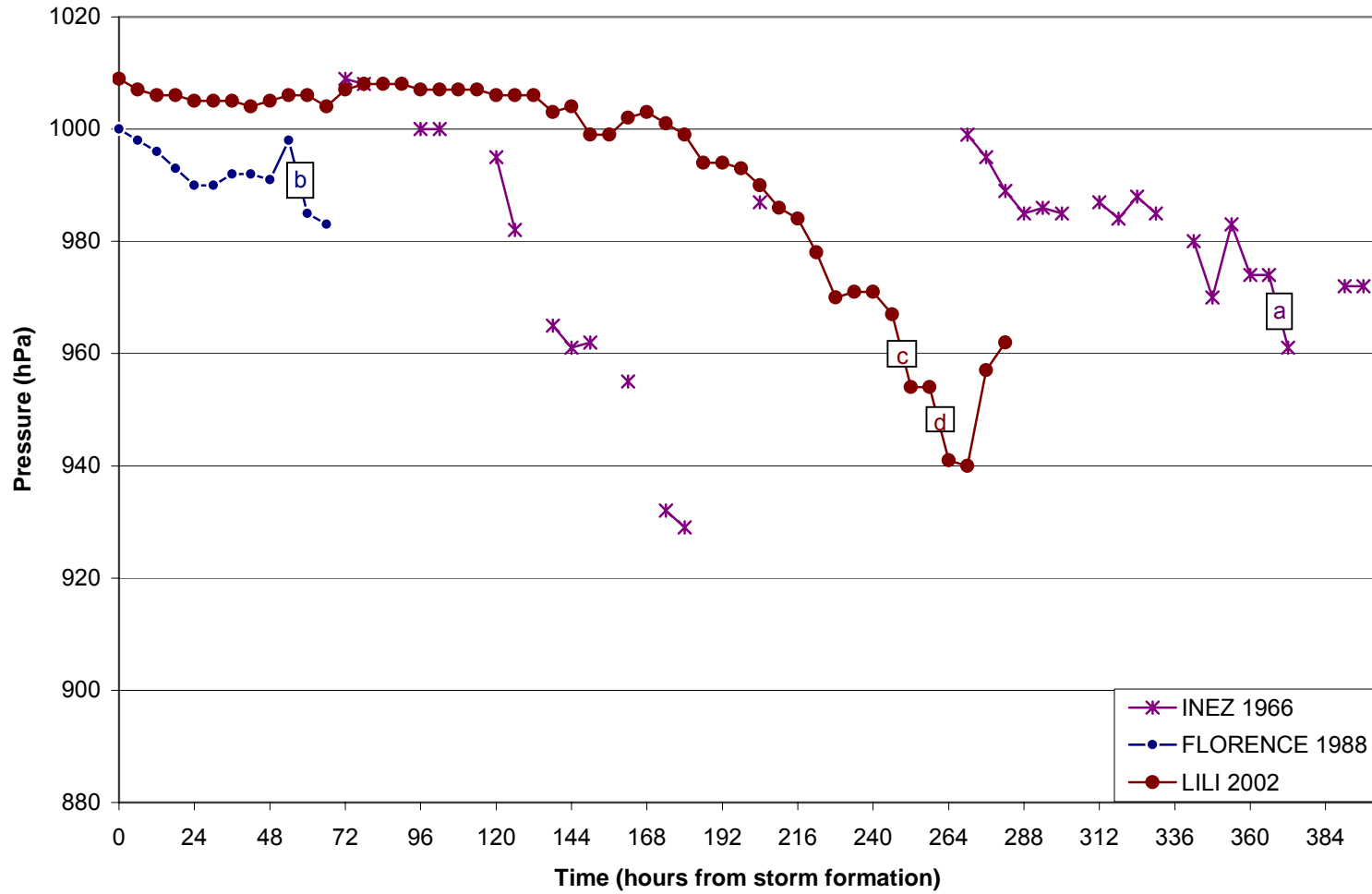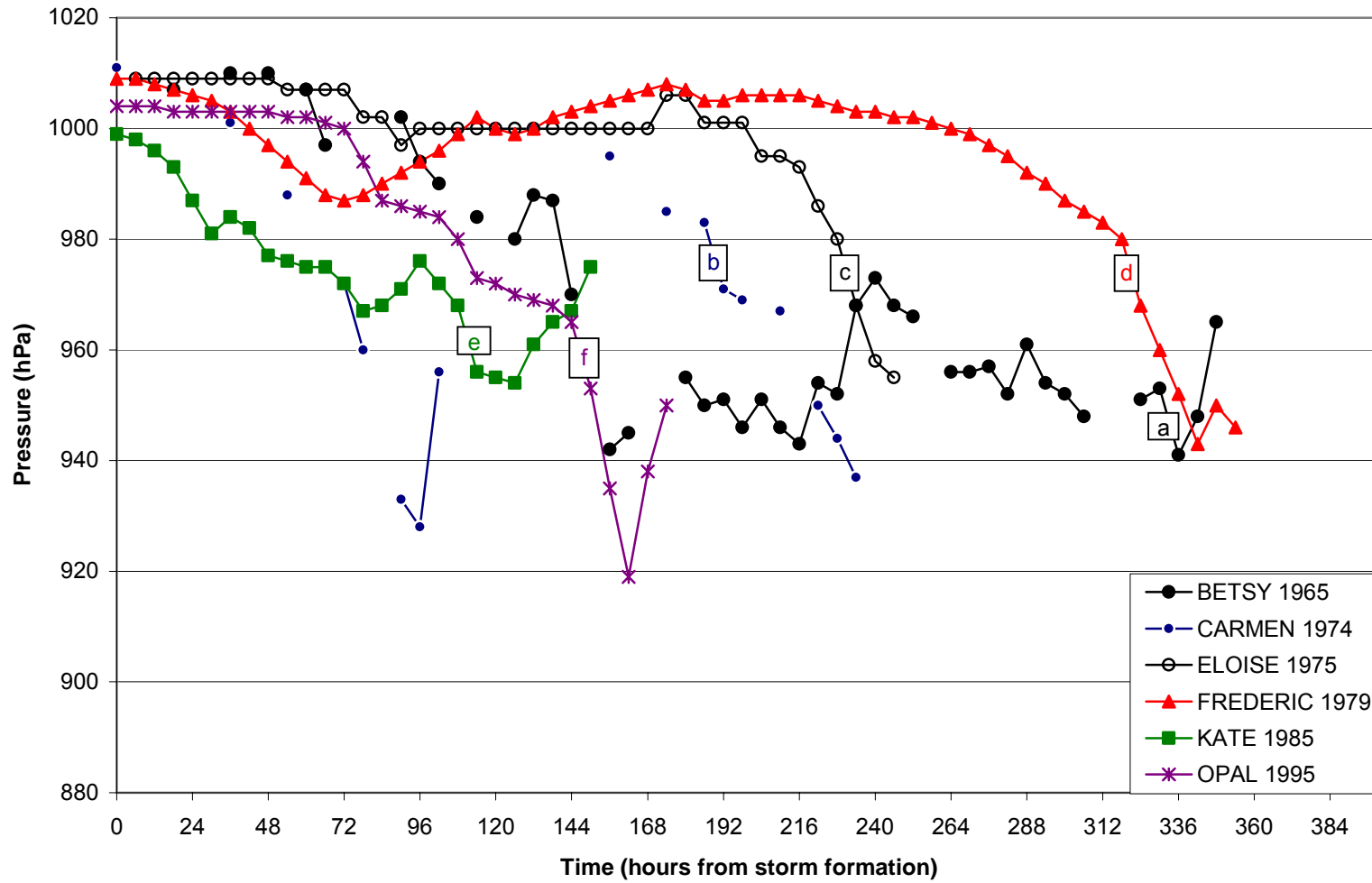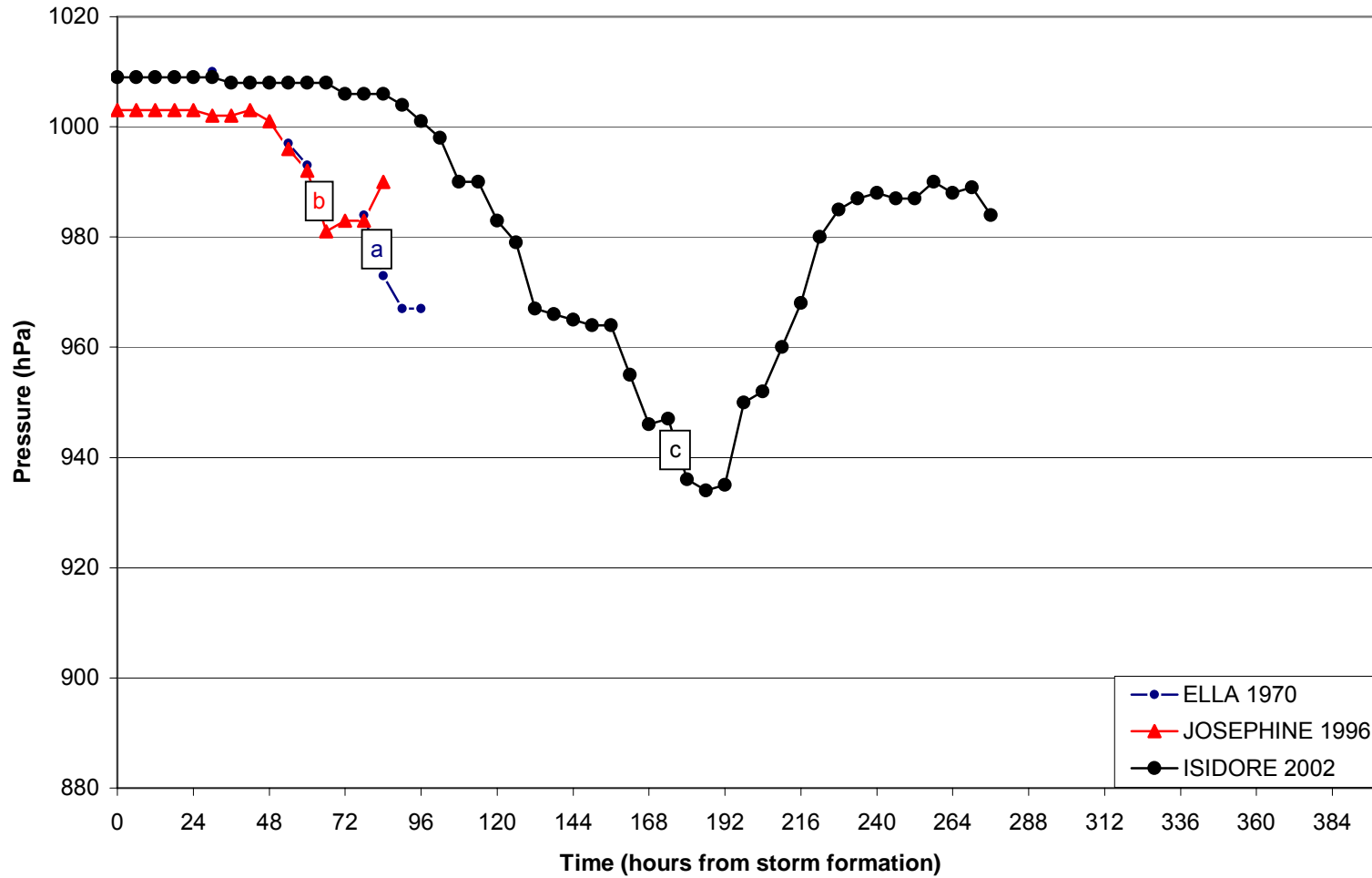**Gulf of Mexico RD1 Events**
Rank 14

Figure 7. GOM RD1 events ranked 14a-d shown by time from storm inception through landfall with the actual location of 6-h pressure events labeled. For ranks with more than one event, the letter is assigned by date order.
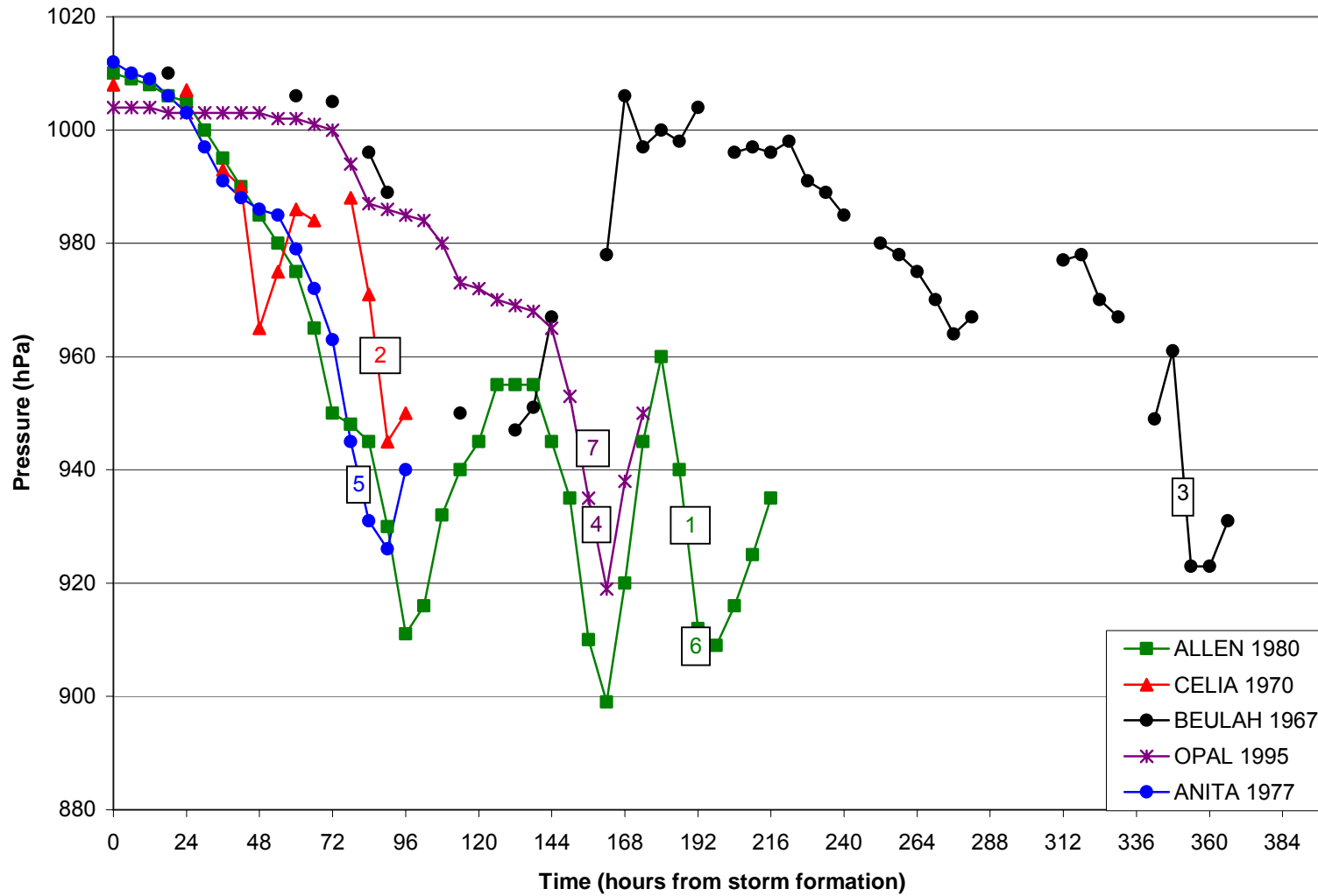
Figure 8. GOM ED2 events shown by time from storm inception through landfall with the actual location of 12 h pressure difference events labeled.

Table 4. Timing of GOM events sorted by hours before landfall.

RD1 Rank	Storm Name	Event Timing Since Storm Formation (h)	Storm Total (h)	Event Timing Before Landfall (h)	Saffir-Simpson Category Change
3	CELIA	90	96	6	Cat2 to Cat3
12b	FLORENCE	60	66	6	TS to Cat1
1	BEULAH	354	366	12	within Cat4
9	CELIA	84	96	12	Cat1 to Cat2
10	OPAL	162	174	12	Cat3 to Cat4
11a	CAROLINE	156	168	12	Cat1 to Cat3
11b	ANITA	84	96	12	Cat3 to Cat5
11c	BARRY	72	84	12	within TS
13a	BETSY	336	348	12	within Cat4
13c	ELOISE	234	246	12	within Cat2
14a	ELLA	84	96	12	Cat1 to Cat2
8a	ANITA	78	96	18	Cat2 to Cat3
8b	OPAL	156	174	18	within Cat3
12d	LILI	264	282	18	Cat3 to Cat4
13b	CARMEN	192	210	18	within Cat1
14b	JOSEPHINE	66	84	18	within TS
2	ALLEN	192	216	24	Cat4 to Cat5
6	BRET	78	102	24	Cat2 to Cat4
12a	INEZ	372	396	24	within Cat3
13f	OPAL	150	174	24	Cat2 to Cat3
7	ALLEN	186	216	30	within Cat4
12c	LILI	252	282	30	Cat2 to Cat3
13d	FREDERIC	324	354	30	within Cat2
13e	KATE	114	150	36	Cat2 to Cat3
4	CELIA	48	96	48	TS to Cat3
5	HILDA	78	144	66	Cat2 to Cat3
14c	ISIDORE	180	276	96	within Cat3
ED2 Rank					
2	CELIA	90	96	6	Cat2 to Cat3
3	BEULAH	354	366	12	Cat4 to Cat5
4	OPAL	162	174	12	Cat3 to Cat4
5	ANITA	84	96	12	Cat3 to Cat5
6	ALLEN	198	216	18	within Cat5
7	OPAL	156	174	18	within Cat3
1	ALLEN	192	216	24	Cat4 to Cat5

days. The fastest development of a GOM ED2 event was in Hurricane Anita (1977) at 84 h after

storm formation. Hurricane Beulah (1967) took the longest to initiate an ED2 event in the GOM

at 354 h. Timing of the GOM RD1 and ED2 events before landfall exhibited a definitive

temporal pattern (Table 4). For the explosive events (ED2), all of the 7 instances occurred ≤ 24

h prior to landfall in the GOM.   More than half of these were within 12 h of landfall. Of the 27

RD1 events, 20 occurred within 24 h of GOM landfall. Half of these 20 events occurred < 12 h

before landfall.

Some intriguing central pressure clusters materialized as well. For ranks 1 through 8 of

RD1 events (Figure 2; Figure 3), each resulted in a pressure of < 955 hPa except for one (Celia

1970). This one exclusion had an RD1 event later which did result in a pressure of < 945 hPa

(Figure 2 [4]). These events all had a -3 hPa h^{-1} rate or higher. The remainder of the GOM RD1

events were more scattered as the pressure drop per hour was weaker (Figures 3 – 6). For the top

14 RD1 events (Table 3 ranks 1 – 11), half also met the ED1 or ED2 criterion. RD1 events are

cross-referenced with the ED1 or ED2 types in the farthest right column of Table 3. For the 7

GOM ED2 events, all but one resulted in a pressure of ≤ 935 hPa (Figure 8). For comparison,

Holliday and Thompson (1979) found that 75% of the rapid deepening cases in the Pacific

resulted in pressures of ≤ 920 mb. These compare reasonably when considering the Pacific has

deeper central pressures (Dodge et al. 1999).

Locations of these RD1 and ED2 events showed that none of these events occurred south

of 22 °N , north of 28.5 °N, or east of 85 °W (Figure 9). If the GOM is divided in half, east-west

by longitude 90 °W, 14 RD1 events occurred in the eastern half of the basin and 13 occurred in

the west (Figure 9 blue dots). Also, the more rapid intensifications (lower number rank)

occurred east of 90 °W. Yearly distribution of these RD1 events was significantly different. For

the eastern RD1 events, 7 occurred from 1965 through 1988 (22 years) and the other 7 from 1995 through 2002 (7 years). The western RD1 events had 12 events between the years of 1964 and 1980 (16 years) and only 2 events over the following 19 years (Opal 1995; Bret 1999). Thus, rapid deepening events have been more frequent on the eastern side of the GOM over the last decade. ED2 events were distributed less evenly across the GOM longitudinally. The eastern half had 2 events and the western side had 5 (Figure 9 red dots). The eastern 2 events both occurred in Hurricane Opal (1995) and thus along one storm path. Four of the western ED2 events clustered around 25 °N and occurred in 3 storms with Hurricane Celia (1970) at the most northern location. RD1 and ED2 locations agree with warmer SSTs of the Loop Current in the eastern GOM and warm core eddy zone in the western GOM (Vukovich et al. 1979; Muller-Karger and Walsh 1991).

Landfall location was also distinct for the 20 storms containing GOM RD1 and ED2 events (Figure 10a-c). For storms with RD1 events, Louisiana had the most landfalls with 6 (Figure 10a). Two were near Marsh Island (Figure 10a; Hilda 1964 [blue dashed line]; Lili 2002 [white solid line]), and 4 eastward of that area (Betsy 1965 [green dashed line]; Carmen 1974 [red dotted line]; Florence 1988 [cyan dashed line]; Isidore 2002 [yellow dashdot line]). Mexico had 4 landfalls (Figure 10b; Inez 1966 [cyan dotted line]; Ella 1970 [red dotted line]; Caroline 1975 [blue dotted line]; Anita 1977 [yellow solid line]). The Texas-Mexico border area had 2 different storms make landfall (Figure 10b; Beulah 1967 [white solid line]; Allen 1980 [red solid line]), and Texas had 2 storms landfall there (Figure 10b; Celia 1970 [blue solid line]; Bret 1999 [green dotted line]). Florida had 5 storms hit with 4 in the panhandle area (Figure 10c; Eloise 1975 [white dashed line]; Kate 1985 [yellow dashed line]; Opal 1995 [green solid line]; Barry 2001 [cyan solid line]) and Hurricane Josephine (1996) in the Big Bend area (Figure 20c red

Figure 9. Location and rank of RD1 events (blue dots and labels) and ED2 events (red dots and labels).
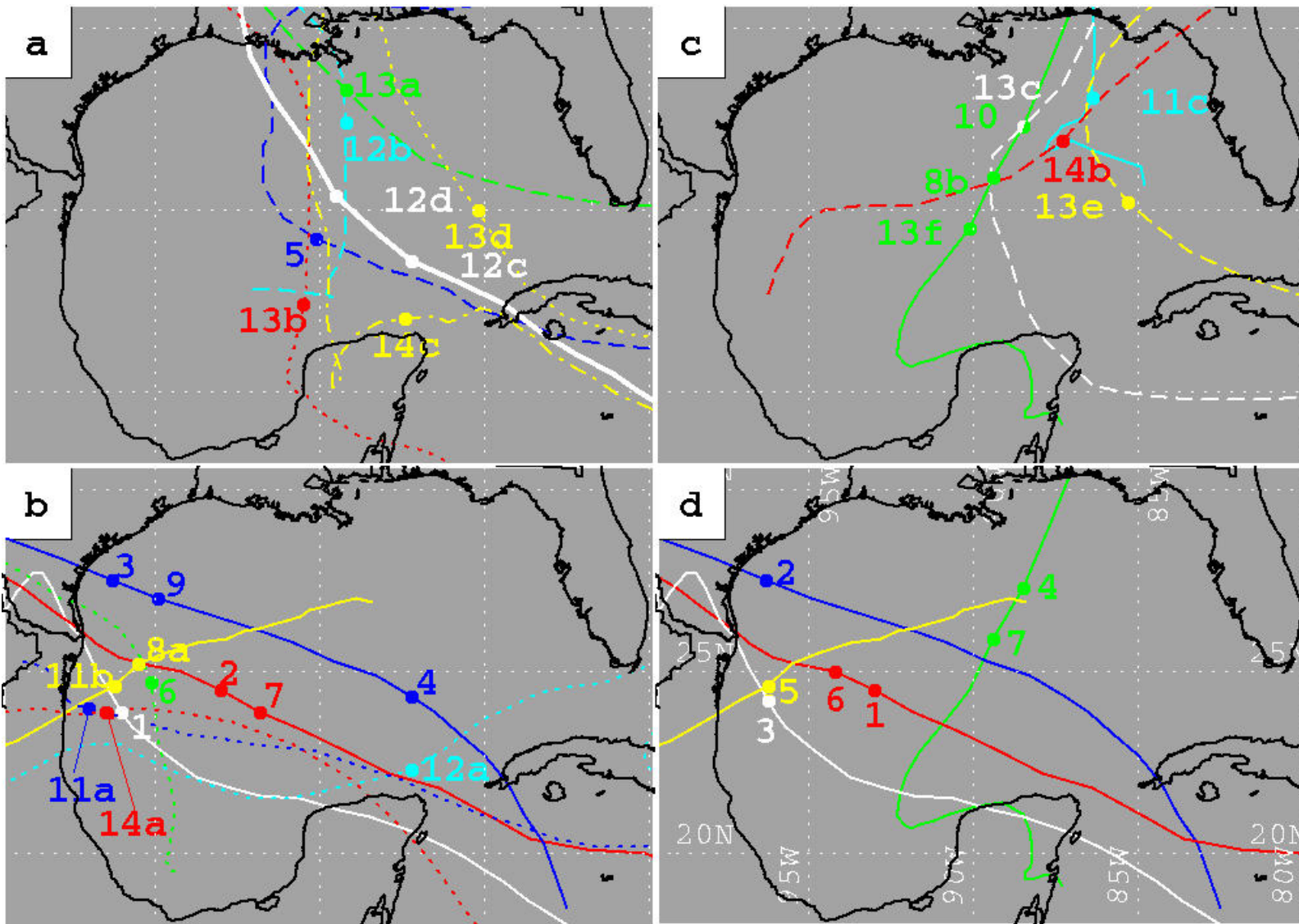
Figure 10. Tracks of storms containing GOM RD1 events broken down by landfall in (a) Louisiana/Mississippi, (b) Texas/Mexico, and (c) Florida. Tracks of storms containing ED2 events are shown in panel (d).

26

dashed line). Hurricane Celia (1970) registered as the storm with the nearest to shore RD1 and ED2 event at 85 km from landfall. Hurricane Frederic (1979) made landfall at the Mississippi-Alabama border (Figure 10a yellow dotted line). Storms with ED2 events spanned the GOM coastline with 2 at the Texas-Mexico border (Figure 10d; Allen 1980 [solid red line]; Beulah 1967 [solid white line]), and one each in Mexico (Figure 10b; Anita 1977 [solid yellow line]), Texas (Figure 10b; Celia 1970 [solid blue line]), and Florida (Figure 10c; Opal 1995 [solid green line]). The north-central GOM coast (Louisiana, Mississippi, Alabama) has not had a landfalling hurricane that underwent an ED2 intensification.

Muller and Stone (2001) constructed a landfall climatology based upon intensity at landfall for coastal locations. Their dataset used the Saffir-Simpson categorization and included data back to 1901. Despite their longer period of record, there was agreement on several locations as to landfalls from storms in general and storms containing RD1 or ED2 events. Southeast Louisiana had the highest frequency of major hurricane landfalls (Muller and Stone 2001). Landfall of storms which included RD1 events agreed with this. However, Louisiana has never had a landfall of an ED2 event storm, so the major hurricanes which made landfall had rapid intensifications or persistent gradual intensifications. Muller and Stone (2001) show Mobile has had the maximum number of strikes for one location with 4, but only 1 RD1 event storm and no ED2 event storms hit there. So at what strength (or category status) these intensifications occur can be very important in terms of coastal impacts.

b. Saffir-Simpson Category Analysis

RD1 and ED1 types were chosen for the Saffir-Simpson category change analysis (Table 5). These were chosen because a singular trend was guaranteed over one pressure difference value, whereas the RD2 and ED2 time criterions might have introduced multiple category change

Table 5. Saffir-Simpson category change analysis for RD1 and ED1 events.

| Category Change | | RD1 1.75 hPa h^{-1} | | ED1 5 hPa h^{-1} drop for 6 h | |
		Full Events 137	GOM Events 27	Full Events 2	GOM Events 1
None	within TS	13	2	1 (suspect)	
	within Cat 1	15	1		
	within Cat 2	9	2		
	within Cat 3	18	3		
	within Cat 4	12	3	1	1
	within Cat 5	4			
One Category	TS to Cat 1	5	1		
	Cat 1 to Cat 2	16	2		
	Cat 2 to Cat 3	20	6		
	Cat 3 to Cat 4	12	2		
	Cat 4 to Cat 5	6	1		
Two Categories	TS to Cat 2				
	Cat 1 to Cat 3	2	1		
	Cat 2 to Cat 4	2	1		
	Cat 3 to Cat 5	1	1		
Three Categories	TS to Cat 3	1	1		
	Cat 1 to Cat 4				
	Cat 2 to Cat 5				
Four Categories	TS to Cat 4				
	Cat 1 to Cat 5				
Five Categories	TS to Cat 5				
	Cat 4 to Cat 3	1	Gladys (1964) winds decreased 2.6 m s^{-1} though pressure deepened		

trends within one difference value. Since ED1 had only 2 events, the break down was very clear

(Table 5) and no useful comparisons can be drawn. Additionally, the Hurricane Gloria (1985)

ED1 event should be disregarded as mentioned earlier. The other ED1 event was in the GOM

during Hurricane Beulah (1967) which remained a category 4 storm. RD1 type had the largest

numbers in both storms and events, thus revealing the most useful information on category

changes of 6 h rapid events. Just over half of the RD1 events experienced no change in Saffir-

Simpson class over both the full basin and GOM (Table 5). Although fairly well distributed,

storms which stayed within the same category were mostly at category 3 intensity. For the GOM

events, storms tended to stay within category 3 or 4. One category jumps occurred around 40%

of the time for RD1 events. The largest category change occurred in Hurricane Celia (1970) in

the GOM where it went from tropical storm to category 3 intensity. The portion of the total

events sharply declined after one category changes. It would be expected that if a pressure drop

over 6 h was large enough to change several Saffir-Simpson categories, then it would more than

likely qualify as an explosive event. This was not seen in the 5 full basin events which qualified

as a two category drop because only 2 were ED2 12 h explosive events. The 3 remaining two

category change events ranked 16th, 17th, and 53rd in the full basin RD1 dataset. Sixty percent of

the two category change RD1 events occurred in the GOM. For both the full basin and the

GOM, a pattern of individual largest number of events (Table 5 blue shaded area) surfaced at the

category 2 to category 3 change. This is the threshold of turnover from a hurricane to a major or

intense hurricane. This pattern revealed itself again in the 20 RD1 events which occurred 24 h

prior to landfall (Table 4). Of the 20 intensifications which occurred $\leq$ 24 h before landfall, 13

resulted in a major hurricane status whether intensification within the same category (4 events), a

one category shift (6 events), or a two category change (3 events) (Table 4).

     c. Comparison to Hurricane Lili (2002)

     A final investigation was the comparison of all GOM RD1 events to Hurricane Lili in

October 2002. Lili's two pressure decreases of 13 hPa (rate of -2.17 hPa h^{-1}) ranked in the 12th

group of RD1 events. Lili had a 17 hPa increase to 957 hPa over the 12 h following the second RD1 13 hPa decrease (Figure 5 brown line). This intensity was higher than the 954 hPa intensity which began the second RD1 event. This raised the question as to how many of the GOM RD1 events were followed by weakening events and to what degree? Pressure differences 24 h prior to and after each GOM RD1 event were investigated for all events ranked 12th or higher (Table 6). For the 18 events including Lili, 2 did not have enough observations in the   54-h time period to produce reliable results. Of the remaining 16 events, 12 exhibited a weakening over 24 h that equaled half of the 24 h intensification amount inclusive of the RD1 event. Even further, 9 of these had pressure increases over 24 h greater than the pressure decrease (Table 6 shaded). So 75% of RD1 events were followed by a pressure increase within 24 h which equaled or exceeded the previous 24-h pressure decrease, and 56% showed a larger decay than the 2/3 ratio found by Emmanuel (2000). Several storms had more than one RD1 event, so the 10 storms were investigated rather than the events. The last RD1 event was used for storms which had more than one (Table 6). Seven GOM storms had a greater pressure increase (weakening) than the total pressure decrease (intensification) the previous 24 h. The proximity of these 7 storms to landfall created a bias in these results as each storm had observations after landfall included in the analysis. For the remaining 3 storms which did not have a substantial weakening, the RD1 event occurred at least 24 h away from landfall.

Since results using 24 h after the RD1 event were biased to landfall, the trend 12 h before and after the RD1 event were scrutinized to match Lili's weakening timescale. Of 17 events, 7 had continued pressure decreases, 3 had pressure increases which nearly equaled the pressure decrease, and 6 had slight pressure increases (Table 6 far column). Hurricane Lili (2002) was the only storm to have a larger total pressure gain than the previous 12-h pressure decrease inclusive

Table 6. Cumulative decreases and increases in central pressure 24 and 12 h prior and after the GOM RD1 event for those events equal or greater than Lili's intensification rate.

GOM RD1 Rank	Storm	Date	24 Hours Prior RD1 (hPa)	After RD1 (hPa)	12 Hours Prior RD1 (hPa)	After RD1 (hPa)
1	BEULAH	9/19/67 1800	ND	ND	-38	8
2	ALLEN	8/9/80 0000	-51	26	-48	4
3	CELIA	8/3/70 1800	-45	47	-43	-40
4	CELIA	8/2/70 0000	-28	19	-28	21
5	HILDA	10/1/64 0600	-56	1	-23	-14
6	BRET	8/22/99 0000	-47	7	-25	-10
7	ALLEN	8/8/80 1800	-51	16	-20	-31
8a	ANITA	9/1/77 1800	-60	52	-27	-19
8b	OPAL	10/4/95 0600	-51	55	-30	3
9	CELIA	8/3/70 1200	-45	47	-17	-21
10	OPAL	10/4/95 1200	-50	63	-34	31
11a	CAROLINE	8/31/75 0000	-31	37	-16	-10
11b	ANITA	9/2/77 0000	-59	72	-32	9
11c	BARRY	8/5/01 1200	-17	18	-14	2
12a	INEZ	10/7/66 0000	ND	ND	-13	ND
12b	FLORENCE	9/9/88 1800	-16	20	-13	3
12c	LILI	10/1/02 0600	-39	17	-17	-13
12d	LILI	10/1/02 1800	-31	36	-13	16

of the RD1 event (Table 6). Thus, the pressure results match the wind speed results of Frederick (2003), that Lili was the only hurricane to weaken at a greater rate (+17 hPa over 6 h or +2.83 hPa h^{-1}) than it intensified (-13 hPa over 6 h or -2.16 hPa h^{-1}).

5. Summary and Conclusions

Rapid and explosive deepening events were frequent over the Atlantic basin for all storms since 1979. Rapid intensifications were quite frequent on both a 6-h (RD1) and 24-h

(RD2) time scale. Explosive intensifications were less frequent because of the greater deepening rate needed to meet the criterion. ED1 $\geq$ -5 hPa h^{-1} rate over 6 h occurred only once, and in the GOM specifically, when a suspect event was discounted. At least half of the storms included more than one rapid intensification event over the full basin. Storms tended to have subsequent RD2 events while RD1 events spread out over days as in Hurricane Andrew (1992). This illustrated delineation between short term oscillations and long term persistent deepening.

The GOM RD1 and ED2 events were chosen for scrutiny to define some regional characteristics of rapid and explosive intensification. Timing of the RD1 and ED2 events since storm formation showed no convincing pattern. Timing before landfall exhibited a significant pattern. For RD1 events, the majority occurred $\leq$ 24 h before landfall, with a third $\leq$ 12 h. More considerable of a discovery was that the stronger ED2 events all occurred $\leq$ 24 h before landfall and half nearer to land at $\leq$ 12 h. These findings contend that the main core of the storm could still be intensifying at an explosive rate although the outer bands would be encountering detrimental land effects. Thus, an important distinction can be made between central pressure and wind speed as a measure of core strength when predicting landfall effects.

Most RD1 events resulted in a minimum pressure of $\leq$ 955 hPa and most ED2 events were $\leq$ 935 hPa. All GOM events were located between 22 °N to 28 °N and 98 °W to 85 °W. This demonstrated that no rapid or explosive events occurred near the coastline in the southwestern, northwestern, or extreme eastern areas of the GOM. RD1 events were split evenly on both sides of 90 °W. Yearly distribution showed more favorable conditions for rapid intensification occurred over the last decade in the eastern Gulf in agreement with the Muller and Stone (2001) landfall climatology. However, this was influenced by specific years and spatial location (Hurricane Opal 1995; Tropical Storm Isidore 2002; Hurricane Lili 2002). The

explosive events occurred more frequently in the western side of the basin around 25 °N. Mechanisms responsible for these yearly and spatial trends were not studied here. Although future research might focus upon the depth of the mixed layer or ocean heat content, favorable or unfavorable upper-level circulation patterns, and GOM storm track climatology as probable factors. Storms containing GOM RD1 events made landfall in Louisiana the most. For the ED2 event storms, the majority made landfall in Mexico or Texas. An explosive deepening event storm has yet to make landfall in Louisiana, Mississippi, or Alabama.

The Saffir-Simpson category change analysis on the RD1 type revealed over half of the events occurred within the same category. The greatest number of RD1 events for both the Atlantic basin and GOM clustered around the category 2 to category 3 change which is the threshold into major hurricane status. The same pattern developed in the timing of the GOM RD1 event before landfall. These numbers reinforced that category status at which these rapid intensifications occur are very important in terms of destructive effects. The GOM contained over half of the stronger category changes. This, in conjunction with the only ED1 event occurring in the GOM, illustrated that the GOM had stronger intensification events than other areas of the Atlantic basin.

Hurricane Lili ranked 12th among all GOM RD1 intensification events. Lili's 48 h intensity behavior was not unique when compared to all GOM rapid deepening events ranked the same or higher. Pressure changes 24 h prior and 24 h after each GOM RD1 event were investigated. The majority were followed by a pressure increase at half the level or greater than the 24 h pressure decrease prior. However, Lili was anomalous because it was the only storm to weaken within 12 h at a greater rate (+17 hPa over 6 h or +2.83 hPa h^{-1}) than its RD1 event rate (-13 hPa over 6 h or -2.16 hPa h^{-1}).

These climatology results exemplify that hurricane intensity forecasting should include recognition of a GOM predisposition to rapid and explosive intensification, especially within 24 h of landfall. Also most GOM tropical cyclones weaken a significant amount after intensification, but not 100% of the time and none has weakened at a greater rate than the intensification, except for this one case in Lili.

CHAPTER 3. RELATIONSHIP BETWEEN LILI'S INTENSITY CHANGES AND SATELLITE MEASURED ATMOSPHERIC WATER VAPOR

1. Introduction

A tropical cyclone is a multi-parameter dependent system which interacts with the environments over and through which it travels. Study and forecasting of a tropical cyclone's life cycle is often plagued by varying interactions of the ocean and atmosphere surrounding environments as well as the cyclone itself. Hurricane Lili was an interesting case within the Gulf of Mexico in October 2002. Lili underwent rapid intensity changes, both strengthening and weakening. Several factors have been identified as possible mechanisms responsible for Lili's intensity changes: 1) drier air to the west of the storm, 2) relatively cool ocean water temperatures after Tropical Storm Isidore one week prior, 3) internal eye dynamics, and 4) an upper-level low to the west. This chapter examines the interaction of Lili and the dry air surrounding it, by means of satellite-derived data. The scientific objective was to investigate the relationship between Lili's intensity changes and a dry air mass based upon previous GOES mid- and upper-level water vapor brightness temperature quantification studies (Martin 2001; Hsu 2002). Additionally, another objective was to find evidence of interaction between Lili and -24 °C vapor front which delineated the dry air mass to the west of the hurricane. It is hypothesized that dry air was advected in proximity to surround and interact with Lili's outer circulation, and thus contributed to the storm weakening more rapidly than it intensified.

2. Literature Review

Most hurricane research attempts to improve track and/or intensity forecasting. While track forecasting has improved over the last decade, intensity change prediction still challenges forecasters, and as a whole has not improved significantly over the past few decades (Ellsberry et al. 1992; Lawrence et al. 1998; Marks and Shay 1998). Since the 1960s, satellite data have been

important in detecting, tracking, and improving the forecasting of tropical cyclones. A main field of satellite meteorology has been water vapor observations of hurricanes and utilization to improve the nowcasting and forecasting of tropical events (Rodgers et al. 1976; Shenk et al. 1976; Shenk and Rodgers 1978; Dvorak 1984; Veldon 1984; Le Marshall et al. 1985; Veldon 1987; Weldon and Holmes 1991; Dvorak 1993; Dvorak and Mogil 1994; Veldon et al. 1997; Goerss et al. 1998; Rodgers et al. 1998; Veldon et al. 1998; Bosart et al. 2000; Titley and Elsberry 2000; Chen et al. 2001; Hanley 2002).   More recently, a study of satellite water vapor brightness temperatures quantified the relationship between drier areas in the atmospheric water vapor column and a cyclone's track (Martin 2001). The Martin (2001) doctoral study used GOES satellite imagery and found that a storm will not move in the direction of a dry core area if the two features are ≥ 620 km apart.. However, Martin (2001) found no dynamic linkage between dry cores within 620 km of a hurricane's center and hurricane intensity because in 4 storms, water vapor temperatures remained constant although dramatic pressure changes occurred. Furthermore, Martin (2001) determined this 620 km distance meant that the dry core was outside of a hurricane's circulation pattern, and thus clear interaction affecting intensity change was improbable. Further research of upper air soundings in the Gulf of Mexico resulted in the identification of a satellite water vapor front threshold of -24 °C (Hsu 2002). This satellite value closely adhered to the K-index number of 28, where the atmosphere is too dry to support substantial convective activity (Hsu 2002). After the Martin (2001) and Hsu (2002) research, Lili provided a good case study to investigate the relationship of this -24 °C vapor front to hurricane intensity changes.

3. Data and Methods

Satellite water vapor brightness temperatures were obtained at the Louisiana State University (LSU) Earth Scan Laboratory (ESL), housed within the Coastal Studies Institute (CSI). More information on ESL research and data capture can be found at http://www.esl.lsu.edu. The ground station hardware and software are the TeraScan™ package developed by SeaSpace Corporation. Components for capture, processing, and image visualization are included. Satellite data from the National Oceanic and Atmospheric Administration (NOAA) Geostationary Operational Environmental Satellite (GOES) series have been captured at the ESL since 1995. The GOES-8 GVAR (GOES Variable Format) sensor was operating during Lili's life cycle with the GOES I-M series sensor configuration (Menzel and Purdom 1994). This imager provided data in five channels sensing the visible, shortwave infrared, mid- and upper-level water vapor, and 2 longwave infrared wavelengths (Table 7). The infrared channel at 6.5 to 7.0 μm (Channel 3), with a spatial resolution of 8 km, was the main data. Channel 3 is sensitive to water vapor in the mid and upper tropospheric levels of the atmosphere (Muller and Fuelberg 1990). In this imagery, colder brightness temperatures (Figure 11 white areas) represent moist areas in the upper troposphere, while warmer temperatures (Figure 11 darker areas) represent drier layers of the middle troposphere around 700 – 200 hPa. Vertical motions can be inferred from these shaded pixels (Rodgers et al 1976; Shenk and Rodgers 1978; Weldon and Holmes 1991), where lighter shades symbolize areas of upward vertical motion and dark characterizes areas of subsidence (Figure 11). Areas of subsidence are indicative of dry air from continental origin associated with high pressure areas in the atmosphere. An additional infrared temperature channel at 10.20 – 11.20 μm (Channel 4) was used as extra confirmation of the center location denoted by the warmest pixel. All temperature calibrations were done by, and according to, satellite operational specifications (Menzel and

Table 7. Imagery sensor specifications onboard the GOES-8 satellite (Menzel and Purdom 1994).

Channel	Resolution	Wavelength Range	Meteorological Objective
Visible (1)	1 km	0.55 - 0.75μm	Daytime cloud cover
Shortwave Infrared (2)	4 km	3.80 – 4.00μm	Nighttime clouds and sea-surface temperature (SST)
Water Vapor (3)	8 km	6.50 – 11.20 μm	Water vapor
Longwave Infrared (4)	4 km	10.20 – 11.20 μm	SST and water vapor
Thermal Infrared (5)	4 km	11.50 – 12.50 μm	SST and low level water vapor compared to channel 4

Purdom 1994) since each downlink site receives rectified data. Once captured by the ESL, the imager data were mapped to a 4 km^2 pixel so channels could be compared more readily in a real-time support role for the state of Louisiana. While this technique oversampled the water vapor channel data, the distance measurements are reliable as the visualization software is a portion of the capture and data processing software package. The National Hurricane Center's (NHC) best track dataset contains measurements of center location, wind speed, and minimum central pressure every 6 h, and was used to define the intensity phases for this study. The HURDAT dataset can be located at http://www.nhc.noaa.gov/pastall.shtml and follows Jarvinen et al. (1984). The images were mapped to the same geographical area (Figure 11). Then each satellite pass was analyzed during Lili's pressure intensity phases of interest. The time frame from 0000 UTC 2 October 2002 through 0600 UTC 3 October 2002 was chosen because it covered two rapid intensification (RI) phases and one rapid weakening (RW) phase categorized by the NHC minimum central pressure measurements. For continuity, time periods in between these phases
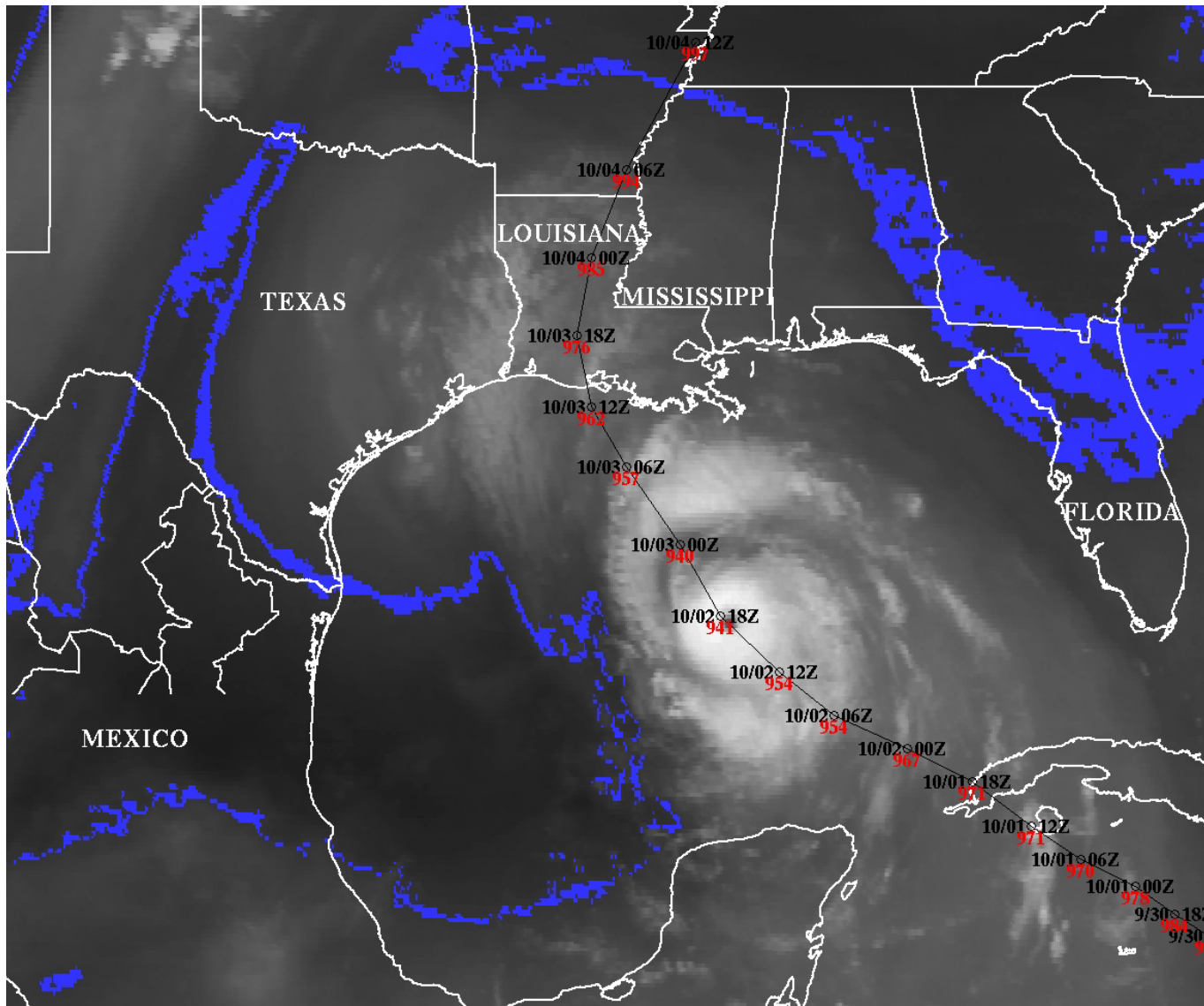
Figure 11. Study area illustrating the specifically designed palette where -24 °C pixels are highlighted blue. Hurricane Lili's track (black) is shown with date, time (UTC or Z), and pressure (hPa; red).

of interest were analyzed as well. There were 98 images over the 30 h time period. The number of images in each of the NHC 6-h time bins varied due to deviances of schedule and planned satellite outages. For these planned outages, the imager function is suspended manually by the satellite operators to avoid damage from direct sun contamination during the solar eclipse season which is routine each fall and spring. Therefore, no imagery is available each day from approximately 0345 UTC through 0645 UTC.

The vapor front defined the edge of the entire dry air mass. It was denoted by applying a specifically designed color palette where the -24 °C pixels were highlighted a contrasting darker blue color (Figure 11). Then for each image, a value for distance in kilometers (km) and azimuth direction were recorded for a line connecting the best determined eye location to the closest point of the -24 °C vapor front. Eye locations for each pass were determined using the warmest pixel temperature in channel 4 and visual interrogation if an eye was discernable. These locations were chosen independently of the NHC track to simulate a real-time nowcasting situation. The nearest -24 °C point was chosen via an interactive method by drawing a line as the distances were simultaneously displayed. The latitude and longitude locations of Lili's center position and the nearest -24 °C point were also documented for later reference and re-creation of the decision process, if necessary. Visually, the outermost feeder band was determined and a distance to the closest -24 °C point was recorded. A companion visual description for each image detailed the width and smooth versus broken signature of the -24 °C vapor front. It became obvious that the warmer water vapor temperature area to the west of Lili (Figure 11 darker area) was the most prevalent and nearest throughout the 30 h time period because dry air on the eastern side formed only half-way into the study period (1500 UTC 2 October 2002). This dry air lobe to the west of Lili expanded in size, elongating against the entire side of the hurricane. A description of the

size of the dry air mass and statistical values of water vapor temperature were completed for the portion over water which directly interacted with Lili. For the hurricane, a visual description of the dense cloud cover surrounding the center was also included as a very informal tracer of convective strength within the main hurricane circulation. Finally, smoothed isopleths of the satellite water vapor temperatures were created to determine the dry core centers for comparison to Martin (2001). Distances to the dry core centers followed the same measurement procedure as previously described.

4. Results

a. Trends in the Time Series

The distances from the -24 °C vapor front to the center of circulation for Hurricane Lili decreased over the 30 h of intensity changes in the Gulf of Mexico (Figure 12). The first GOES GVAR channel 3 image on 0015 UTC 2 October 2002 showed that the vapor front and the center of the hurricane were 507 km apart. The final best determined center of circulation and the -24 °C vapor front were 193 km apart on 0332 UTC 3 October 2002. The trend of falling distance was not a smooth, continuous pattern, but instead had oscillations (Figure 12). Oscillations in distance were caused by individual sections truncating from the -24 °C vapor front which approached closer to Lili than the vapor front. These oscillations are believed to be evidence of the interaction between the more stable air and the storm's outer convection. These were often short-lived features over several images which moved closer to the storm and then either became more moist after interaction with the outer convection of the storm or were reabsorbed by the dry area itself. These variations in trend clustered more during the rapid intensification (RI) cycles of Lili from 0000 - 0600 UTC 2 October 2002 and 1200 -1800 UTC 2 October 2002. In contrast, the two final 6-h time periods (1800 UTC 2 October 2002 through 0600 UTC 3 October
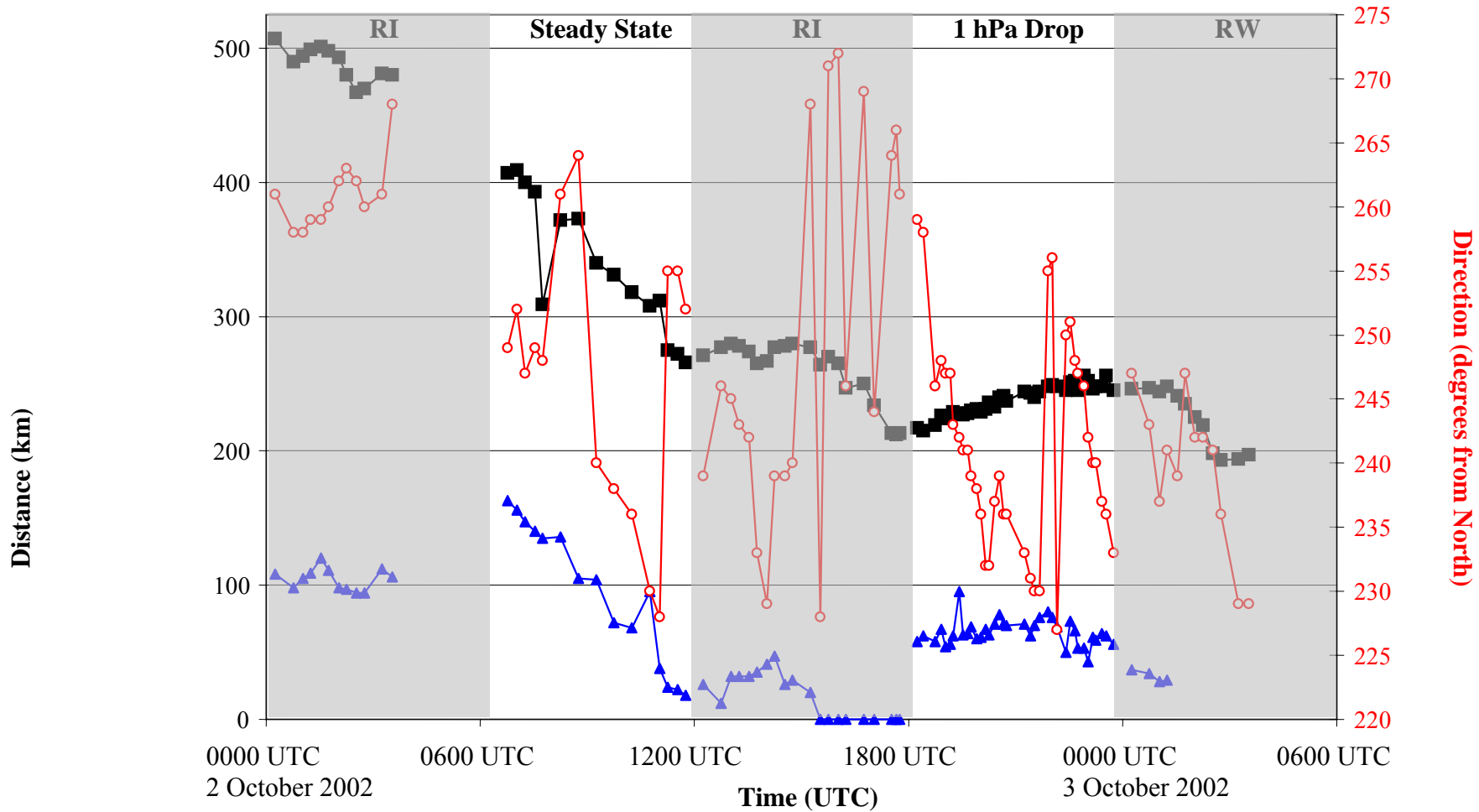
Figure 12. Distances from Lili's center to the -24 °C vapor front nearest point (squares) and the direction of that nearest point (circles) for the entire 30-h time series. Also included are the distances between Lili's center and the outermost feeder band (triangles). Rapid intensity phases are shaded and each phase is labeled.

2002) both had steadier trend lines. Distance between the vapor front and Lili decreased the most during a steady state phase for Lili (0600 – 1200 UTC 2 October 2002) after the first RI phase. Radial direction between Lili's center and the closest -24 °C point was inconsistent from image to image, although the measurements did stay within the southwest quadrant between 225° and 275°. The directional variance of the nearest -24°C point contributed additional confidence to the notion that the vapor front severed at specific points of interaction between the dry, stable air and moist, unstable air.

It became apparent after detailed analysis of the imagery that quantifying the distance between the-24 °C vapor front and outermost feeder band might also provide valuable information. The trend of these measurements mimicked very closely the other distance measurements (Figure 12). The vapor front and outer edge of Lili's convection touched continuously during the final two hours of the second RI stage (1545 – 1745 UTC 2 October 2002). Afterward, a 1 hPa pressure decrease occurred, followed by the only rapid weakening (RW) phase. The nearest point to the outer convection distance rose from directly interacting to 58 km around 1800 UTC 2 October 2002 because the outer convection of Lili dissipated and the next convective band was chosen. Data for this analysis ended at 0115 UTC 3 October 2002 as the outer bands became indiscernible due to the convection weakening on the western periphery of the hurricane.

The strength of the -24 °C vapor front at the boundary with Lili was visually described to help interpret what effect the two systems had upon each other. There was a great deal of variance in the vapor front visual descriptions as was shown in the distances. Over time, the line of highlighted values took on a number of diverse visual characteristics across differing locations. Sometimes the vapor front became broken or took on variable widths. There were a

number of instances when one section of the -24 °C vapor front was wider and thus slightly stronger, while another section would be weaker. As mentioned in the distance measurements, it is believed that these self-contained smaller areas of warmer temperatures characterized interaction between the rising convective tendency of the moist air and the stableness of the dry air (Figure 11).

Additional distances related Lili's center to the core of the dry air for direct comparison to Martin (2001) that a storm will not move in the direction of a dry core area if the two are 620 km apart. For these distances, only the initial images of each NHC 6-h time intervals were analyzed (Figures 13 – 18). The trend here was a decrease, however the core of the dry area never moved closer than 702 km from the center of Lili for the western area of stable air or any closer than 808 km for the dry air mass to the east.

Over the 30 h imagery time series, the mass of dry air to the west of Lili grew from a thin east-west orientated tongue (Figure 13) to a taller and wider lobe extending all along the entire western side of the hurricane (Figure 17). A more in-depth hourly scrutiny of the lobe's area and sample count confirmed this areal orientation trend (Table 8). These statistics were gathered by drawing a box specifically for each hourly image incorporating the tallest extent offshore. The portion of the lobe from the Texas coastline out to the -24 °C vapor front became drier as evidenced by the mean and maximum temperatures growing warmer with each hourly image (Table 8). Table 9 details the extent of the lobe along with the latitude and longitude location separated by the NHC 6-h time bins.
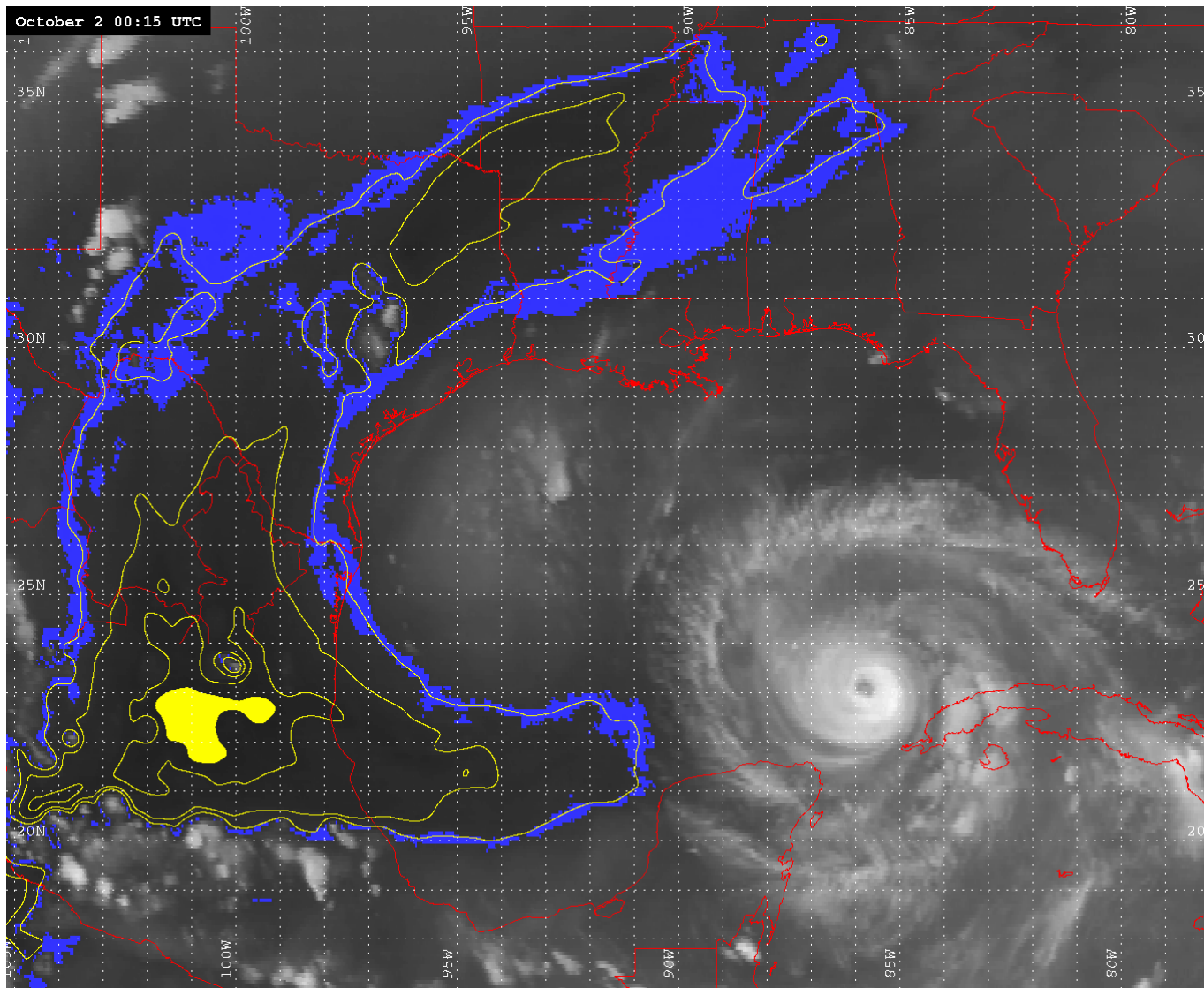
Figure 13. GOES-8 water vapor image on 0015 UTC 2 October 2002 with the -24 °C vapor front (blue) and isotherms (yellow) highlighted. The area of the dry core (-19 °C) is filled in yellow.
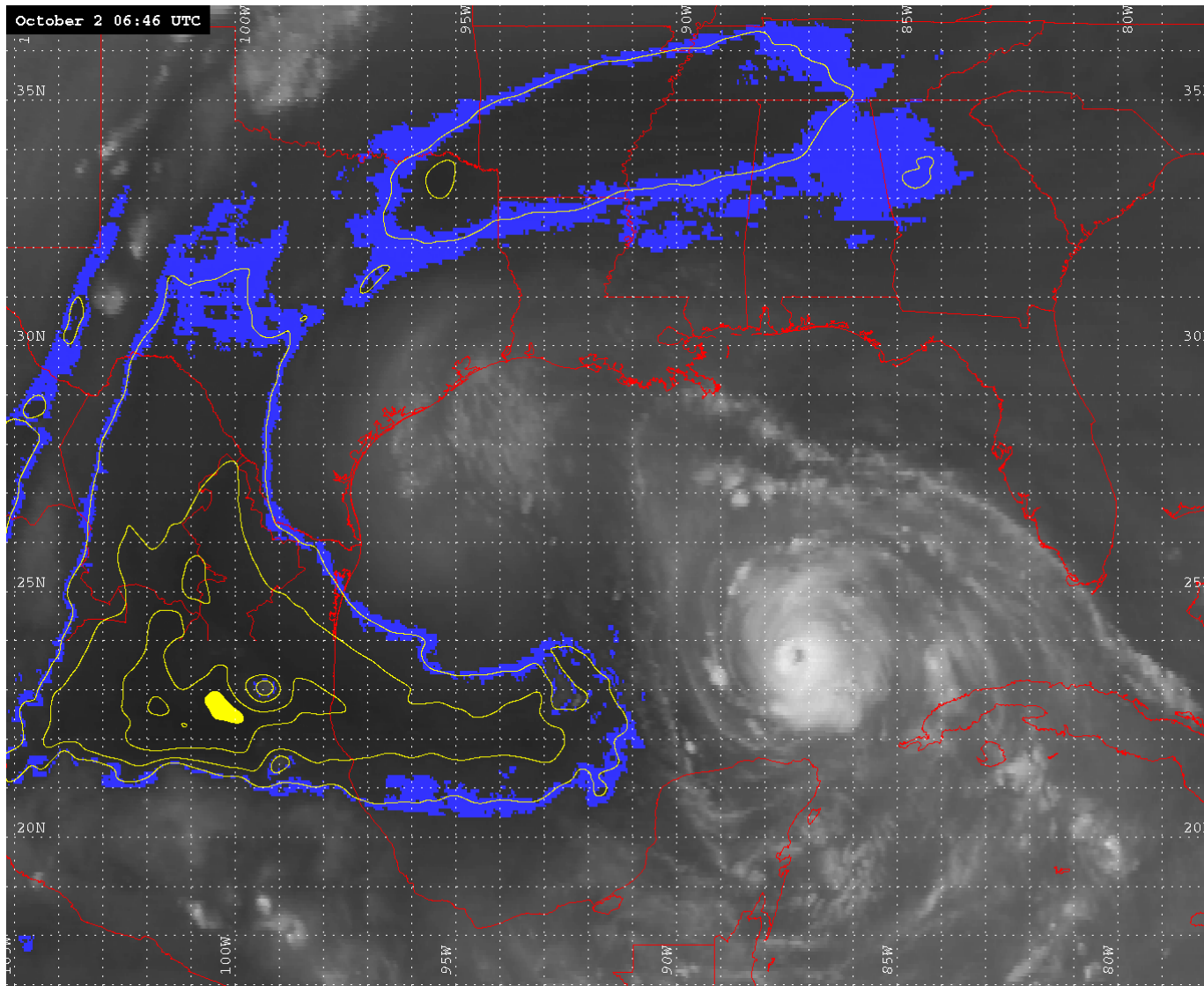
45

Figure 14. GOES-8 water vapor image on 0646 UTC 2 October 2002 with the -24 °C vapor front (blue) and isotherms (yellow) highlighted. The area of the dry core (-19 °C) is filled in yellow.
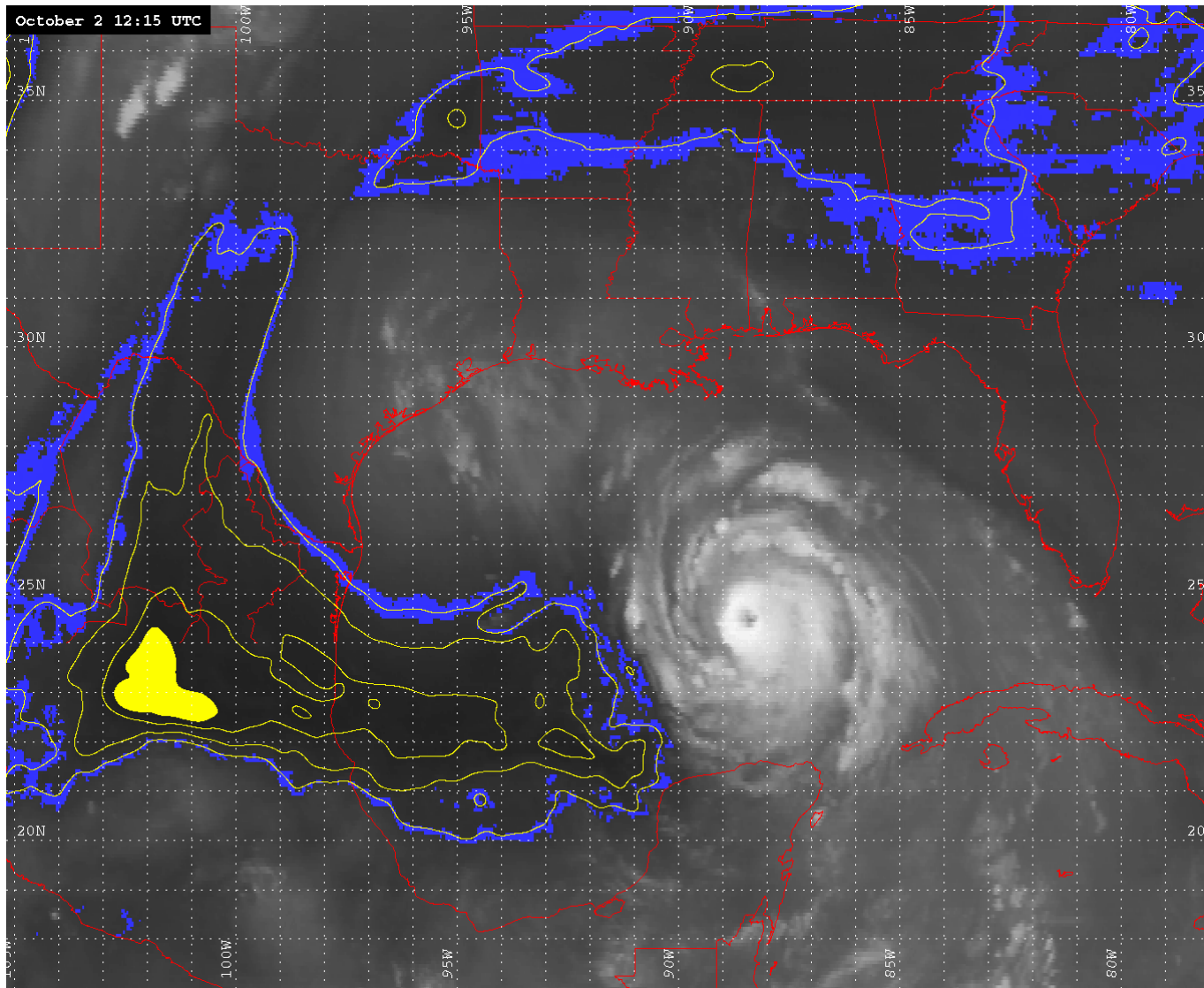
Figure 15. GOES-8 water vapor image on 1215 UTC 2 October 2002 with the -24 °C vapor front (blue) and isotherms (yellow) highlighted. The area of the dry core (-19 °C) is filled in yellow.
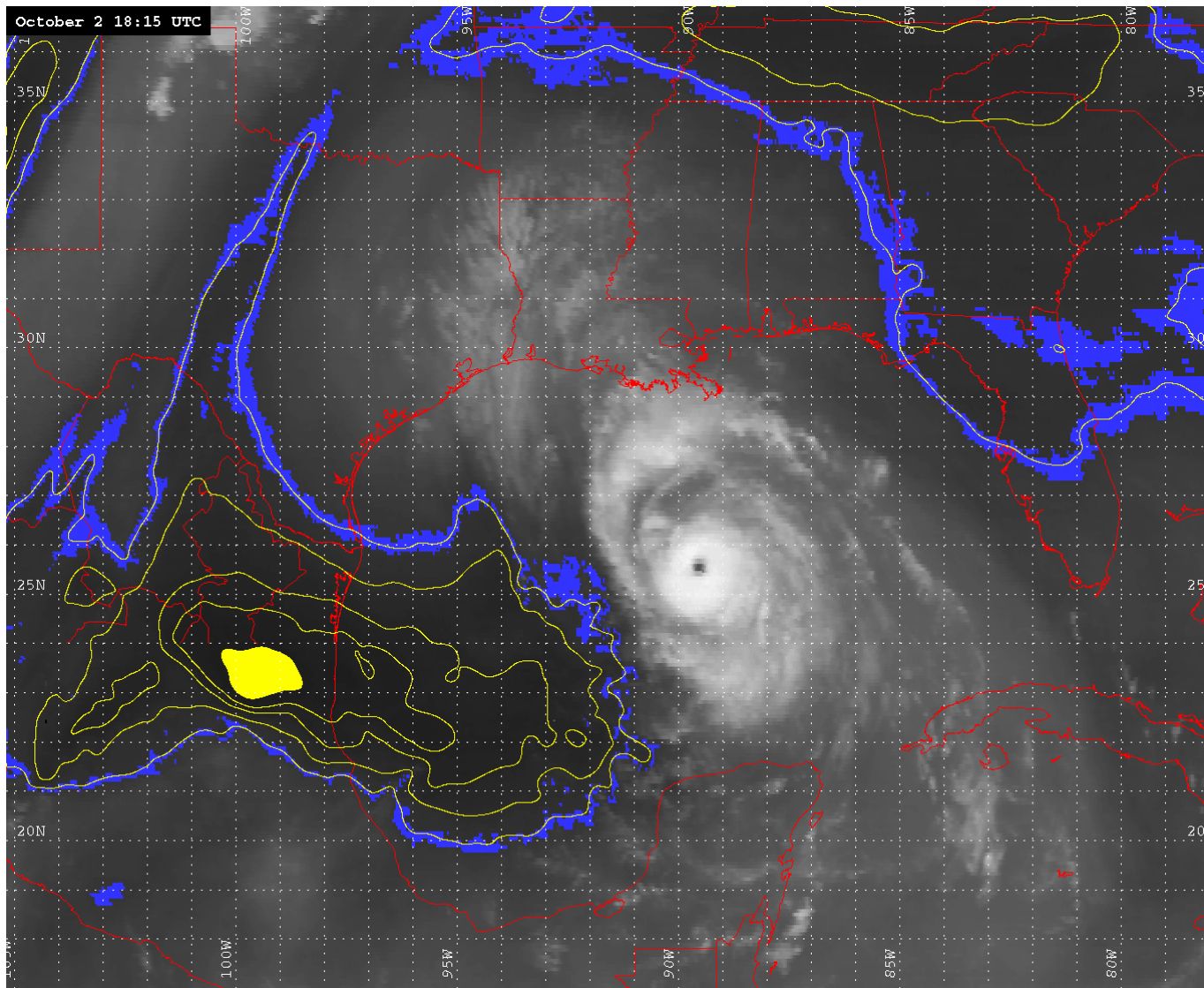
Figure 16. GOES-8 water vapor image on 1815 UTC 2 October 2 2002 with the -24 °C vapor front (blue) and
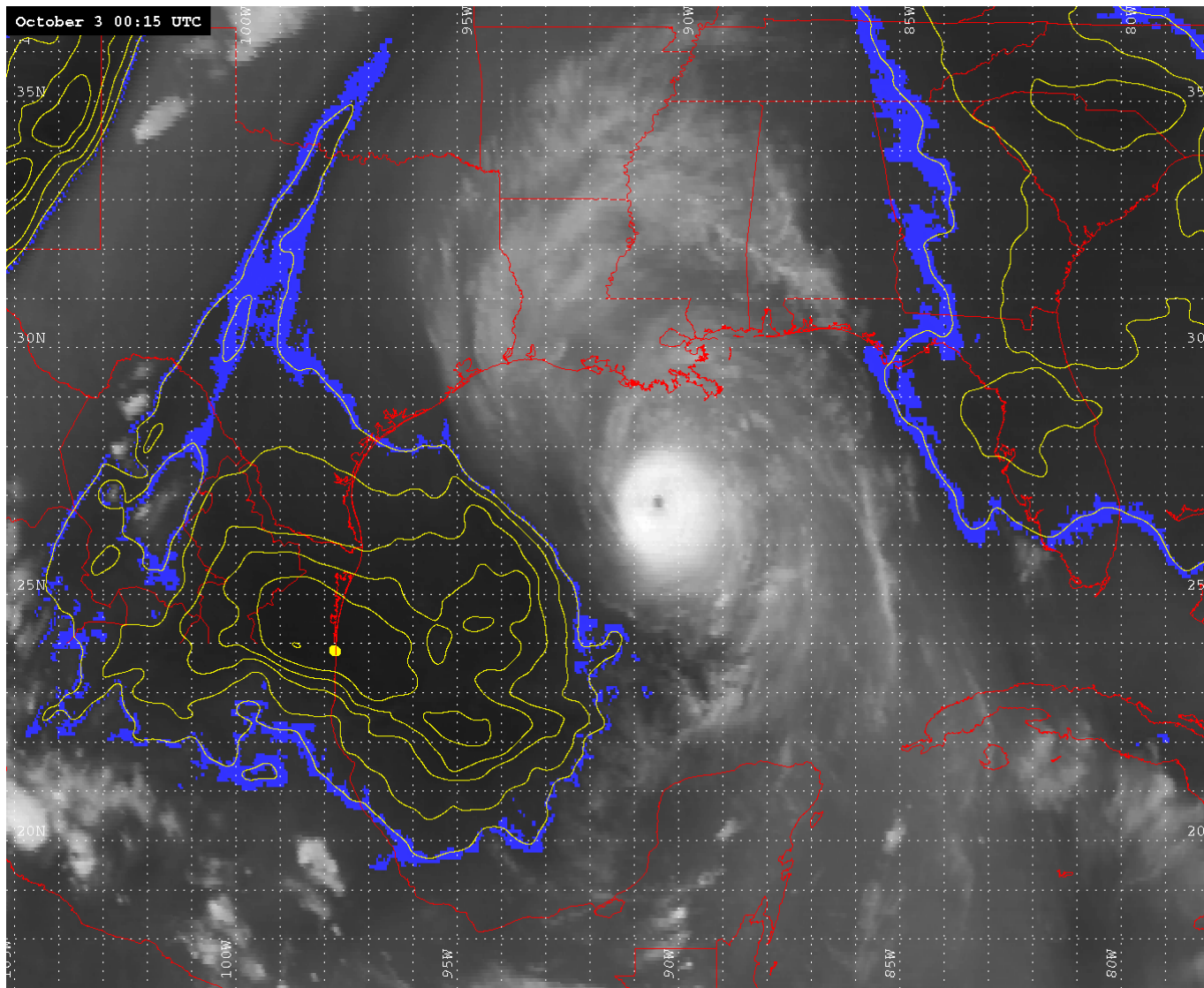 isotherms (yellow) highlighted. The area of the dry core (-18 °C) is filled in yellow.

Figure 17. GOES-8 water vapor image on 0015 UTC 3 October 2002 with the -24 °C vapor front (blue) and
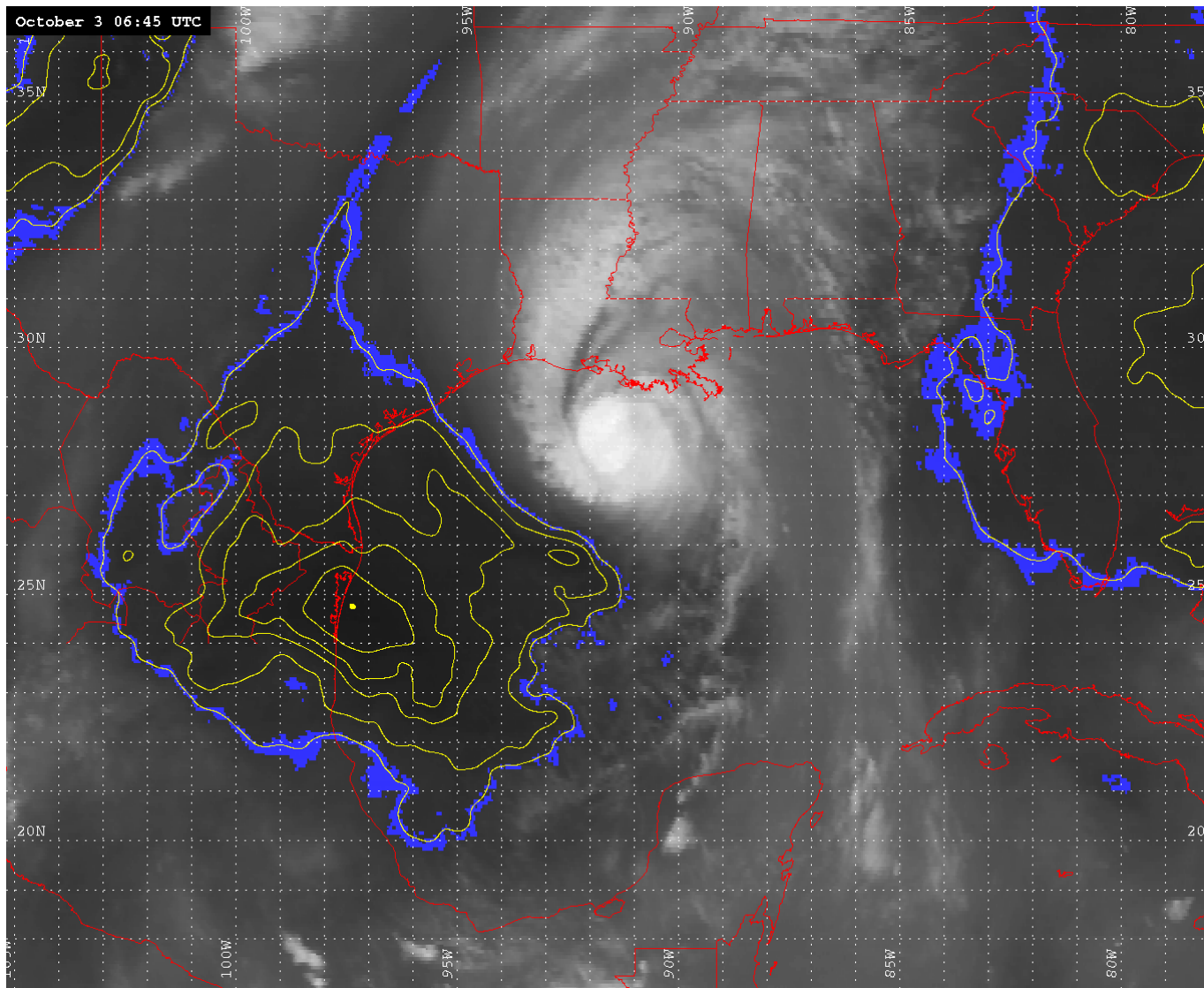 isotherms (yellow) highlighted. The area of the dry core (-17 °C) is filled in yellow.

Figure 18. GOES-8 water vapor image on 0645 UTC 3 October 2002 with the-24 °C vapor front (blue) and
 isotherms (yellow) highlighted. The area of the dry core (-17 °C) is filled in yellow.

Table 8. Hourly representative statistics of the satellite water vapor brightness temperature (channel 3) for the offshore dry air lobe to the west of Lili throughout the 30-h time series of imagery. ND is no data.

	Image Time (UTC)	Water Vapor Temperature Max (°C)	Mean (°C)	Std. Dev (°C)	Area (km²)	Pixel Count
	2 October 2002					
	0145	-20.06	-22.37	0.90	80,327	5,056
Rapid	0245	-19.88	-22.36	0.89	80,327	5,056
Intensification	0332	-19.88	-22.36	0.97	80,327	5,056
(RI)	0445	ND	ND	ND	ND	ND
	0545	ND	ND	ND	ND	ND
	0646	-20.34	-22.67	1.06	85,855	5,412
	0745	-19.88	-22.29	1.00	114,917	7,216
Steady State	0845	-19.88	-21.93	1.06	100,386	6,256
	0945	-19.43	-21.83	1.17	117,542	7,383
	1045	-19.52	-21.57	1.25	117,542	7,383
	1145	-19.08	-21.26	1.38	117,542	7,383
	1245	-18.90	-21.34	1.43	136,435	8,468
Rapid	1345	-18.47	-20.92	1.31	136,435	8,468
Intensification	1445	-18.47	-20.67	1.30	136,435	8,468
(RI)	1545	-18.55	-20.78	1.37	164,769	10,064
	1645	-18.21	-20.50	1.30	164,769	10,064
	1745	-18.38	-20.41	1.17	164,769	10,064
	1845	-18.21	-20.50	1.32	171,869	10,720
	1945	-18.29	-20.30	1.39	171,869	10,720
1 hPa drop	2045	-17.95	-20.24	1.47	145,529	9,359
	2145	-17.86	-19.94	1.40	145,529	9,359
	2245	-17.61	-19.88	1.49	147,474	9,292
	2345	-17.18	-19.68	1.45	170,744	10,752
	3 October 2002					
	0045	-17.27	-19.57	1.41	170,744	10,752
	0145	-17.18	-19.65	1.50	170,744	10,752
	0245	-17.44	-19.49	1.38	224,122	14,062
Rapid	0332	-17.10	-19.47	1.33	213,585	13,356
Weakening	0445	ND	ND	ND	ND	ND
(RW)	0545	ND	ND	ND	ND	ND
	0645	-16.93	-19.58	1.05	172,183	11,050

b. 6 Hour Intensity Phases

Since the research objective was to investigate the relationship between dry air and Lili's intensity changes, the previously mentioned distances between the vapor front and both Lili's center and outermost feeder band plus visual imagery descriptions will be discussed in 6-h time increments based upon the NHC best track dataset. The minimum, maximum, mean, and range of distance measurements are presented in Tables 10 and 11. Throughout the imagery of Lili's intensity changes, the dry air mass to the west always contained the nearest point of the -24 °C vapor front. All distance measurements unless otherwise noted refer to the dry air mass to the west of Lili.

1) Rapid Intensification 0000 – 0600 UTC 2 October 2002

The initial time period analyzed was the first RI phase covering 0000 – 0600 UTC 2 October 2002. The NHC best track report detailed that Lili's pressure began at 967 hPa and decreased to 954 hPa, and thus achieved a drop of 13 hPa over 6 h. This rate satisfied the criterion for an RI event presented in chapter 2. This was a Saffir-Simpson category change from category 2 to 3. However, the imagery was not available for approximately 3 h during the final stages of this time increment as a result of the GOES eclipse season. Only 12 images over 3.25 h were available.

Distance between Lili's center and the -24 °C vapor front during this phase decreased, however it was not a steady drop but rather had variation (Figure 12). The distances between the -24 °C vapor front and Lili's center for this RI period averaged 488 km, with a minimum of 467 km and a maximum of 507 km (40 km range). These numbers were a bit misleading since the final 2.5 h of imagery were unavailable. If the 0645 UTC 2 October 2002 image is interpolated as the final 0600 UTC 2 October 2002 measurement for this phase, the minimum would have

Table 9. Extent of the dry air mass lobe as measured offshore from the Texas coastline for the initial and ending images within the NHC best track 6-h time periods.

	Image Time (UTC)	Height (km)	Southern Edge (°N)	Northern Edge (°N)	Width (km)	Western Edge (°W)	Eastern Edge (°W)
2 October 2002							
Rapid Intensification (RI)	0015	348	20	23	742	-97.72	-90.5
	0332	382	20	23.5	695	-97.72	-91
Steady	0646	395	20.5	24	715	-97.72	-91
	1145	557	20	25	800	-97.72	-90
Rapid Intensification (RI)	1215	556	20	25	801	-97.72	-90
	1745	792	20	27	700	-97.72	-91
1 hPa drop	1815	792	20	27	700	-97.72	-91
	2345	935	20	28	675	-97.72	-91
3 October 2002							
Rapid Weakening (RW)	0015	935	20	28	675	-97.72	-91
	0332	1017	19.5	28.5	565	-97.72	-92

decreased to around 409 km and the range would have doubled to 102 km. Also, the distance between the outermost convective band of Lili and nearest -24°C point averaged 104 km with a minimum of 94 km and a maximum of 120 km. The range of 26 km again was misleading. If the same interpolation is made for the 0600 UTC 2 October 2002 image, then the maximum increased to 163 km and the range to 69 km. It would be too difficult to interpolate over the 2.5 h for a mean value. Even though the statistics and component distances were incomplete, it seemed plausible that the two features remained far enough apart so that Lili's inner core strength was not affected negatively.

Table 10. Minimum, maximum, mean, and range of distances between Lili's center and the -24 °C vapor front.

	Image Times (UTC)	Minimum (km)	Maximum (km)	Mean (km)	Range (km)
Rapid Intensification 12 images	0015 – 0332 UTC 2 October 2002	467	507	488	40
Steady 15 images	0646 – 1145 UTC 2 October 2002	266	409	339	143
Rapid Intensification 20 images	1215 – 1745 UTC 2 October 2002	213	280	260	67
1 hPa drop 37 images	1815 – 2345 UTC 2 October 2002	215	256	238	41
Rapid Weakening 12 images	0015 – 0332 UTC 3 October 2002	193	247	224	54

Visually, the -24 °C vapor front began rather thick, approximately 36 km along the entire north-south oriented border with the hurricane (Figure 19a). This thick nature and smoothness of the highlighted -24 °C vapor front denoted that the two systems were not interacting directly in the mid and upper level moisture patterns. Beginning with the 0132 UTC 2 October 2002 image, this stout width began to breakdown slightly as the width varied throughout the entire border with Lili. However, there were no complete breaks through this vapor front or drastic shape transformations (Figure 19b) which would have been indicative of increased interaction between the two features. This variation in the width of the -24 °C vapor front indicated that the two systems were interacting minimally, though still not at a substantial level to alter the overall

Table 11. Minimum, maximum, mean, and range of distances between Lili's outermost convective band and the -24 °C vapor front.

	Image Times (UTC)	Minimum (km)	Maximum (km)	Mean (km)	Range (km)
Rapid Intensification 12 images	0015 – 0332 UTC 2 October 2002	94	120	104	26
Steady 15 images	0646 – 1145 UTC 2 October 2002	18	163	95	145
Rapid Intensification 20 images	1215 – 1745 UTC 2 October 2002	0	47	17	47
1 hPa drop 37 images	1815 – 2345 UTC 2 October 2002	43	95	65	52
Rapid Weakening 4 images	0015 – 0332 UTC 3 October 2002	28	37	32	9

hurricane intensity trend. Since the imager did not scan the latter 3 h of this time frame, it can be inferred from the 0646 UTC 2 October 2002 image (Figure 14) that this increased broken pattern of the -24 °C vapor front continued through 0600 UTC 2 October 2002 which was the end of this RI phase. The areal coverage of the dry air mass extended by 0.5° latitude for both the north and east edges over the 3.25 h of imagery. The northern boundary began along 23 °N (Figure 19a) and by the 0332 UTC 2 October 2002 image was along 23.5 °N (Figure 19d). This translated to a slight increase in the northern extent, but the width drew in somewhat (Table 9) and both values were under 50 km change. Even though the edges changed slightly, the box drawn was representative for the entire time period so the area and pixel count were unchanged (Table 8). Water vapor hourly temperatures confirmed that the entire lobe of dry air remained fairly
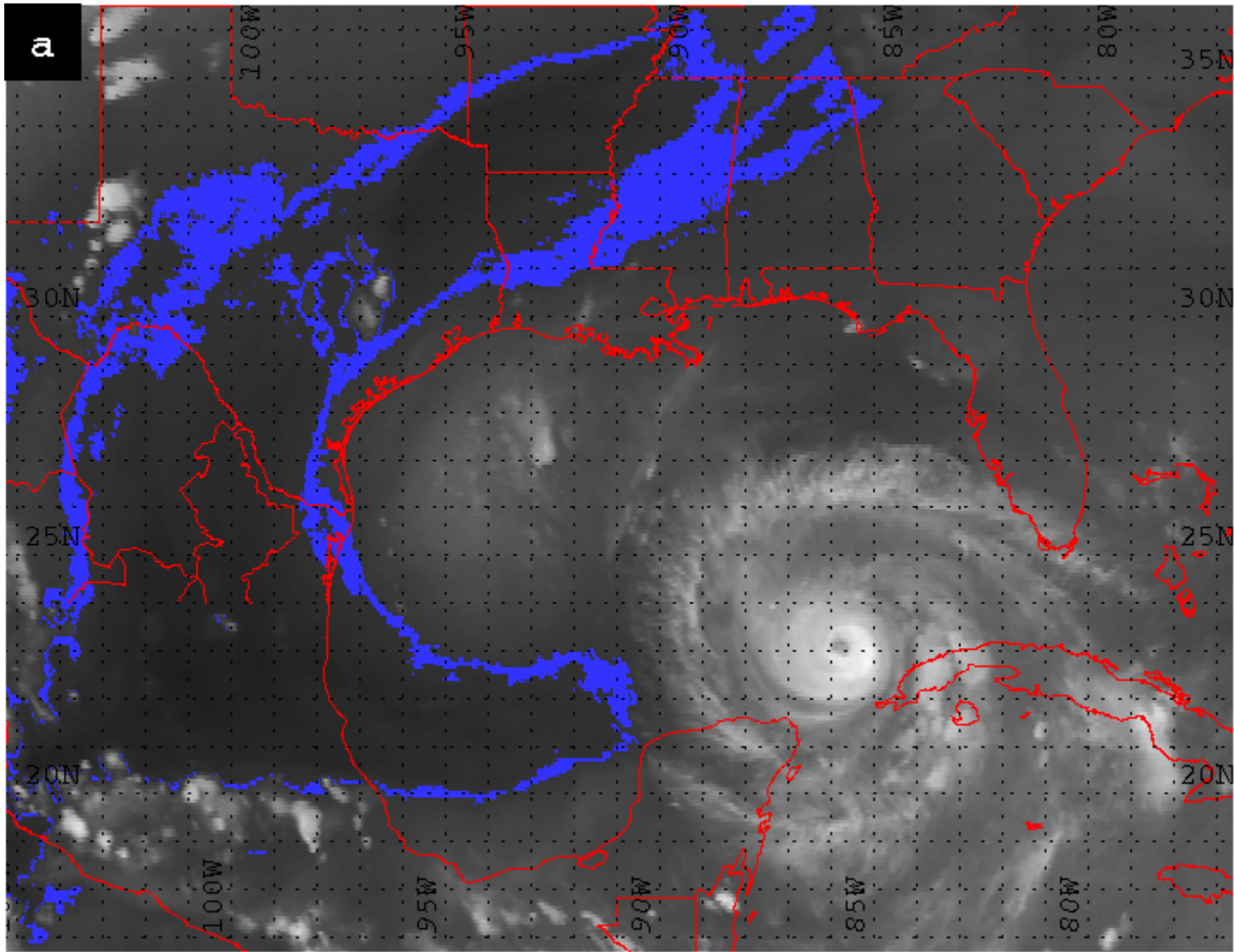
Figure 19a. GOES-8 water vapor image during the first RI phase on 0015 UTC 2 October 2002 with the -24 °C vapor front (blue) highlighted.
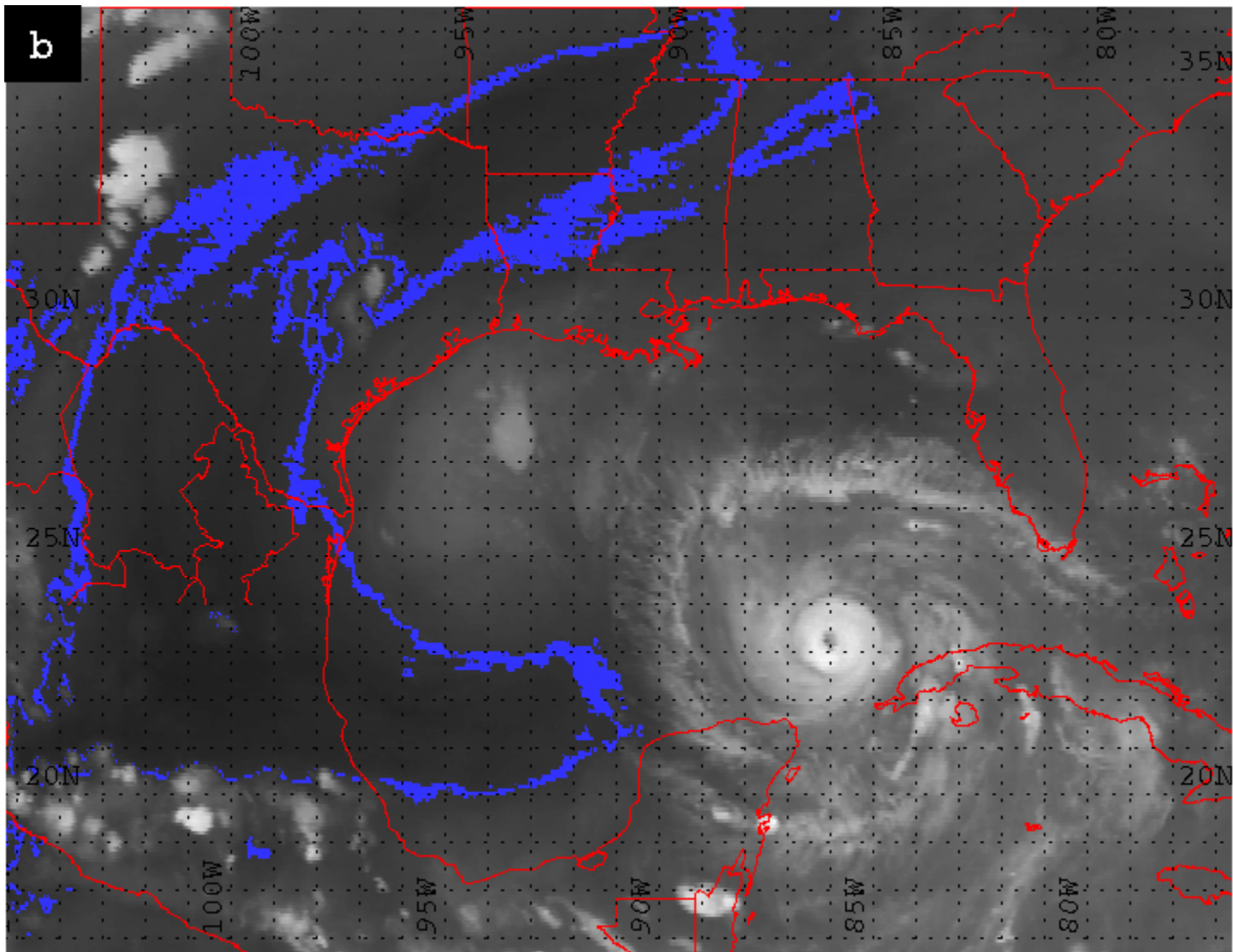
Figure 19b. GOES-8 water vapor image during the first RI phase on 0132 UTC 2 October 2002 with the -24 °C vapor front (blue) highlighted.
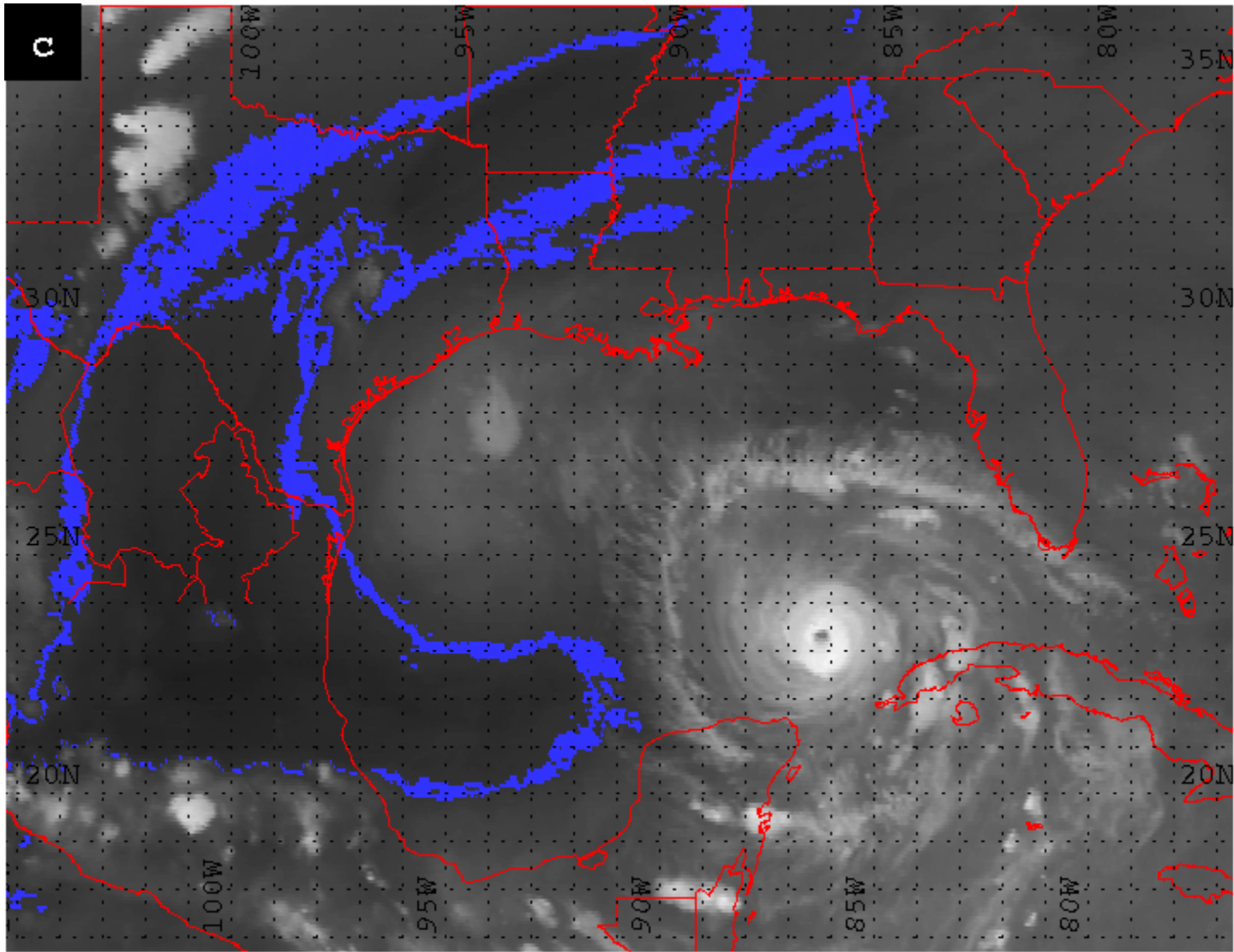
Figure 19c. GOES-8 water vapor image during the first RI phase on 0215 UTC 2 October 2002 with the -24 °C vapor front (blue) highlighted.
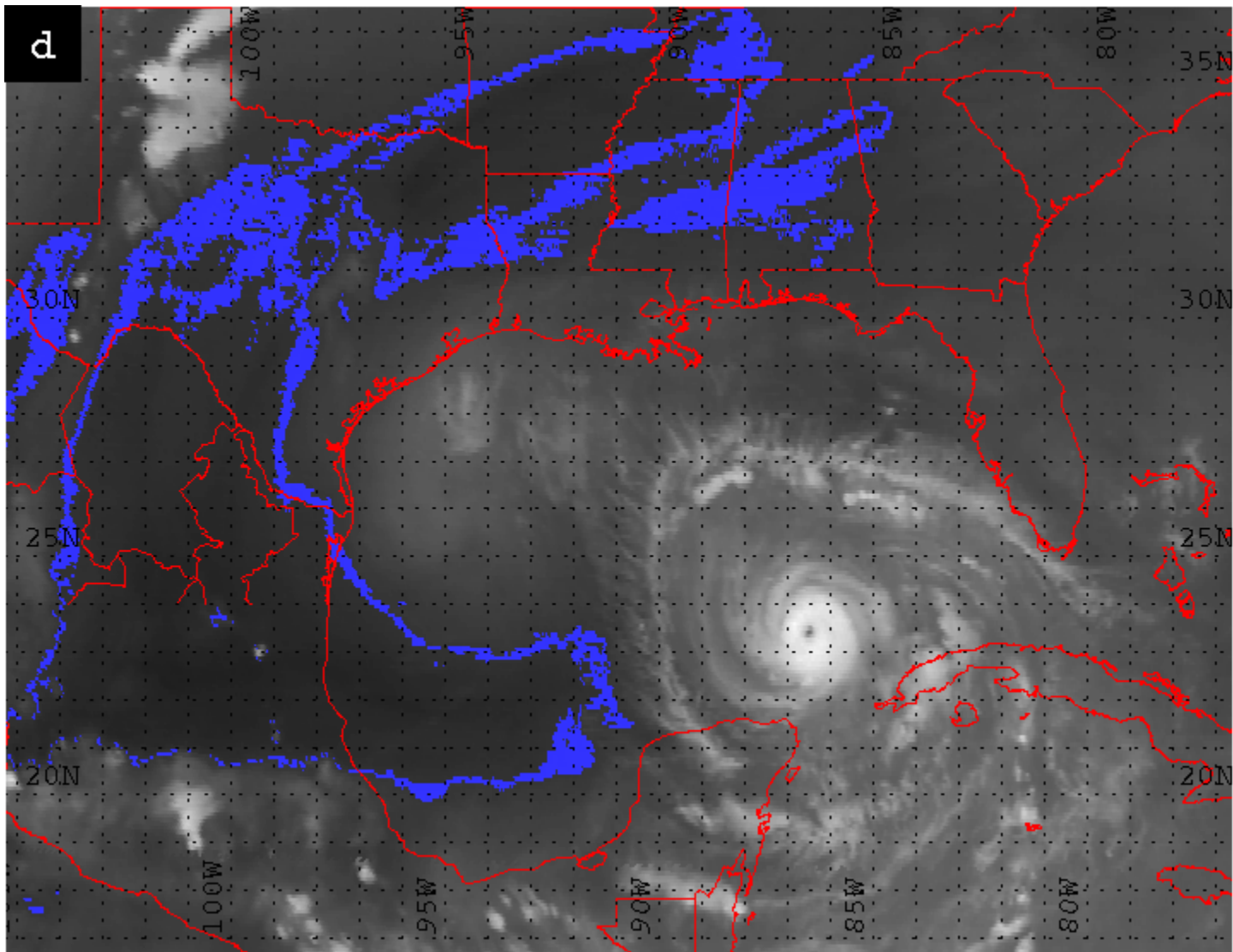
Figure 19d. GOES-8 water vapor image during the first RI phase on 0332 UTC 2 October 2002 with the -24 °C vapor front (blue) highlighted.

consistent with the mean approximately -22.4 °C and a +0.2 °C change in the maximum temperature, all while Lili strengthened (Table 8).

The entire circulation of Lili expanded around the center during this RI phase. It resembled the more classic low pressure comma shape in the first image (Figure 19a), but by the 0332 UTC 2 October 2002 image there was complete symmetrical enclosure of the eye (Figure 19d). The 0646 UTC 2 October 2002 image (Figure 20a) illustrated an even better expansion of the main convection area when used to interpolate during the data outage covering the 0600 UTC 2 October 2002 end of this RI phase. This growth of circulation agreed with previous research that inner core strengthening coincides with deepening (Croxford and Barnes 2002). The outflow pattern was a good distance from the cyclonic circulation throughout (Figure 19).

2) Steady State 0600 – 1200 UTC 2 October 2002

The next 6-h NHC best track report time period covered 0600 – 1200 UTC 2 October 2002. Lili's pressure remained constant at 954 hPa and category 2 status, marking a period of no intensity loss or gain following the previous RI event. The GOES eclipse season outage only impacted the first 45 minutes of this time period, therefore 15 images over 5 h were available for study.

Distances decreased between the -24 °C vapor front and both Lili's center (Figure 12) and the outermost convective band (Figure 12). The distance between the -24 °C vapor front and the center of Lili averaged 339 km from a low of 266 km to a peak of 409 km. This 143 km range illustrated the two features moved closer at a faster pace because the large range was over the same 6 h time frame as the other phases. The distance from the outer edge of Lili's convective bands to the nearest -24°C point had a low of 18 km and a peak of 163 km, with a

60

mean of 95 km. The range of 145 km again showed the two features moved closer more efficiently during this phase.

The -24 °C vapor front started out thick in most places, but was thinner at 21.75 °N and 91.25 °W (Figure 20a). For the first time, the front had definitive breaks with the most broken signature at 0915 UTC 2 October 2002 (Figure 20c). Shape transformations were prevalent throughout the imagery as well. Between 0915 and 1102 UTC 2 October 2002 (Figure 20c; 20e), there was an extension of the lobe toward the southwest side of Lili's circulation at 21.5 °N and 90 °W. The vapor front re-strengthened farther eastward by the end of the time period (Figure 20f). The more broken nature of the -24 °C line exhibited throughout this steady intensity time period signified that the two features interacted more so than the previous RI phase. However, no pixels representative of -24 °C entrained in Lili's circulation nor did any of the convective bands completely diminish at the boundary with the dry air mass. Since Lili did not change in intensity during this time period, it was viable to assume that the interaction between the two features still was not significant enough to directly alter Lili's intensity.

The dry air mass extended on the north, south, and eastern sides throughout this time period to span from 20 to 25 °N and from 97.7 to 90 °W (Table 9). This resulted in the second highest growth in height and the only increase in width over the entire time series. While extending in coverage, the dry air mass also increased in stability with > +1 °C warming in both the mean and maximum temperatures (Table 8).

Visually, Lili's circulation pattern grew more symmetrical and more expansive (Figure 20 a-f), although the pressure remained constant. Some well defined convective bands appeared at 0845 UTC 2 October 2002 (Figure 20b). There seemed to be an eyewall replacement cycle between 0915 and 1115 UTC 2 October 2002 (Figure 20c; 20f). Eyewall replacement cycles
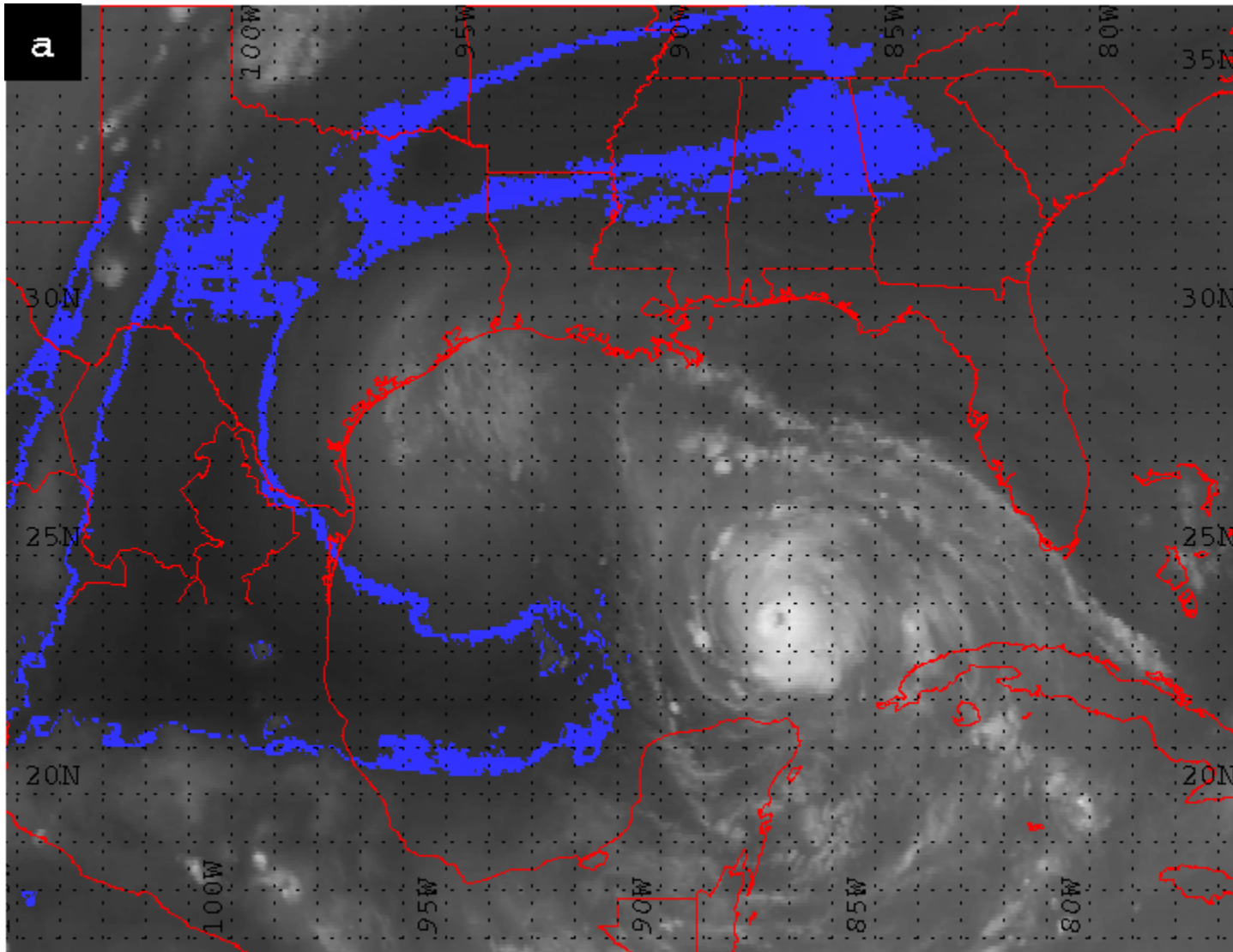
Figure 20a. GOES-8 water vapor image during the steady state phase on 0646 UTC 2 October 2002 with the -24 °C vapor front (blue) highlighted.
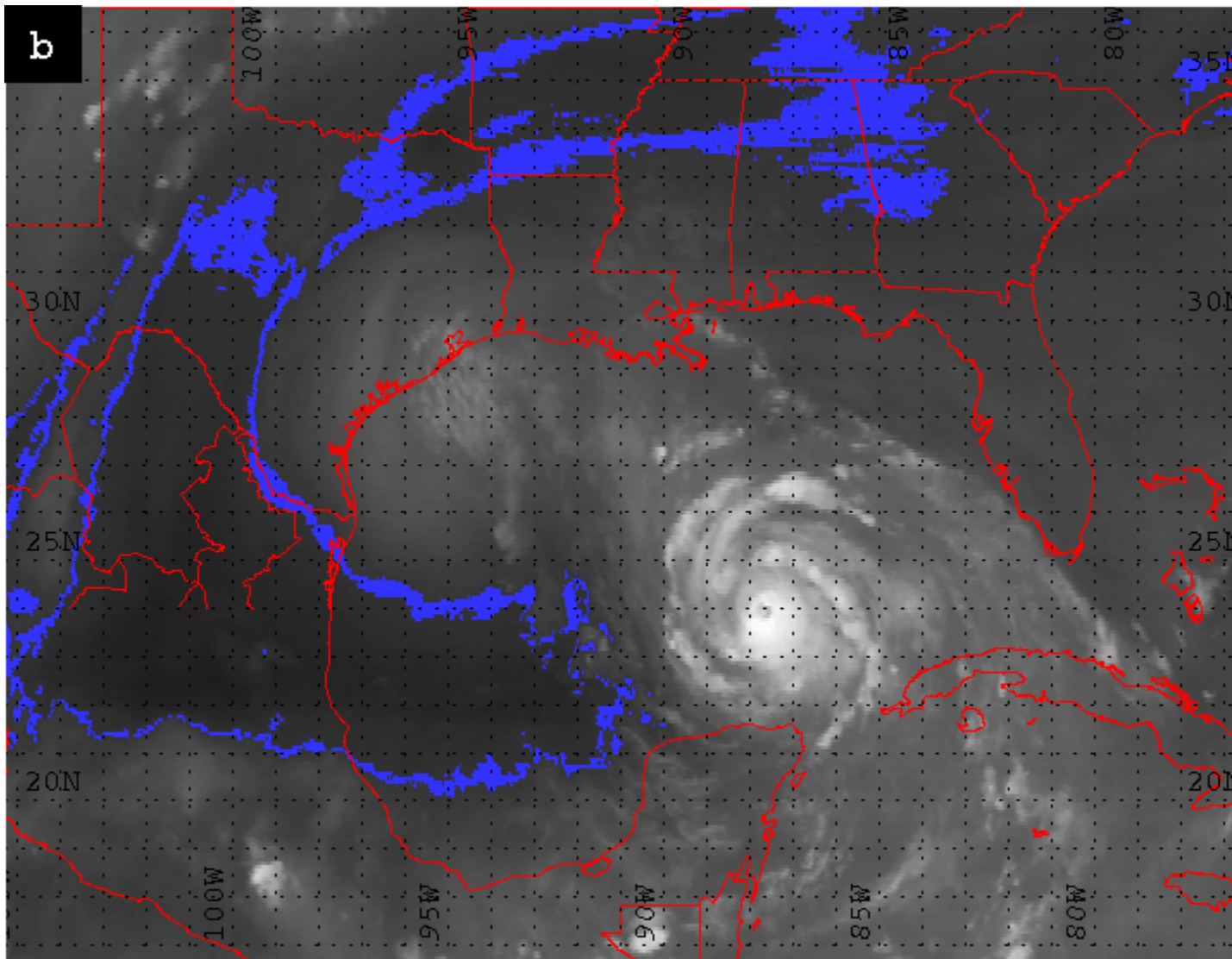
Figure 20b. GOES-8 water vapor image during the steady state phase on 0845 UTC 2 October 2002 with the -24 °C vapor front (blue) highlighted.
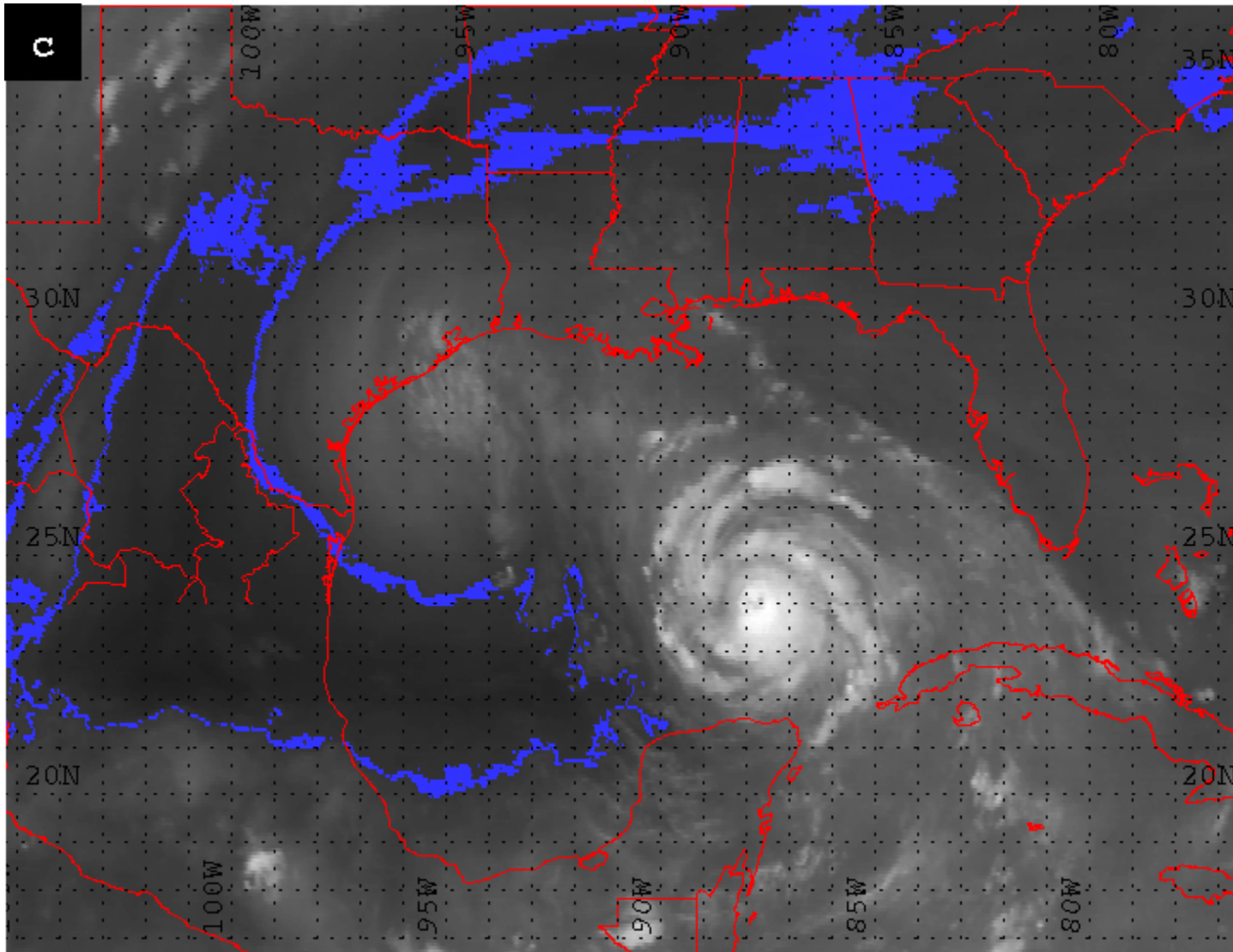
Figure 20c. GOES-8 water vapor image during the steady state phase on 0915 UTC 2 October 2002 with the -24 °C vapor front highlighted in blue.
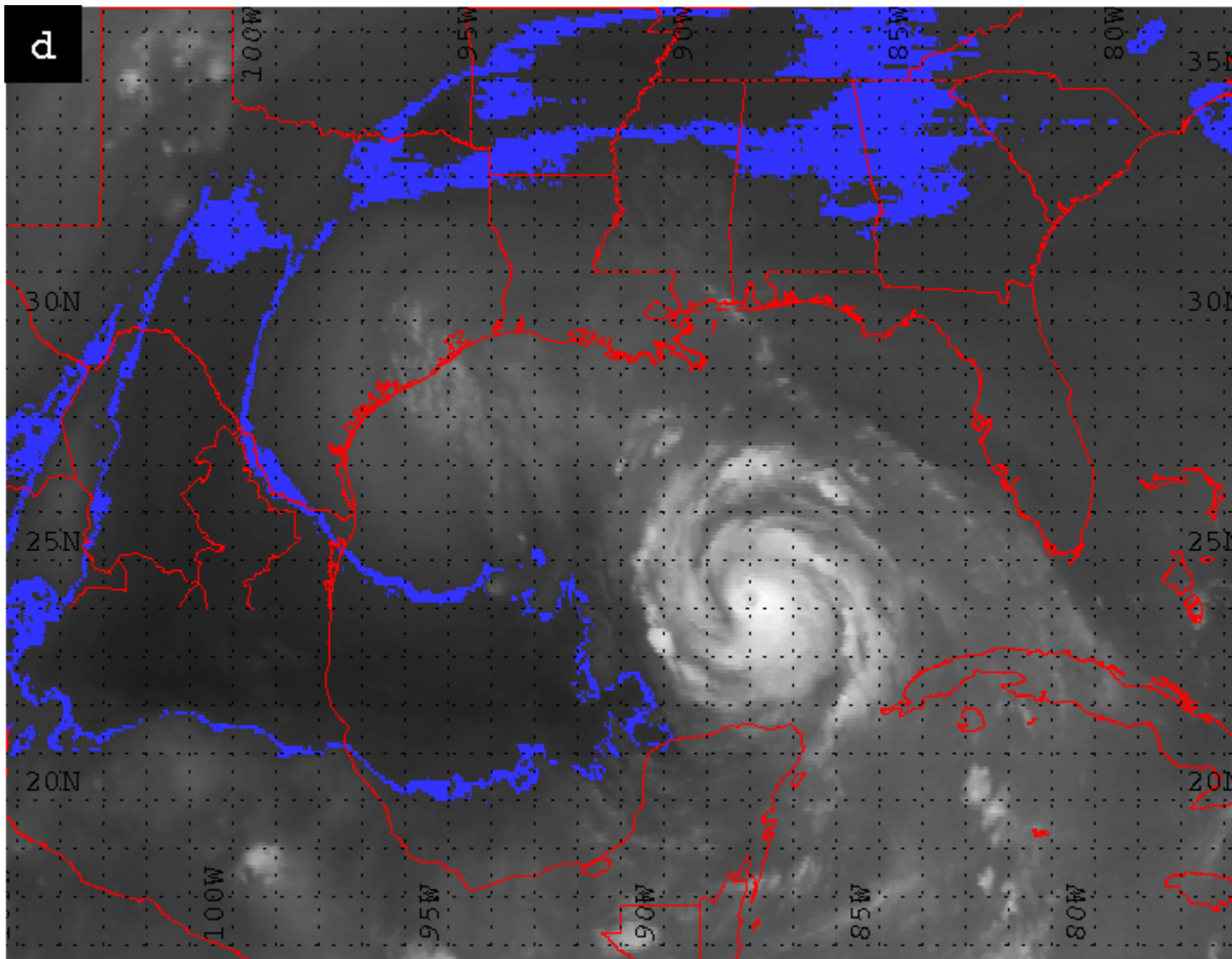
Figure 20d. GOES-8 water vapor image during the steady state phase on 1015 UTC 2 October 2002 with the -24 °C vapor front (blue) highlighted.

Figure 20e. GOES-8 water vapor image during the steady state phase on 1102 UTC 2 October 2002 with the -24 °C vapor front (blue) highlighted.

Figure 20f. GOES-8 water vapor image during the steady state phase on 1145 UTC 2 October 2002 with the -24 °C vapor front (blue) highlighted.
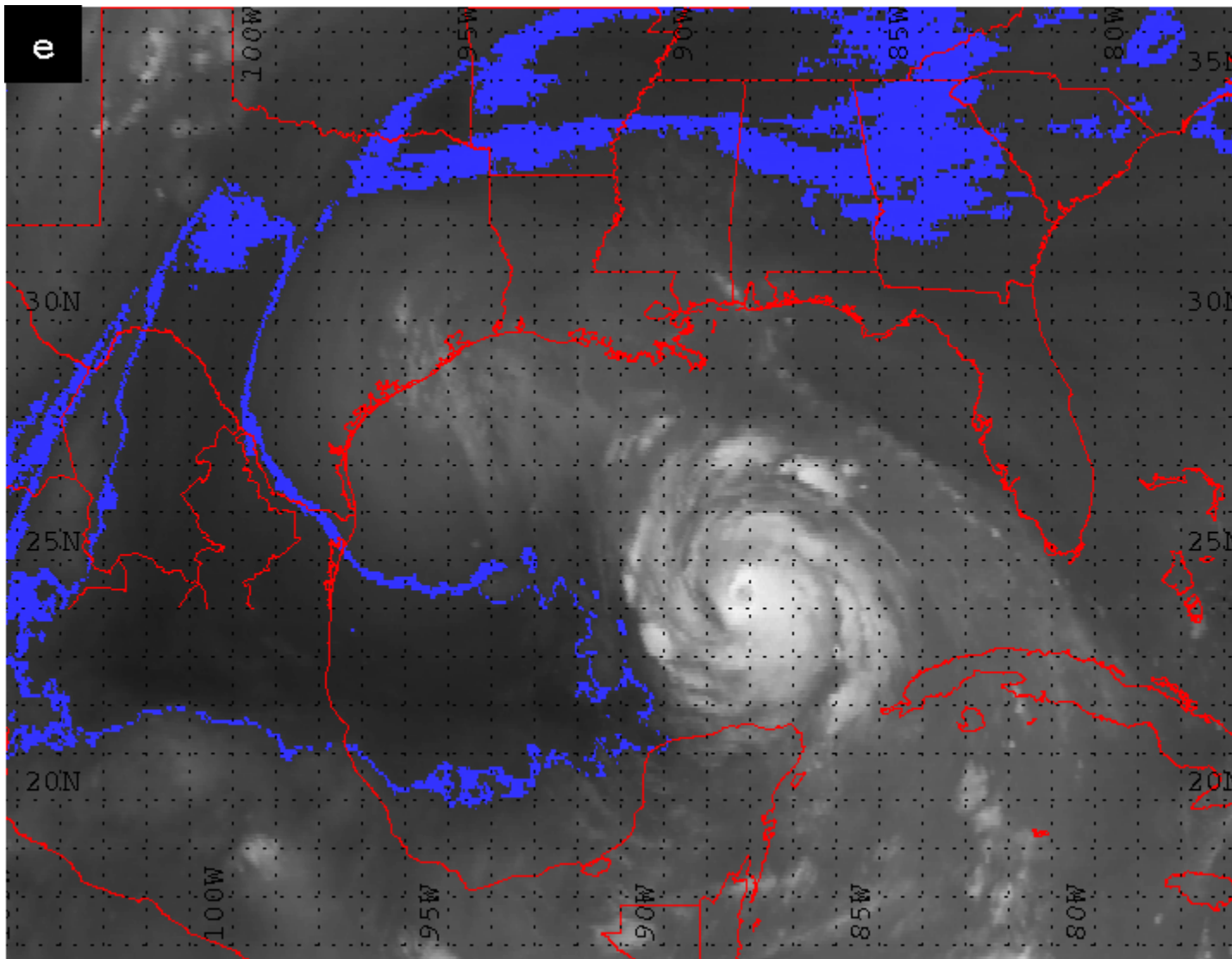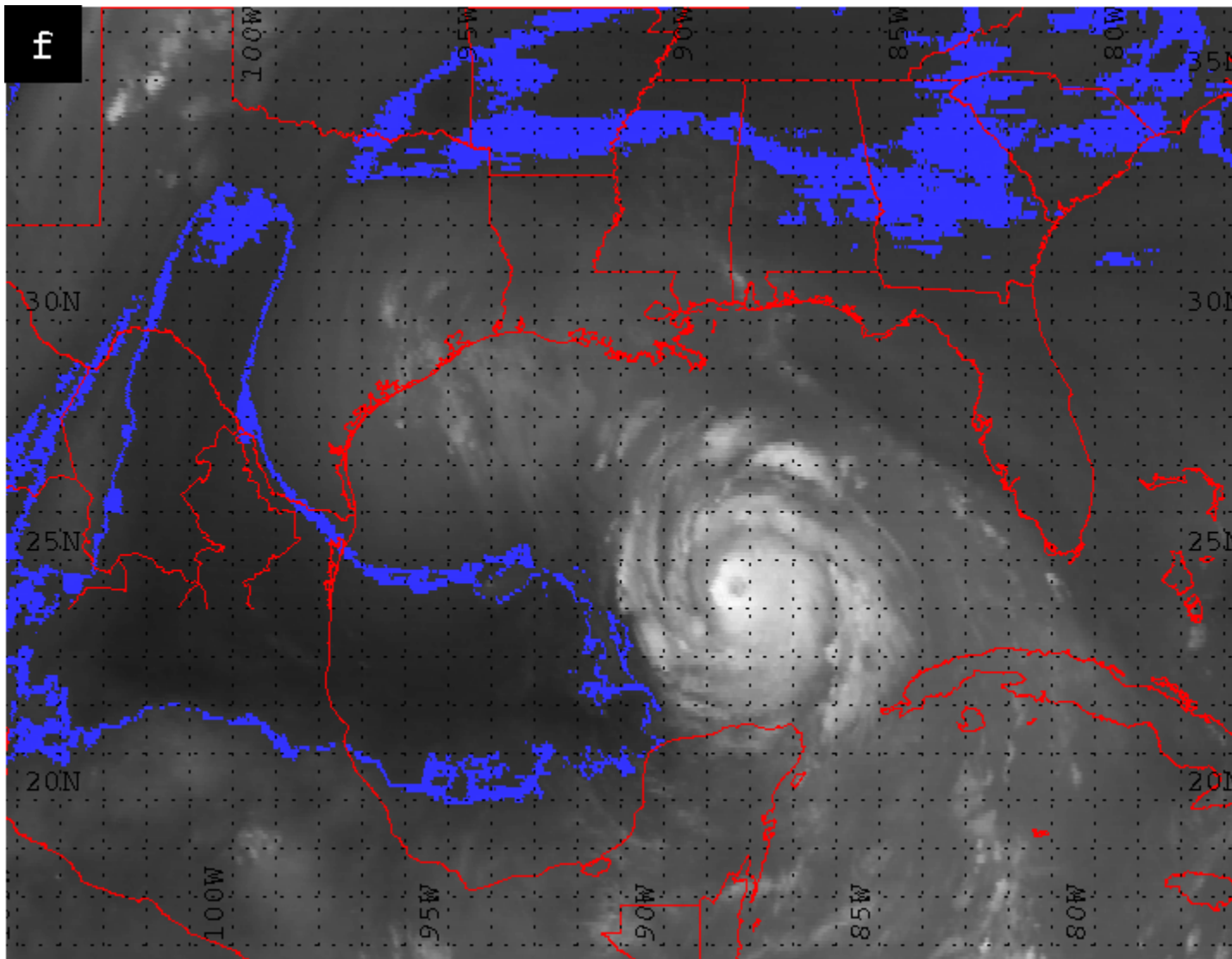
(ERC) occur in major hurricanes when a small concentric eye and radius of maximum winds are overtaken by surrounding outer eyewall of formed rainbands. During the cycle, intensity may weaken, but is often equal to, or greater, once the outer eyewall replaces the inner eyewall. Convective bands expanded farther outward on each side of Lili while this ERC was occurring. This provided visual corroboration that during an ERC intensity of the entire storm and strength of the inner core are out of phase (Croxford and Barnes 2002). After the ERC in the 1145 UTC 2 October 2002 image (Figure 20f), the core convection became more symmetrical about the eye though slightly elongated on the north-south axis. The main cyclonic circulation and the outflow pattern converged producing a more widespread storm overall (Figure 20f). Diameter measurements were approximately 438 km at 0646 UTC 2 October 2002 and 644 km at 1145 UTC 2 October 2002 across the width of Lili's circulation.

3) Rapid Intensification 1200 – 1800 UTC 2 October 2002

For this NHC best track time period, Lili's pressure was observed at 954 hPa (category 3 status) and dropped to 941 hPa (category 4 status). This pressure drop of 13 hPa over 6 h classified as Lili's second RI phase in 18 h. This time frame contained 20 images.

The individual image distances and the directions between the -24 °C vapor front oscillated again during this RI period (Figure 12). The mean distance was 260 km, covering a minimum of 213 km and a maximum of 280 km. The mean distance decreased by 79 km from the previous steady state phase. The range decreased to 67 km from 143 km. This was a result of the maximum distance declining by 129 km from the previous steady phase. The distances from the outer edge of Lili's convective bands to the nearest -24 °C point averaged 17 km (Figure 12) and the range also decreased to 47 km, covering a zero distance to a maximum of 47 km. This mean distance was the closest the vapor front and Lili's center had been to date. For

this particular period as of 1532 UTC 2 October 2002 (Figure 21e), the outer convective bands of

Lili and -24 °C line boundary were directly in contact. The mean distances from the outer band

had 2.25 h of zero values included in the calculation (Figure 12). If these distances from 1532 -

1745 UTC 2 October 2002 are removed, the mean distance increased to 30 km from Lili's

outermost band to the -24 °C vapor front.

The -24 °C vapor front started with a large area separate from the lobe of dry air at 23.5

°N and 91°W (Figure 21a). The vapor front exhibited a more broken nature beginning at 1315

UTC 2 October 2002 (Figure 21b). At 1402 UTC 2 October 2002 (Figure 21c), it took on a

more linear signature on a northwest-southeast axis, in contrast to other images where the broken

signature seemed to be actual protrusions or sections of interaction. The separated portions of

dry air returned around 1515 UTC 2 October 2002 (Figure 21d). The 1702 UTC 2 October 2002

image (Figure 21g) displayed the most broken signature. A less defined area of the -24 °C vapor

front was located on the southeast section of the dry air lobe around 22 °N and 91° W. This

broken area of the vapor front corresponded to the southwest side of Lili's circulation where

lower water vapor temperatures, lower infrared temperatures, and less structured visible satellite

imagery for that quadrant over the whole time period signified weaker convective development.

The entire offshore lobe of dry air grew significantly northward throughout this period.

The northern boundary began along 25 °N latitude (Figure 21a) and by the 1745 UTC 2 October

2002 image was along the 27 °N (Figure 21h). Table 9 provided confirmation that the dry air

lobe did indeed extend more northward and had the largest increase in areal extent for the entire

time series. The dry air lobe statistics in Table 8 showed that while growing along the axis of the

hurricane track, the dry air mass water vapor temperature was also steadily warming and thus

reinforcing the stableness.

Figure 21a. GOES-8 water vapor image during the second RI phase on 1215 UTC 2 October 2002 with the -24 °C vapor front (blue) highlighted.

Figure 21b. GOES-8 water vapor image during the second RI phase on 1315 UTC 2 October 2002 with the -24 °C vapor front (blue) highlighted.

Figure 21c. GOES-8 water vapor image during the second RI phase on 1402 UTC 2 October 2002 with the -24 °C vapor front (blue) highlighted.

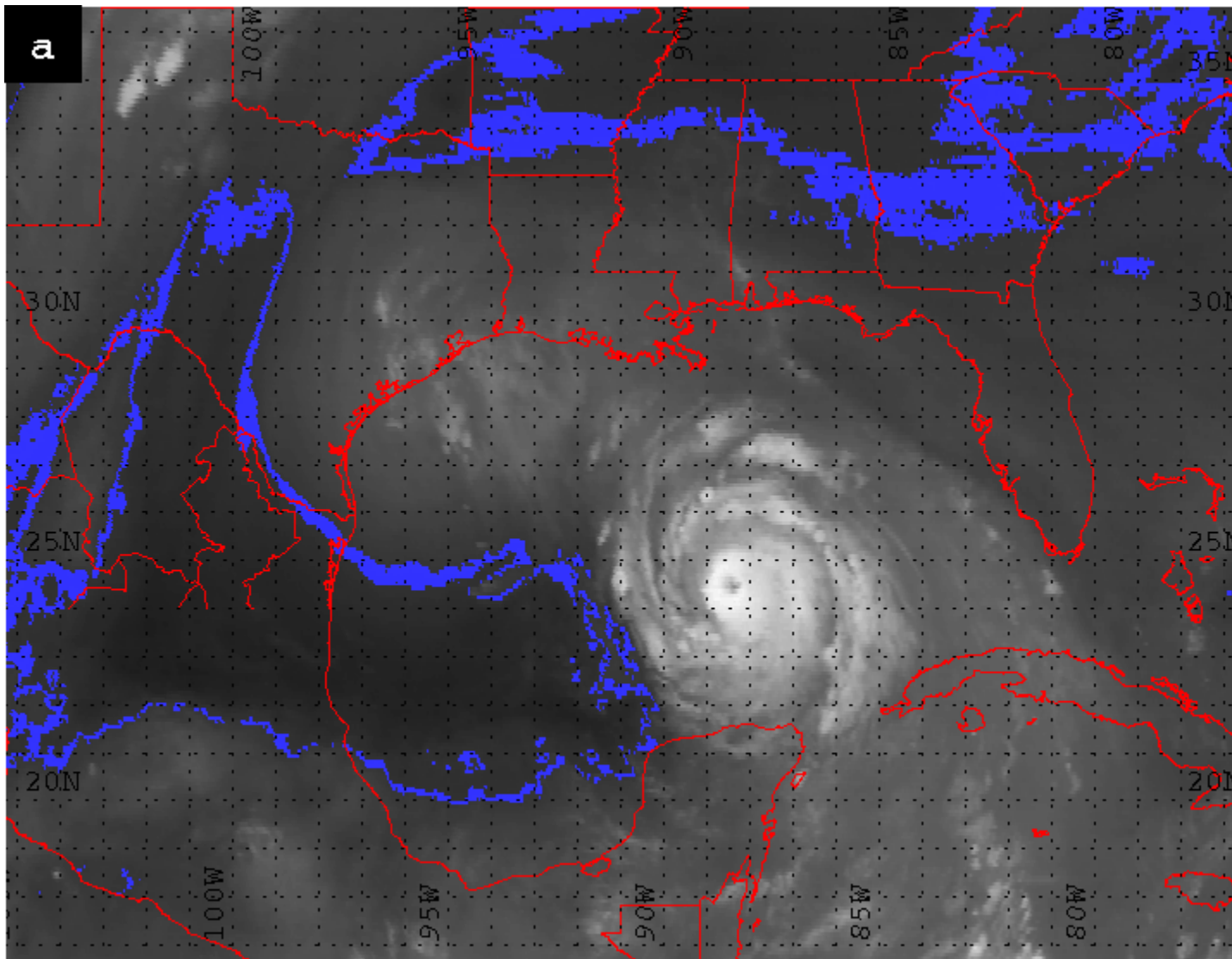Figure 21d. GOES-8 water vapor image during the second RI phase on 1515 UTC 2 October 2002 with the -24 °C vapor front (blue) highlighted.
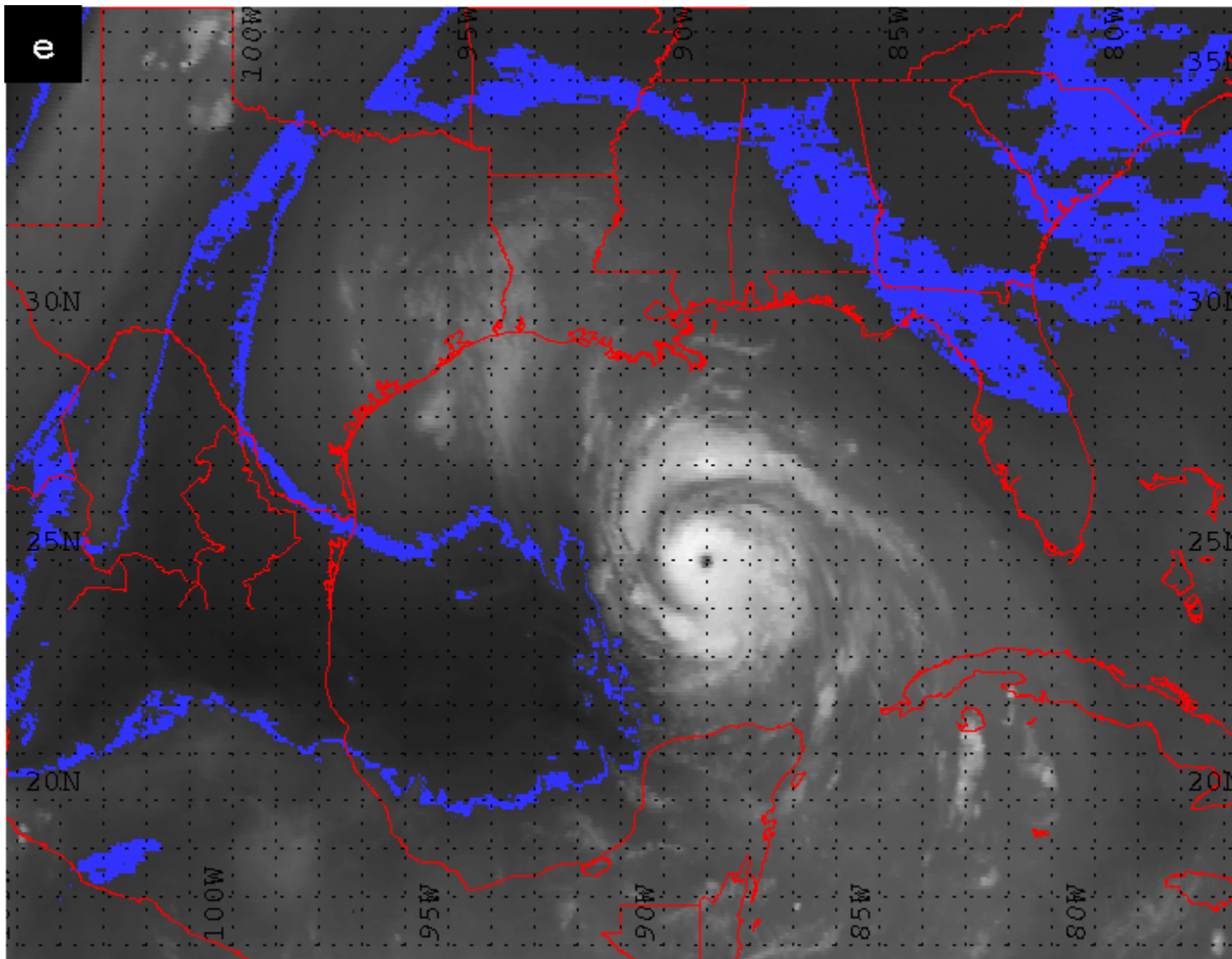
Figure 21e. GOES-8 water vapor image during the second RI phase on 1532 UTC 2 October 2002 with the -24 °C vapor front (blue) highlighted.
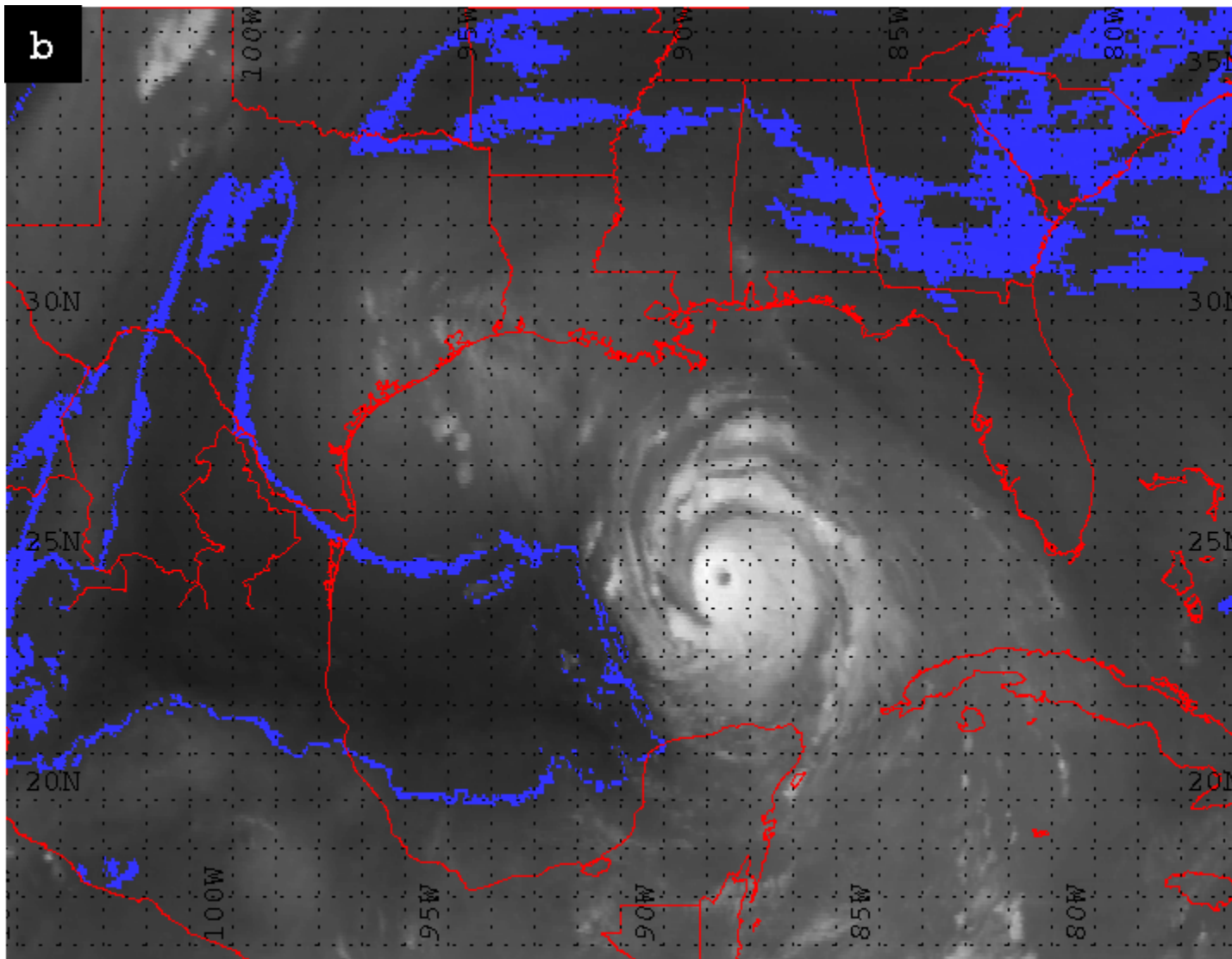
Figure 21f. GOES-8 water vapor image during the second RI phase on 1645 UTC 2 October 2002 with the -24 °C vapor front (blue) highlighted.
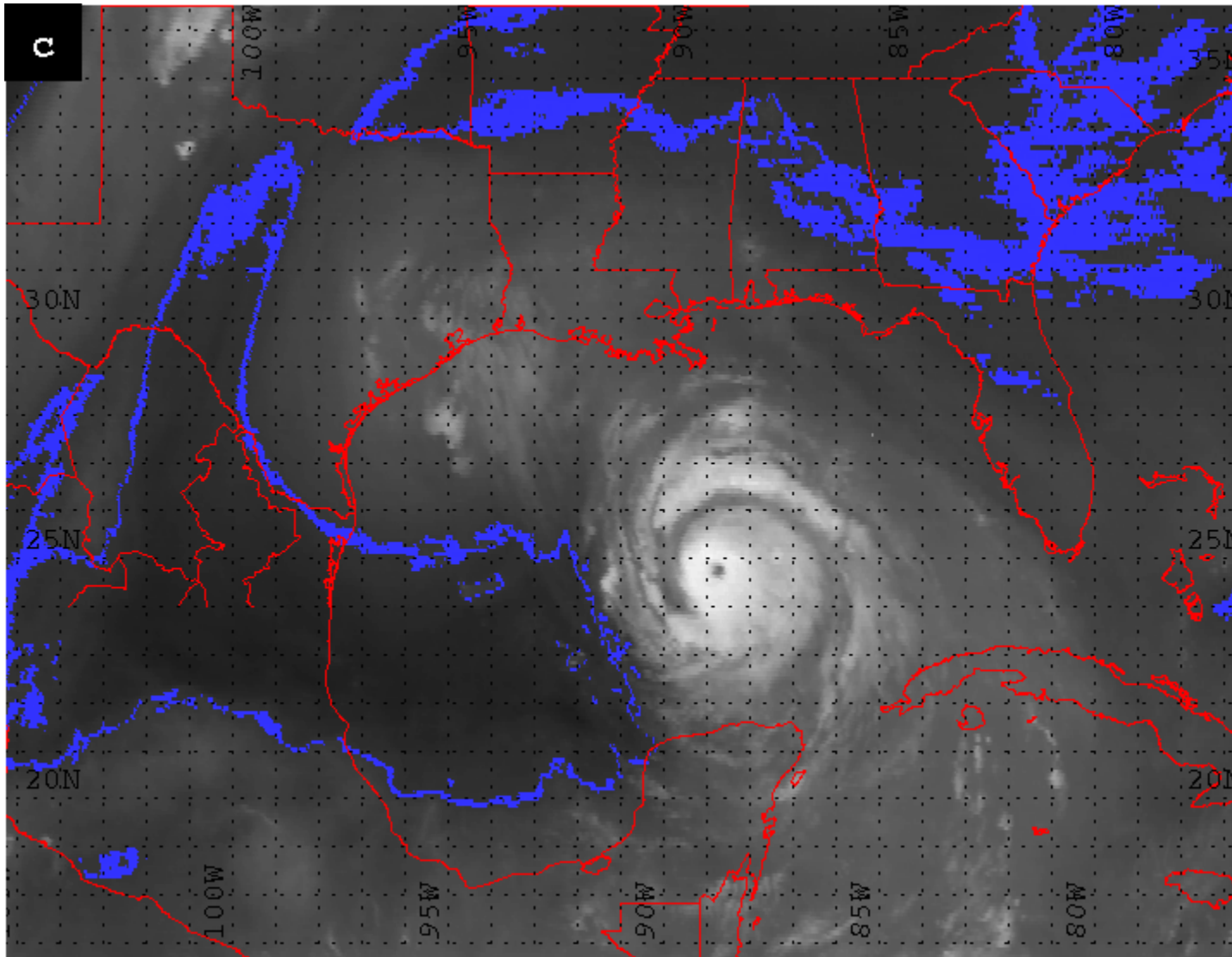
Figure 21g. GOES-8 water vapor image during the second RI phase on 1702 UTC 2 October 2002 with the -24 °C vapor front (blue) highlighted.
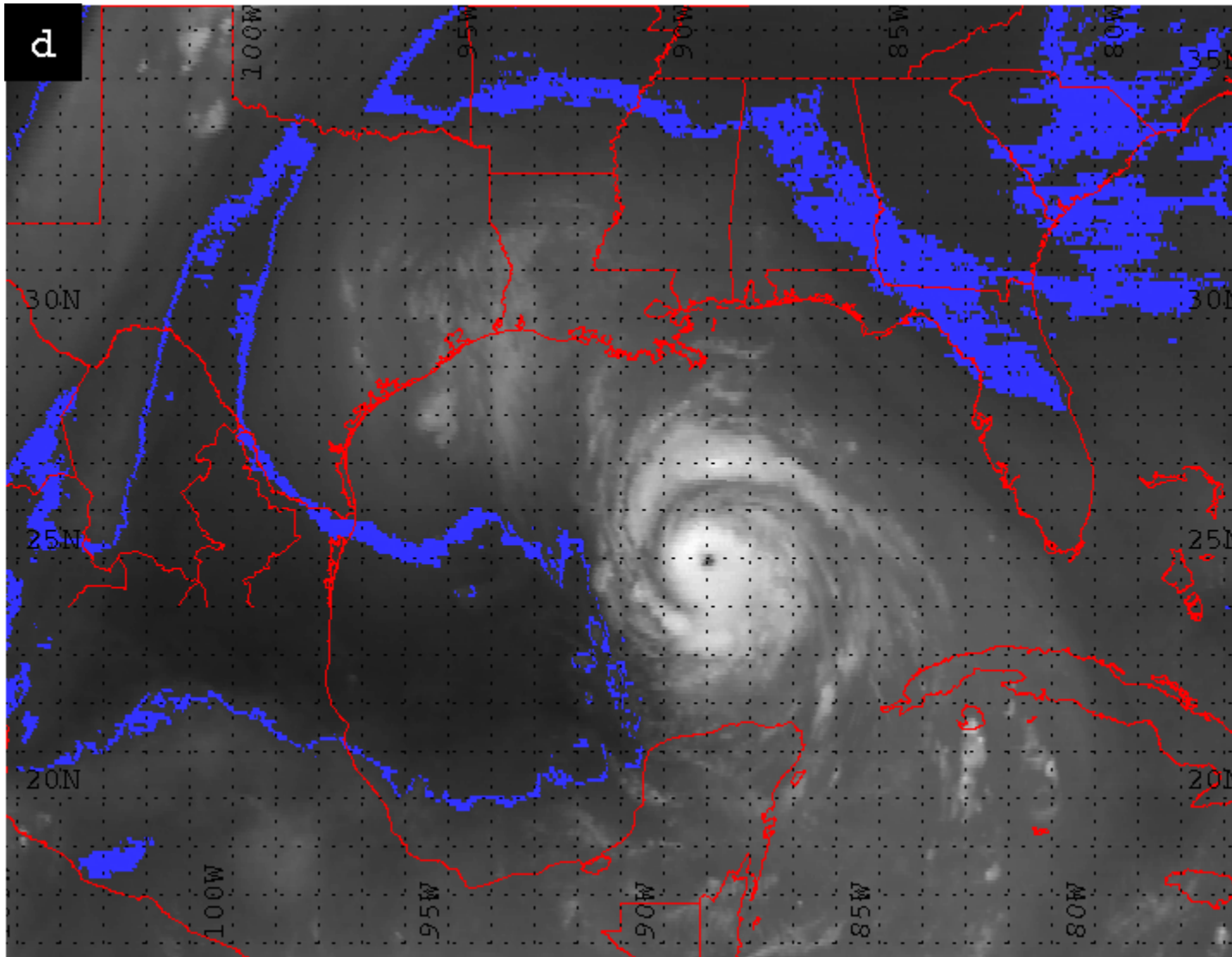
Figure 21h. GOES-8 water vapor image during the second RI phase on 1745 UTC 2 October 2002 with the -24 °C vapor front (blue) highlighted.
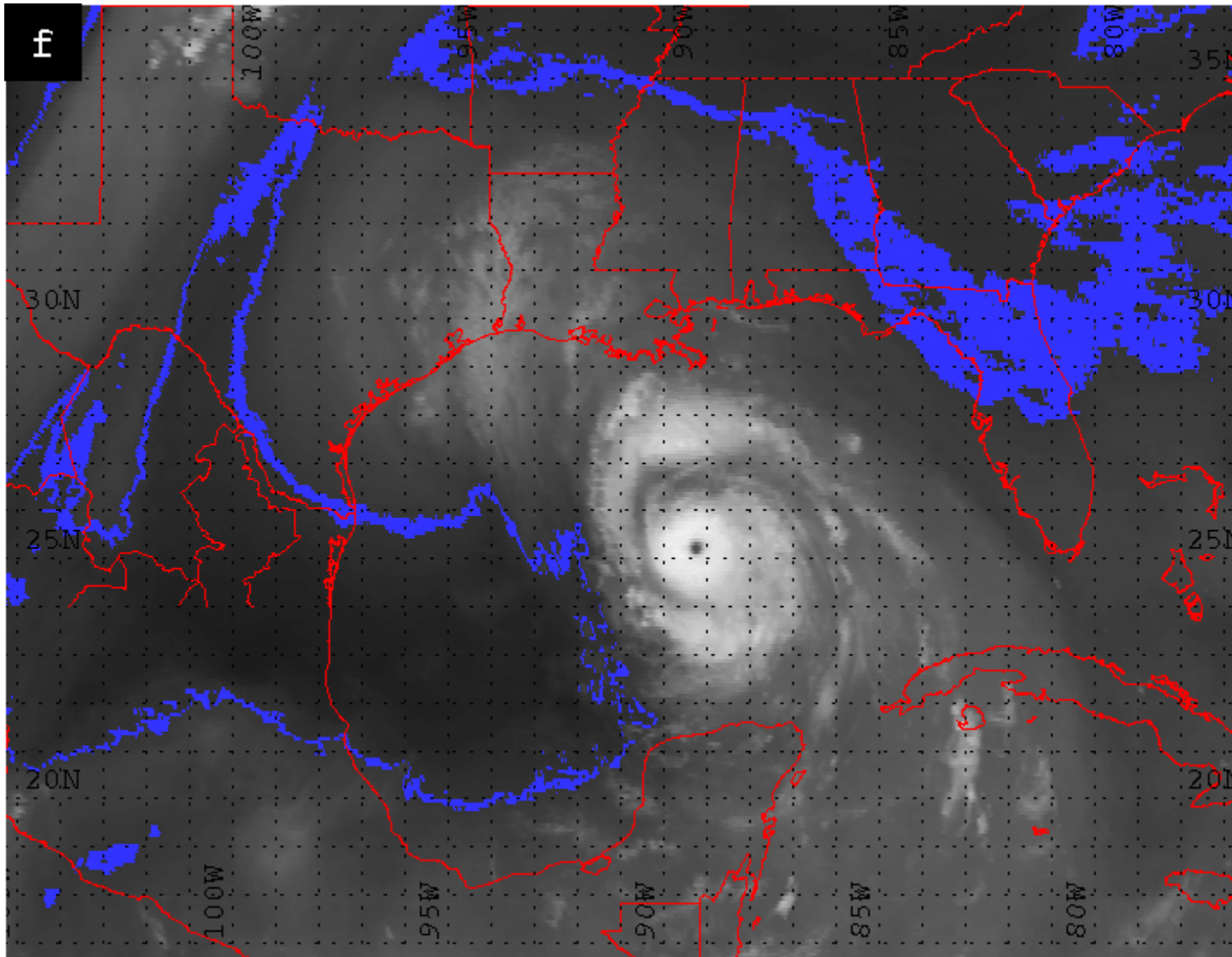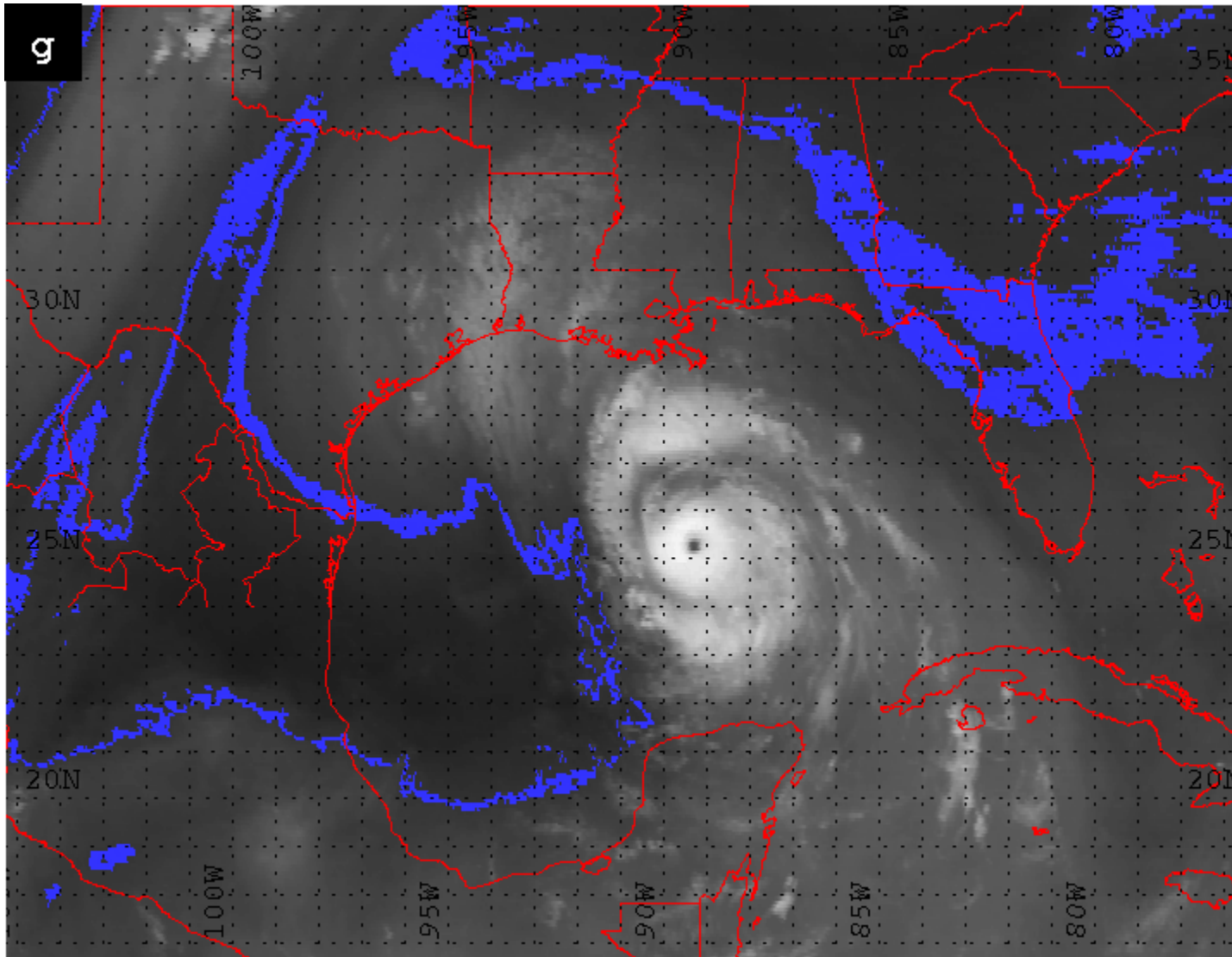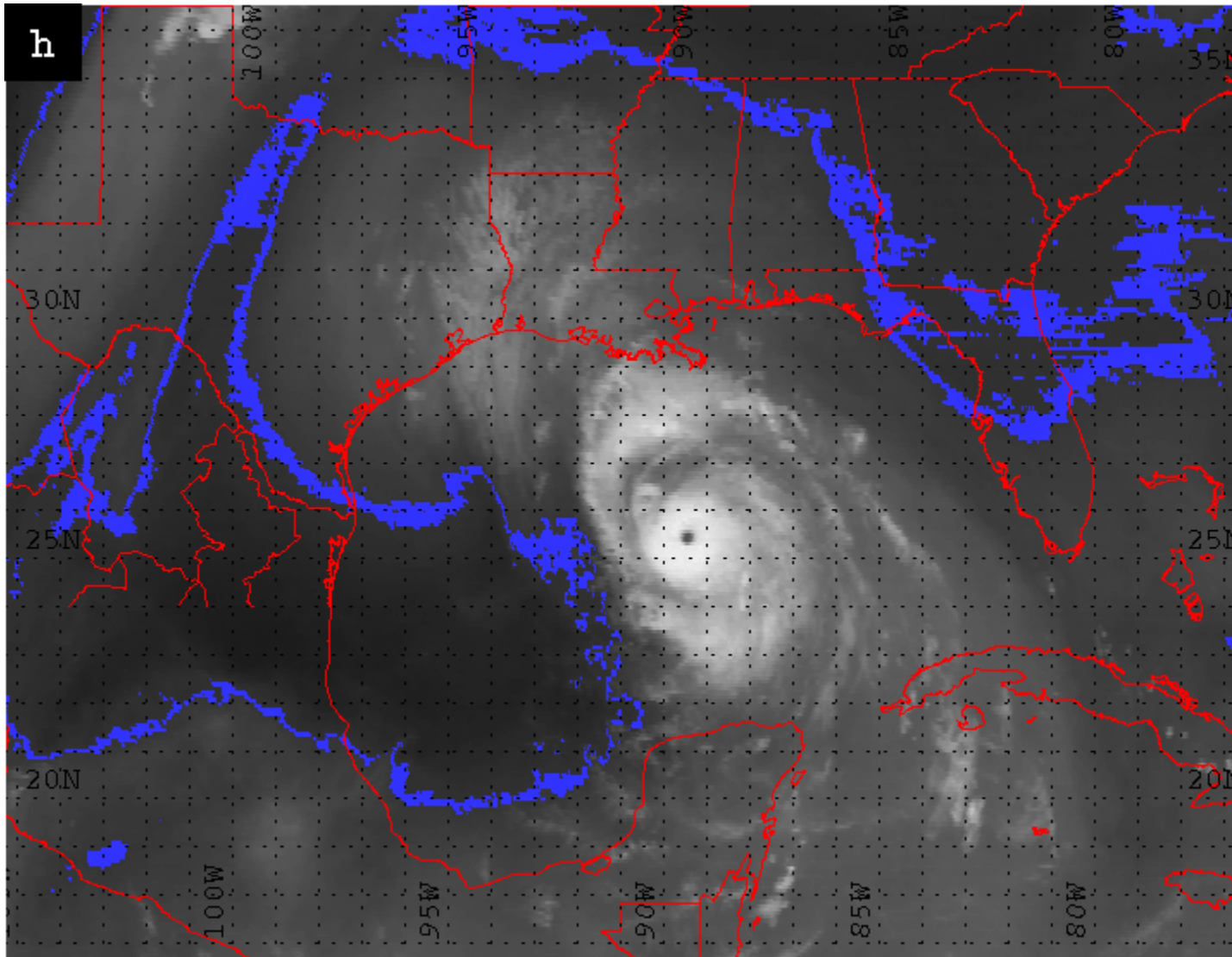
Visually, Lili became more elongated rather than symmetrical beginning at 1645 UTC 2 October 2002 (Figure 21f) as the southwest side of the storm lost its convection. However, during this time, Lili's eye remained tightly compact and symmetrically consistent. The main area of convection surrounding the eye exhibited a more elongated signature as well. Croxford and Barnes (2002) believe that the inner and outer core portions of tropical cyclone circulation are controlled by different physical mechanisms. The changes started due east of Lili's center, then extended far south from the center. Around 1645 UTC 2 October 2002 (Figure 21f), this southerly elongation separated from the area around the eye because of drier air entrainment, although less stable than the -24 °C threshold at approximately -30 °C. After this separation, the main circulation recovered and was more symmetrical about the eye through to the end of the time period. Outflow circulation was less pronounced until after 1102 UTC 2 October 2002 when it developed well on the east and southeast sides (Figure 21e-f).

4) 1 hPa Drop 1800 UTC 2 October 2002 through 0000 UTC 3 October 2002

For this NHC best track time period, Lili's pressure at 1800 UTC 2 October 2002 was 941 hPa and dropped only 1 hPa to 940 by 0000 UTC 3 October 2002 which kept Lili at a category 4 status. This time period contained the most images with 37.

The mean distance between the -24 °C vapor front and the center of Lili continued a decreasing trend. Distance averaged 238 km, from a low of 215 km to a peak of 256 km spanning a range of 41 km. The dry air vapor front and Lili's center were the closest yet both in mean distance and maximum distance (Table 10). The individual image distances increased slightly (Figure 12) though the mean distance decrease was due to a tightening of the range between minimum and maximum (Table 10). This increase in the individual image distances resulted from a portion of the vapor front which had separated, was closer, and then dissipated.

Additionally, the vapor front oriented toward a more north-northwest to south-southeast line (Figure 22a-b). This orientation change was seen in the directions decreasing (Figure 12) which showed that the vapor front nearest point migrated toward a more southwesterly trend overall. The distance from the outer edge of Lili's convective bands to the nearest -24 °C point increased to a mean of 65 km, a minimum of 43 km, and a maximum of 95 km (Table 11). This can be attributed to a convective band dissipating during the final 2 h of the last time period and so the next feeder band was utilized. Lili's outer convection and the vapor front grew apart considerably due to the vapor front taking on a more angled orientation (Figure 22a-f). This brought the vapor front closer the southwestern quadrant of Lili rather than the western or west-southwestern section of the storm.

The vapor front still exhibited a broken signature at 1815 UTC 2 October 2002 (Figure 22a). The vapor front resembled more of a line as shape transformations and protrusions diminished (Figure 22b-c). By the 2040 UTC 2 October 2002 image, the -24 °C edge was less broken, had fewer shape transformations, and the width remained fairly consistent (Figure 22c). The vapor front continued to be well defined through the remainder of this time period. It is believed this smoothness and consistent width of -24 °C vapor front illustrated Lili's outer circulation was influenced by the dry air, although the main circulation was able to slightly intensify by 1 hPa. This again demonstrated the probability of different mechanisms driving separate areas of circulation (Croxford and Barnes 2002).

The entire dry air mass lobe continued its growth northward by 1 °N latitude (Table 9). It exhibited a more rounded shape (Figure 22f) as a result of northward extension by 143 km and reduction in width by 25 km. There was some areal variation throughout the time frame, although the overall trend was growth (Table 8). Hourly statistics within this lobe again

Figure 22a. GOES -8 water vapor image during the 1 hPa drop phase on 1815 UTC 2 October 2002 with the -24 °C vapor front (blue) highlighted.

Figure 22b. GOES-8 water vapor image during the 1 hPa drop phase on 1915 UTC 2 October 2002 with the -24 °C vapor front (blue) highlighted.
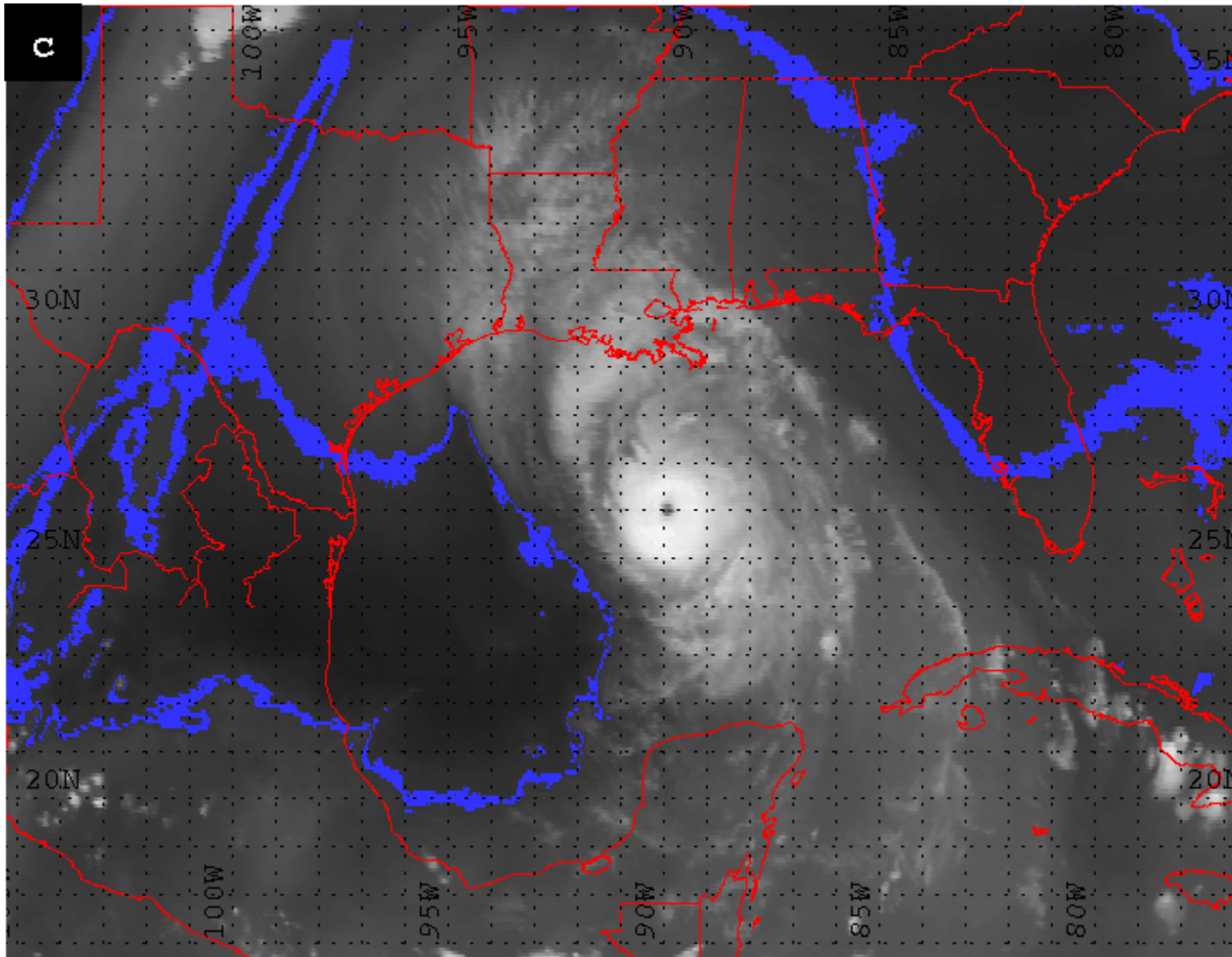
Figure 22c. GOES-8 water vapor image during the 1 hPa drop phase on 2040 UTC 2 October 2002 with the -24 °C vapor front (blue) highlighted.

Figure 22d. GOES-8 water vapor image during the 1 hPa drop phase on 2115 UTC 2 October 2002 with the -24 °C vapor front (blue) highlighted.
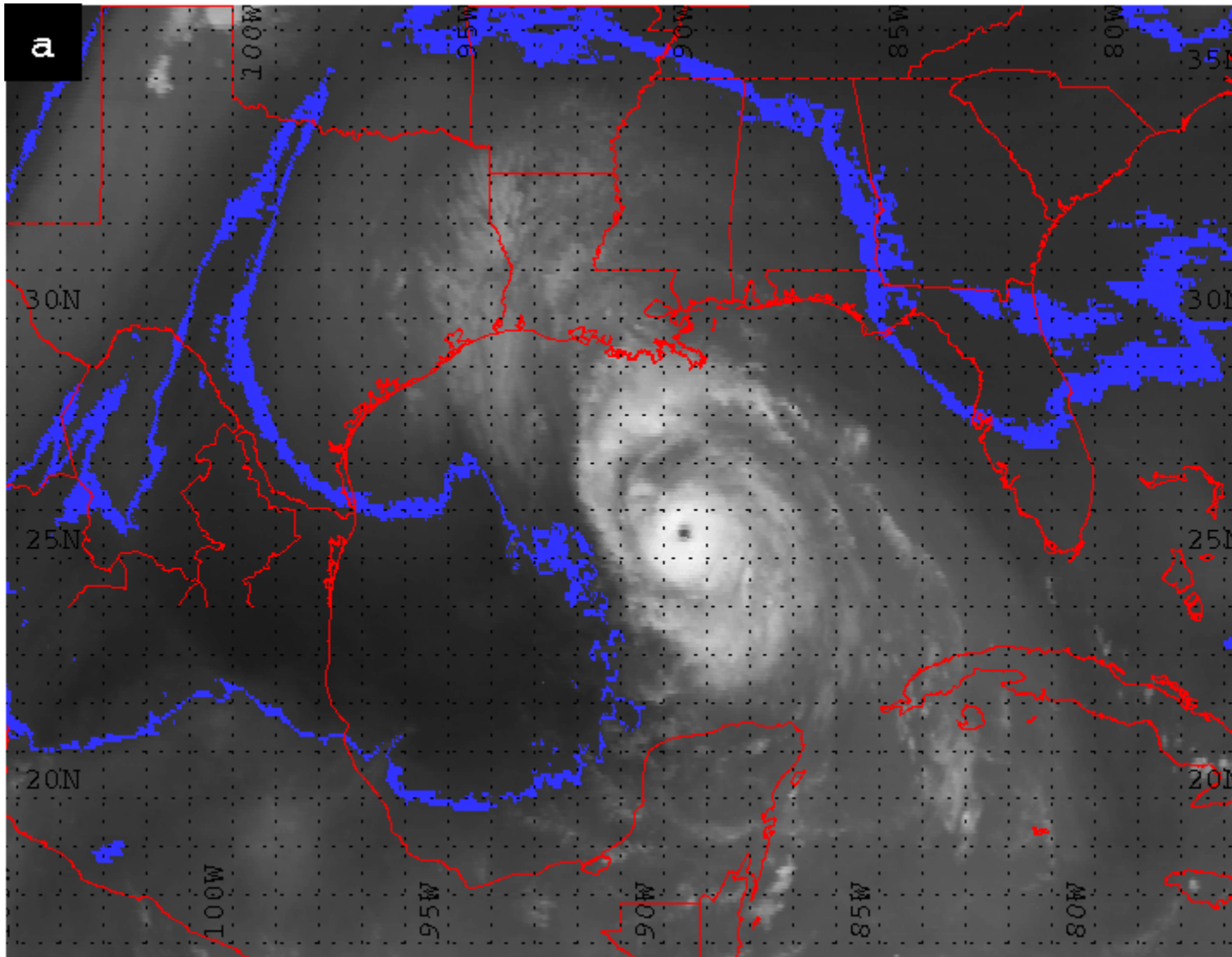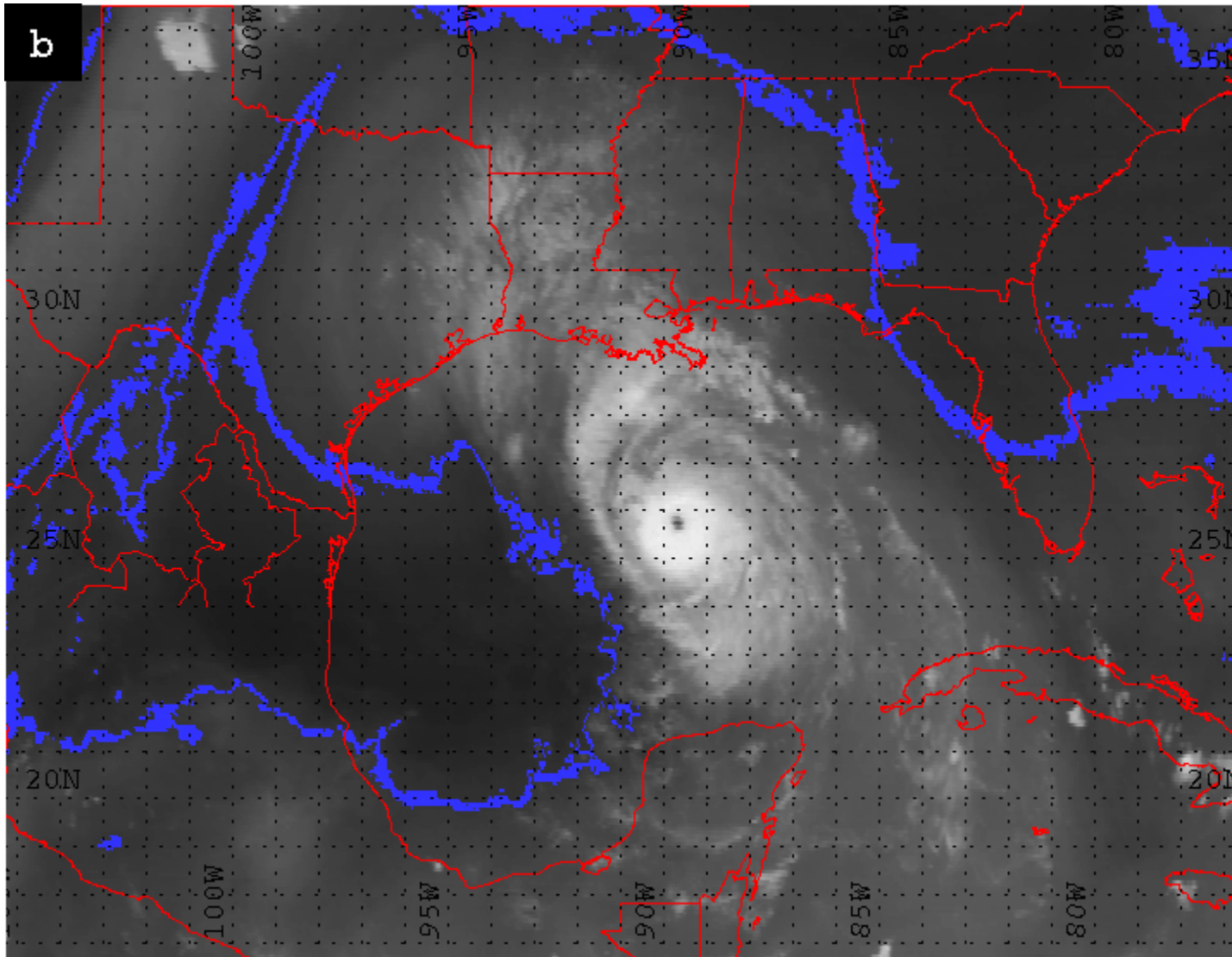
Figure 22e. GOES-8 water vapor image during the 1 hPa drop phase on 2230 UTC 2 October 2002 with the -24 °C vapor front (blue) highlighted.
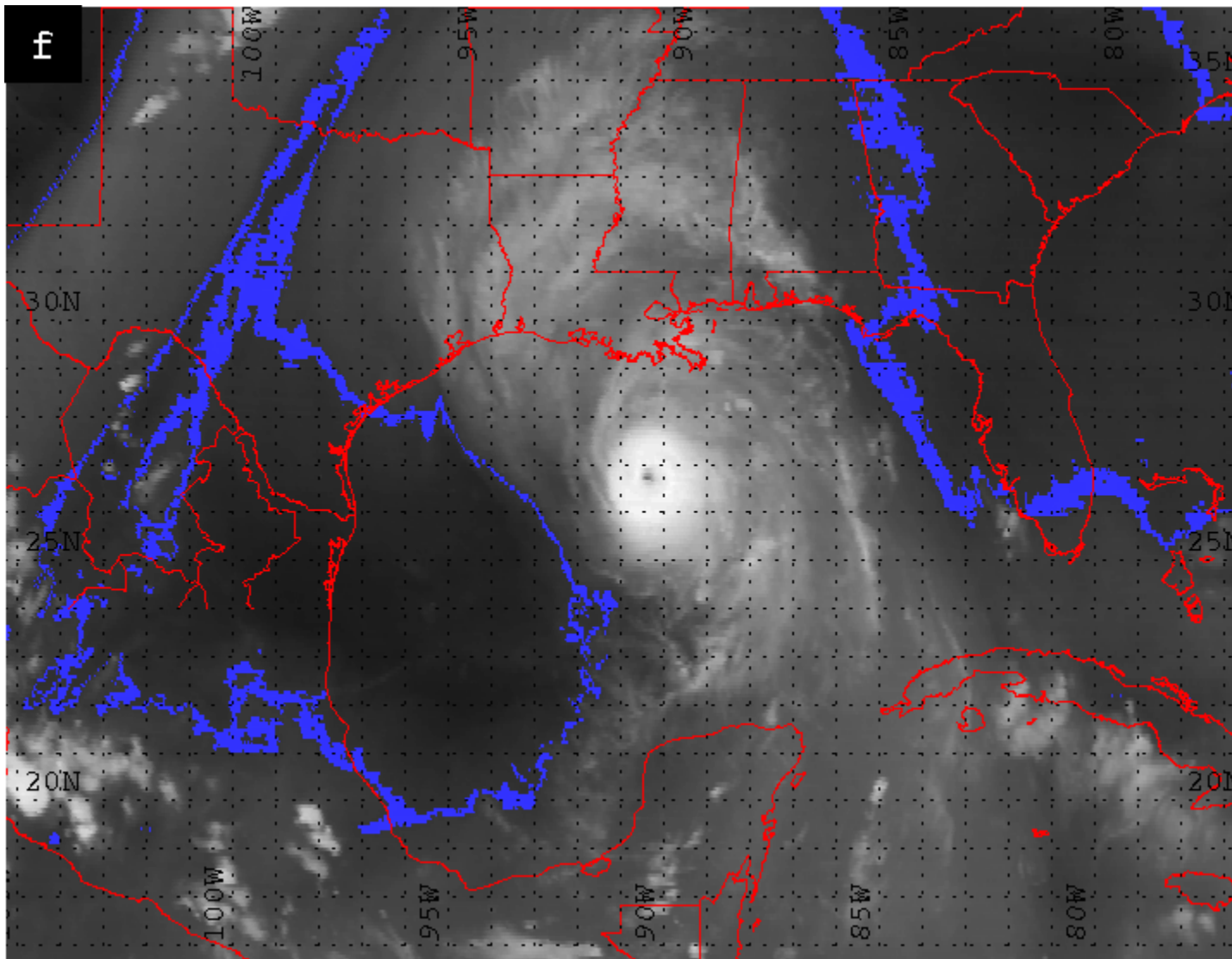
Figure 22f. GOES-8 water vapor image during the 1 hPa drop phase on 2345 UTC 2 October 2002 with the -24 °C vapor front (blue) highlighted.

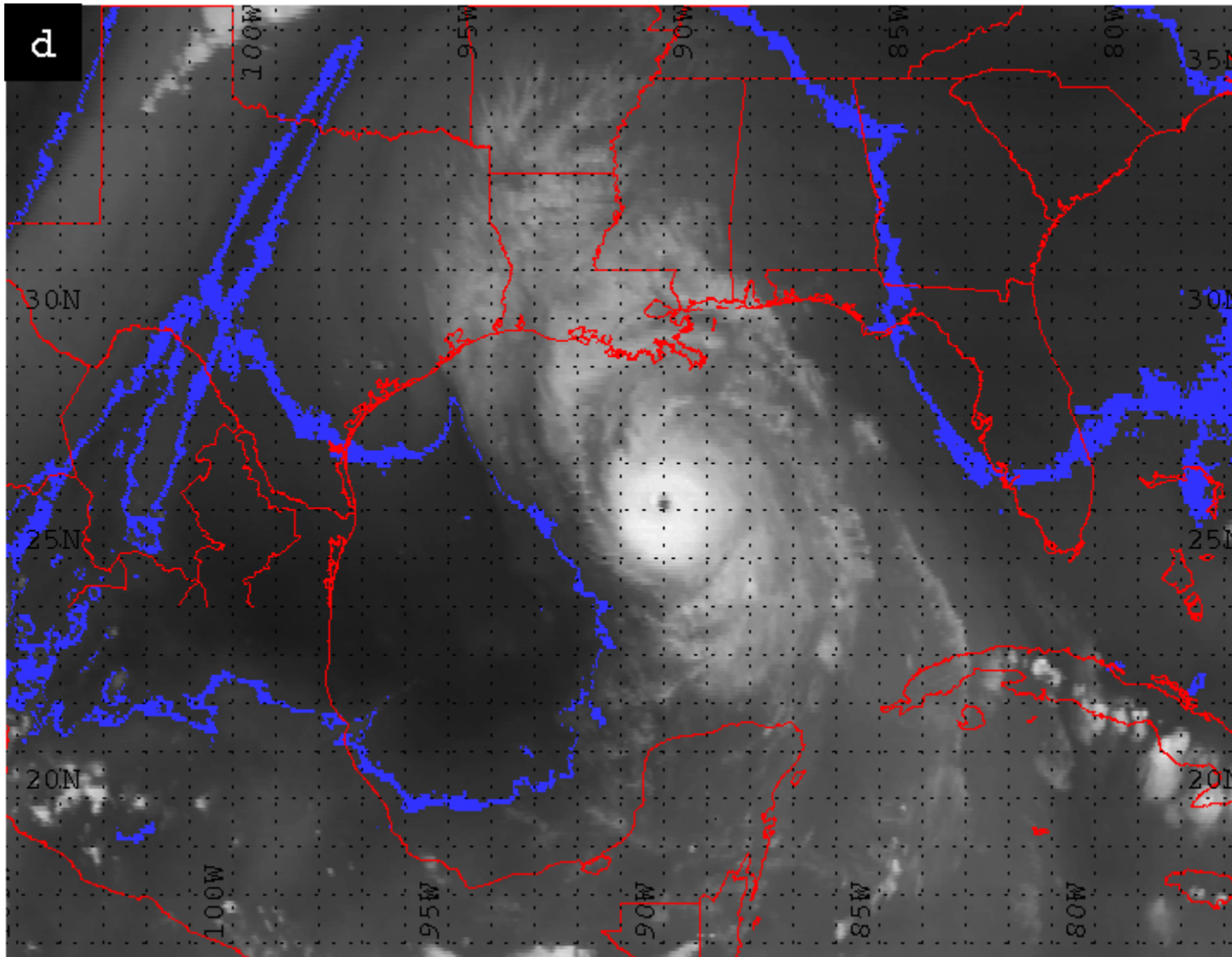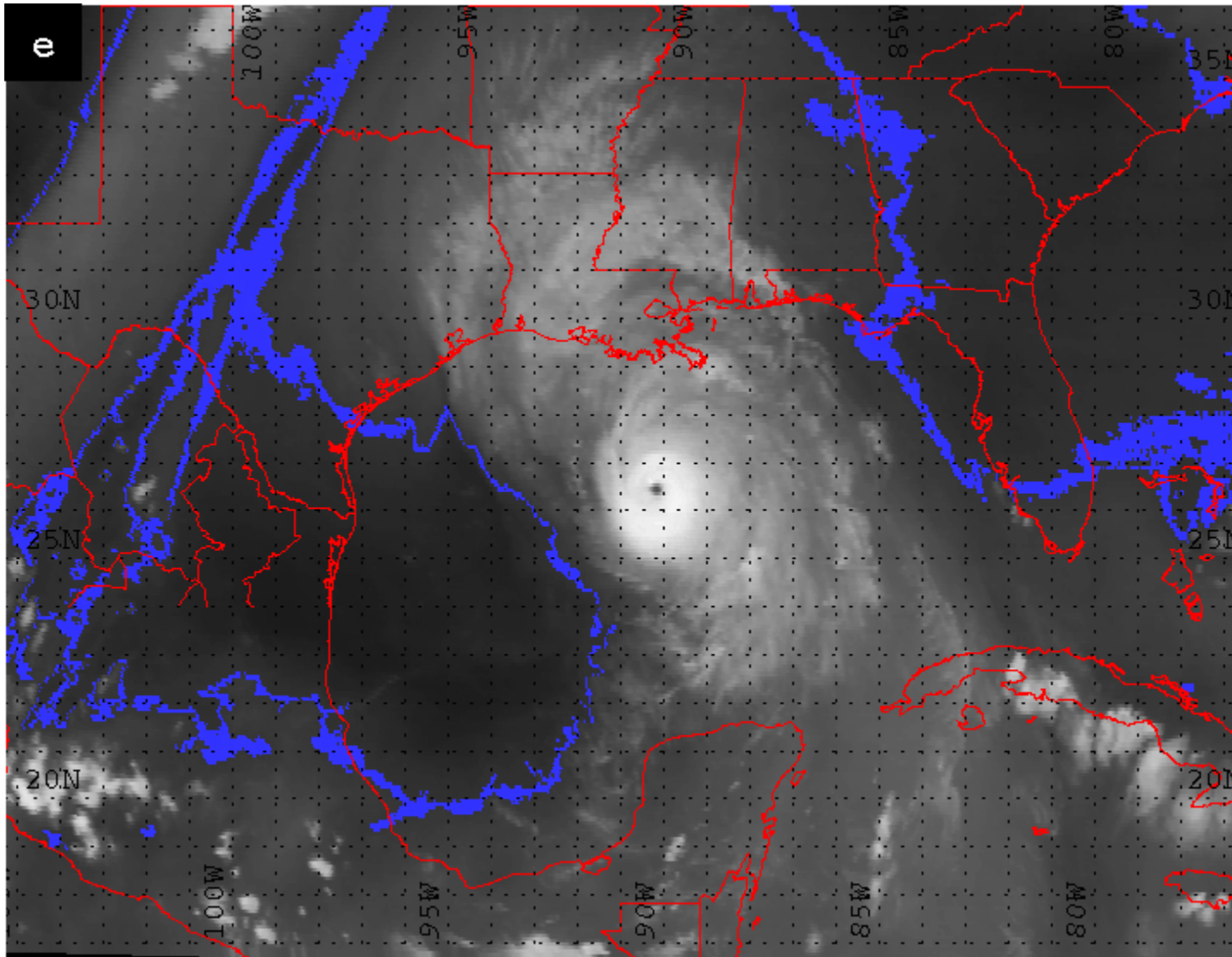indicated that the mass grew drier by +0.1 °C in the maximum and mean water vapor temperatures.

Less defined feeder bands converged with the vapor front at 27 °N and 91 °W on the northwest side of Lili (Figure 22c). This interaction was approximately 425 km away from the center, however it seemed to essentially affect the symmetrical balance of the outer convection. The thunderstorms diminished and thus were not available to formulate well-defined bands in the circulation. The main convection about the center of Lili was more broken and variable over the entire time period than before. Croxford and Barnes (2002) found intensity responds more readily to the collapse of convection in the eyewall, and so the inner core could have still been strengthening although the outer circulation was affected by dry air. Also the more broken nature of the convection about the center could signify an onset of weakening. By the 1815 UTC 2 October 2002 image, Lili's entire circulation pattern elongated. Stretching along the north-south axis continued through the end of this time period (Figure 22a; 22f), and convection weakened as a result of this spreading. This was illustrated by the darker shades of gray in the last water vapor image (Figure 22f) and warming of the cloud-top temperatures outside of the circulation about the center (Figure 23). The anti-cyclonic outflow pattern appeared healthy only in the northeast (30 °N and 89 °W) and southeast (23 °N and 88 °W) quadrants of the storm. The uneven distribution of circulation and marked decrease in convective strength indicated significant breakdown of the cyclonic system before the rapid pressure drop. Abraham et al. (2004) showed that Hurricane Michael had a low level stable area which they collocated to dry air wrapping around the storm in water vapor imagery. They suggested future research could find a decoupling of the main tropospheric tropical cyclone circulation from the boundary layer. For Lili, the dry air entrainment began towards the end of the second RI phase (1645 UTC 2

86
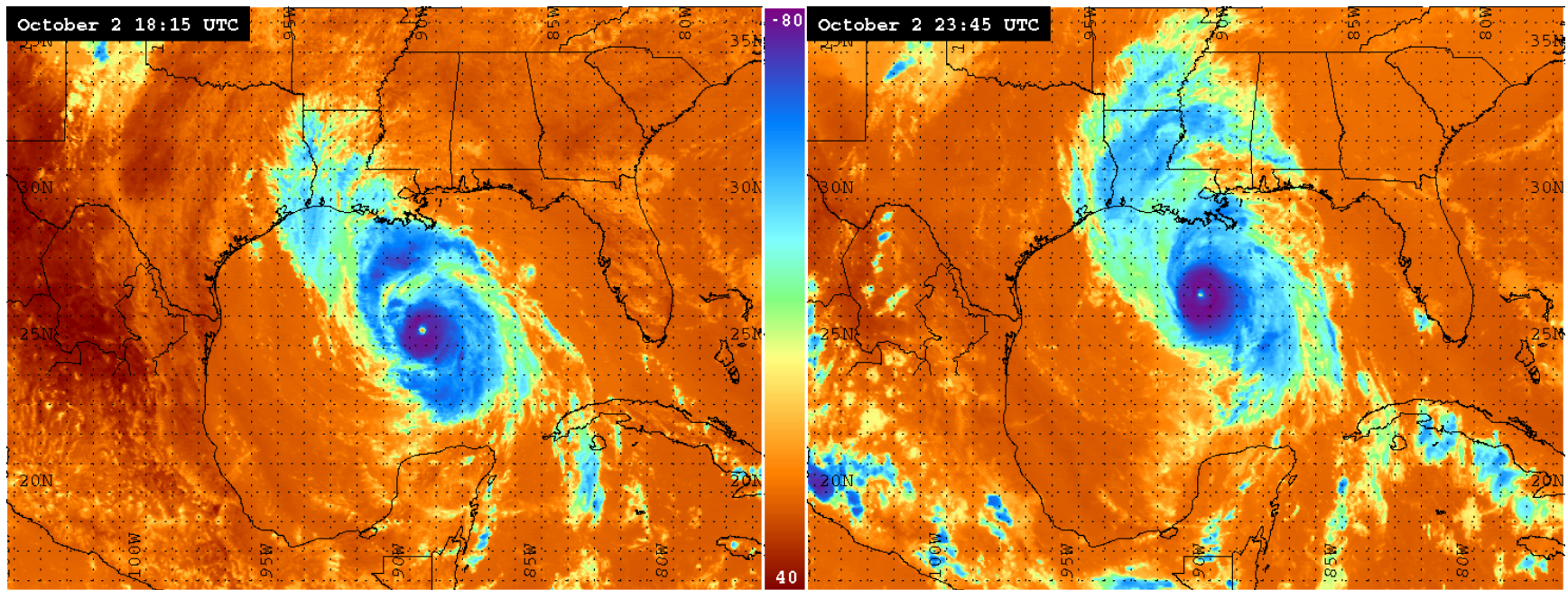
Figure 23. GOES-8 channel 4 infrared temperature images during the 1 hPa drop phase at (a) 1815 UTC 2 October 2002 and (b) 2345 UTC 2 October 2002.

October 2002). Possibly for Lili, the tropical depression and maybe the tropical storm force circulation were impacted during this phase while the hurricane level minimum pressure still dropped slightly.

5) Rapid Weakening 0000 -0600 UTC 3 October 2002

For this final intensity stage, Lili's pressure was 940 hPa at category 4 status and rose significantly to 957 hPa making it a category 3. This 17 hPa increase over 6 h can be defined as rapid weakening (RW) since the rate exceeds the process criterion in chapter 2. No imagery between 0345 UTC and 0600 UTC 3 October 2002 were available due to the GOES eclipse outages, so this RW period contained 12 images over 3.5 h.

The distance between the -24 °C vapor front and the determined center of Lili continued a general decreasing trend (Figure 12). Individual distances ranged 54 km with a minimum of 193 km to a maximum of 247 km. The mean distance was 224 km. The dry air vapor front and Lili's center of circulation were the nearest during this phase indicated by the lowest values for the mean, minimum, and maximum distances (Table 10). Directions of measurement for this period varied some but were less erratic than the second RI phase (Figure 12). The outermost feeder bands were not well defined for this time period. Therefore, distances between the outermost convection and the -24 °C vapor front represented Lili's southwest quadrant where bands of convection were more discernable, but only based on 4 images through 0115 UTC 3 October 2002. The distances here decreased slightly over the time period (Figure 12). The mean distance was second lowest yet at 32 km, behind the second RI phase. The minimum was 28 km from the outermost feeder band and the maximum distance was 37 km for a very tight 9 km range. The vapor front and Lili's convection met along the western edge of the hurricane (Figure 24a-d).

The -24 °C vapor front was nearest to both Lili's center and outermost feeder band during this period. The -24 °C vapor front remained a continuous line, fairly wide with only small breaks intermittently (Figure 24a-d). The interaction zone was contained more southward of Lili, depicted by areas breaking off and shape transformations south of 25 °N (Figure 24a). In the 0145 UTC 3 October 2002 image, the vapor front began to overtake Lili's outer convection and moved inward toward the storm at 26 °N and 93 °W (Figure 24b). The vapor front grew stronger at this location gaining in width throughout until the 0332 UTC 3 October 2002 image, last before the eclipse outage.

The dry air mass extended by 0.5° latitude to the north and south over this RW period. The easternmost extent started at 91 °W (Table 9) in the 0015 UTC 3 October 2002 image because of a protrusion at 24 °N (Figure 24a). This easternmost extent retracted at the end once the vapor front reformed into more of a continuous line (Figure 24d). The lobe increased northward by 82 km, but decreased in width by 110 km, as it became more round. The water vapor temperatures in this dry air mass offshore grew warmer still while increasing in area (Table 8). The maximum and mean hourly water vapor temperatures warmed to the lowest for the time series, indicating that the dry air mass was strongest during this RW phase of Lili (Table 8). The water vapor temperatures and infrared temperatures warmed within Lili's entire over this time period (Figure 24; Figure 25). Gray shaded pixels were more numerous over bright white pixels surrounding the entire storm and the eye disappeared in the water vapor temperature and infrared temperature imagery.

Visible imagery were not available since this was during local nighttime. By 0245 UTC 3 October 2002, Lili's eye diminished completely. At that point, Lili was surrounded by significant pockets of drier air interlaced with the feeder bands on the northwest, south, and

Figure 24a. GOES-8 water vapor image during the RW phase on 0015 UTC 3 October 2002 with the -24 °C vapor front (blue) highlighted.
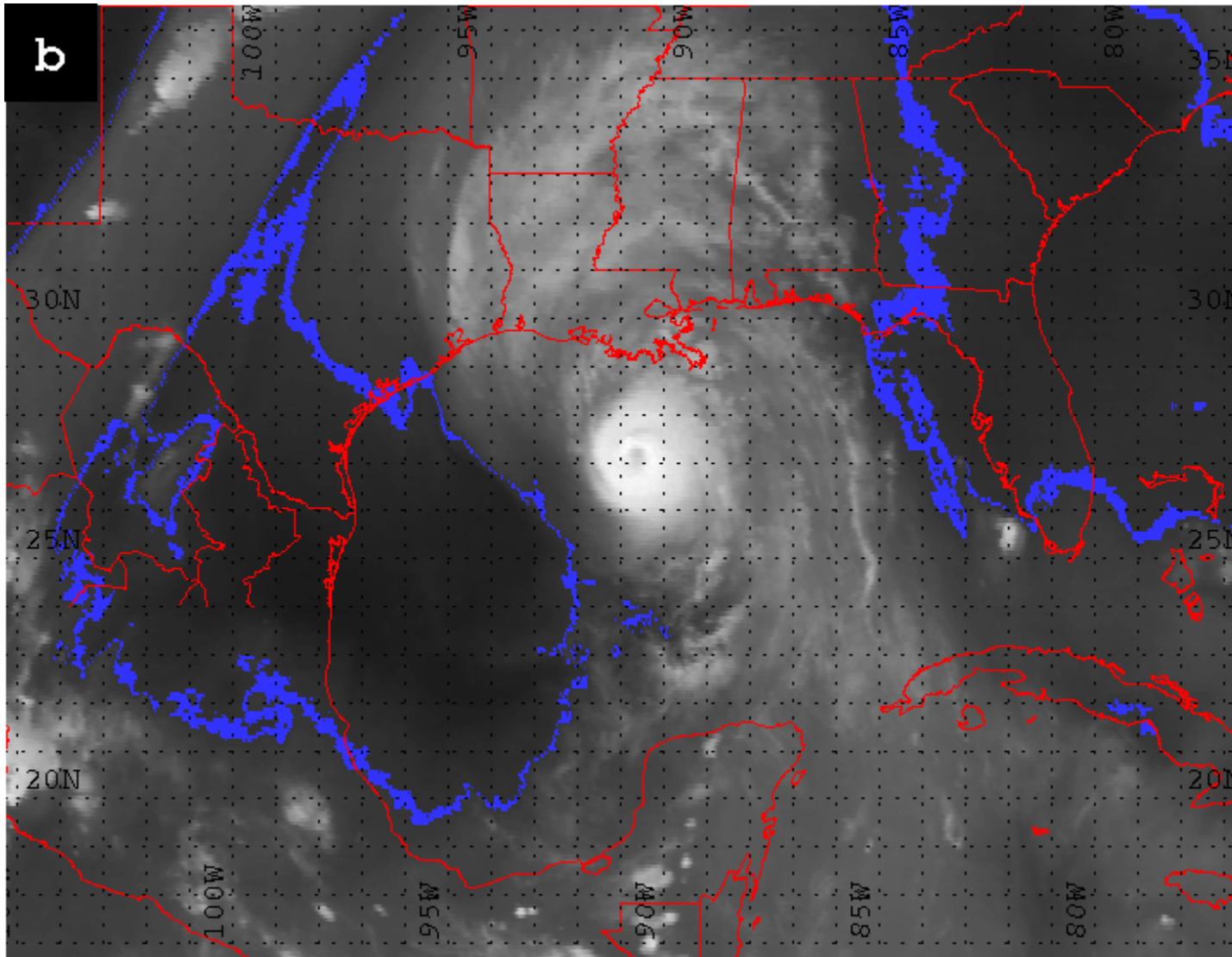
Figure 24b. GOES-8 water vapor image during the RW phase on 0145 UTC 3 October 2002 with the -24 °C vapor front (blue) highlighted.
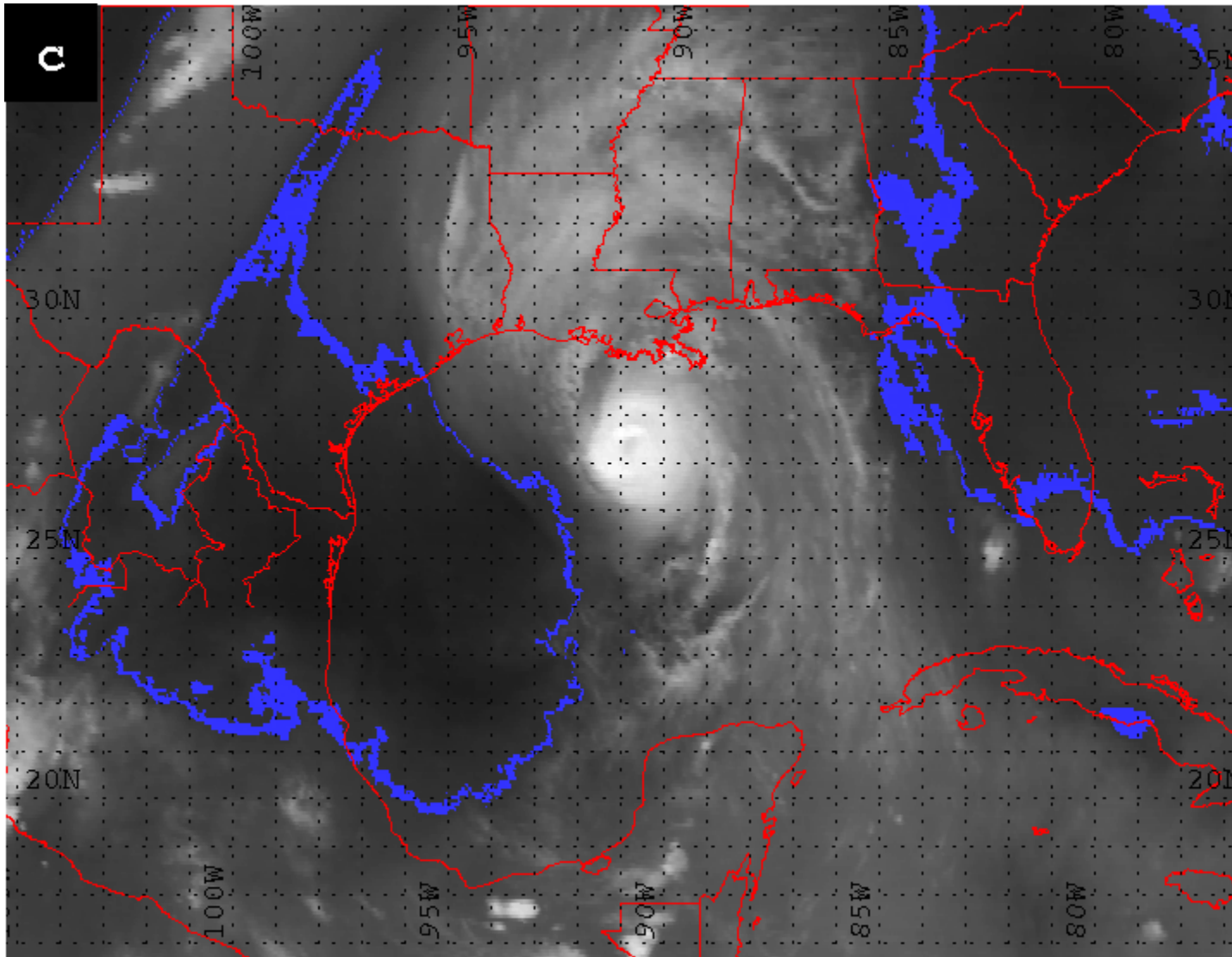
Figure 24c. GOES-8 water vapor image during the RW phase on 0245 UTC 3 October 2002 with the -24 °C vapor front (blue) highlighted.
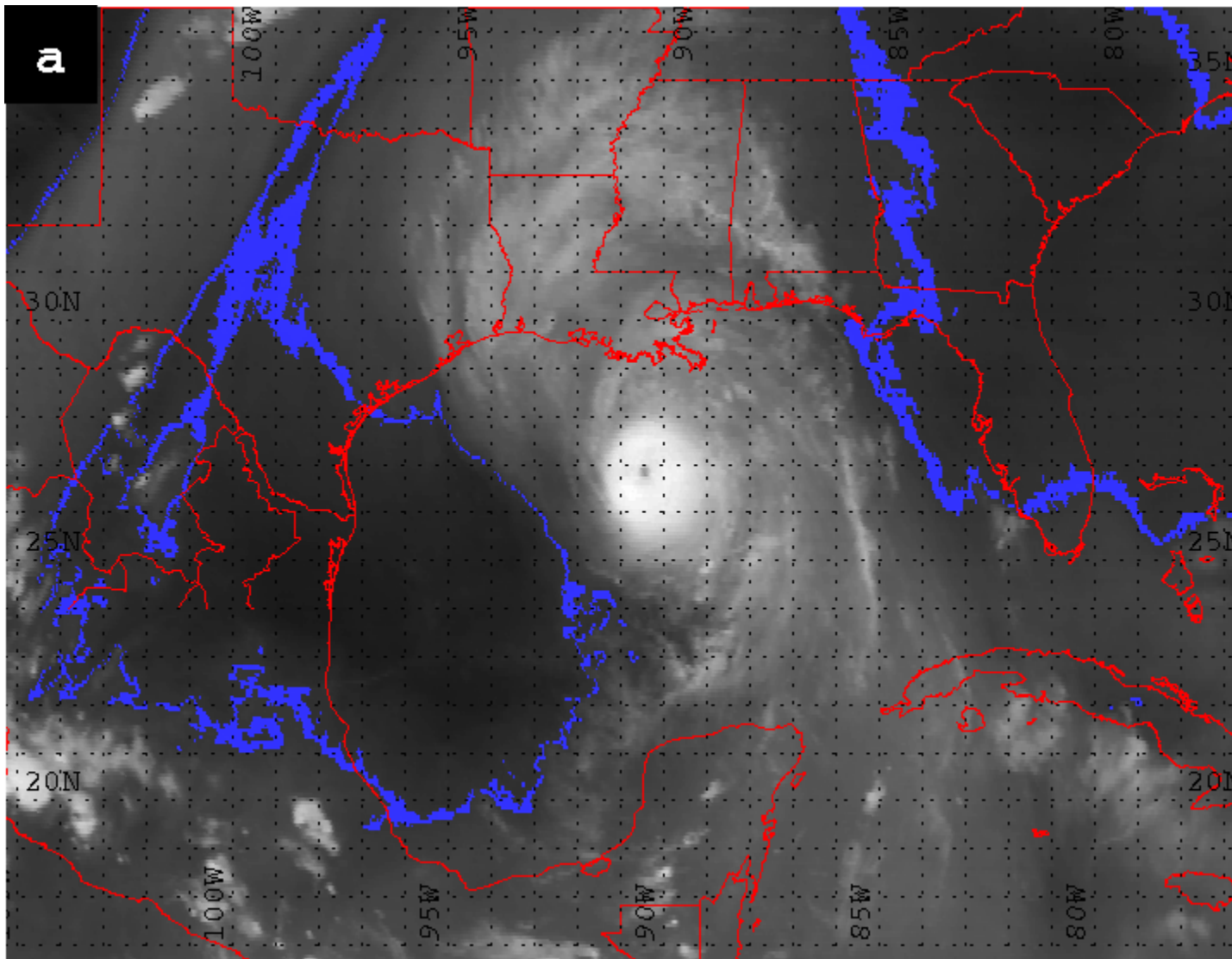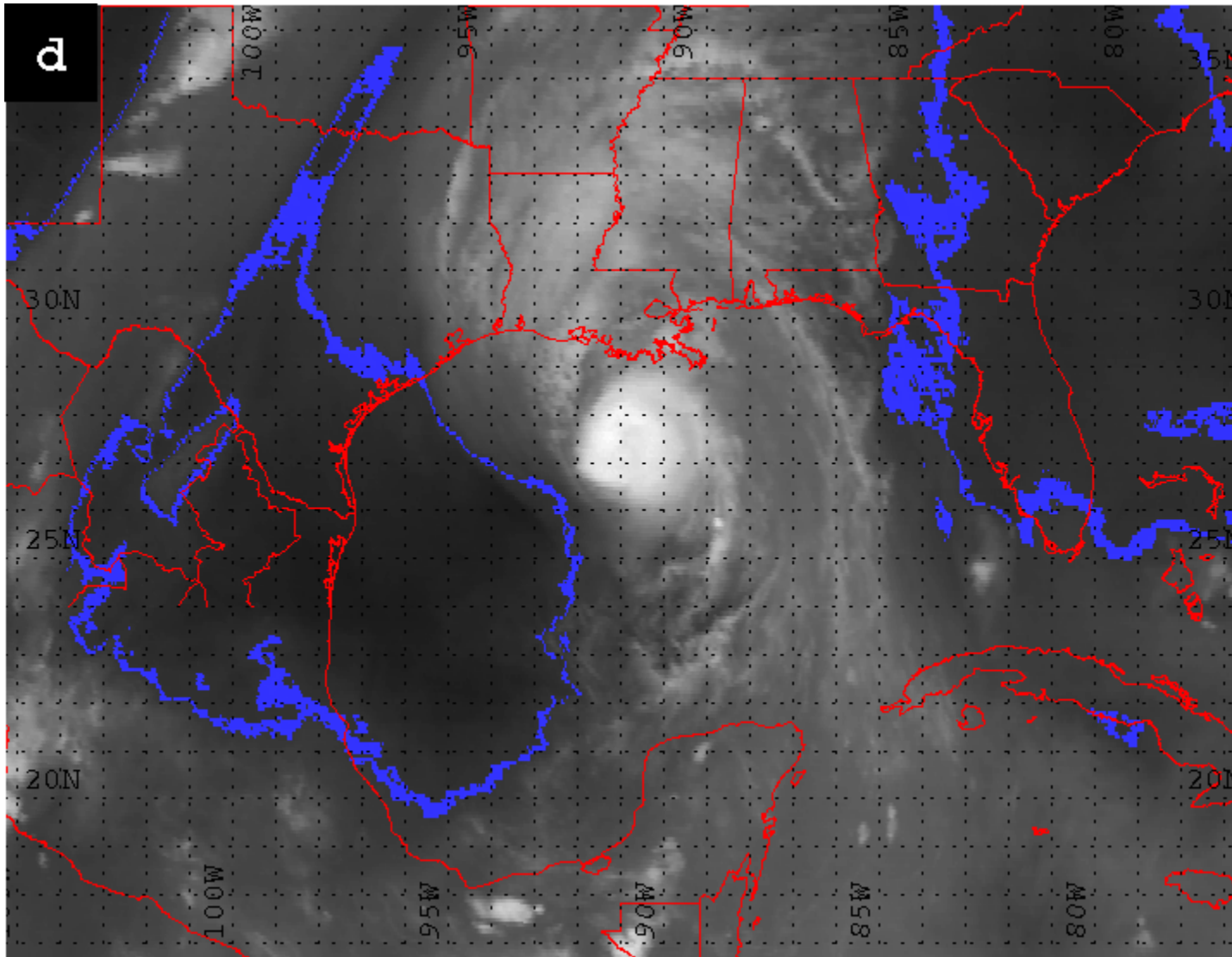
Figure 24d. GOES-8 water vapor image during the RW phase on 0332 UTC 3 October 2002 with the -24 °C vapor front (blue) highlighted.
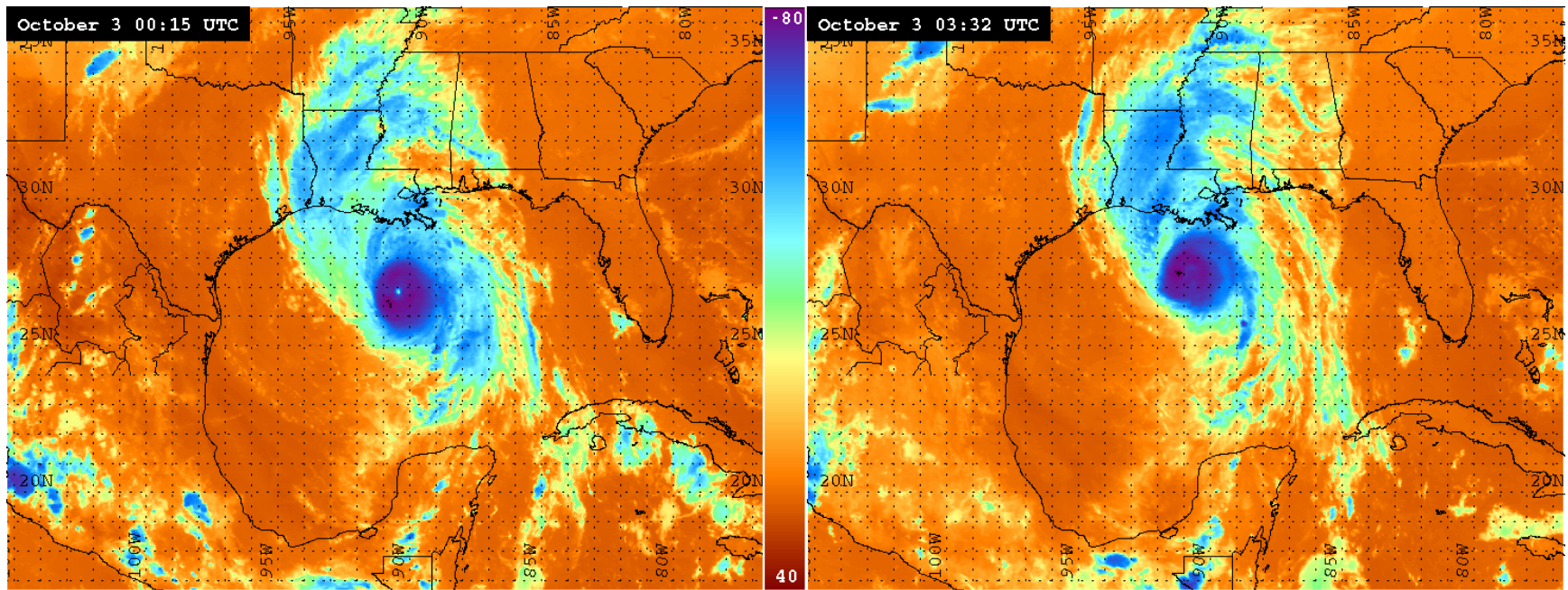
Figure 25. GOES-8 channel 4 infrared temperature images during the RW phase at (a) 0015 UTC 3 October 2002 and (b) 0032 UTC 3 October 2002.

southeast (Figure 24c darker areas). Additionally, the feeder bands were not defined on Lili's western side as the convection was broader but weaker there. After the 0232 UTC 3 October 2002 image, Lili resembled the low pressure comma shape rather than a tropical cyclone center vortex. The core circulation about the center of Lili remained elongated through this period and began a trend of warming as illustrated in the infrared satellite imagery (Figure 25). The outflow pattern stretched far onshore over Louisiana, Mississippi, and Alabama for the northern side and was somewhat cut-off on the eastern side by a dry air mass and vapor front over Florida (Figure 24). An outflow pattern was non-existent in the southwestern quadrant and barely discernable due west and south of Lili (Figure 24d). Again this indicated that the venting was not symmetrical and unfavorable for intensification. The continuation of uneven circulation, decrease in convective strength, and eye collapse indicated overall weakening of the storm from the satellite perspective. This supported the RW over this time period in the NHC minimum central pressure measurements. This satellite perspective illustrated that intensity responded quickly to collapse of convection in the eyewall or loss of an outflow channel (Croxford and Barnes 2002).

c. Dry Core Distance Analysis

Distances to the nearest dry core were recorded for direct comparison Martin (2001) who found that a storm will not move in the direction of a dry core area if the two are ≥ 620 km apart. The initial images of each NHC 6-h time intervals were analyzed (Figures 13 - 18) and Table 12 details the distances between the dry core and Lili's center, the dry core contoured temperature, and the area of the dry core temperature. At the beginning of the first RI phase, the nearest dry air core was over central Mexico around 22.5 °N and 101 °W (Figure 13). This core had a temperature of -19 °C and covered an area of 22,409 km. The core was 1,150 km away from

Lili's center. The dry air mass extended in a concave pattern along the northern and western

Gulf coasts, spanning Mexico, Texas, Louisiana, Mississippi, Tennessee, and Arkansas.

By 0646 UTC 2 October 2002 at the start of the steady state phase, the dry core was over

Mexico still near °23 N and 100 °W (Figure 14). Temperature remained constant at -19 °C, but

the area of the temperature decreased to 3,538 km because the previous one large core split into

several smaller ones. The core and Lili's center moved 200 km closer (Table 12). The extent of

the dry air mass was smaller because the entire mass split into two separate features around 32

°N and 98 °W (Figure 14).

The second RI phase initial image at 1215 UTC 2 October 2002 showed the core had

stretched offshore and formed a dominant horizontal signature (Figure 15). The core

encompassed 25,129 km and remained around 1,330 km away from the hurricane's center (Table

12). The extension offshore combined with the narrowing of the portion over land showcased a

funneling of more stable air into the core. Temperature corroborated this idea as the other

contours of water vapor temperature grew in area, although the core remained the same at -19 °C

and nearly the same area.

The 1 hPa drop phase began at 1815 UTC 2 October 2002. This image illustrated a more

pronounced horizontal orientation and the core migrated near the Mexican coast (Figure 16).

Temperatures warmed and a new dry core of -18 °C formed at 13,383 km in size. The dry core

and Lili's center drifted about 300 km closer. The entire dry air mass decreased its latitude

extent over land, again narrowing as the mass concentrated farther south and offshore.

The RW stage began with the 0015 UTC 3 October 2002 image and again the dry mass

had grown in size offshore and strength (Figure 17). A smaller -17 °C dry core formed right on

the coastline spanning an area of 330 km. Lili's center and this dry core were the closest

Table 12. Distance, temperature, and area of the dry core nearest to Hurricane Lili's center.

	Image Time (UTC)	Distance (km)	Temperature (°C)	Area (km)
Rapid Intensification (RI) Begin	0015 UTC 2 October 2002	1,550	-19	22,409
Rapid Intensification (RI) End	0646 UTC 2 October 2002	1,351	-19	3,538
Steady State End	1215 UTC 2 October 2002	1,330	-19	25,129
Rapid Intensification (RI) End	1815 UTC 2 October 2002	1,034	-18	13,383
1 hPa Drop End	0015 UTC 3 October 2002	811	-17	330
Rapid Weakening (RW) End	0645 UTC 3 October 2002	702	-17	34

yet at 811 km. The extent of the dry air mass contracted some on the southeast and thus had a less horizontal signature at its base. To get a final distance from the dry core to Lili's center, the 0645 UTC 2 October 2002 image was analyzed even though the intensity phases of interest were complete. The two features were the closest yet at 702 km, although still the under Martin (2001) track influential distance of 620 km throughout all intensity phase changes.

An interesting pattern emerged when these initial images are interpolated as the end state of the previous intensity phase. The dry air core moved significantly closer to Lili's center after each RI stage, by 199 km (0000 – 0600 UTC 2 October 2002) and 296 km (1200 – 1800 UTC 2 October 2002). Also after the 1hPa phase (1800 UTC 2 October 2002 – 0000 UTC 3 October

2002), the two features moved considerably closer as well by 223 km. The distance between the dry core and Lili's center remained initially the same after a steady state phase while Lili was at category 3 status and moved closer by only 109 km after the RW stage down from a category 4 to a category 3. Lili's center and the dry core moved closer by 479 km as a result of the 12 h combination of the second RI stage and the 1 hPa drop. This was indicative of the dry air strengthening and moving closer to Lili even though the circulation about the center was still intensifying, again in agreement with Croxford and Barnes (2002). The RW phase occurred after later.

5. Summary and Conclusions

Distances between the -24 °C vapor front and Lili's center had an overall trend of decrease shown in the mean, minimum, and maximum distance statistics for each intensity phase. The range did not show a definitive pattern. Mean and maximum distance underwent the largest decrease between the first RI phase and the steady state phase. Maximum distance had the largest decrease from the steady state phase to the second RI phase when the range tightened the most. The two RI events seemed to be characterized by a trend of oscillations in the distance between the -24 °C vapor front nearest point and the center of circulation. These oscillations are believed to be groups of -24 °C temperatures which broke away from the vapor front and indicated that the storm's convection was overpowering the dry air at that spatial position and time. Conversely, the rapid weakening phase, period of no change in pressure, and the slight intensification phase each illustrated steadier trends in these distance measurements. After the RI phases, the dry air was close enough to begin impacting Lili. A mean distance of 250 km from the center of Lili to the vapor front, or a minimum of 215 km, appeared to be the critical

values. The distances from the outer feeder band to the vapor front were more dependent upon the particular intensity phase as no real pattern surfaced.

The second RI phase visual descriptions of the -24 °C vapor front exhibited the most broken signature. The vapor front had definitive breaks, shape changes, and protrusions while Lili underwent the steady state phase and second RI phase. These descriptions indicated the vapor front was weaker as Lili was maintaining or increasing intensity. The vapor front was smoother and resembled a true linear signature during the final two phases. The -24 °C vapor front and Lili's center were closest yet then, and the dry air was interacting more with the hurricane as Lili was barely intensifying or rapidly weakening. These two phases coincided with distances near or less than the 250 km mean and 215 minimum distance critical values. The line was also smooth and sturdy in width during the first RI phase when the two features were the greatest distance apart.

The -24 °C vapor front delineated the edge of an offshore dry air lobe to the west of Lili. This lobe grew in size during all of the intensity phases. Additionally, this lobe continually strengthened as evidenced by the warming of the hourly mean and maximum water vapor temperatures. The dry air lobe had the largest areal coverage and was strongest during Lili's decay. The signature of the -24 °C vapor front became more consistent in width and had a smoother signature after the second RI phase because the entire dry air mass advected stronger, drier air into the offshore portion reinforcing the vapor front boundary with Lili's convection.

Lili's entire circulation expanded and well-defined banding appeared during the steady state phase. An eye replacement cycle also occurred during the steady state phase. During the latter hours of the second RI phase, Lili's circulation elongated but the eye remained tight and the outflow well defined. Lili's main circulation showed no impact until the two features were a

mean of 250 km apart after the second RI phase. At this point the dry air vapor front held its ground and was expanding more northward offshore. GOES GVAR water vapor (channel 3) and infrared temperatures (channel 4) both warmed after this second RI phase where outflow was healthy to the northeast and southeast. After the slight intensification stage, the eye collapsed as Lili was surrounded by drier air on the northwest, southwest, and southeast. The outflow was not good except to the north. Uneven circulation, decreased convective strength, and the eye collapse all correlated with RW phase seen in the NHC minimum central pressure measurements. These findings agreed with Croxford and Barnes (2002) that positive correlation between intensity and inner core strength ends after collapse of the eyewall or loss of outflow channel.

Lili's center and the nearest dry core to the west were ≥ 702 km apart throughout the imagery time series and > 620 km (Martin 2001 critical distance). The mean temperature value of this dry core grew warmer and thus drier. The area of the dry core varied, but was always less after an RI Phase. The dry core and Lili's center moved closest together at the fastest rate during the second RI phase. This was the same period where Lili's circulation began elongating and feeder bands met with the -24 °C vapor front. The next fastest rate of movement together was during the 1 hPa drop phase when Lili's center and the vapor front were closest in the mean and maximum distances. Also the feeder bands and the vapor front met in the northwest quadrant of Lili as the entire circulation continued elongating north and south. The > 620 km dry core distances for Lili agreed with the Martin (2001) that no dynamic linkage can be drawn for intensity change and dry core distance at this level apart. However, the dry air core can be far removed from the edge delineated by the -24 °C vapor front. This study found the -24 °C vapor front can be more directly linked to Lili's intensity changes.

Conclusions can be drawn about Lili's intensity changes based on these satellite observations. First, oscillations in mean distance values clustered during the rapid intensification periods showing more interaction than other phases. The two features were still not interacting at a level to impact Lili's main circulation because the hurricane was still intensifying. Second, Lili began to weaken in structure reflected in the pressure observations when the distances between the -24 °C vapor front and center reached critical values of 250 km mean and 215 minimum distances. Also, visual descriptions of the -24 °C vapor front were more broken during times when Lili was intensifying and smoother resembling a continuous line when Lili was farther away or weakening in strength. All of these conclusions suggest the eventual weakening of Lili was a result of this western side interaction with dry air which began towards the end of the second RI period. It is very plausible there was a lag effect as Lili broke down outward in, such that the main circulation could have been intensifying still even though the entire circulation pattern was weakening. This agreed with previous collocation of a low level stable area to dry air wrapping around Hurricane Michael in water vapor imagery (Abraham et al. 2004). They suggested future research could reveal a decoupling between the upper circulation of a tropical cyclone and the boundary layer.

Hurricane track forecasting has steadily improved and satellite water vapor has been found to steer hurricane tracks. Through this research, a satellite water vapor temperature signature and hurricane intensity change relationship has been developed. Intensity forecasting can be improved from application of this 250 km critical distance of when dry air will begin affecting a hurricane's intensity. Figure 26 depicts the 250 km mean distance visually on satellite imagery as an aid to implementing this technique. Vapor front descriptions showed a broken signature when Lili was rapidly intensifying and the two features were ≤ 250 km. A

smoother vapor front was evident when the two features were not interacting because of distance apart or decrease in feeder band activity around a hurricane's circulation. These results provide tools to interpret satellite water vapor imagery which can help local meteorologists and responders make decisions before coastal networks observe hurricane intensity or in the absence of reconnaissance data. For states with large coastal populations and/or underdeveloped evacuation routes, any additional realistic information about hurricane intensity change can improve sheltering and pre-storm response, especially in the 24 h before landfall. Even if evacuation had been called and followed by citizenry, first responders can benefit from information if impact severity effects were lessening prior to landfall. Additionally for storms larger in physical circulation extent, how rapidly the main core decreases in intensity after feeder bands move onshore can be assessed. Warming and/or growth in areal extent of the water vapor dry core temperatures can provide predictive information as to the strength of the dry air mass in comparison to the tropical cyclone. Also in Lili's case, stable air temperatures $\geq$ -24 °C threshold did not have to entrain into the core circulation to negatively affect the convective processes and symmetrical nature of the hurricane. Future research will provide interpretive tools which apply across more than just this one case study. However in the short-term, these results can be at the very least another set of data to investigate during tropical cyclone operations. While intensification is very important to predict, weakening is equally as important to accurately forecast or nowcast.
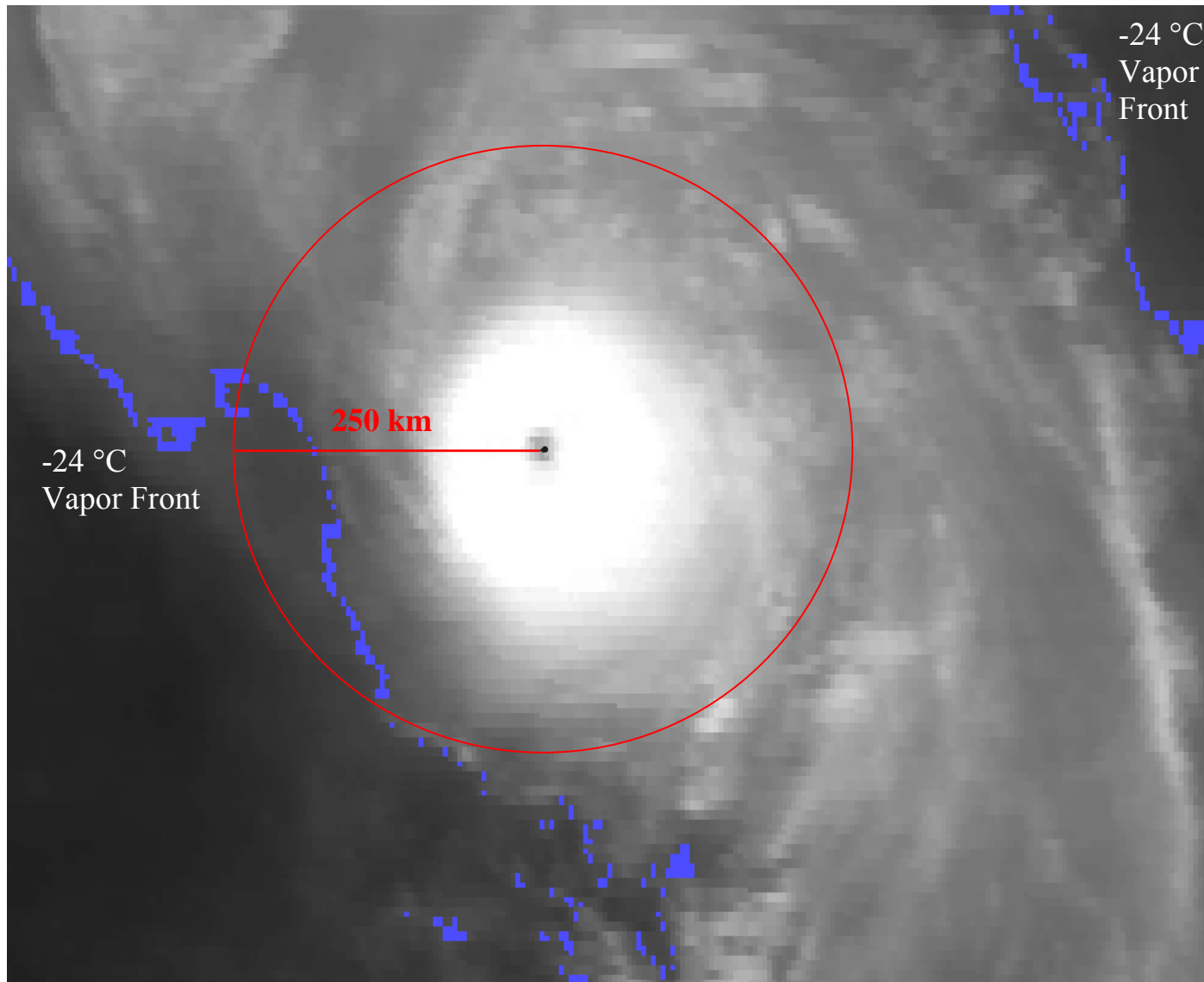
Figure 26. GOES-8 channel 3 image from 0015 UTC 3 October 2002 with the -24 °C vapor fronts highlighted blue. A schematic of the 250 km mean distance is superimposed in all radial directions with the line drawn toward the closest vapor front in the Lili case.

CHAPTER 4. SEA-SURFACE TEMPERATURE AND AIR-SEA INTERACTION CHARACTERISTICS

1. Introduction

The ocean provides fuel for large scale convection and thus is one factor necessary in the formation of tropical cyclones (Byers 1944; Palmen 1948; Riehl 1954; Miller 1958; Malkus and Riehl 1960) and their convective growth (Gray 1979). Several studies examined the resultant effects upon tropical cyclone intensification (Bosart et al. 2000; Hong et al. 2000; Shay et al. 2000) or weakening (Dunn and Miller 1964) from warmer or cooler waters. Therefore it is necessary to include an investigation of the oceanic contribution in this research of Hurricane Lili's intensity changes. Sea-surface temperature (SST) characteristics were studied using ocean buoy surface measurements and satellite data. Air-sea interactions were analyzed using heat flux calculations from buoy data. The main objective was to investigate the SST and heat flux characteristics during Lili's intensity changes in the Gulf of Mexico (GOM). Variation before and after Isidore will be quantified using a temporal comparison analysis to determine what effects Isidore had upon Lili. Heat flux levels will be compared to tropical ocean and GOM normal conditions, Atlantic basin tropical cyclone conditions, and Hurricane Opal (1995). Air-sea interactions near two central GOM buoys (42001 and 42041) will be investigated hourly for an in-depth focus upon Lili's intensity changes. A sensitivity analysis was performed to investigate heat flux variability in response to higher and lower water temperatures under Lili's wind regime. Ocean heat content will be mentioned briefly as satellite altimeter data was used to locate ocean features traversed by Lili during the intensity changes.

2. Literature Review

Warm water temperature ≥ 26 °C is one of the critical factors necessary for tropical cyclone formation (Palmen 1948) and maintenance (Gray 1979). There is some disagreement on

an SST lower threshold for intensity change, with values ranging from 26.5 °C to 28 °C (Miller 1958; Holliday and Thompson 1979; Merrill 1988; DeMaria and Kaplan 1994b; Shay et al. 2000; Cione et al. 2000). Inoue et al. (2002) correlated several environmental factors to tropical storm formation patterns in the Caribbean Sea. They found that minor SST variability is linked to the dominance of tropical storm formation in the southwestern Caribbean.

Historically, studies on the relationship of ocean temperatures and tropical storm intensity have taken slightly different perspectives of positive influence and negative feedback. Several reports covered the positive correlation between water temperature and storm intensity (Byers 1944; Miller 1958; Malkus and Riehl 1960; Merrill 1988; Bosart et al. 2000; Shay et al. 2000). Studies of rapid intensification (RI) focus on climatological and other characteristics of all events (Holliday and Thompson 1979; DeMaria and Kaplan 1994a; Kaplan and DeMaria 2003) or individual storm case studies (Shenk and Rodgers 1978; Rodgers et al. 1998; Bosart et al. 2000; Hong et al. 2000; Shay et al. 2000; Titley and Elsberry 2000; Chen et al. 2001). Hurricane Opal (1995) case studies concluded that a warm water eddy did in some way enhance or initiate rapid intensification (Bosart et al. 2000; Hong et al. 2000; Shay et al. 2000). While Rodgers et al. (1998) thought the higher SSTs worked in concert with lower atmospheric temperatures for Opal's rapid intensification. In relating SST to tropical cyclone RI, Holliday and Thompson (1979) suggested 28 °C is necessary for rapid intensification of typhoons. Titley and Elsberry (2000) agree that high sea-surface temperatures are a necessary condition for intense tropical cyclones, but found these high SSTs do not guarantee rapid intensification. Merrill (1988) viewed SST as a descriptive factor of the upper bound of tropical cyclone intensity and found storms which failed to reach their potential intensity encountered adverse atmospheric effects such as vertical shear, mean upper level flow above the center, and weaker outflow.

Oceanic cooling after a storm is the secondary perspective mentioned when studying SST as related to intensity changes. It is generally agreed upon that ocean waters can cool $1 - 3$ °C after a tropical cyclone as a result of wind induced upwelling and vertical mixing (Kraus 1972; Anthes 1982; Bender et al. 1993; Bender et al. 2000), and this cooling can occasionally reach between 4–5 °C (Price 1981; Black 1983). An inverse barometer effect initiates a sea level rise of approximately 1 cm mb^{-1} (Bishop 1984), creating the Eckman pumping effect. However, Cione and Ulhorn (2003) actually found less chilling on the order of only 0-1 °C using AXBT measurements dropped into the immediate storm eyewall area. Schade (2000) found that tropical cyclone intensity is more sensitive to the actual SST under the eye area than the entire SST field around the complete storm outflow.

Air-sea interaction studies presented a range of values covering sensible and latent heat flux values for the general tropical ocean (Fairhall et al. 1996) and more specifically, the Gulf of Mexico (Hsu 1997). A quantitative range of heat flux values within a tropical cyclone is more applicable here. Several studies have been published ranging from a summary of early case studies on latent heat release through the entire atmospheric column of a tropical cyclone (Riehl 1954) to a statistical study categorizing the surface heat fluxes by radial distance from the eye (Cione et al. 2000). Heat flux values during rapidly intensifying Hurricane Opal (1995) were studied in detail via observations (Shay et al. 2000), model simulation (Hong et al. 2000), and satellite data (Rodgers et al. 1998; Bosart et al. 2000).

Emmanuel (2000) found an average Atlantic basin intensity change rate of 12 m s^{-1} for both intensification and weakening. Emmanuel (2000) found decay rates to be similar over warm or cool waters and that a hurricane successively decays at 2/3 the rate of the previous intensification. Rodgers et al. (1998) found for Hurricane Opal (1995), a dry air intrusion on the

southwestern quadrant of outer circulation as the cause of latent heat rate rapid decline and eventual decay. Hurricane Lili's decay rate of 20.6 m s^{-1} over the 24 hours after rapid intensification ranked in the first percentile of cyclones since 1851 and was the only storm to have weakened at a stronger rate than it intensified (Frederick 2003).

3. Data and Methods

Meteorological and surface oceanographic measurements were obtained from the National Weather Service's (NWS) moored buoys. Detailed technical information is located at the National Data Buoy Center (NDBC) website (http://www.noaa.ndbc.gov). The shallow water coastal stations of the WAVCIS program are provided in the appendix and were not included in the main discussion because Lili's intensity changes were not in the vicinity of the coastal stations. Additionally, humidity measurements were not available at all WAVCIS coastal stations.

Buoy locations and the storm tracks of Isidore and Lili are provided in Figure 1. Sensible and latent heat flux values were calculated for NDBC buoys 42001, 42041, 42002, and 42003 over the time period 15 September 2002 through 15 October 2002. The month long time period was chosen to include the conditions in the GOM immediately prior to Isidore, through the life spans of both Isidore and Lili, and after Lili's effects had subsided to compare non-storm conditions and storm effects.

Hourly heat flux computations used the following equations. Sensible heat flux during unstable conditions, defined as when water temperature (t_{sea}) > air temperature (t_{air}), was calculated using (Smith 1980, Eq. [4])

$$H_s = \rho C_P C_T (t_{sea} - t_{air}) U_{10},$$

(1)

where ρ is the air density, C_P is the specific heat capacity at a constant pressure, C_T is the sensible heat flux transfer coefficient, t_{air} is referenced to a height of 10 m, and U_{10} is the wind speed also at the reference height of 10 m. Standard values were used for ρ at 1.15 kg m^{-3}, C_P at 1004 J kg^{-1} K^{-1}, and C_T at 1.1 x 10^{-3}. U_{10} was available at all stations except Buoy 42041 wherein a correction factor 1.08 m s^{-1} was applied.

Subsequently, the latent heat flux was calculated using Roll (1965)

$$H_l = L_T E = L_T C_E \rho (q_{sea} - q_{air}) U_{10} \; ,$$

(2)

where L_T is the latent heat of vaporization, E is the evaporation which can be broken down into its component parts of C_E the latent heat flux transfer coefficient, ρ the air density, q_{sea} the specific humidity of the seawater, q_{air} the specific humidity of the air, and U_{10} the wind speed referenced to the 10 m height. Standard values were used for L_T at 2.5 x 10^6 J kg^{-1}, C_E at 1.12 x 10^{-3}, and ρ at 1.15 kg m^{-3}. The correction factor 1.08 m s^{-1} mentioned earlier was again applied for buoy 42041. The variables of q_{sea} and q_{air} were not measured specifically. These values were calculated from the saturation vapor pressure (Hsu 1988)

$$q_{sea} = 0.62 \frac{e_{sea}}{P} \, ,$$

(3)

where

$$e_{sea} = 6.1078 \times 10^{[(7.5 t_{sea})/(237.3 + t_{sea})]} ,$$

(4)

in which P is the atmospheric pressure. Additionally,

$$q_{air} = 0.62 \frac{e_{air}}{P} \, ,$$

(5)

where

$$e_{air} = 6.1078 \times 10^{[(7.5t_{dew})/(237.3+t_{dew})]},$$

(6)

and t_{dew} is the dewpoint temperature. Hourly total heat flux vales were calculated from the addition of the hourly sensible heat flux and the hourly latent heat flux values. Missing data were interpolated because disruptions were sporadic and in one hour increments.

The temporal comparison analysis of non-storm effects was created by averaging over a valid statistical sample of 72 hours before Isidore (17 September 2002 through 20 September 2002), between the two storms (28 September 2002 through 1 October 2002), and after Lili (4 October 2002 through 7 October 2002). The mean periods were chosen from wind speed plots of all stations (Figure 27) to ensure that any tropical system wind effects had subsided and the same periods could be used for each station.

GOES-8 satellite infrared temperature composites were created using the multi-channel algorithm of Walker et al. (2003). This method utilizes GOES-8 infrared channels 2, 4, and 5 (Table 7) to compute SSTs. Then, a maximum SST at each pixel location is determined from contributing imagery between 0215 UTC - 1115 UTC. This produces a daily composite that is de-clouded. Satellite altimetry data were obtained from Dr. Bob Leben at the Colorado Center for Astrodynamics Research (CCAR), University of Colorado, Boulder. TOPEX/Poseidon and ERS-2 satellite data were used to create daily sea-surface height (SSH) maps referenced to a mean altimetry as described in Leben et al. (2002).

The sensitivity analysis covered the time period of 1200 UTC 2 October 2002 through 0700 UTC 3 October 2002 when Lili was closest to buoys 42001 and 42041. The positive sensitivity analysis simulated what the heat flux values could have been under pre-Isidore

109
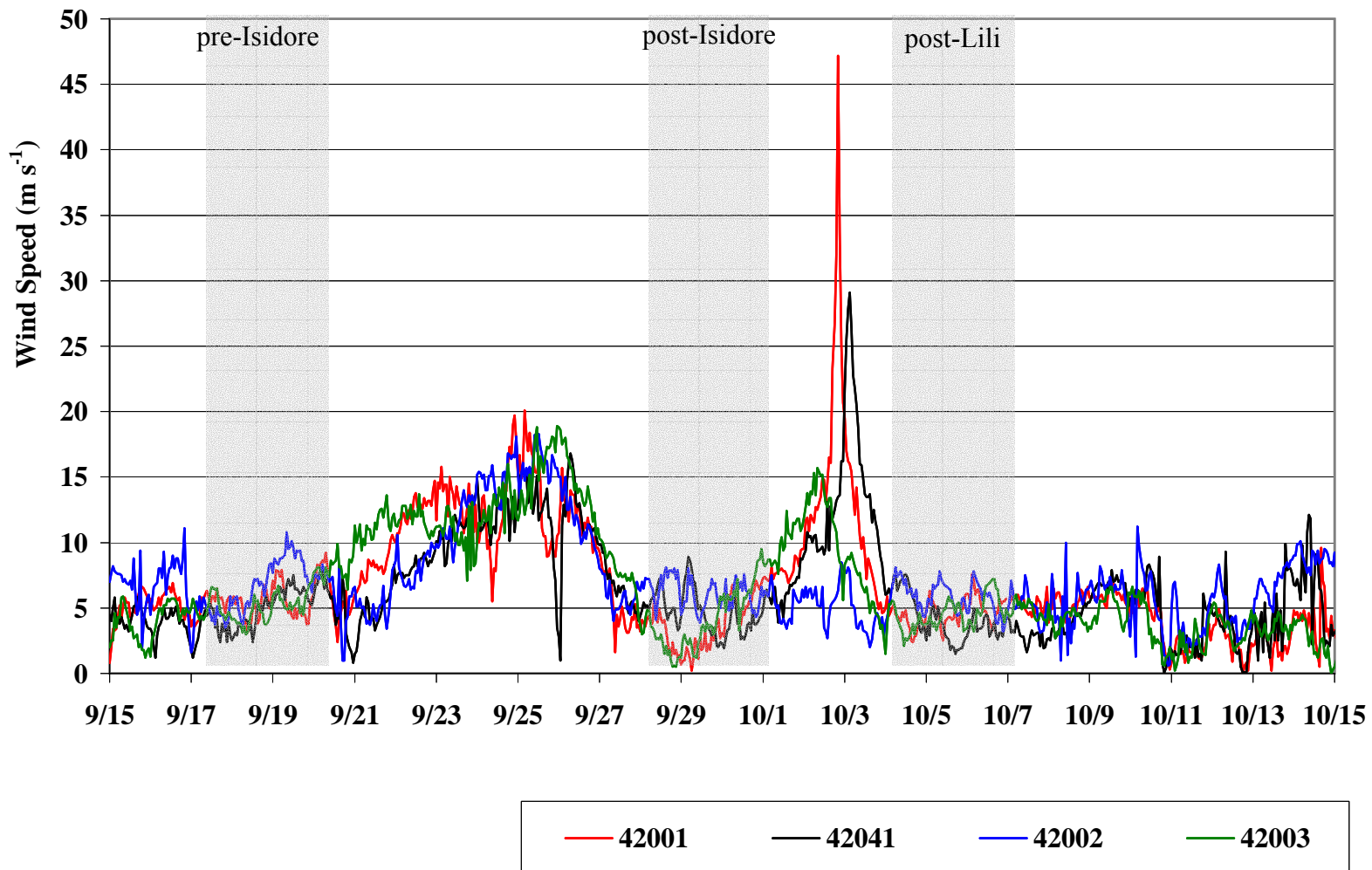
Figure 27. Wind speed (m s[1]) for each of the NDBC buoys with the time periods of pre-Isidore, post-Isidore, and post-Lili shaded.
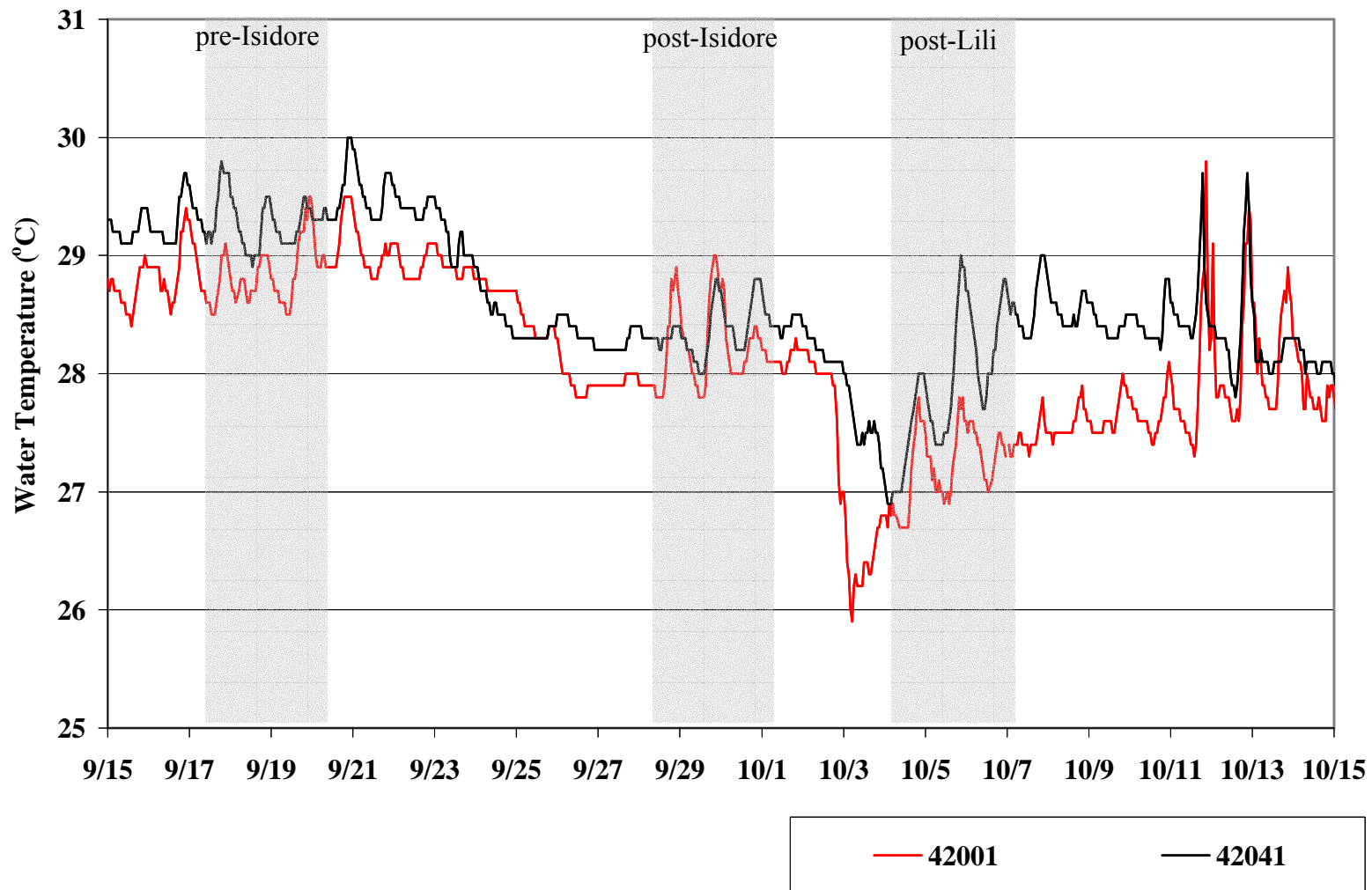
Figure 28. Water temperature (°C) for each of the NDBC buoys with the time periods of pre-Isidore, post-Isidore, and post-Lili shaded.

warmer water temperature conditions (Figure 28). A value of 0.84 °C was added to hourly

observed water temperatures at buoy 42001. This value was chosen based upon initializing the

first observation (28 °C; 1200 UTC 2 October 2002) to the pre-Isidore mean (28.84 °C). At

buoy 42041, 1.09 °C was added to observed hourly water temperatures based upon initializing

the first observation (28.20 °C; 1200 UTC 2 October 2002) at the pre-Isidore mean water

temperature (29.29 °C). This method was used because it factored in the cooling during the

higher winds of Lili whereas keeping the water temperature steady at the pre-Isidore mean would

have introduced additional overestimating. This analysis will be referenced as the +1 °C

sensitivity analysis. In the same manner, a -2 °C sensitivity analysis was performed to show

what impact increased cooling would have had upon heat fluxes. To simulate maximized

cooling, pre-Isidore mean water temperatures were decreased by 2 °C to 26.84 °C at 42001 and

27.29 °C at 42041. Then the first observation (1200 UTC 2 October 2002) was initialized to this

-2 °C lower value and the difference was subtracted from the observed hourly water

temperatures. For 42001, 1.16 °C was subtracted from observed water temperature values and

0.91 °C was subtracted from 42041 observed water temperatures. This method was chosen

instead of subtracting 2 °C from observed water temperatures as the latter would have

overestimated the cooling during Lili's high winds.

4. Results

Table 13 summarizes results of the temporal comparison analysis covering temperatures

of water, air, and dewpoint along with the latent, sensible, and total heat flux values.

Additionally, included in Table 13 are the variable parameters of the heat flux calculations, t_{sea} -

t_{air}, q_{sea} - q_{air}, and wind speed for reference purposes. Figures 29-31 provide time series of these

same parameters.

Table 13. NDBC station means, differences, and comparison ratios for each time period.

	Pre-Isidore 9/17/02 - 9/20/02	Post-Isidore 9/28/02 - 10/1/02	Post-Lili 10/4/02 - 10/7/02	Pre-Isidore/Post-Isidore		Post-Lili/Post-Isidore		Post-Lili/Pre-Isidore	
				Ratio	Difference	Ratio	Difference	Ratio	Difference
water temperature (°C)									
42001	28.8	28.2	27.2		-0.6		-1.0		-1.6
42041	29.3	28.4	27.8		-0.9		-0.5		-1.4
42002	29.9	28.4	29.0		-1.4		0.5		-0.9
42003	28.7	27.9	27.5		-0.8		-0.4		-1.2
air temperature (°C)									
42001	28.3	28.0	27.8		-0.3		-0.1		-0.5
42041	28.3	27.1	27.4		-1.2		0.3		-0.9
42002	29.2	27.8	28.5		-1.4		0.7		-0.7
42003	28.2	27.5	27.3		-0.7		-0.2		-1.0
dewpoint temperature (°C)									
42001	23.3	23.1	24.7		-0.2		1.6		1.4
42041	24.1	22.6	24.8		-1.5		2.2		0.7
42002	25.1	23.9	24.9		-1.2		0.9		-0.3
42003	25.1	24.3	24.8		-0.8		0.5		-0.3
sensible heat flux (W m^{-2})									
42001	3.5	2.8	0.9	80%	-0.7	32%	-1.9	26%	-2.6
42041	6.0	8.5	2.2	142%	2.5	26%	-6.3	36%	-3.8
42002	4.9	3.3	2.1	68%	-1.6	64%	-1.2	43%	-2.8
42003	3.0	1.4	1.7	46%	-1.6	122%	0.3	57%	-1.3

(table continued)

	Pre-Isidore 9/17/02 - 9/20/02	Post-Isidore 9/28/02 - 10/1/02	Post-Lili 10/4/02 - 10/7/02	Pre-Isidore/Post-Isidore Ratio	Difference	Post-Lili/Post-Isidore Ratio	Difference	Post-Lili/Pre-Isidore Ratio	Difference
latent heat flux (W m^{-2})									
42001	114.5	69.3	48.3	60%	-45.3	70%	-20.9	42%	-66.2
42041	103.9	112.3	48.0	108%	8.4	43%	-64.3	46%	-55.9
42002	127.5	114.7	96.0	90%	-12.8	84%	-18.7	75%	-31.5
42003	73.9	51.0	49.1	69%	-22.8	96%	-1.9	67%	-24.7
total heat flux (W m^{-2})									
42001	118.0	72.1	49.2	61%	-46.0	68%	-22.8	42%	-68.8
42041	109.8	120.8	50.2	110%	11.0	42%	-70.6	46%	-59.7
42002	132.4	118.0	98.1	89%	-14.4	83%	-19.9	74%	-34.3
42003	76.9	52.5	50.9	68%	-24.4	97%	-1.6	66%	-26.0
q_{sea} - q_{air} (g kg^{-1})									
42001	0.0068	0.0061	0.0030		-0.0007		-0.0031		-0.0038
42041	0.0065	0.0068	0.0037		0.0003		-0.0031		-0.0028
42002	0.0063	0.0057	0.0052		-0.0005		-0.0006		-0.0011
42003	0.0046	0.0044	0.0033		-0.0002		-0.0010		-0.0013
t_{sea} - t_{air} (°C)									
42001	0.5315	0.2329	-0.6236		-0.2986		-0.8565		-1.1551
42041	0.9658	1.2603	0.4375		0.2945		-0.8228		-0.5283
42002	0.6959	0.6562	0.4938		-0.0397		-0.1624		-0.2021
42003	0.4863	0.3986	0.2451		-0.0877		-0.1535		-0.2412
wind (m s^{-1})									
42001	5.3	3.6	4.7		-1.7		1.0		-0.6
42041	4.6	4.7	4.2		0.0		-0.5		-0.4
42002	6.5	6.2	5.8		-0.3		-0.3		-0.7
42003	5.0	4.0	4.5		-1.0		0.5		-0.5

Figure 29a. Latent heat flux and component variables for buoy 42001.
Temporal comparison time periods (non-storm) are shaded.

Figure 29b. Latent heat flux and component variables for buoy 42041.
Temporal comparison time periods (non-storm) are shaded.

Figure 29c. Latent heat flux and component variables for buoy 42002.
Temporal comparison time periods (non-storm) are shaded.

Figure 29d. Latent heat flux and component variables for buoy 42003.
Temporal comparison time periods (non-storm) are shaded.

Figure 30a. Sensible heat flux and component variables for buoy 42001.
Temporal comparison time periods (non-storm) are shaded.

Figure 30b. Sensible heat flux and component variables for buoy 42041.
Temporal comparison time periods (non-storm) are shaded.

120
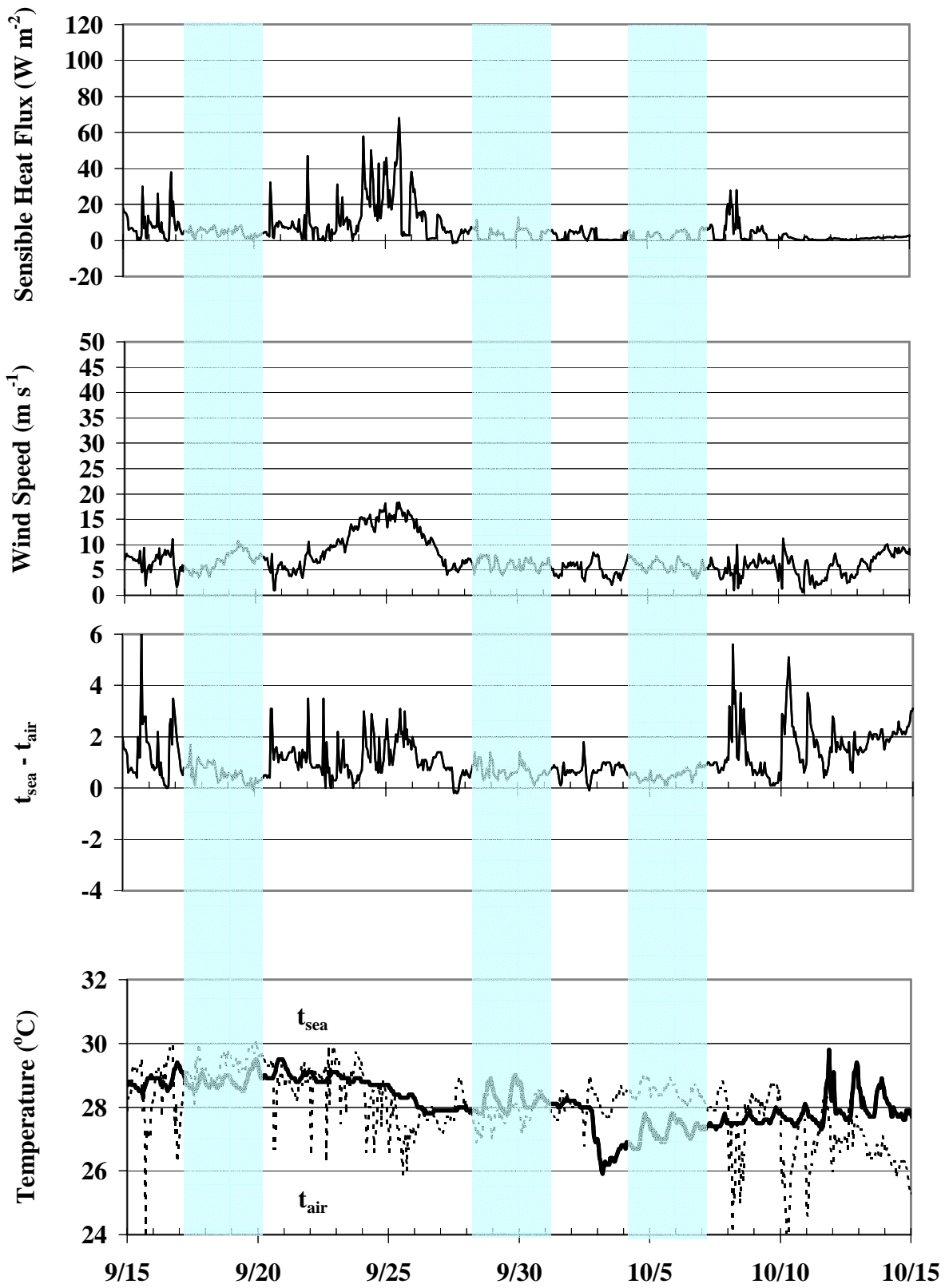
Figure 30c. Sensible heat flux and component variables for buoy 42002.
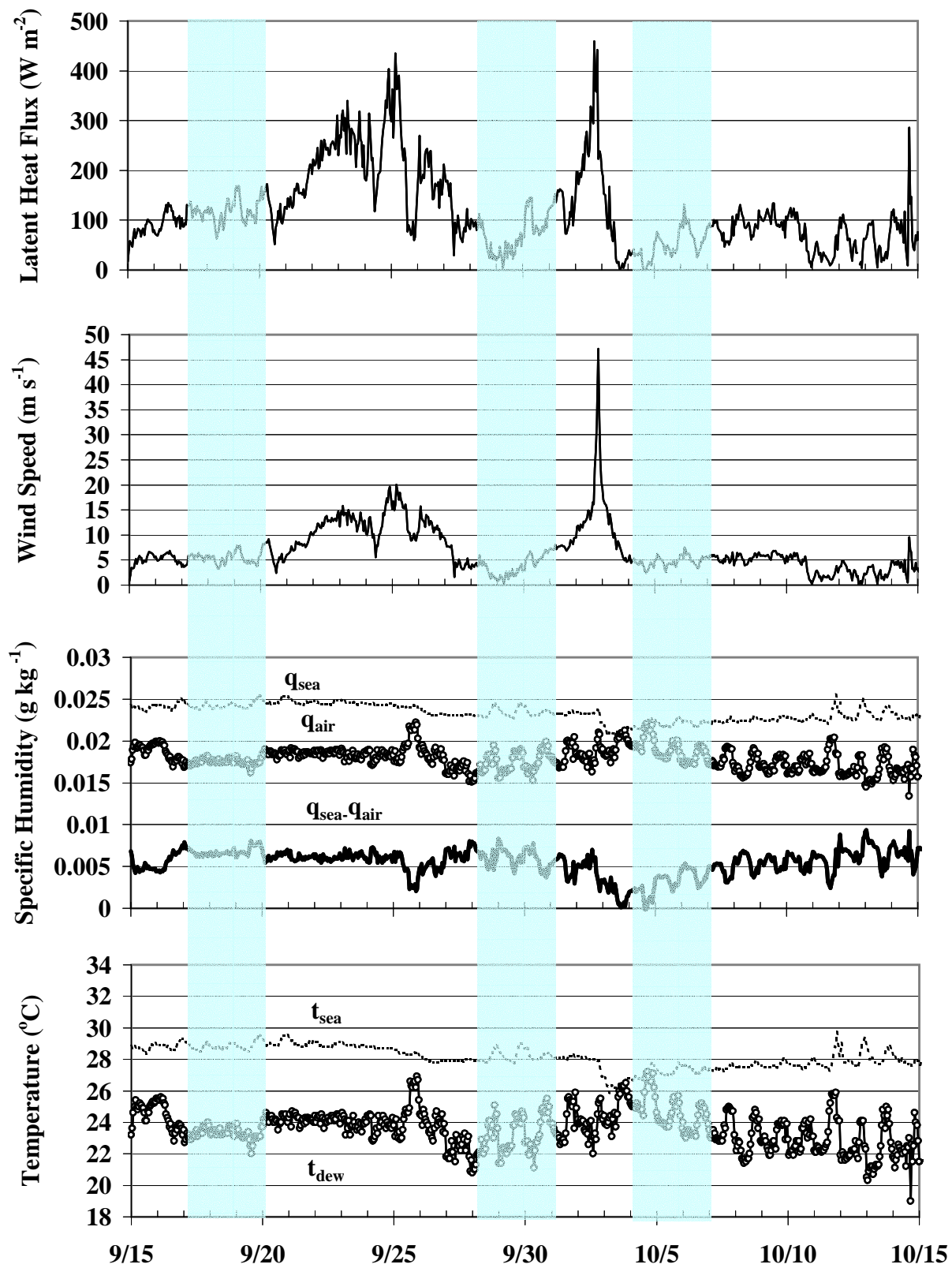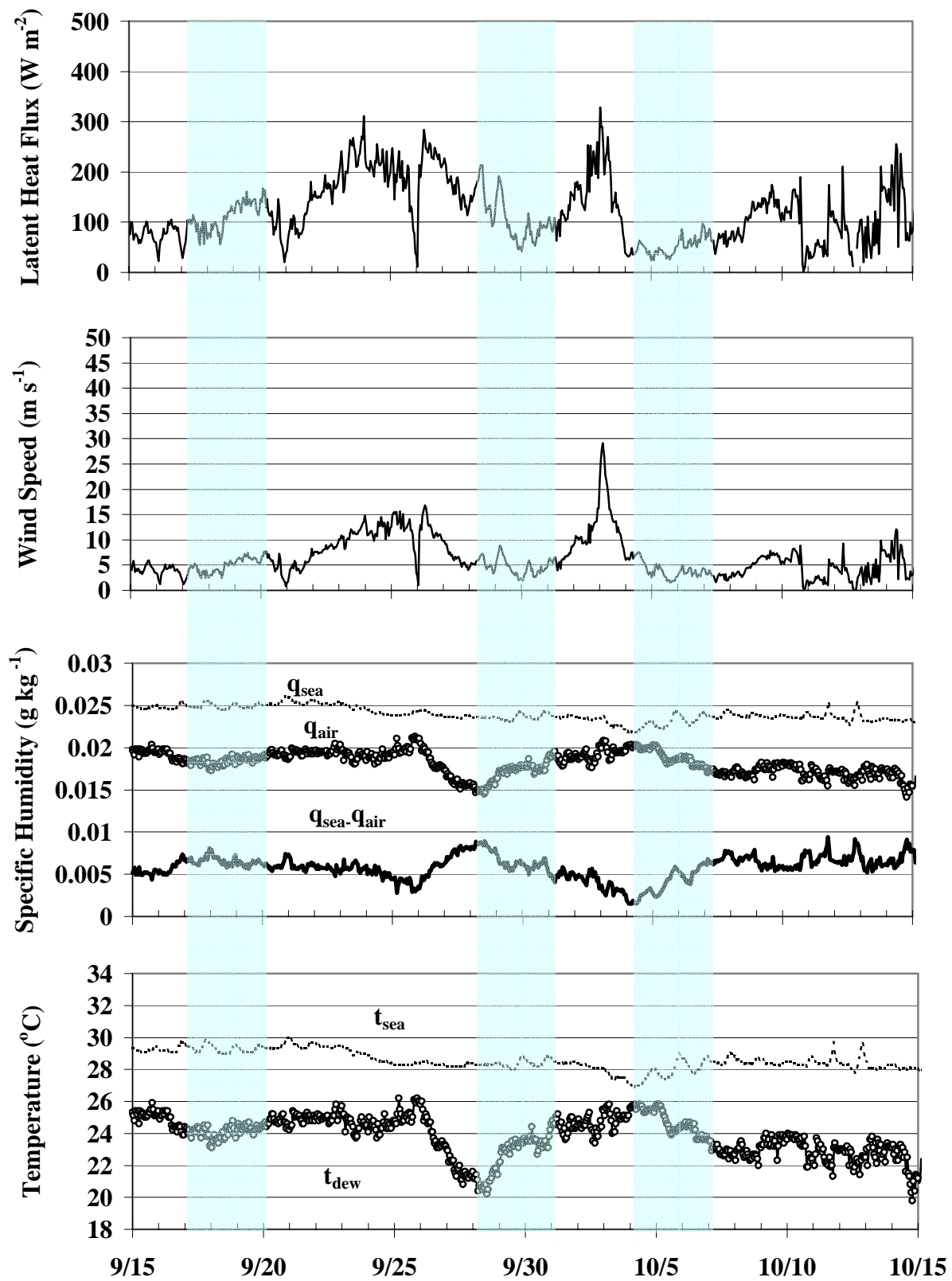Temporal comparison time periods (non-storm) are shaded.
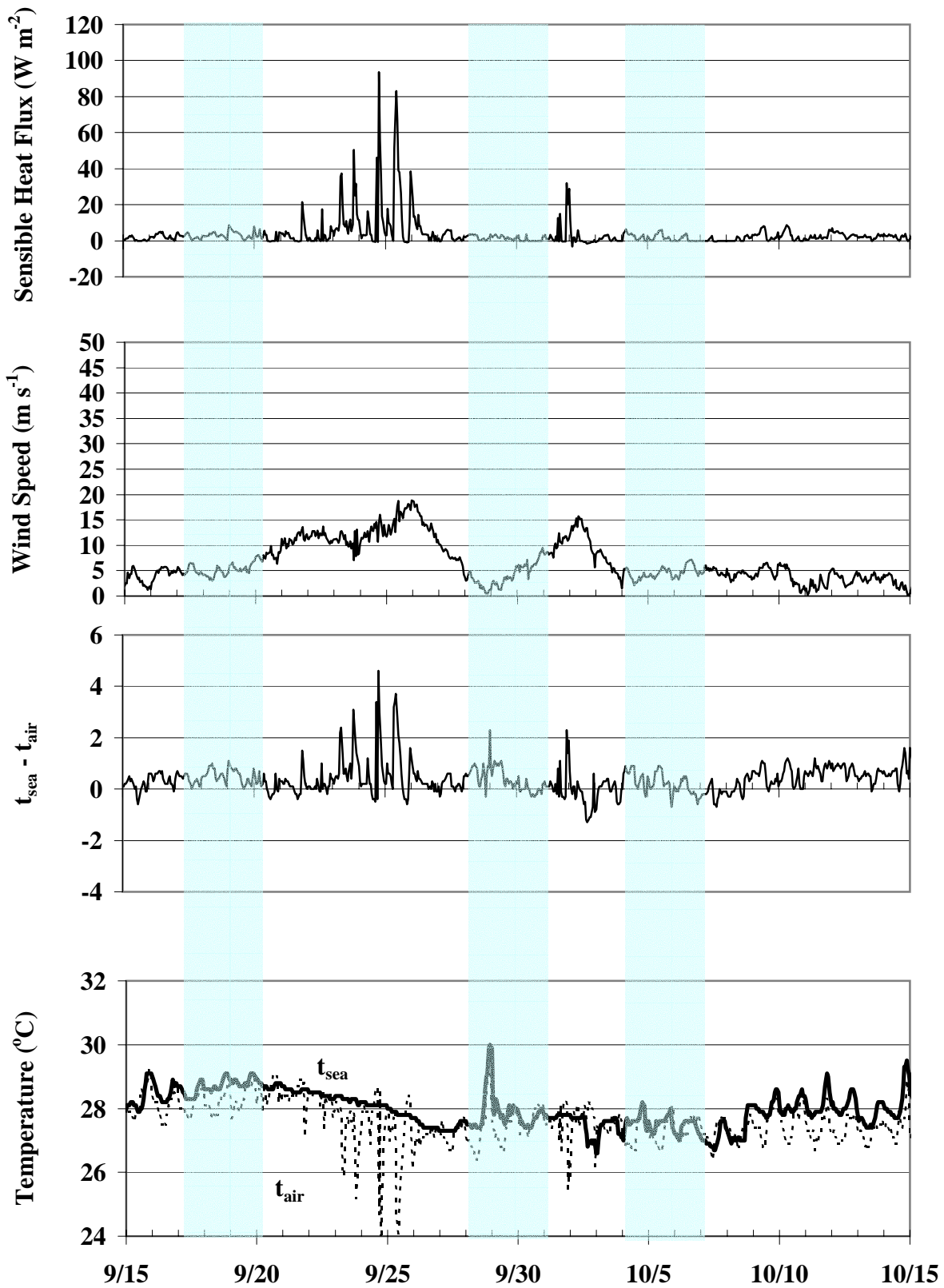
Figure 30d. Sensible heat flux and component variables for buoy 42003.
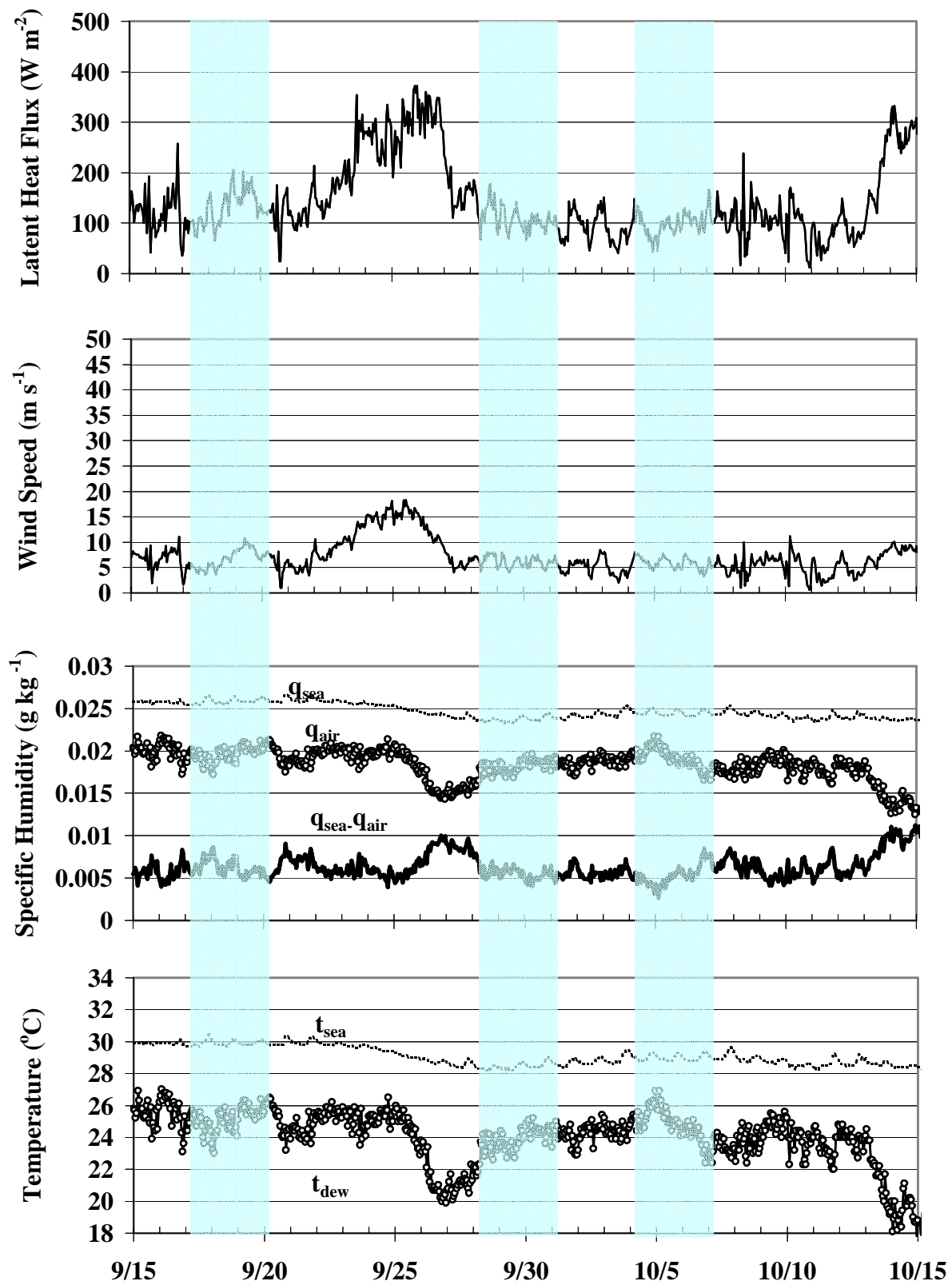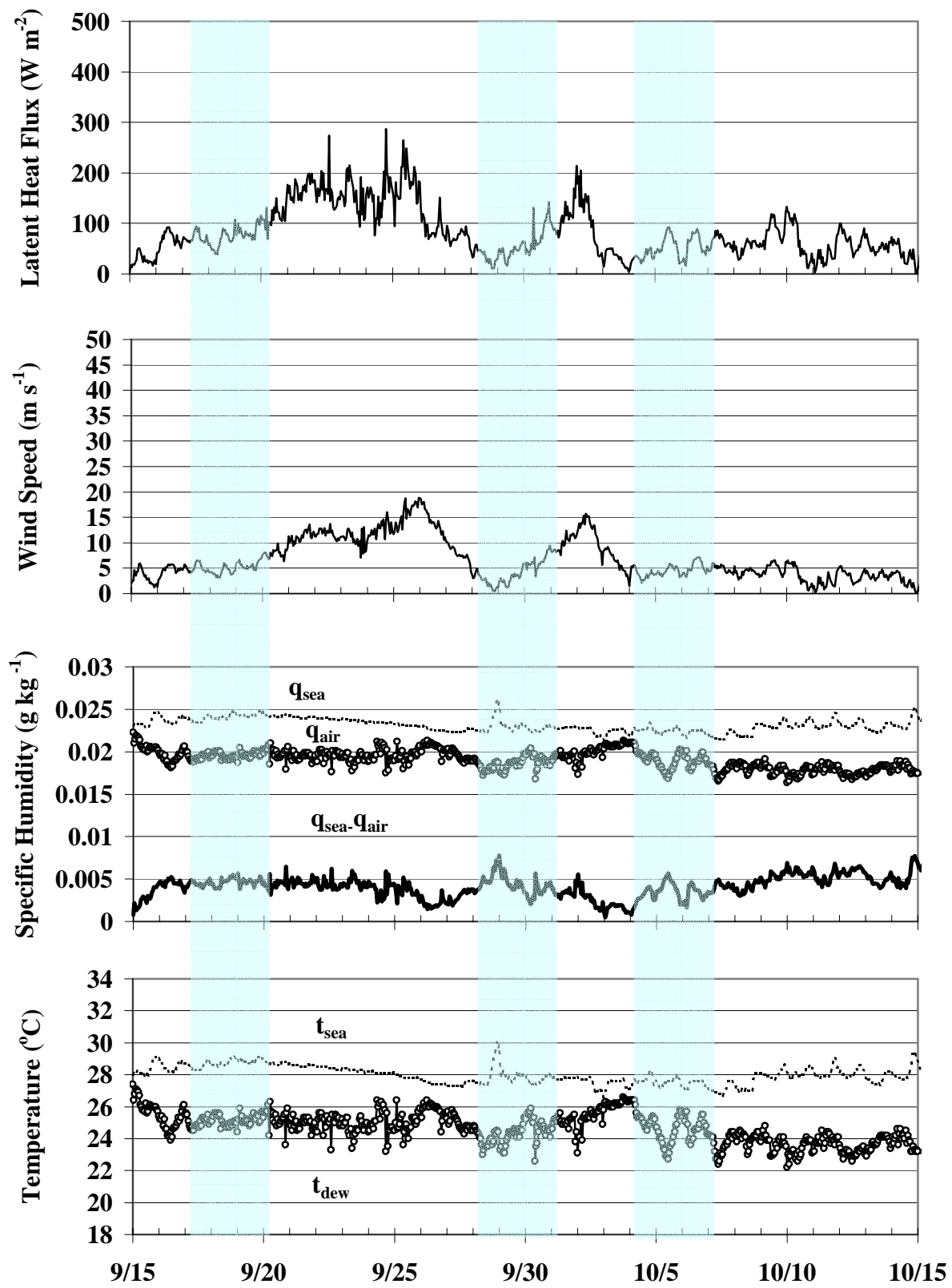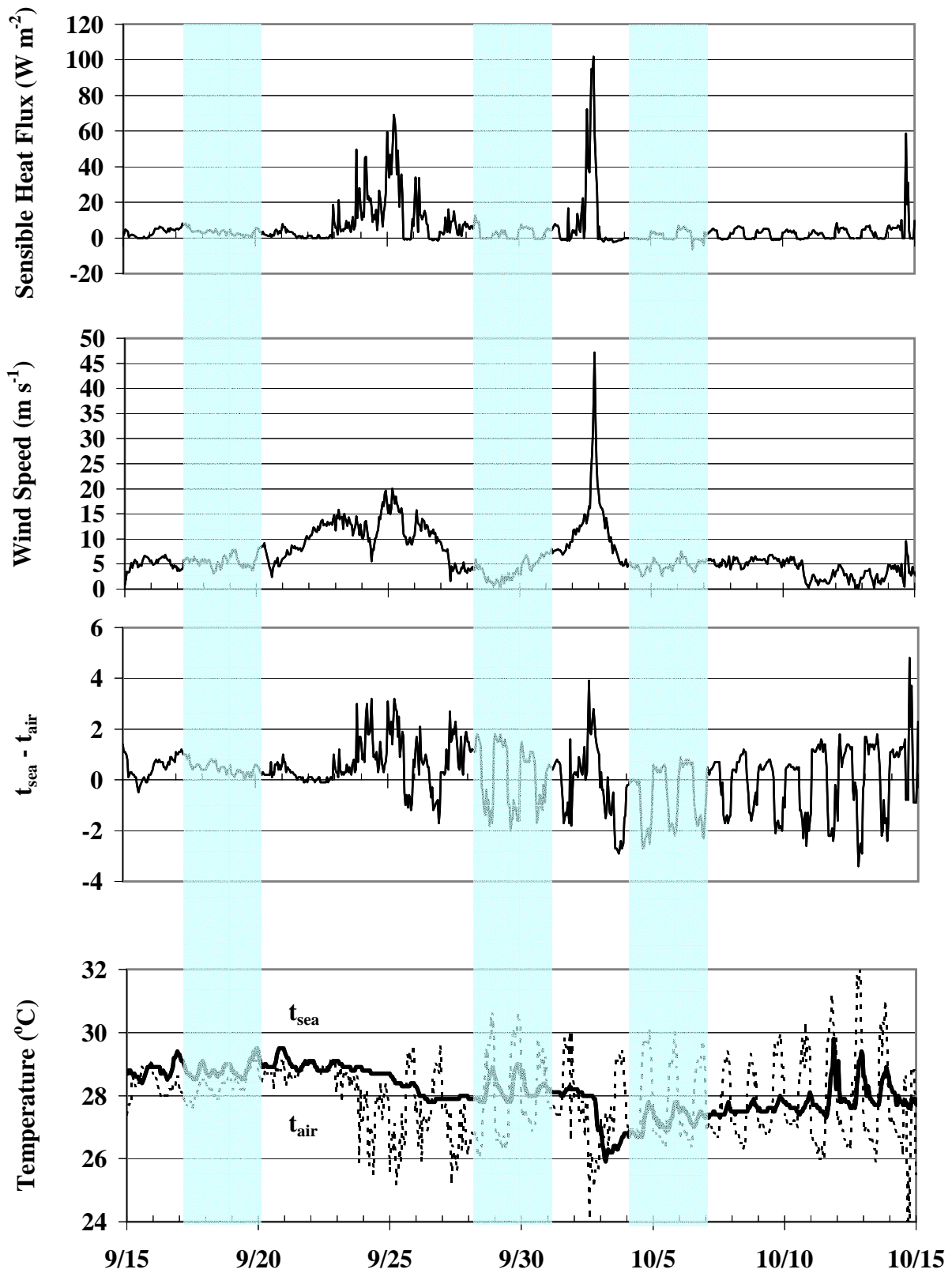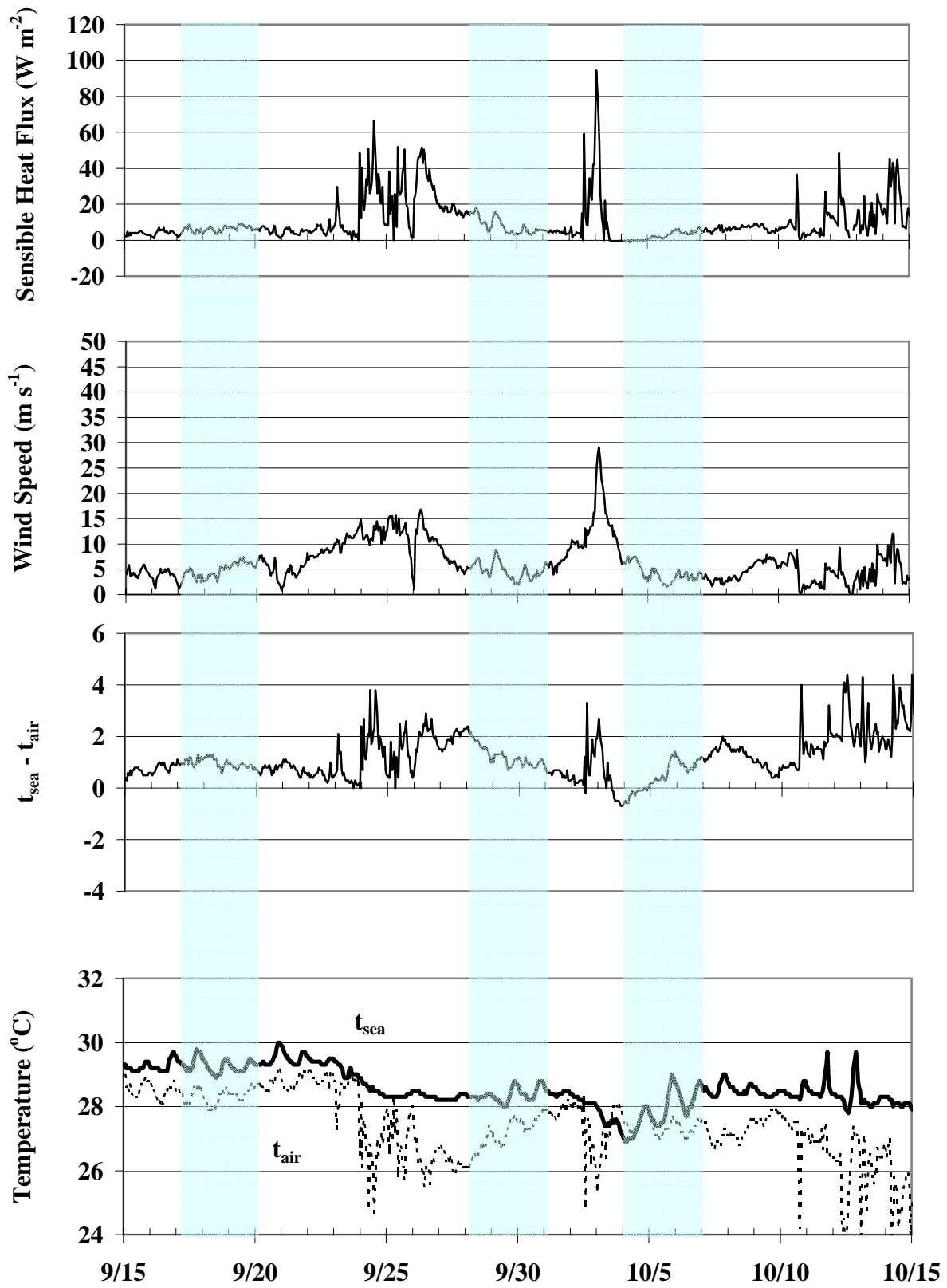Temporal comparison time periods (non-storm) are shaded.
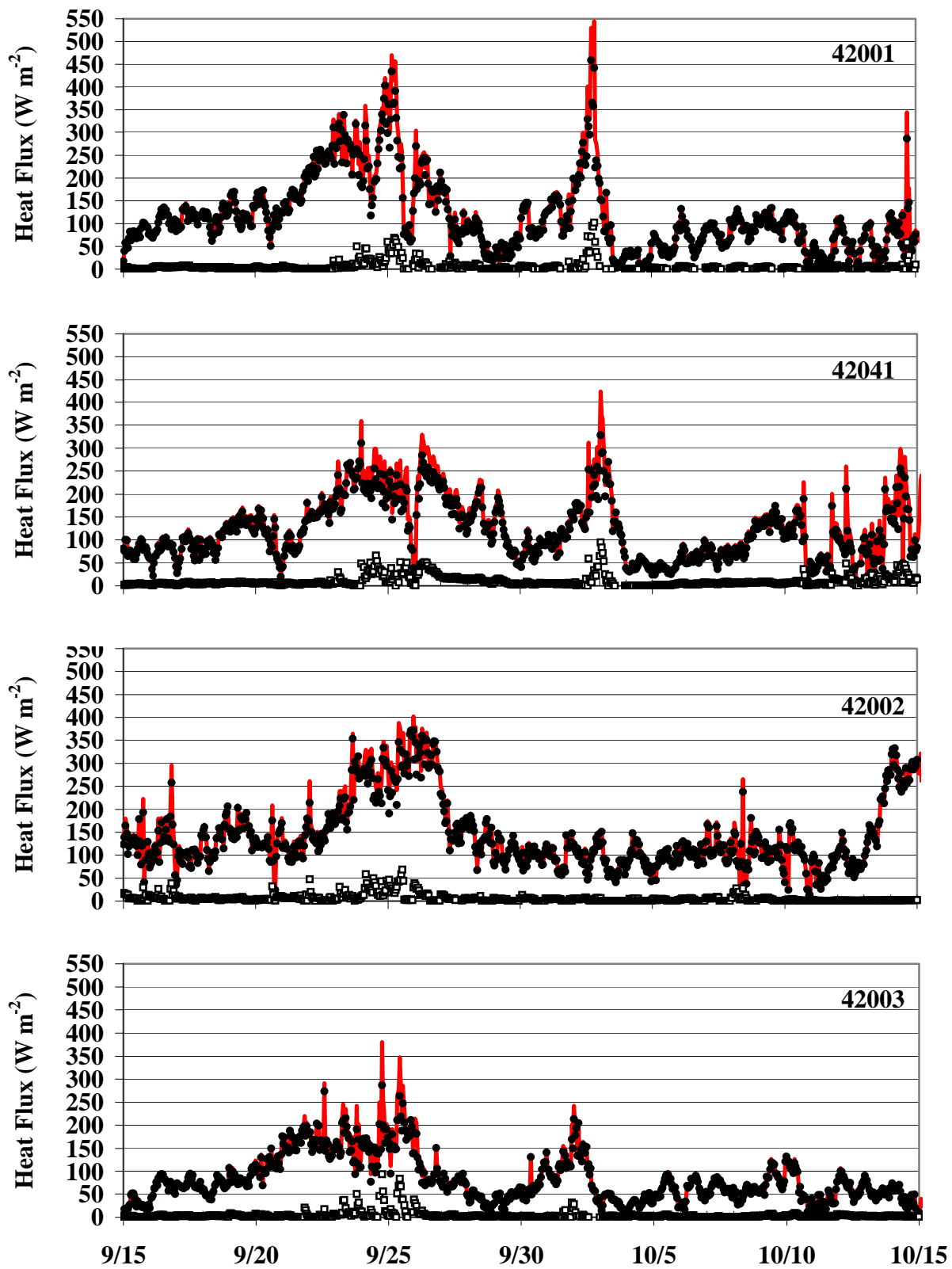
Figure 31. Total (red line), latent (circles), and sensible (squares) heat flux for each buoy.

123

a. SST Characteristics

1) NDBC Buoy Temperature Comparison Analysis

First, it is relevant to discuss general trends of the water temperature before and after Tropical Storm Isidore. For the 72-h mean time period before Isidore, GOM water temperatures averaged > 28.5 °C at each NDBC buoy and exceeded the aforementioned ocean temperature boundary of > 26 °C for tropical storm formation (Palmen 1948) and the ≥ 28 °C for convective growth (Gray 1979). It has been proven that water temperatures cool following tropical cyclones because of wind induced upwelling and vertical mixing (Kraus 1972; Price 1981; Anthes 1982; Black 1983; Bishop 1984; Bender et al. 1993; Bender et al. 2000). Most buoys showed a ≤ 1 °C decrease in water temperature following Isidore, and each were still ≥ 28 °C (Table 13). Buoy 42002 in the western GOM had the largest temperature decrease after Isidore (1.45 °C), but still averaged 27.8 °C. Additionally after Lili, water temperatures at all buoy locations were warm enough to support tropical activity with mean temperatures > 27 °C. Central GOM buoy 42001 registered the largest surface cooling effect following Lili (Table 13; -1 °C). Buoy 42001 also had the greatest water temperature decrease (1.6 °C) over the entire two storm time period, but remained > 26 °C (Table 13). It decreased the most because the centers of both Isidore and Lili were 64 and 14 kilometers westward of this location. Water temperatures at 42001 decreased more significantly after Lili because the storm was stronger when encountering 42001 than 42041.

2) Satellite Temperature Comparison Analysis

Figures 32 and 33 illustrate the GOES-8 SST composite images for the pre-Isidore and post-Isidore time periods which lend some spatial perspective to the in-situ point measurements. Figure 32 included only 19 September 2002 and 20 September 2002 because data were

unavailable for 17 September 2002 and 18 September 2002. Although these SST satellite mean temperatures were produced with only nocturnal data and thus included just under half of the in-situ mean observations, they agreed well (Figure 32; Figure 33; Table 14). Satellite temperatures ranged from ≤ 0.5 °C lower than the buoy in-situ mean water temperatures (42001 pre-Isidore) or just slightly higher than the in-situ (42002 post-Isidore). A difference image of pre-Isidore and post-Isidore composites is shown in Figure 34. Satellite composites showed a maximum water temperature decrease of 1-2 °C after Isidore in the area Lili would traverse the next week (Figure34 green areas). This satellite difference representation also correlated well with the in-situ water temperature mean differences (Figure 34; Table 14 far columns). Buoy 42003 showed the most disparity between satellite and in-situ measurements (-0.7 °C) when comparing pre-Isidore and post-Isidore time periods. The slight disparities between in-situ and satellite water temperatures fall within the buoy instrumentation field accuracy (± 1 °C) and satellite radiometric accuracy of 0.25 °C. These satellite measurements represent only the surface skin temperatures, while buoy measurements are bulk temperatures over 1 m depth. Previous research has demonstrated that ocean heat content is more important than SST (Shay et al. 2000).

b. Heat Flux Characteristics

1) 15 September 2002 through 15 October 2002

Latent heat is the driving mechanism for tropical cyclone warm core convection. Latent heat flux measures the heat energy involved in the phase change of water during evaporation which is stored in water molecules without raising the temperature. This heat energy is then released during condensation as sensible heat. Latent heat flux is driven by wind speed and humidity gradient between sea and air (Figure 29a-d). Over this month, wind speed exhibited the largest variability and highest values. Thus, greater heat flux events over the month reflected

125
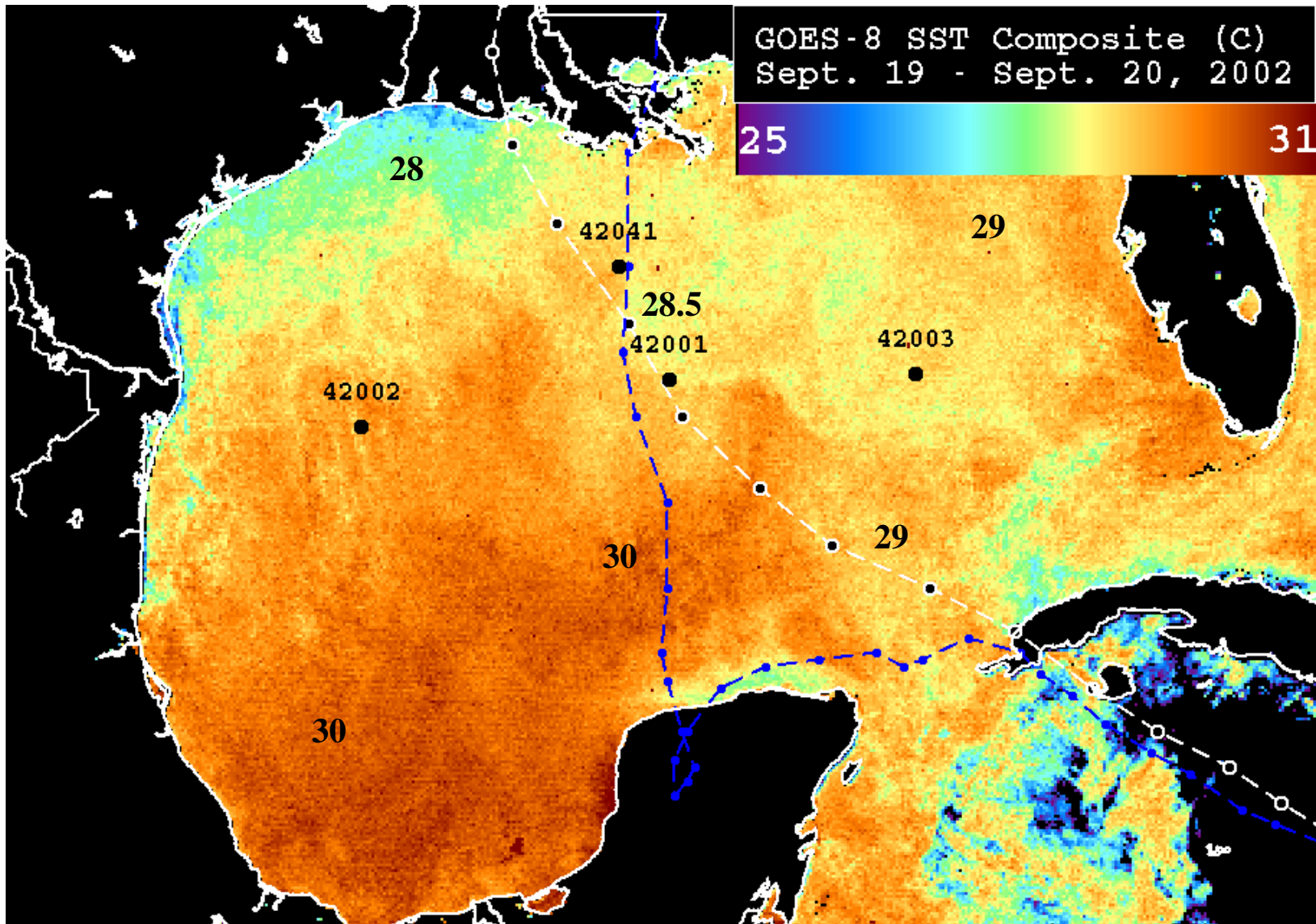
Figure 32. GOES-8 SST composite image (°C) matching the pre-Isidore statistical time period with NDBC buoys (black dots), Isidore's track (blue dashed) and Lili's track (white dashed) overlain. Representative temperatures are labeled throughout.
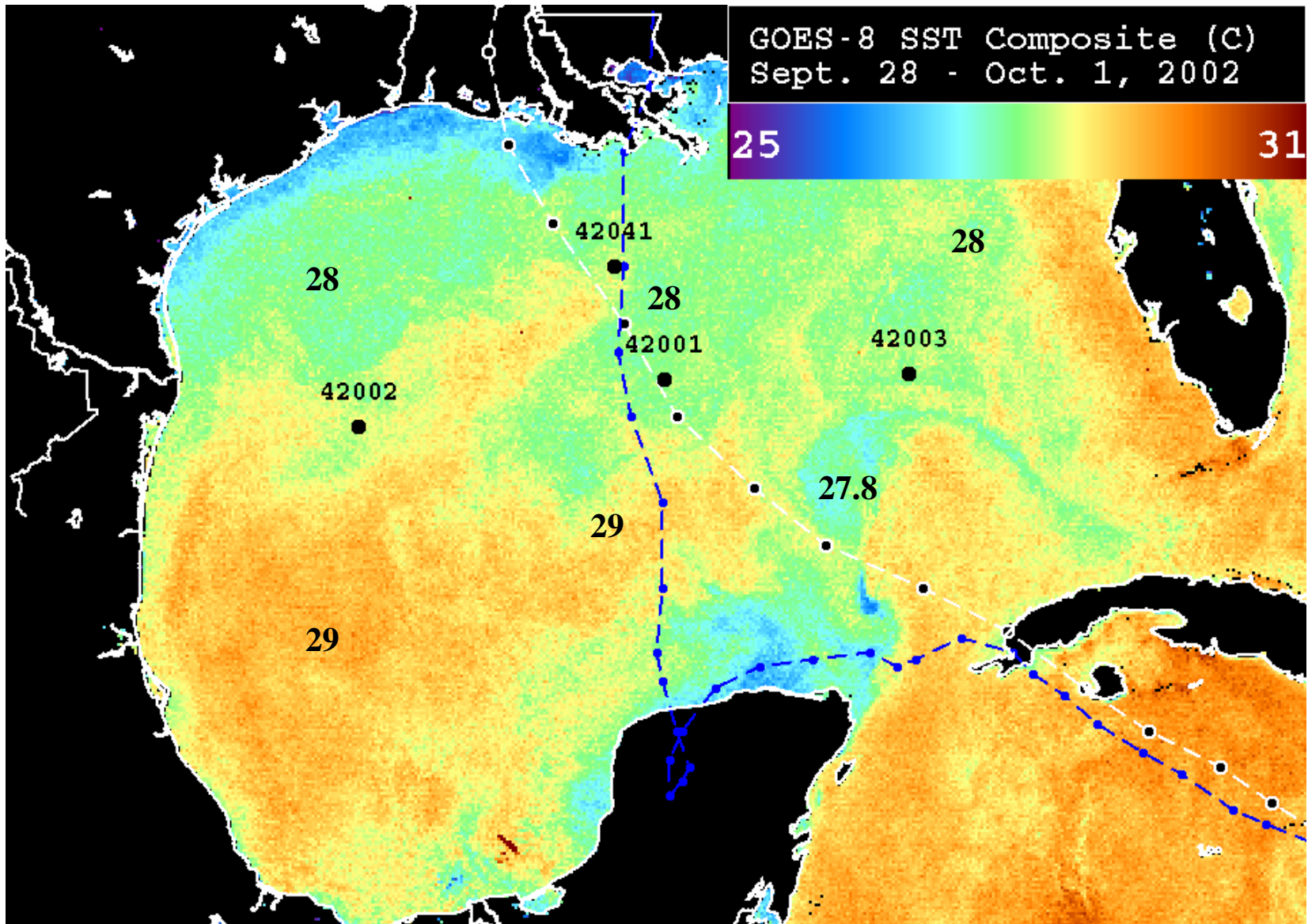
Figure 33. GOES-8 SST composite image (°C) matching the post-Isidore statistical time period with NDBC buoys (black dots), Isidore's track (blue dashed), and Lili's track (white dashed) overlain. Representative temperatures are labeled throughout.
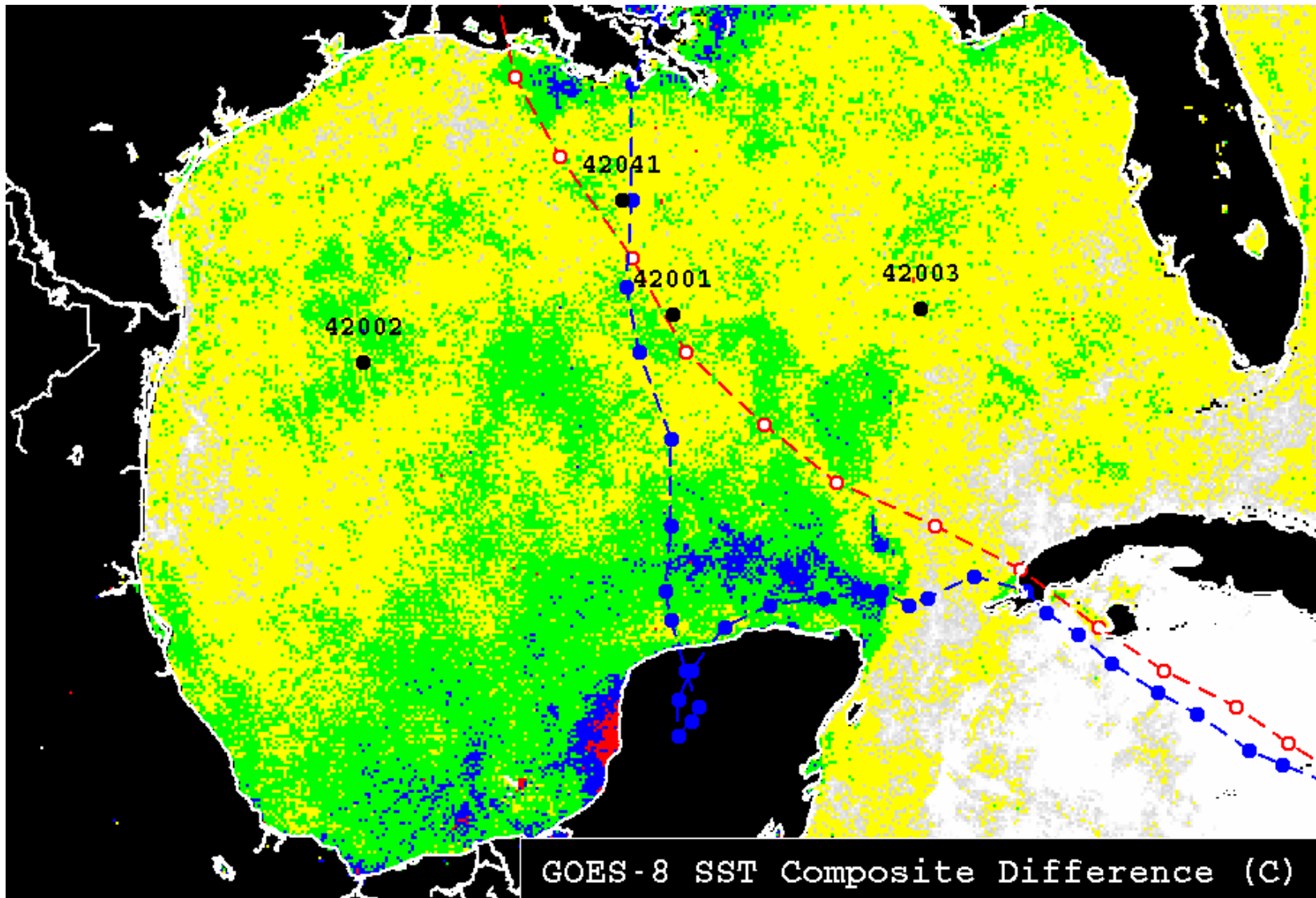
Figure 34. GOES-8 SST composite difference image (°C) illustrating the spatial temperature change resultant from subtracting post-Isidore (Figure 33) from pre-Isidore (Figure 32). Temperature decreases of 0-1 °C (yellow), 1-2 °C (green), and 2-3 °C (blue) are colored.

Table 14. Mean temperature (°C) at NDBC buoys with satellite composite SST (°C) corresponding values at those locations.

| | Pre-Isidore | | Post-Isidore | | Difference Pre to Post-Isidore | |
	In-situ (°C)	Satellite (°C)	In-situ (°C)	Satellite (°C)	In-situ (°C)	Satellite (°C)
42001	29.3	28.8	28.4	28.2	-0.9	-0.6
42041	28.8	28.8	28.2	28.1	-0.6	-0.7
42002	28.7	29	27.9	28.3	-0.8	-0.7
42003	29.9	29.5	28.4	28.7	-1.5	-0.8

the Isidore and Lili high wind periods at 42001 and 42041 (Figure 29a-b). Specific humidity has a very small range of values and generally has a less significant effect in Eq. (2). But, q_{sea} - q_{air} factored in more when it increased during wind speeds of < 10 m s^{-1}, such as around 14 October 2002 at buoy 42002 (Figure 29c). This q_{sea} - q_{air} increase was usually a result of dewpoint temperature decrease, creating a higher potential for the exchange of moisture from the water to the air.

Sensible heat is the transfer of physical heat energy between the water and atmosphere. Sensible heat flux signature generally reflected the sea-air temperature difference and the wind speed (Figure 30a-d). During sharply increased wind speed, sensible heat flux exhibited the largest values such as at buoy 42001 during Lili (Figure 30a). Variable t_{air} had a strong diurnal component when solar radiation was a factor (non-storm time periods). During the tropical cyclone time periods, air temperature declined steadily as high wind speed evaporated the moisture and cooled the air. Increased t_{sea} - t_{air} was also generally a result of decreased air

temperature, although when t_{sea} decreased it had a significant effect (Figure 30c). Total heat flux is a combination of both latent and sensible heat flux. Latent heat flux accounted for 85 – 90% of total heat flux (Figure 31) as generally expected.

2) Heat Flux Comparison Analysis (Non-Storm Mean Time Periods)

Table 13 and Figures 29-31 contain the data discussed in this heat flux temporal comparison analysis. Sensible, latent, and total heat fluxes decreased with each successive non-storm period. For sensible heat, 42041 increased after Isidore when compared to pre-Isidore conditions. Conversely, 42001, 42002, and 42003 decreased for this time period. After Isidore, latent heat and total heat flux decreased for all buoys except 42041. Although 42041 was closest in proximity to Isidore's eye wall, it quickly recovered to register a slight increase in evaporative energy. A comparison of post-Isidore and post-Lili revealed that all buoys decreased in sensible, latent, and total heat flux except for 42003 which exhibited a minor gain in sensible heat. Both Isidore and Lili in combination caused a decrease in all heat flux categories.

Following a discussion of the general heat flux value trends, it is now appropriate to compare each time period means to ranges found in the literature. Fairhall et al. (1996) calculated the air-sea fluxes over the tropical ocean during the Tropical Ocean-Global Atmosphere (TOGA) program's Coupled Ocean-Atmosphere Response Experiment (COARE). Their findings set a range of sensible heat flux at $6 - 11$ W m^{-2} and the latent heat flux at $88 - 113$ W m^{-2} for the steady state tropical Pacific Ocean (hereafter COARE). It is important to note that these findings were during a winter period of November 1992 through February 1993 using ship measurements. A frame of reference for general GOM heat flux values can be found in Hsu (1997) where one year of data at buoy 42002 was analyzed. For September, Hsu (1997) found a mean value of 7 W m^{-2} for sensible heat flux and 94 W m^{-2} for latent heat exchange. And for

130

October, the values increased to 17 W m^{-2} for sensible heat flux and 146 W m^{-2} for latent. These referenced Gulf of Mexico values from Hsu (1997) shall hereafter be referred to as GOM-HF.

For the 17 September 2002 through 20 September 2002 period before Isidore, all the NDBC buoys exhibited a lower sensible heat mean (1-6 W m^{-2}) than both the GOM-HF September value of 7 W m^{-2} and the COARE minimum value of 6 W m^{-2}, except buoy 42041 which barely satisfied the COARE minimum. Post-Isidore (28 September 2002 through 1 October 2002), three buoys averaged lower (1-3 W m^{-2}) sensible heat values than the GOM-HF (7 W m^{-2}) and COARE (6-11 W m^{-2}) values, while 42002 at 9 W m^{-2} fit closer to the COARE mid-range. Post-Lili (4 October 2002 through 7 October 2002), sensible heat values at all buoys ranged from $1 - 2$ W m^{-2}, falling well short of both the GOM-HF October mean of 17 W m^{-2} and the COARE range. Variable t_{sea} - t_{air} seemed to be the most influential on the large sensible heat decline between the pre-Isidore conditions and the post-Lili conditions. Water temperature decreased on the order of 1-1.6 °C of the pre-Isidore values in comparison to the air temperatures which declined < 1 °C of pre-Isidore conditions. A more detailed comparison analysis of the pre-Isidore and post-Isidore time periods is covered in subsequent paragraphs investigating Lili's rapid intensity stages.

Latent heat values for the pre-Isidore time period ranged from $70 - 128$ W m^{-2}. Three of the four buoys exceeded the GOM-HF September mean value of 94 W m^{-2} while buoy 42003 registered a mean of 70 W m^{-2}. When compared to COARE ($88 - 113$ W m^{-2}), 42003 was again below the range, 42001 and 42041 were within the range at 114 and 104 W m^{-2}, respectively, and 42002 exceeded the range at 127 W m^{-2}. Post-Isidore showed more variability within the latent heat flux results. Buoy 42003 at 51 W m^{-2} and buoy 42001 at 69 W m^{-2} both had mean values lower than the GOM-HF and COARE referenced values. Buoy 42041 exceeded the GOM-HF

index but came just below the maximum COARE value of 113 W m^{-2}, while the mean at buoy 42002 of 115 W m^{-2} exceeded both indices. Post-Lili, latent heat flux values reduced the most and all buoys were well below both the GOM-HF October index of 146 W m^{-2} and COARE range. Buoy 42002 had the largest mean value after Lili at 95 W m^{-2}. Buoy 42002 wind speed averaged over 5 m s^{-1} and q_{sea} - q_{air} increased over the time period as a result of a > 4 °C dewpoint temperature decrease. Buoy 42003 was the lowest at 46 W m^{-2}. Closest in proximity to Lili, 42001 and 42041 logged means of 48 and 49 W m^{-2}. The air-sea parameter (q_{sea} - q_{air}) was more of a factor in the latent heat flux value decreases during the comparison of these low wind speed periods.

These heat flux results during non-storm periods provided definitive proof that each storm impacted the heat exchange between sea and air, with Lili significantly so. The latent and total heat flux percentages comparing pre-Isidore to post-Isidore conditions were most significant to this chapter's objective of the determinable effect from Isidore. The largest post-Isidore decrease in latent heat flux occurred at buoy 42001 which later encountered the northeast quadrant of convection near the edge of Lili's eyewall area. At this location, the latent heat flux mean registered at only 60%, the sensible heat flux at 80%, and the total at 61% of pre-Isidore conditions. However, Lili was still strengthening a few days later while in the vicinity of 42001. Although Isidore diminished the water, air, and dewpoint temperatures, and thus the air-sea exchange rate parameters (q_{sea} - q_{air} and t_{sea} - t_{air}) prior to Lili, it is well within reason to postulate that this 60% latent flux decrease factor alone could not have been the all encompassing reason for Lili's rapid weakening. Also curious, is that the buoy closest to Isidore (42041) actually increased in all heat flux values post-Isidore on the order of approximately 10% for latent and total, but 42% for sensible. Later the next week, Lili would weaken while in proximity of this

buoy 42041. Since the heat flux means increased at 42041 between the two storms, Lili's demise might be better explained as a combination effect from eye mechanics, atmospheric conditions such as dry air advection, and some SST temperature influence.

c. Intensification and Weakening Stages

NDBC buoys 42001 and 42041 heat flux values provided a unique opportunity to study Lili's intensity changes since both a rapid intensification and weakening stage occurred near these locations. Lili underwent a rapid intensification of 13 hPa over the 6 h from 1200 UTC 2 October 2002 until 1800 UTC 2 October 2002, while 61 km southeast of buoy 42001. The eye of Lili passed 14 km west of 42001 during a 1 hPa drop over 6 h from 1800 UTC 2 October 2002 through 0000 UTC 3 October 2002. Lili underwent a rapid weakening phase of 17 hPa over 6 h, while passing 29 km west of 42041 during the time frame of 0000 UTC 3 October 2002 through 0600 UTC 3 October 2002. Table 15 provides the hourly time series calculations for NDBC buoys 42001 and 42041 during these intensity changes of interest.

Latent and sensible heat flux ranges from studies presented earlier focused upon the tropical ocean and GOM general conditions. Heat flux values during tropical cyclone events are of greater significance to this study. Cione et al. (2000) used surface buoy observations during tropical cyclone events to form a database (hereafter TCBD) from which they conducted a statistical study and formulated a range of heat flux values for tropical cyclones. TCBD values had a wide variance inherently since this study covered the entire spectrum from tropical storms to hurricanes and results were radially averaged for distance from the center. As a comparison to the heat flux values presented here during Lili's strength changes, the most applicable TCBD results were inside $0.75°$ radius from the center, had SST ≥ 27 °C, and had wind speed > 17.5 m s^{-1}. TCBD sensible heat flux ranged from 17 to 813 W m^{-2} with a mean of 220 W m^{-2}. The

133

Table 15. NDBC buoy measurements for 42001 and 42041 during Hurricane Lili's intensity phases while nearest to the buoys.

	Wind (m s^{-1})	Air Temp (°C)	Water Temp (°C)	Dewpoint Temp (°C)	$t_{sea} - t_{air}$	Sensible Heat Flux (W m^{-2})	$q_{sea} - q_{air}$	Latent Heat Flux (W m^{-2})	Total Heat Flux (W m^{-2})
42001									
10/2/02 1200	14.80	27.70	28.00	24.10	0.30	6	0.005	228	234
10/2/02 1300	13.10	25.90	28.00	23.10	2.10	35	0.006	248	283
10/2/02 1400	14.60	24.10	28.00	22.00	3.90	72	0.007	329	401
10/2/02 1500	16.50	26.10	28.00	23.10	1.90	40	0.006	313	352
10/2/02 1600	16.10	26.20	28.00	23.30	1.80	37	0.006	294	331
10/2/02 1700	23.30	25.60	28.00	22.90	2.40	71	0.006	459	530
10/2/02 1800	26.70	25.10	27.90	24.50	2.80	95	0.004	366	461
10/2/02 1900	32.00	25.60	27.90	25.20	2.30	93	0.003	358	452
10/2/02 2000	47.20	25.90	27.60	25.40	1.70	102	0.003	442	544
10/2/02 2100	33.70	25.70	27.10	25.50	1.40	60	0.002	223	283
10/2/02 2200	25.10	25.70	26.90	24.50	1.20	38	0.003	238	276
10/2/02 2300	20.70	26.00	27.00	24.20	1.00	26	0.003	227	253
10/3/02 0000	19.50	27.30	27.00	24.40	-0.30	-1	0.003	199	198
10/3/02 0100	17.00	26.50	26.80	23.90	0.30	6	0.003	189	196
10/3/02 0200	16.20	26.80	26.40	23.90	-0.40	-1	0.003	153	153
10/3/02 0300	16.00	26.70	26.30	23.80	-0.40	-1	0.003	150	150
10/3/02 0400	15.40	27.10	26.00	24.00	-1.10	-2	0.002	115	114
10/3/02 0500	13.80	27.40	25.90	24.30	-1.50	-2	0.002	83	81
10/3/02 0600	12.10	27.40	26.20	24.40	-1.20	-1	0.002	83	81
10/3/02 0700	14.20	26.20	26.30	23.10	0.10	0	0.004	167	167

(table continued)

	Wind (m s^{-1})	Air Temp (°C)	Water Temp (°C)	Dewpoint Temp (°C)	t_{sea} - t_{air}	Sensible Heat Flux (W m^{-2})	q_{sea} - q_{air}	Latent Heat Flux (W m^{-2})	Total Heat Flux (W m^{-2})
42041									
10/2/02 1200	9.10	27.00	28.20	24.40	1.20	15	0.005	149	164
10/2/02 1300	9.60	28.30	28.10	24.20	-0.20	0	0.005	160	160
10/2/02 1400	13.10	24.80	28.10	23.50	3.30	59	0.006	253	312
10/2/02 1500	9.40	27.10	28.10	24.10	1.00	13	0.005	160	173
10/2/02 1600	12.80	27.60	28.10	23.40	0.50	9	0.006	252	261
10/2/02 1700	11.80	27.60	28.10	24.30	0.50	8	0.005	192	201
10/2/02 1800									
10/2/02 1900	13.20	26.20	28.10	23.80	1.90	34	0.005	241	276
10/2/02 2000	13.50	26.70	28.10	24.30	1.40	26	0.005	221	247
10/2/02 2100	13.60	26.90	28.10	24.80	1.20	22	0.004	196	218
10/2/02 2200	16.20	26.20	28.10	24.40	1.90	42	0.005	260	302
10/2/02 2300	16.20	26.20	28.10	25.50	1.90	42	0.003	188	230
10/3/02 0000	21.70	25.80	28.00	25.40	2.20	65	0.003	252	317
10/3/02 0100	25.50	25.30	28.00	25.10	2.70	94	0.004	329	423
10/3/02 0200	27.80	25.70	27.90	25.60	2.20	84	0.003	289	373
10/3/02 0300	29.10	26.10	27.90	25.70	1.80	72	0.003	291	362
10/3/02 0400	26.40	26.30	27.80	25.70	1.50	54	0.003	250	304
10/3/02 0500	22.80	26.90	27.70	25.80	0.80	25	0.002	195	220
10/3/02 0600	21.80	27.20	27.60	25.20	0.40	12	0.003	230	242
10/3/02 0700	20.5	27.2	27.5	25	0.3	8	0.003	240	248

latent heat flux values ranged from 550 W m^{-2} on the low side to 1,992 W m^{-2} as a maximum

with a mean of 1,108 W m^2. To evaluate the heat flux values from Lili against the TCBD,

relevant times where Lili's center was within 0.75° latitude radially of each buoy was considered

(Figure 1). For 42001, the applicable times were 1600 UTC 2 October 2002 through 2300 UTC

2 October 2002 covering the final 2 h during a rapid intensification and through all but 1 h of the

subsequent minor intensification. For 42041, the relevant times were during the rapid weakening

phase (0000 UTC 3 October 2002 until 0700 UTC 3 October 2002). Sensible heat flux values

for 42001 during the intensification periods ranged from a minimum of 26 W m^{-2} to a maximum

of 102 W m^{-2} with a mean of 61 W m^{-2}. While the Lili 42001 minimum was larger than the 17

W m^{-2} of the TCBD, the mean and maximum calculations still registered much lower. This

maximum hourly sensible heat flux value at 42001 occurred during the hour of highest wind

speed (Table 15 10/2/02 2000) All of the sensible heat flux values at 42041 fell far short of the

TCBD results. At 42041, sensible heat flux values ranged from a minimum of 12 W m^{-2} to a

maximum of 94 W m^{-2} with a mean of 52 W m^{-2}. The maximum at 42041 resulted from the

largest t_{sea} - t_{air} value over the considered time period (Table 15 10/3/02 0100) even though the

wind speed had not reached its peak. For latent heat flux numbers, 42001 showed a mean of 314

W m^{-2} with a low value of 223 W m^{-2} and the highest reaching close to the TCBD minimum

value of 550 W m^{-2}. Lili's maximum latent heat flux value at 42001 resulted from wind speed >

20 ms^{-1} and a -0.4 °C dewpoint temperature change (Table 15 10/2/02 1700). At 42041 the

latent heat flux values were even lower than at 42001, and thus farther from the TCBD values.

Buoy 42041 showed a minimum of 195 W m^{-2}, a maximum of 329 W m^{-2}, and a mean of 259 W

m^{-2} for latent heat flux values. All of the TBCD referenced latent heat flux values were higher

than the Lili values for both 42001 and 42041. However, TCBD surface moisture parameters

were calculated with only 14 measurements contained within about 10 cyclones. With a minimum latent heat flux value of 550 W m^{-2} for those 14 measurements, it is quite possible that the TCBD calculations consisted mainly of storms which traversed over the warmer and deeper Atlantic waters, Gulf Stream, or GOM Loop Current. Also, wind speed-dependent bulk aerodynamic transfer coefficients ($C_T = C_E = (a + bU_{10}) \times 10^{-3}$) were used in the TCBD calculations, where constants a and b were chosen for $U_{10} > 20$ m s^{-1} conditions. These transfer coefficients, which increase as wind speed increases, caused TCBD heat flux calculations to be larger than values here from Eq. (2) and Eq. (3). Garratt (1992) validated that the best datasets over a wide range of wind speeds (up to 25 m s^{-1}) only yielded $C_T \approx C_E \approx 1.1 \times 10^{-3}$ with an error of $\pm 15\%$. So these TCBD ranges could be overestimates.

Hurricane Opal, a Gulf of Mexico storm in 1995, underwent a similar rapid intensification stage and a less dramatic weakening event as Lili. For Opal, buoy 42001 observations yielded values of latent heat flux between 300 and 1,200 W m^{-2} and a sensible heat flux maximum around 200 W m^{-2} (Shay et al. 2000). These values were calculated during an intense atmospheric and oceanic forcing time frame which included encountering a warm eddy (Shay et al. 2000). They estimated total air-sea heat fluxes values of 2,000 W m^{-2}, as a percentage of the total ocean heat content loss. A model study of Opal inferred a surface heat flux of 2,000 – 3,000 W m^{-2} over the same period (Hong et al. 2000). Heat flux calculations during Lili were much lower than these Opal studies. This again was because Shay et al. (2000) used wind speed-dependent bulk aerodynamic transfer coefficients, although no formula is presented in their manuscript. Thus, Shay et al. (2000) heat flux values would expectedly be larger than the calculations in this study using Eq. (2) and Eq. (3) because their transfer coefficients of C_T and C_E increased with higher wind speeds. Hong et al. (2000) also did not

include a formula or any information about transfer coefficients. Since the Hong et al. (2000) model numbers matched the buoy heat flux values (Shay et al. 2000), the same assumptions about higher transfer coefficients can be made. Lili and Opal heat flux values were more comparable when 42001 data from Opal were calculated using Eq. (1) and Eq. (2) (Table 16). Shay et al. (2000) assumed 85% relative humidity (RH) because 42001 did not have a humidity sensor during Opal. Since Lili's RH averaged 81% at 42001 and 83% at 42041, the Lili data was calculated with the higher 85% RH and the Opal data with the lower 81% RH (Table 16). Water temperatures were warmer during Opal by ≈1.2 °C. Lili heat flux values were superior to Opal heat flux values at 85% RH because the wind remained higher for a longer period of time.

A temperature sensitivity analysis was initiated to determine what effect oceanic cooling from Isidore had upon the intensity changes specifically. The +1 °C sensitivity analysis simulated what heat flux values could have been if buoy 42001 and 42041 water temperatures had remained at pre-Isidore levels. The -2 °C sensitivity analysis was based upon the observed maximum SST change along Lili's path in the GOES-8 composites (Figure 34). Since the comparison analysis earlier showed water temperature cooling from Isidore was < 1 °C for both 42001 and 42041 (Table 13), this substitution of lower water temperatures simulated what heat flux values might have been if the ocean temperature had not rebounded somewhat before Lili. Figures 35 and 36 graphically depict the sensitivity calculations and the congruent water temperatures. The most significant results were revealed in the +1 °C sensitivity analysis for latent heat flux values (Figures 35 and 36 circles). At 42001 (1600 UTC 2 October 2002 through 2300 UTC 2 October 2002), sensible flux values ranged from 48 to 152 W m^{-2} with a mean of 95 W m^{-2}, which were still inferior to TCBD values. The latent heat values were lower than the TCBD ranges as well only registering from 301 to 625 W m^{-2} with a mean of 431W m^{-2}.

Table 16. Hurricane Opal (1995) and Hurricane Lili (2002) heat flux value ranges calculated with Eq. (1) and Eq. (2).

	Latent Heat Flux (W m^{-2})	Sensible Heat Flux (W m^{-2})	Total Heat Flux (W m^{-2})
85 % RH			
Opal 42001	200-620	9-108	211-728
Lili 42001	183-840	-1-102	180-942
Lili 42041	195-535	1-87	197-620
81% RH			
Opal 42001	244-689	9-108	254-796
Lili 42001	199-459	-1-102	198-544
Lili 42041	188-329	8-94	218-423

For 42041 during the Lili relevant time period of 0000 UTC 3 October 2002 through 0700 UTC 3 October 2002, the rates were closer to the TCBD ranges though still overall less. At 39 W m^{-2}, the 42041 sensible heat flux rate exceeded the TCBD minimum, but the mean and maximum (88 and 133 W m^{-2}) still did not come close to the TCBD numbers. For latent heat flux at 42041, the levels were actually lower than at 42001 because Lili was undergoing a rapid weakening stage. Thus, 42041 latent heat values were appreciably less than the TCBD values ranging from 315 to 465 W m^{-2} and averaging 389 W m^{-2}. Again when evaluating the seemingly large difference between the Lili +1 °C sensitivity analysis and TCBD database latent heat flux values, it is prudent to keep in mind the higher transfer coefficients and statistical shortcoming mentioned earlier. When compared to the Opal studies, +1 °C sensitivity latent heat flux values met the Shay et al. (2000) minimum of 300 W m^{-2}, but registered only half the maximum of 1,200 W m^{-2}. Total heat flux values from the Hong et al. (2000) model simulation were still significantly higher than the +1 °C sensitivity analysis.

Figure 35. 42001 sensitivity analysis heat flux values and water temperatures for +1 °C (circles), observed (solid line), and -2 °C (squares). Wind speed is included for reference.
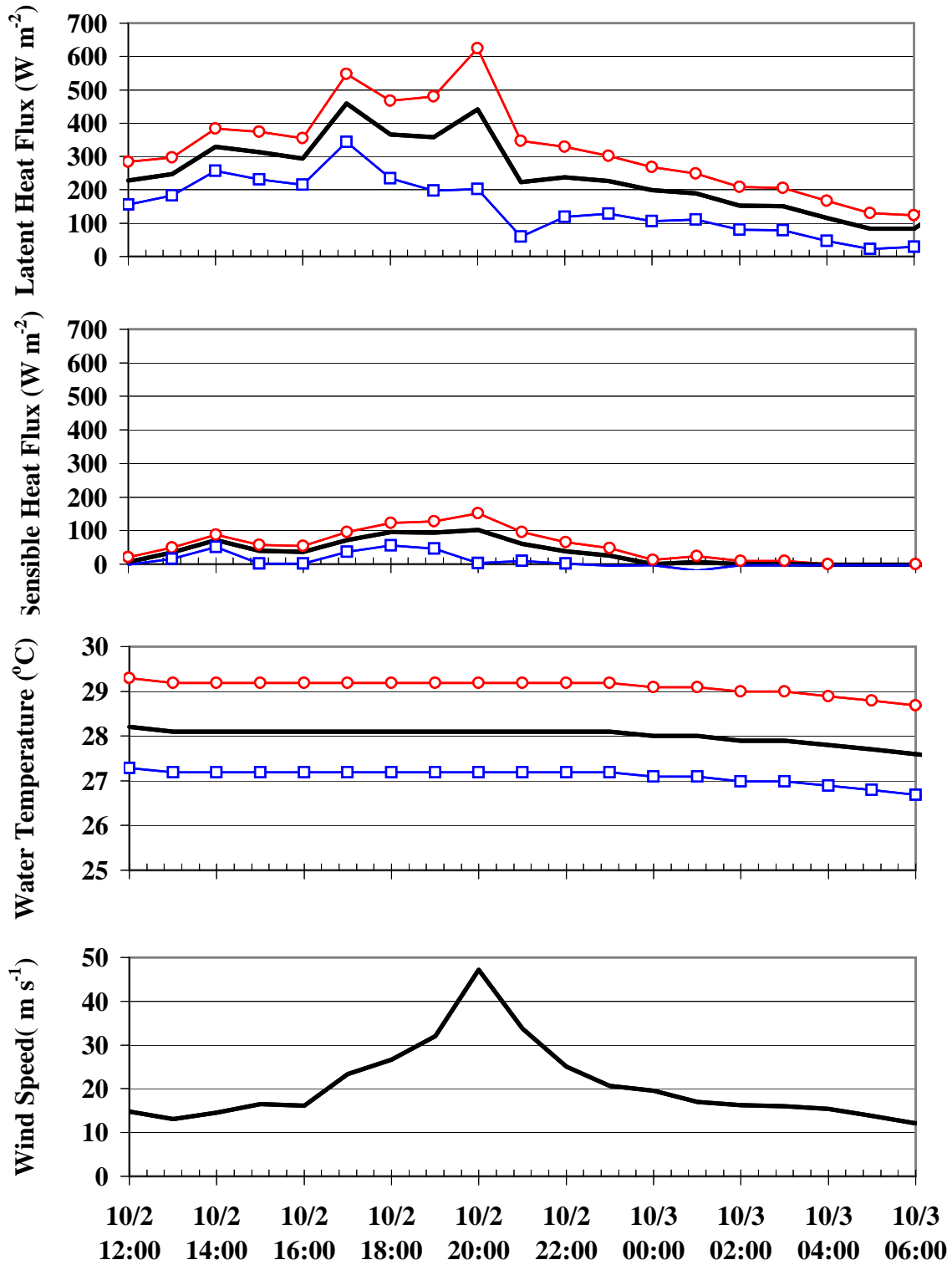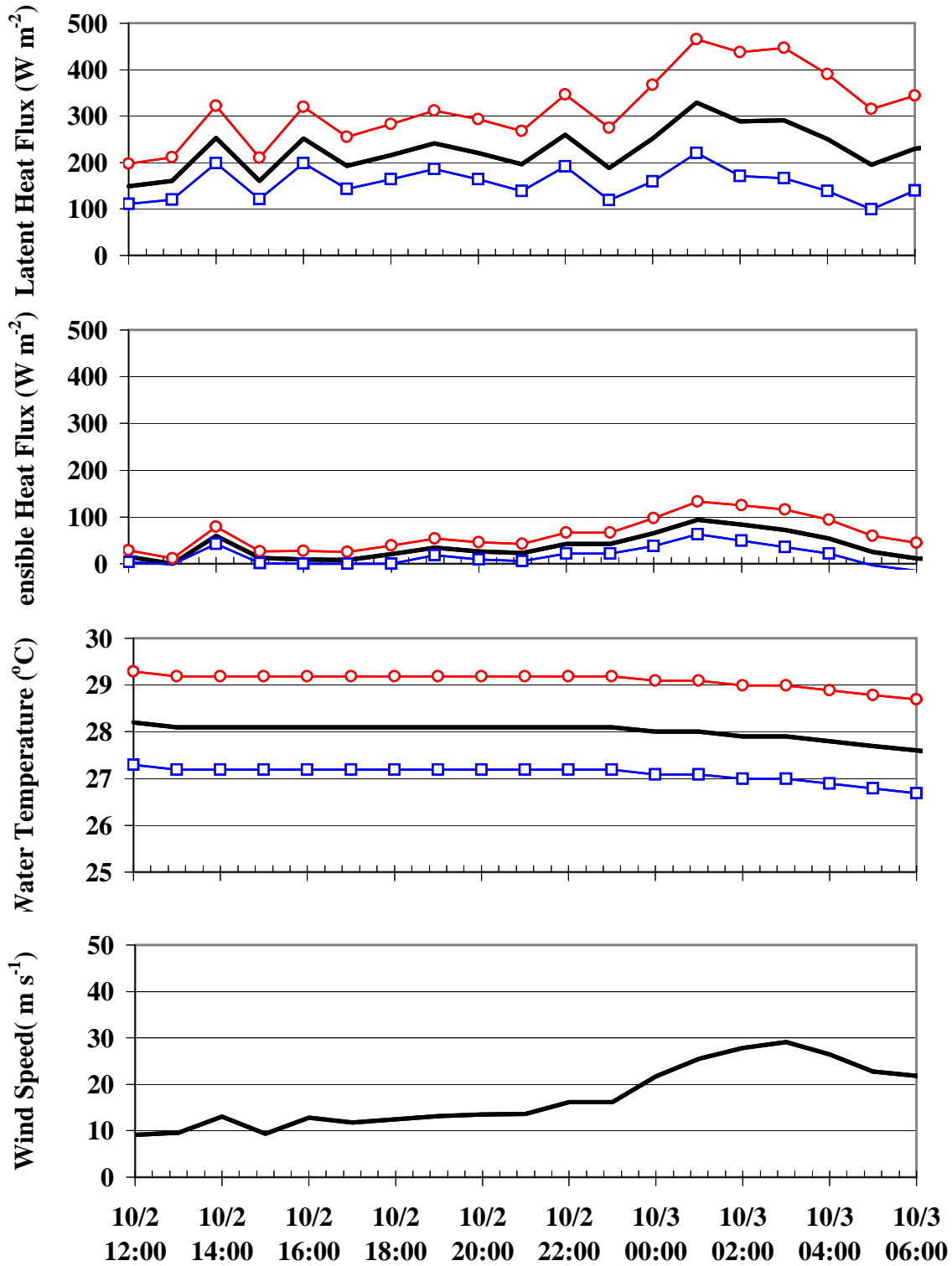
Figure 36. 42041 sensitivity analysis heat flux values and water temperatures for +1 °C (circles), observed (solid line), and -2 °C (squares). Wind speed is included for reference.

141

The next question was to investigate if the increase between the observed heat flux calculations and the +1 °C sensitivity analysis remained consistent throughout the higher wind speed conditions encountered at 42001 and 42041. It was hoped that this would further isolate the effect warmer water temperatures would have had upon the rapid weakening phase of Lili. Sensible heat flux values showed the largest percentage increases in the +1 °C sensitivity analysis (Table 17). This would be expected as the t_{sea} - t_{air} component increased. At both 42001 and 42041, maximum effects of +1 °C were during higher wind speeds (Table 17; Figure 35 - 36). Although 42001 had the largest increase in latent heat flux at the wind speed peak (Table 17; 182 W m^{-2}), 42041 had a longer trend increase because of the slightly higher water temperature used in the analysis. Raising water temperature had more of an effect during the decay phase as illustrated by 42041 latent heat flux increases all > 100 W m^{-2}.

d. Ocean Heat Content

Ocean heat content in the well-mixed upper-ocean layer has been shown to be more significant than SST when discussing tropical cyclone intensification (Shay et al. 2000). DeMaria and Kaplan (1994b) found upper layer climatological SSTs explained the large variation in tropical cyclone wind speed increases. The Loop Current is a permanent circulation feature which brings warm waters into the Gulf of Mexico from the Caribbean Sea. This circulation meanders and often sheds off eddies, but general temperature structure has been demonstrated (Vukovich et al. 1979; Muller-Karger and Walsh 1991). Satellite altimetry sea-surface height (SSH) data aids in detecting oceanic features such as the Loop Current in summer when surface temperature is not representative of the total water column heat content. SSH depicts anti-cyclonic regions of downwelling and cyclonic regions of upwelling (Figure 37). Satellite altimeter data on 1 October 2002 illustrated that the first rapid intensification (RI) phase

Table 17. Increase over the observed heat flux values for the +1 °C sensitivity analysis during direct storm effect at each buoy. Wind speed is included for reference.

	Wind (m s^{-1})	Water Temperature Increase (°C)	Sensible Heat Flux Increase (W m^{-2})		Latent Heat Flux Increase (W m^{-2})	
42001						
10/2/02 1600	16.1	0.84	17	47%	60	21%
10/2/02 1700	23.3	0.84	25	35%	88	19%
10/2/02 1800	26.7	0.84	28	30%	101	27%
10/2/02 1900	32	0.84	34	37%	122	34%
10/2/02 2000	47.2	0.84	50	49%	182	41%
10/2/02 2100	33.7	0.84	36	60%	124	56%
10/2/02 2200	25.1	0.84	27	70%	91	38%
10/2/02 2300	20.7	0.84	22	84%	75	33%
42041						
10/3/02 0000	21.7	1.09	32	50%	116	46%
10/3/02 0100	25.5	1.09	38	40%	137	42%
10/3/02 0200	27.8	1.09	42	50%	149	52%
10/3/02 0300	29.1	1.09	44	61%	156	54%
10/3/02 0400	26.4	1.09	39	73%	141	56%
10/3/02 0500	22.8	1.09	34	136%	120	62%
10/3/02 0600	21.8	1.09	33	271%	114	50%
10/3/02 0700	20.5	1.09	31	363%	106	44%

of Lili occurred when the center of Lili went over the deep Loop Current (Figure 37 red contours), but the second RI phase and rapid weakening (RW) phase were when Lili's center was over less deep features (Figure 37 black contours). During second RI and other intensification phases, the eastern side of Lili's circulation did encounter an anticyclone (26 °N, 87.5 °W). However, the main core of convection about the center did not directly traverse any higher sea-surface heights after the first RI phase. Along Lili's track, satellite-derived SST remained above 28 °C through her entire life cycle until the center passed 28 °N latitude (Figure 38). Since rapid intensifications only took place in the GOM, heat content in the Loop Current and its eddies
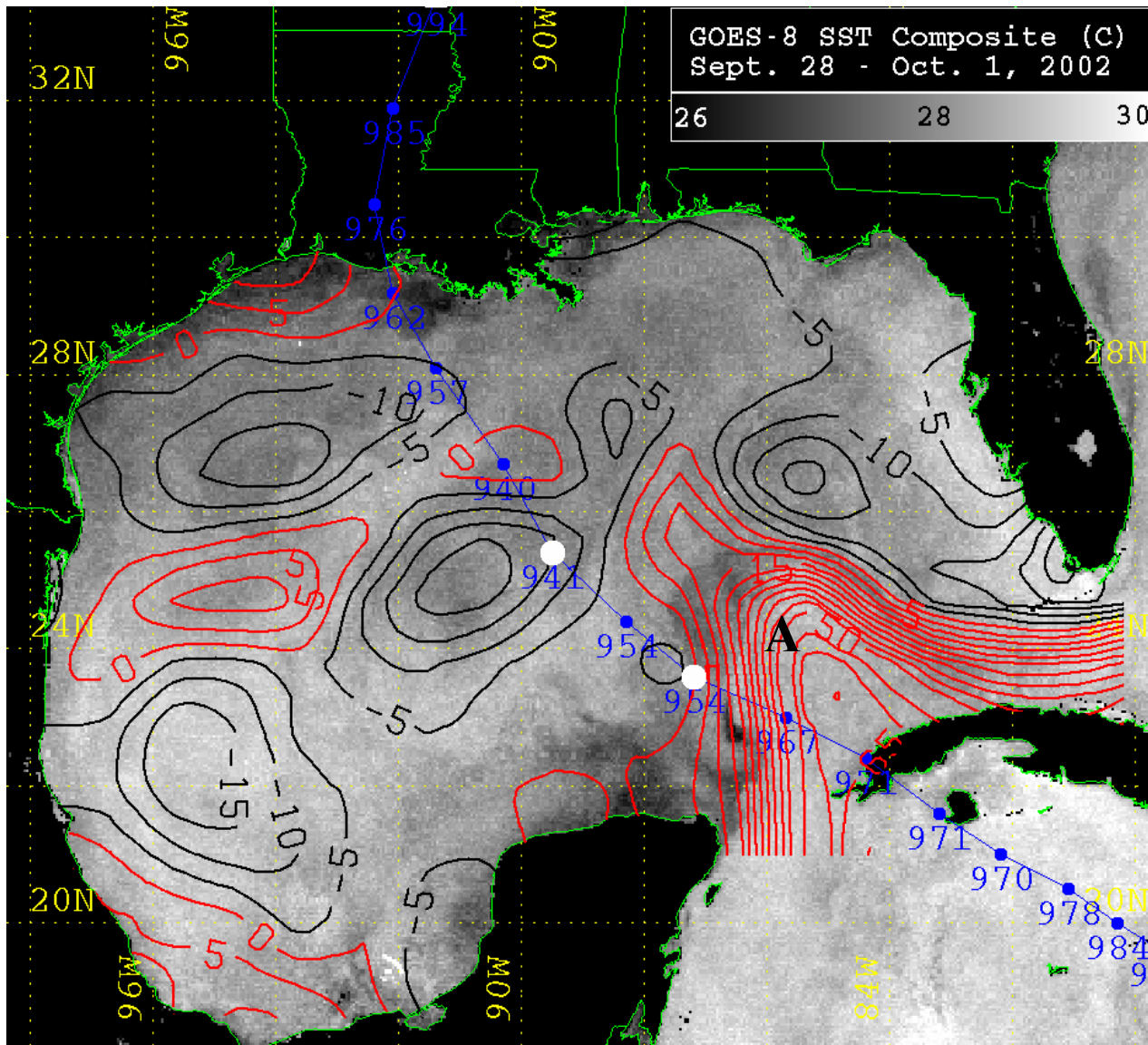
Figure 37. Post-Isidore GOES-8 SST (°C) composite with 1 October 2002 altimetry data (cm) superimposed showing the Loop Current (A), anticyclones (red contours), and cyclones (black contours). Lili's track (blue line) is included with the end of the two RI periods (white dots) marked.
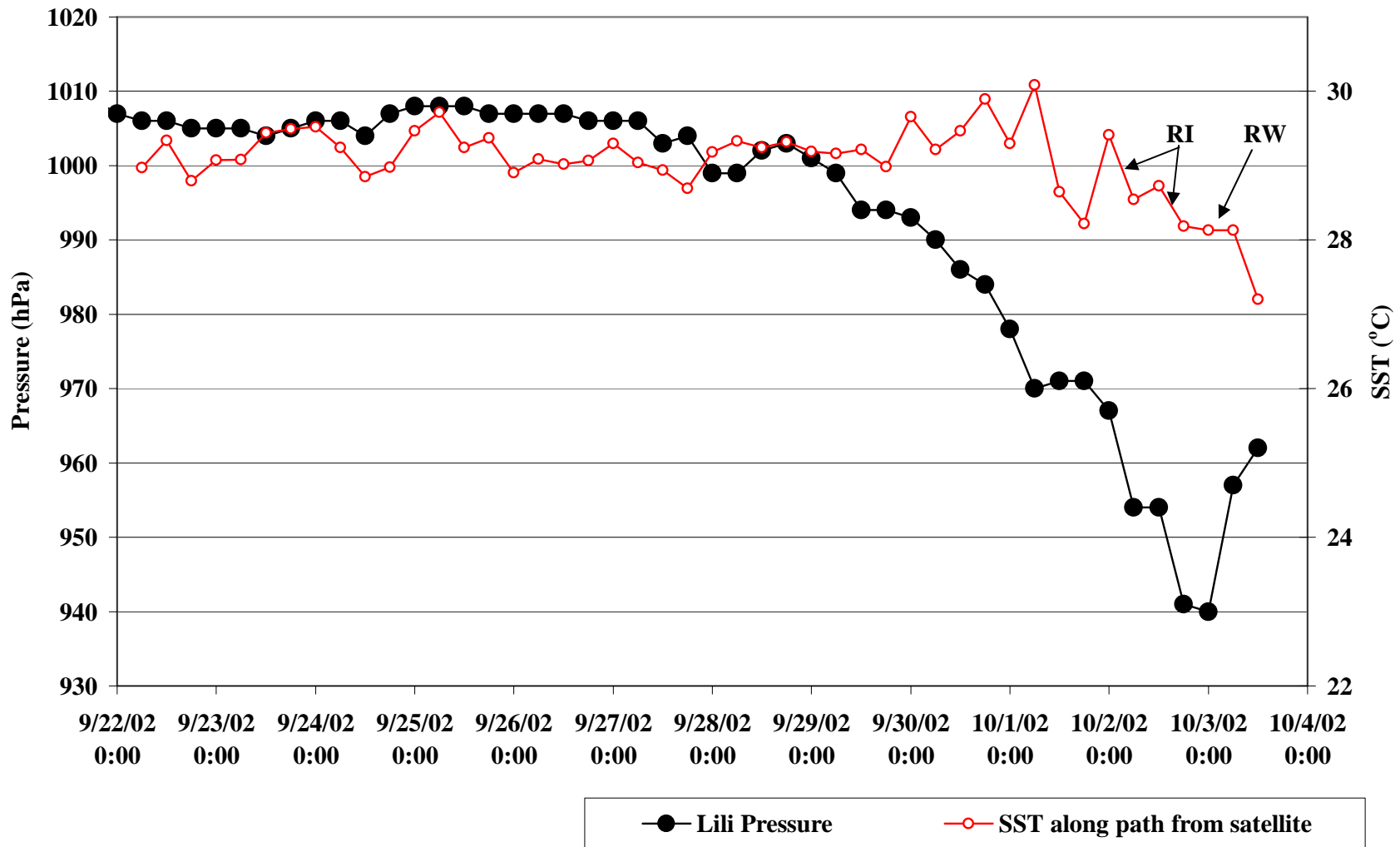
Figure 38. Post-Isidore GOES-8 SST composite temperatures (°C; red line) sampled along Lili's track at the NHC 6 h best track center locations until landfall. Pressure (hPa; black dots) is provided for reference.

should be considered in rapid intensification. Schade (2000) described that tropical cyclone intensity is more sensitive to SST directly under the center of circulation than the surrounding SST field. The influence of the temperature field under all of a hurricane's circulation is not meant to be underestimated here as it does provide necessary latent heat energy for the microscale convective processes of the cyclone. However, ocean heat content directly under the center of the hurricane appears more essential for rapid intensification as seen in Hurricane Opal (Shay et al. 2000) and Lili's first RI phase.

5. Summary and Conclusions

Temporal comparison results showed that SST in the Gulf of Mexico pre and post-Isidore was > 28 °C and thus warm enough to support a hurricane. The largest water temperature decrease was west of Isidore's track at 42002 (1.4 °C) and not nearest to the track at 42001 and 42041. GOES-8 SST composite imagery correlated well with in-situ buoy data and showed a post-Isidore maximum water temperature change of -2 °C along Lili's future path. Heat flux variation during the month inclusive of Isidore and Lili illustrated that wind speed was the driving mechanism when >10 m s^{-1}. During lower wind speed events, latent heat flux was driven more by the q_{sea} - q_{air} parameter and usually resulted from a decrease in dewpoint temperature. Sensible heat flux during low wind events was driven by increased t_{sea} - t_{air} which usually resulted from a decrease in air temperature. Decreases in the heat flux values after Isidore exist and therefore Isidore's path had some impact upon the ocean conditions for Lili, especially right along her track at buoys 42001 and 42041. Buoy 42001 exhibited the largest latent and total heat flux decrease post-Isidore, but a day later Lili strengthened while near this buoy. Buoy 42041 was closest to Isidore's track yet showed a gain in evaporative energy post-Isidore. Two days

later, Lili would weaken while in the vicinity of 42041. This shows the variability inherent in-situ surface point observations and relating those to the larger environmental feature cyclone.

Non-storm sensible heat flux values were generally lower than tropical ocean conditions determined during the COARE program (Fairhall et al. 1996) and Gulf of Mexico (GOM-HF) September and October conditions (Hsu 1997). Pre-Isidore latent heat flux values were within the ranges of COARE and GOM-HF, but varied slightly post-Isidore. Both 42001 and 42041 along Isidore's track were lower than general tropical ocean latent heat flux values. Heat flux values for 42001 and 42041 during Lili's intensity phases were compared to a tropical cyclone buoy measurement database (TCBD; Cione et al. 2000) and another rapidly intensifying hurricane (Opal 1995). During an intensification stage of Lili, the maximum latent heat flux values at 42001 only reached the TCBD minimum value. During the weakening stage of Lili, buoy 42041 was considerably below the tropical cyclone database. When compared to Opal studies (Hong et al. 2000; Shay et al. 2000), heat flux values for Lili were significantly lower. Wind-speed dependent energy transfer coefficients were offered as an explanation for the large differences. Lili and Opal heat flux values were more comparable when buoy 42001 Opal data was calculated using the same equations. Lili values were slightly higher because of a longer period of high wind speeds. When humidity levels between the two storms were equalized, Opal values were higher because of approximately 2 °C warmer water temperatures.

The +1 °C sensitivity analysis illustrated that warmer water temperatures influenced sensible heat flux as evidenced by large percentage increases. Observed and +1 °C sensitivity analysis water temperatures were $\geq$28 °C threshold in the literature. Maximum effects of the +1 °C sensitivity analysis were seen during the higher wind speeds. Latent heat flux at buoy 42041 increased > 100 W m^{-2} (+ 40%) between the +1 °C sensitivity analysis and observed values.

147

This demonstrated that cooler waters may have had an impact on Lili's weakening phase at 42041 through a reduction in evaporation. Satellite-derived SSH illustrated one of Lili's rapid intensification phases occurred over the deep Loop current. However, Lili's eye was not over a higher SSH area when a subsequent rapid intensification occurred. Based upon Opal studies and the location of Lili's first rapid intensification phase, ocean heat content influences rapid intensification more so when the center passes directly over a deeper reservoir of warm water.

CHAPTER 5. SUMMARY AND CONCLUSIONS

Rapid intensity changes of Hurricane Lili in the Gulf of Mexico were studied in three distinct ways: climatology, satellite remote sensing, and surface meteorological and oceanographic measurements. Each research methodology provided characteristics of Hurricane Lili's intensity behavior.

To lend perspective, rapid intensity change events were assessed through the creation of a minimum central pressure climatology. Results showed rapid and explosive intensification events were frequent, especially in the GOM. Timing of the event since storm formation exhibited no convincing pattern. Timing before landfall clustered around ≤ 24 h for the majority of GOM rapid events and all of the GOM explosive events. This illustrated an important consideration for emergency management officials, that a hurricane's core intensity could be intensifying although the rest of the circulation could be weakening from detrimental land effects. Louisiana had the most storms containing rapid intensification events landfall there. However, an explosive deepening event storm has yet to make landfall in Louisiana, Mississippi, or Alabama. No rapid or explosive events occurred near the coasts in the southwestern, northwestern, or extreme eastern areas of the GOM. However, conditions have been more favorable for rapid intensification within the GOM east of 90 °W over the last decade. Lili emerged anomalous as the only hurricane to weaken at a greater rate (+17 hPa over 6 h or +2.83 hPa h^{-1}) than its rapid intensification event rate (-13 hPa over 6 h or -2.16 hPa h^{-1}). These climatology results exemplify that hurricane intensity forecasting should include recognition of a GOM predisposition to rapid and explosive intensification, especially within 24 h of landfall. Also, most GOM tropical cyclones weaken a significant amount after intensification, but not

100% of the time and none has weakened at a greater rate than the intensification except for the case of Hurricane Lili.

GOES-8 satellite water vapor brightness temperature data were investigated using a -24 °C vapor front to delineate a dry air mass west of Lili. Drier air west of Lili was shown to affect the hurricane during a rapid weakening phase once the two features were less than 250 km mean or 215 km minimum distance apart. These critical distances are offered as possible criterion for a relationship between tropical cyclone intensity weakening and dry air advection. Water vapor brightness temperatures cooler than the -24 °C threshold did not have to entrain into Lili's core circulation to negatively affect the convective processes and symmetrical nature of the hurricane. During the time periods when Lili was rapidly intensifying or maintaining intensity, the -24 °C vapor front exhibited more broken signatures of definitive interruptions, shape changes, and protrusions. The -24 °C vapor front was a smooth, strong, and wide boundary line during the rapid weakening phase and early in the 30-h time period when Lili's center and the vapor front were the greatest distance apart. The dry air mass was shown to have the greatest effect upon Lili during phases after rapid intensification. In the hours before rapidly weakening, Lili was slightly intensifying and a lag effect of convective breakdown from outer circulation into the main core was offered as explanation. Dry air core distances have been related to track forecasting (Martin 2001), but the -24 °C vapor front distance and visual descriptions were more directly linked to intensity changes here. These results provide tools to interpret satellite water vapor imagery which can help to forecast and nowcast rapid intensity changes in absence of other measurements such as coastal observation networks or flight-level reconnaissance data. Future research on other tropical cyclones may substantiate the critical distances as an important forecasting technique for tropical cyclone intensity changes.

Tropical Storm Isidore cooled surface water temperatures by approximately 1 °C at buoy locations a week prior to Lili. GOES-8 SST composites showed a maximum loss along Lili's path of -2 °C. Pre-Isidore water temperatures were shown to increase latent heat flux values by > 100 W m^{-2} (+ 40%) over observed values during Lili's weakening phase. Lili's values were lower than those in a tropical cyclone database (Cione et al. 2000) and Hurricane Opal studies (Hong et al. 2000; Shay et al. 2000). Lili's heat flux calculations were comparable to Opal when humidity level and transfer coefficients in the equations were equalized between the two storms. Wind speed was shown to be the driving mechanism in heat flux values when > 10 m s^{-1}. During lower wind periods, latent heat flux responded more to q_{sea} - q_{air} increase usually a result of dewpoint temperature decrease. Sensible heat flux during low wind periods was driven by the t_{sea} - t_{air} parameter which usually resulted from air temperature decrease. SST and heat flux calculations illustrated that oceanic contributions into hurricane intensity were more significant during rapid intensification periods. SSH data confirmed Lili's first rapid intensification phase occurred over the Loop Current, and illustrated ocean heat content directly under the center of a hurricane appears more essential for rapid intensification

Different mechanisms appeared to be more significant in the separate rapid intensification and weakening phases of Lili. Oceanic contributions were proven to be the dominate factor in rapid intensification based on analyses of water temperature, sea-surface height, and heat fluxes. Dry air advection was proven to be the governing factor in rapid weakening as satellite data showed Lili was affected 7 or 8 h prior to, and during a rapid weakening phase. Because both the atmospheric and oceanic contributions are important in the complicated tropical cyclone system, these results will help to focus attention on specific parameters when forecasting and nowcasting intensity.

Climatology results showed a predisposition in the GOM to rapid and explosive intensification ≤24 h before landfall, with general confidence that significant weakening occurs afterward. Since the level of weakening is not always equal to or greater than the previous intensification, any additional information assessing the realistic situation can be helpful to those forecasting and making decisions, especially within the 48 h before landfall. Future research goals include analyzing other storms to verify the relationship between intensity changes and the -24 °C vapor front in satellite imagery. Verification of the 250 mean and 215 minimum critical distances will provide interpretive tools which apply across more than just this one case study.

REFERENCES

Abraham, J., J.W. Strapp, C. Fogarty, and M. Wolde, 2004: Extratropical transition of Hurricane Michael: An aircraft investigation. *Bull. Amer. Meteor. Soc.*, **85**, 1,323-1,338.

Anthes, R. A., 1982: *Tropical Cyclones:Their Evolution, Structure, and Effects*. American Meteorological Society, 208 pp.

Bender, M. A., I. Ginnis, and Y. Kurihara, 1993: Numerical simulation of tropical cyclone-ocean interaction with a high-resolution model version 4 (MM4), *J. Geophys. Res.*, **98**, 23,245-23,263.

--------, M. A., I. Ginnis, and Y. Kurihara, 2000: Real case simulation of hurricane-ocean interaction using a high-resolution coupled model: Effects on hurricane intensity. *Mon. Wea. Rev.*, **128**, 917-946.

Bishop, J.M., 1984: *Applied Oceanography*. John Wiley & Sons, 251 pp.

Black, P.G., 1983: Ocean temperature changes induced by tropical cyclones. Ph.D. dissertation, The Pennsylvania State University, 278 pp.

Bosart, L. F., C. S. Velden, W. E. Bracken, J. Molinari, and P. G. Black, 2000: Environmental influences on the rapid intensification of Hurricane Opal (1995) over the Gulf of Mexico. *Mon. Wea. Rev.,* **128**, 322-352.

Byers, H.R.,1944: *General Meteorology*. McGraw-Hill, 645 pp.

Cione, J. J., P. G. Black, and S. H. Houston, 2000. Surface observations in the hurricane environment. *Mon. Wea. Rev.*, **128**, 1550-1561.

-------, J. J. and E. W. Ulhorn, 2003. Sea surface temperature variability in hurricanes: Implications with respect to intensity change. *Mon. Wea. Rev.*, **131**, 1783-1796.

Chen, K.S., J.T. Wang, and L.M. Mitnik, 2001: Satellite and ground observations of the evolution of Typhoon Herb near Taiwan. *Rem. Sens. Env.*, **75**, 397-411.

Croxford, M. and G.M. Barnes, 2002: Inner core strength of Atlantic tropical cyclones. *Mon Wea. Rev.*, **130**, 127-139.

DeMaria, M. and J. Kaplan, 1994a: A Statistical Hurricane Prediction Scheme (SHIPS) for the Atlantic Basin. *Wea. Forecasting*, **9**, 2309-220.

----- 1994b: Sea surface temperature and the maximum intensity of Atlantic tropical cyclones. *J. Climate*, **7**, 1,324-1,334.

Dodge, P., R. W. Burpee, and F. D. Marks, 1999: The kinematic structure of a hurricane with sea level pressure less than 900 mb. *Mon. Wea. Rev.*, **127**, 987-1,004.

Dunn, G. E. and B. I. Miller, 1964: *Atlantic Hurricanes*. Louisiana State University Press, 377 pp.

Dvorak, V.F., 1984. Satellite observed upper level moisture patterns associated with tropical cyclone movement. *Proc. 15th conference on Hurricanes and Tropical Meteorology*, Miami, FL, Amer. Met. Soc., 163-168.

---------, V.F., 1993. A workbook on tropical clouds and cloud systems observed in satellite imagery. NOAA/NESDIS/NWS 43AANE802322, 359 pp.

---------, V.F. and H.M. Mogil, 1994. Tropical cyclone motion forecasting using satellite water vapor imagery. NOAA Tech. Rep. NESDIS 83, 42 pp.

Elsberry, R.L., G. Holland, H. Gerrish, M. DeMaria, C. Gourd, and K.A. Emmanuel, 1992: Is there any hope of tropical cyclone intensity prediction?- A panel discussion. *Bull. Amer. Meteor. Soc.*, **73**, 264-275.

Emanuel, K., 2000: A statistical analysis of tropical cyclone intensity. *Mon. Wea. Rev.*, **128**, 1,139-1,152.

Fairhall, C. W., E. F. Bradley, D. P. Rogers, J. B. Edson, and G. S. Young, 1996: Bulk parameterization of air-sea fluxes for Tropical Ocean-Global Atmosphere Coupled-Ocean Atmosphere Response Experiment, *J. Geophys. Res.*, **101**, 3,747-3,764.

Frederick, W. J., The rapid intensification and subsequent rapid weakening of Hurricane Lili as compared with historical hurricanes. *Wea. Forecasting*, **18**, 1,295-1,298.

Garratt, J.R., 1992: *The Atmospheric Boundary Layer*. Cambridge University Press, 316 pp.

Goerss, J.S., C.S. Veldon, and J.D. Hawkins, 1998: The impact of multispectral GOES-8 wind information on Atlantic tropical cyclone track forecasts 1995. Part II: NOGAPS forecasts. *Mon. Wea. Rev.*, **126**, 1219-1227.

Gray, W.M. 1979: Hurricanes: Their formation, structure, and likely role in the tropical circulation. *Meteorology over the Tropical Oceans*, D. B. Shaw, Ed., Roy. Meteor. Soc., 155-218.

-------------- 1990: Strong association between West African rainfall and U.S. landfall of intense hurricanes. *Science*, **249**, 1,251-1,256.

Hanley, D.E., 2002: The evolution of a hurricane-trough interaction from a satellite perspective. *Wea. Forecasting*, **17**, 916-926.

Hart, R.E. and J.L. Evans, A climatology of extratropical transition of Atlantic tropical cyclones. *J Climate*, **14**, 546-564.

Holliday, C.R., and A.H. Thompson, 1979: Climatological characteristics of rapidly intensifying typhoons. *Mon. Wea. Rev.*, **107**, 1022-1034.

Hong, X., S. W. Chang, S. Raman, L. K. Shay, and R. Hodur, 2000: The interaction between Hurricane Opal (1995) and a warm core eddy in the Gulf of Mexico. *Mon. Wea. Rev.*, **128**, 1347-1365.

Hsu, S. A., 1988: *Coastal Meteorology*. Academic Press, 260 pp.

------------- 1997: Effects of cold-air outbreaks on evaporation and heat loss from three regions in the Gulf of Mexico. *Gulf Mex. Sci.*, **2**, 71-76.

------------ 2002: Coastal meteorology. *Encyclopedia of Physical Science and Technology*, Robert Meyers, Ed., Academic Press, 155-173.

Inoue, M., I.C. Handoh, and G.R. Bigg, 2002: Bimodal distribution of tropical cyclogenesis in the Caribbean: characteristics and environmental factors. *J Climate*, **15**, 2,897-2,905.

Jarvinen, B.R., C.J. Neumann, and M.A.S. Davis, 1984: A Tropical Cyclone Data Tape for the North Atlantic Basin, 1886-1983: Contents, Limitations, and Uses. NOAA Tech. Memo NWS NHC 22, 21 pp.

Jordan, C. L., 1961: Marked changes in the characteristics of the eye of intense typhoons between the deepening and filling stages. *J. Meteo.*, **18**, 779-789.

Kaplan, J. and M. DeMaria, 2003: Large-scale characteristics of rapidly intensifying tropical cyclones in the North Atlantic Basin. *Wea. Forecasting*, **18**, 1093-1108.

Kraus, E. B., 1972: *Atmosphere-Ocean Interaction*. Clarendon Press, 362 pp.

Landsea, C.W., 1993: A climatology of intense (or major) Atlantic hurricanes. *Mon Wea. Rev.*, **121**, 1,703-1,713.

Lawrence, M.B., B.M. Mayfield, L.A. Avila, R.J. Pasch, and E.N. Rappaport, 1998: Atlantic hurricane season of 1995. *Mon. Wea. Rev.*, **126**, 1,124-1,151.

Leben, R.R., G.H. Born, and B.R. Engebreth, 2002: Operational altimeter data processing for mesoscale monitoring. *Mar. Geod.*, **25**, 3-18.

Le Marshall, J.F., W.L. Smith, and G.M. Callan, 1985: Hurricane Debby-An illustration of the complementary nature of VAS soundings and cloud and water vapor motion winds. *Bull. Amer. Meteor. Soc.*, **66**, 258-263.

Malkus, J.S. and H. Riehl, 1960: On the dynamics and energy transformations in steady-state hurricanes. *Tellus*, **12**, 1-20.

Marks, F.D., and L.K. Shay 1998: Landfalling tropical cyclones: Forecast problems and associated research opportunities. *Bull. Amer. Meteor. Soc.*, **79**, 867-876.

Martin, Jr., M.F., 2001: The relationship of water vapor and hurricane track using the GOES-8 satellite. Ph.D. dissertation, Louisiana State University, 543 pp.

Menzel, W.P. and J.F.W. Purdom, 1994: Introducing GOES-I:The first of a new generation of geostationary operational environmental satellites. *Bull. Amer. Meteor. Soc.*, **75**, 757-781.

Merrill, R.T., 1988: Environmental influences on hurricane intensification. *J. Atmo. Sci.*, **45**, 1,678-1,687.

Miller, B. I., 1958: On the maximum intensity of hurricanes. *J. Meteor.*, **15**, 184-195.

Muller, B.M. and H.E. Fuelberg, 1990: A simulation and diagnostic study of water vapor image dry bands. *Mon. Wea. Rev.*, **118**, 705-722.

Muller, R.A. and G.W. Stone, 2001: A climatology of tropical storm and hurricane strikes to enhance vulnerability prediction of the Southeast U.S. coast. *J Coast. Res.*, **17**, 949-956.

Muller-Karger, F.E. and J.J. Walsh, 1991. On the seasonal phytoplankton concentration and sea-surface temperature cycles of the Gulf of Mexico as determined by satellites. *J. Geophys. Res.*, **96**, 12, 645-12,665.

Neumann, C. J., B. R. Jarvinen, C. J. McAdie, and J. D. Elms, 1993: *Tropical Cyclones of the North Atlantic Ocean, 1871-1992*. Historical Climatology Series, 6-2, National Climatic Data Center, 193 pp.

Palmen, E., 1948: On the formation and structure of tropical cyclones. *Geophysica*, **3**, 26-38.

Pasch, R.J., M.B. Lawrence, L.A. Avila, J.L. Beven, J.L. Franklin, and S.R. Stewart, 2004: Atlantic hurricane season of 2002. *Mon. Wea. Rev.*, **132**, 1,829-1,859.

Price, J.F., 1981: Upper ocean response to a hurricane. *J. Phys. Oceanogr.*, **11**, 153-175.

Riehl, H., 1954: *Tropical Meteorology*. McGraw-Hill, 392 pp.

Rodgers, E.B., V.V. Salomonson, and L. Kyle, 1976: Upper tropospheric dynamics as reflected by Nimbus 4 THIR 6.7 µm data. *J. Geophys. Res.*, **81**, 5,749-5758.

---------, E. B., W. S. Olson, V. M. Karyampudi, and H. F. Pierce, 1998: Satellite-derived latent heating distribution and environmental influences in Hurricane Opal (1995). *Mon. Wea. Rev.*, **126**, 1,229-1,247.

Rogers, R. F., and R. E. Davis, 1993: The effect of coastline curvature on the weakening of Atlantic tropical cyclones. *Int. J. Clima,.* **13**, 287-299.

Roll, H. U., 1965: *Physics of the Marine Atmosphere*. Academic Press, 426 pp.

Schade, L. R., 2000: Tropical cyclone intensity and sea surface temperature. *J. Atmos. Sci.*, **57**, 3,122-3,130.

Shay, L. K., G. J. Goni, and P. G. Black, 2000: Effects of a warm oceanic feature on Hurricane Opal. *Mon. Wea. Rev.*, **128**, 1,366-1,383.

Shenk, W.E., R.J. Holub, and R.A. Neff, 1976: A multispectral cloud type identification method developed for tropical ocean areas with Nimbus 3 MRIR measurements. *Mon. Wea. Rev.*, **104**, 284-291.

--------, W.E. and E.B. Rodgers, 1978: Nimbus 3/ATS 3 observations of the evolution of Hurricane Camille. *J. Appl. Meteor.*, **17**, 458-476.

Simpson, R. H., and H. Riehl, 1981: *The Hurricane and Its Impact*. Louisiana State University Press, 398 pp.

Smith, S.D., 1980: Wind stress and heat flux over the ocean in gale force winds. *J. Phys. Oceanogr.*, **10**, 709-726.

Stone, G. W., X.P. Zhang, W. Gibson, and R. Fredericks, 2001: A new wave-current online information system for oil spill contingency planning (WAVCIS). Proc. 24th Arctic and Marine Oilspill Program Technical Seminar, Edmonton, Alberta, Canada, Environment Canada, 401-425.

Titley, D.W., and R.L. Elsberry, 2000: Large intensity changes in tropical cyclones: A case study of Supertyphoon Flo during TCM-90. *Mon. Wea. Rev.*, **128**, 3,556-3,573.

Veldon, C.S., 1984: Applications of VAS and TOVS to tropical cyclones. *Bull. Amer. Meteor. Soc.*, **65**, 1059-1067.

--------, C.S, 1987: Satellite observations of Hurricane Elena (1985) using the VAS 6.7 μm "Water Vapor" channel. *Bull. Amer. Meteor. Soc.*, **68**, 210-215.

--------, C.S., C.M. Hayden, S.J. Nieman, W.P. Menzel, and J.S. Goerss, 1997: Upper-troposheric winds derived from geostationary satellite water vapor observations. *Bull. Amer. Meteor. Soc.*, **78**, 173-195.

--------, C.S., T.L. Olander, and S. Wanzong, 1998: The impact of multispectral GOES-8 wind information on Atlantic tropical cyclone track forecasts 1995. Part I: Dataset Methodology. *Mon. Wea. Rev.*, **126**, 1202-1218.

Vukovich, F.M., B.W. Crissman, M. Bushnell, amd W.J. King, 1979. Some aspects of the oceanography of the Gulf of Mexico using satellite and in situ data. *J. Geophys. Res.*, **84**, 7,749-7,768.

Walker, N.D., S. Myint, A. Babin and A. Haag, 2003: Advances in satellite radiometry for the surveillance of surface temperatures, ocean eddies and upwelling processes in the Gulf of Mexico using GOES-8 measurements during summer. *Geophys. Res. Lett.*, **30**, 1,854-1,858.

Weldon, R.B., and S.J. Holmes, 1991: Water vapor interpretation and applications to weather analysis and forecasting. NOAA Tech. Rep. NESDIS 57, 213 pp.

Zhang, X. P., 2003: Design and implementation of an ocean observing system : WAVCIS (Wave-Current-Surge Information System) and its application to the Louisiana coast. Ph.D. dissertation, Louisiana State University, 194 pp.

APPENDIX: WAVCIS

Stations within the Wave-Current Information System (WAVCIS) field program operated by the Louisiana State University (LSU) Coastal Studies Institute (Stone et al. 2001; Zhang 2003) are included here (Figure 39). WAVCIS particulars are available at http://www.wavcis.lsu.edu/. The WAVCIS stations did not have dewpoint temperature inherently. CSI-3 was the only WAVCIS station where dewpoint temperature could be determined from the humidity sensor by way of the saturation vapor pressure (Hsu 1988)

$$T_{dew} = (237.2 \; x \, \log(e/6.1078)) \; / \; (7.5 - \log(e/6.1078)) \qquad (7)$$

Table 18 provides the temporal comparison analysis results. And Figures 40–42 are the latent and sensible heat flux with the variable parameters graphed over the entire monthly time series.
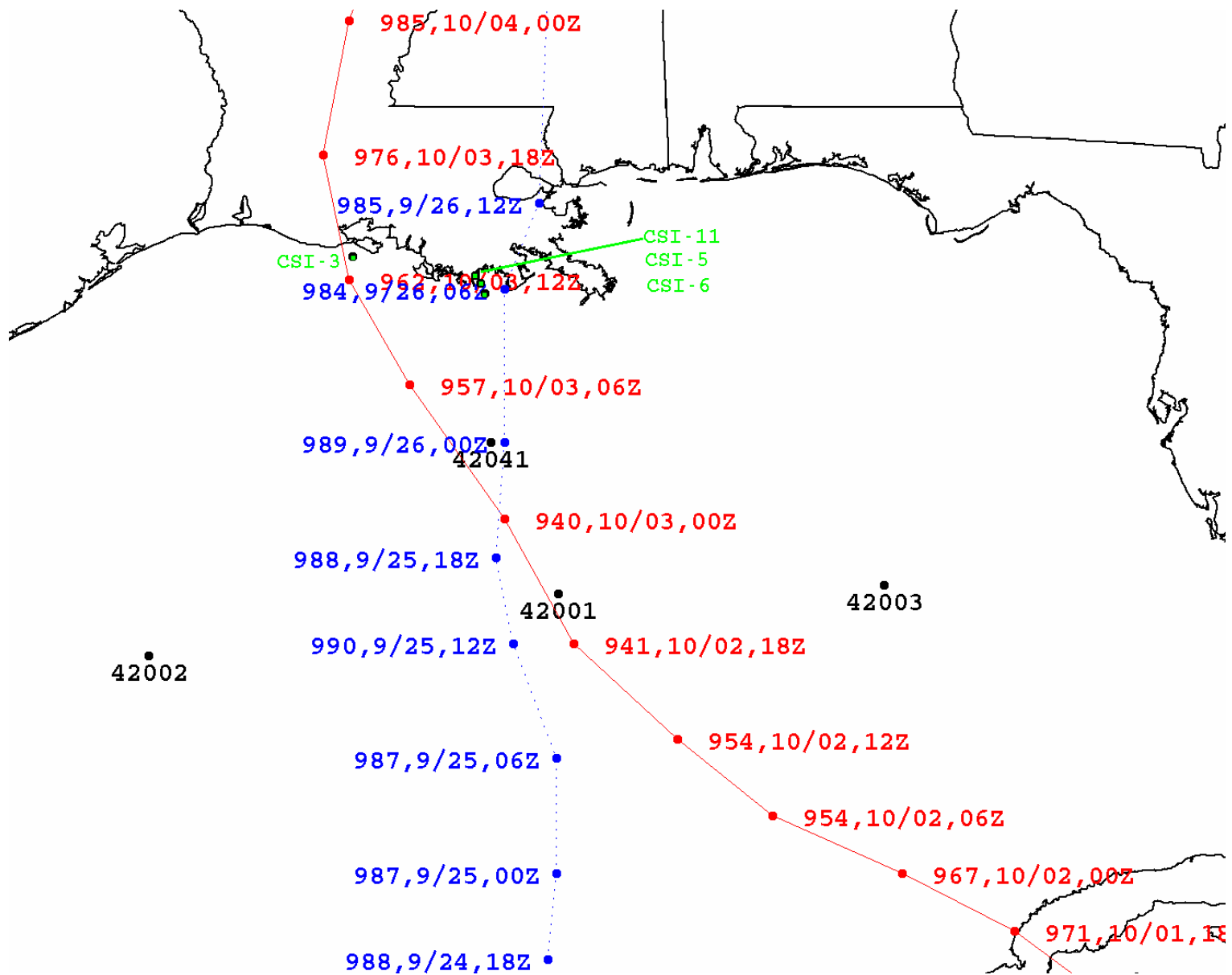
Figure 39. WAVCIS stations (green dots) in relation to Isidore's (blue line) and Lili's (red line) storm tracks.

Table 18. WAVCIS station means, comparison ratios, and comparison differences for each time period.

	Pre-Isidore 9/17/02 - 9/20/02	Post-Isidore 9/28/02 - 10/1/02	Post-Lili 10/4/02 - 10/7/02	Pre- Isidore/Post-Isidore		Post-Lili/Post-Isidore		Post-Lili/Pre-Isidore	
				Ratio	Difference	Ratio	Difference	Ratio	Difference
water temperature (°C)									
CSI-3	30.4	28	27.9		-2.4		-0.03		-2.5
CSI-5	30.8	28.7	28.9		-2.1		0.3		-1.8
CSI-6	30.6	29.2			-1.4				
CSI-11	30.8	27.5	28.9		-3.3		1.4		-1.8
air temperature (°C)									
CSI-3	28.1	26.1	26.8		-1.9		0.7		-1.3
CSI-5	28.1	26.1	27.3		-2.1		1.2		-0.9
CSI-6	28.2	26.4	27.6		-1.8		1.2		-0.6
CSI-11	27.7	25.6	27		-2.2		1.4		-0.8
dewpoint temperature (°C)									
CSI-3	24.1	21.3	23.9		-2.9		2.6		-0.3
sensible heat flux (W m^2)									
CSI-3	17.1	8.2	4.9	47.9%	-8.9	60%	-3.3	28.7%	-12.2
CSI-5	16.6	14.2	8.7	85.7%	-2.4	61.2%	-5.5	52.4%	-7.9
CSI-6	15.4	17.8		115.6%	2.4				
CSI-11	18.5	9.2	9.1	49.5%	-9.4	98.5%	-0.1	48.7%	-9.5
latent heat flux(W m^2)									
CSI-3	160.6	82.6	48.7	51.5%	-78	59%	-33.9	30.3%	-111.9
total heat flux(W m^2)									
CSI-3	177.7	90.8	53.6	51.1%	-86.9	59.1%	-37.2	30.2%	-124

(table continued)

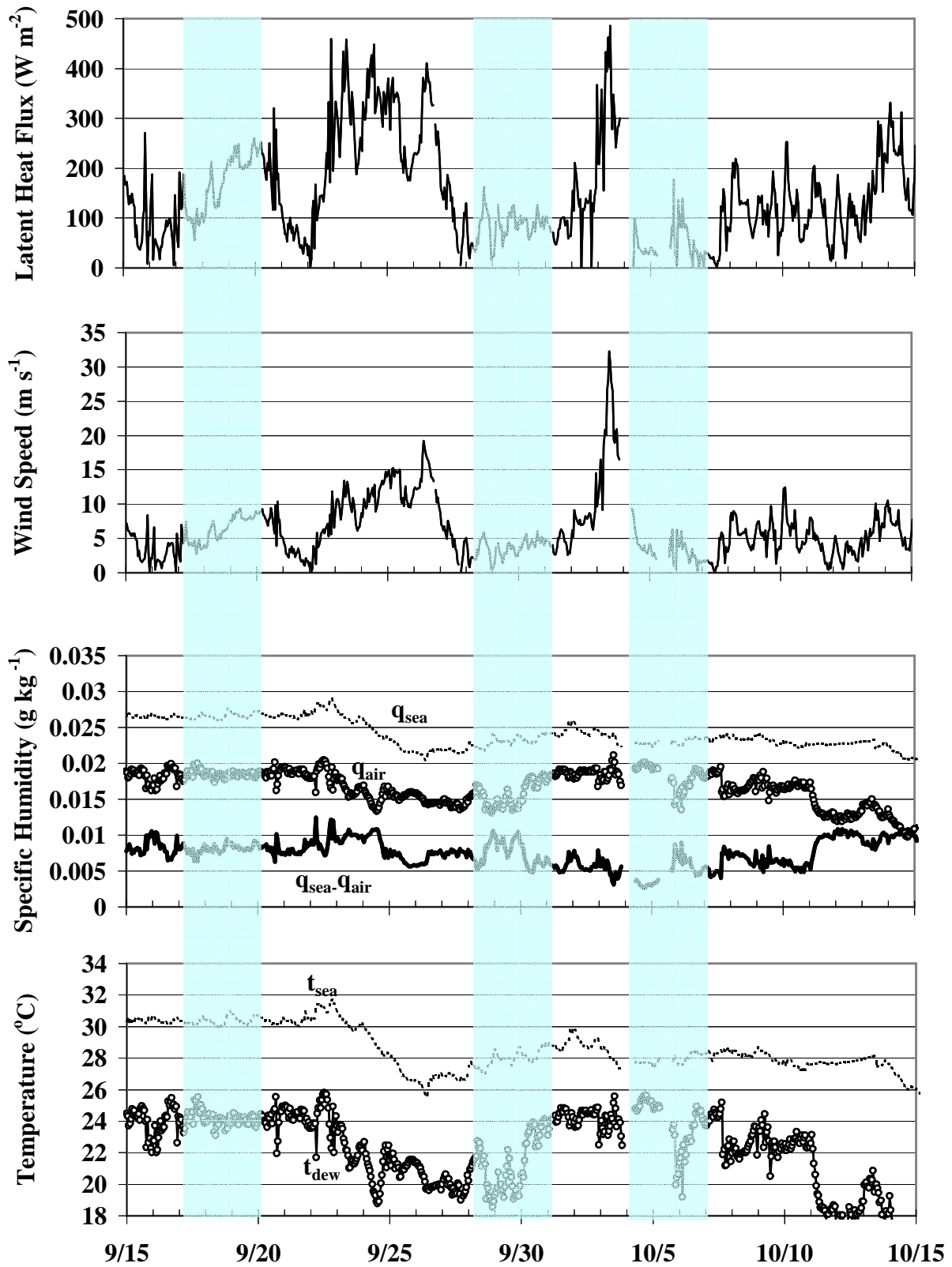|	Pre-Isidore 9/17/02 - 9/20/02	Post-Isidore 9/28/02 - 10/1/02	Post-Lili 10/4/02 - 10/7/02	Pre- Isidore/Post-Isidore		Post-Lili/Post-Isidore		Post-Lili/Pre-Isidore	
				Ratio	Difference	Ratio	Difference	Ratio	Difference
t_{sea} - t_{air} (°C)									
CSI-3	2.3	1.8	1.1		-0.5		-0.7		-1.2
CSI-5	2.6	2.6	1.6		0		-1		-1
CSI-6	2.4	2.8			0.4				
CSI-11	3	1.9	1.9		-1.1		0		-1.1
q_{sea} - q_{air} (g kg^{-1})									
CSI-3	0.0081	0.0075	0.0048		-0.0006		-0.0027		-0.0033
wind (m s^{-1})									
CSI-3	6.1	3.5	3.4		-2.5		-0.1		-2.7
CSI-5	5	4.4	4.5		-0.6		0.1		-0.5
CSI-6	5	5.1	5		0.1				
CSI-11	4.8	3.8	4.3		-1		0.5		-0.5

Figure 40. Latent heat flux and component variables for CSI-3.
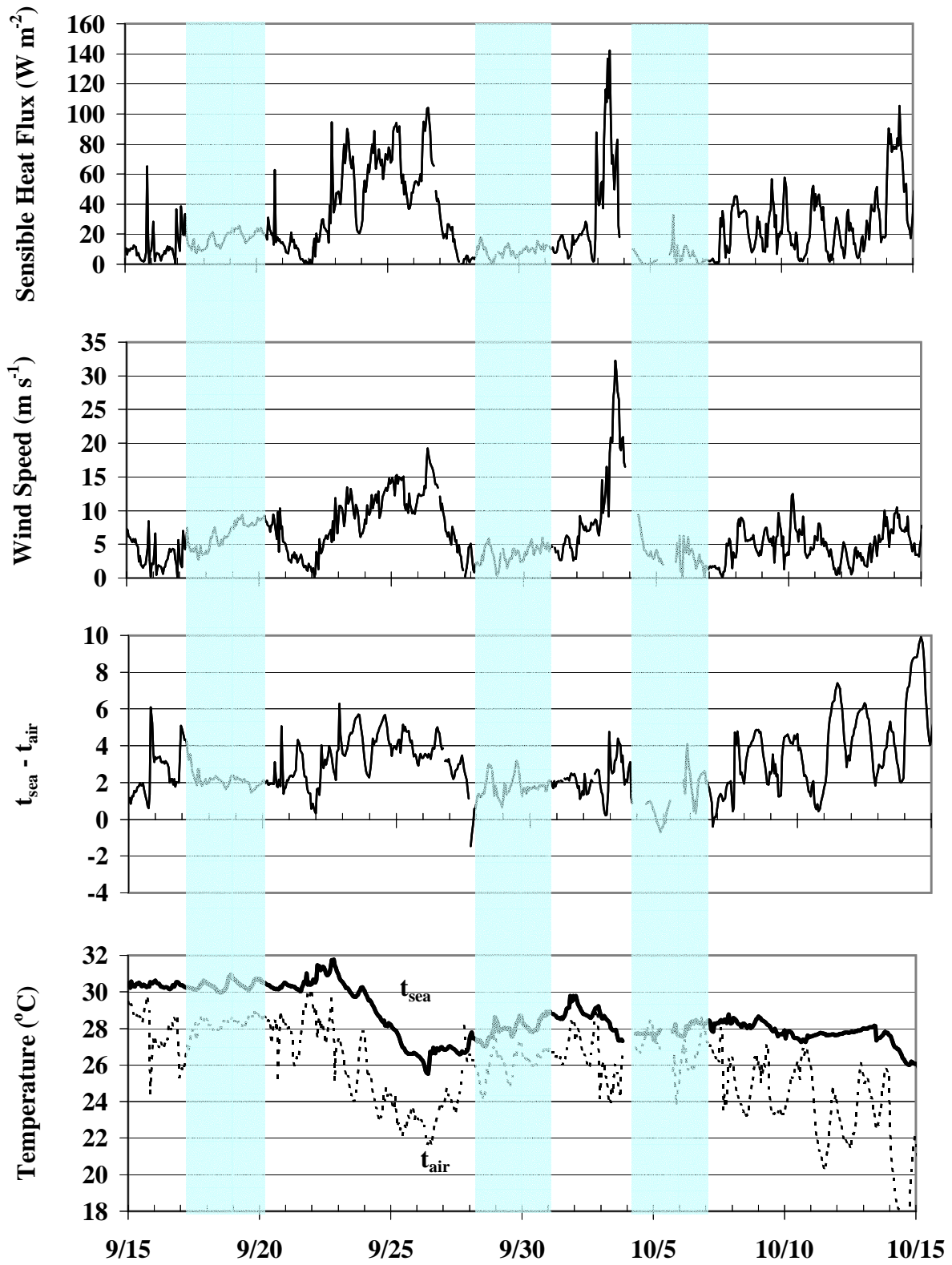Temporal comparison time periods (non-storm) are shaded.

Figure 41. Sensible heat flux and component variables for CSI-3.
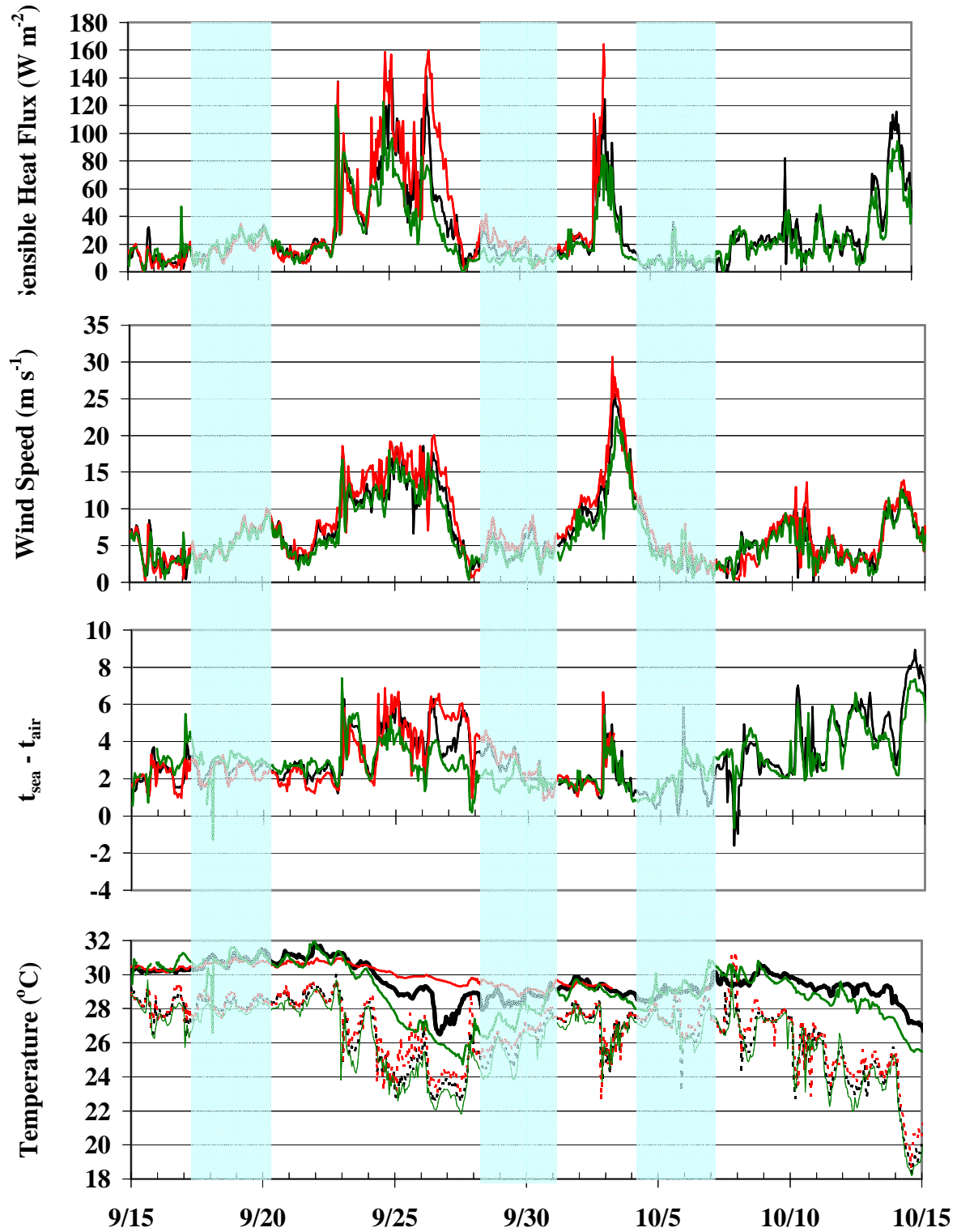Temporal comparison time periods (non-storm) are shaded.

Figure 42. Sensible heat flux and component variables for CSI-5 (black), CSI-6 (red), and CSI-11 (green). Temporal comparison time periods (non-storm) are shaded. In the final panel t_{air} (dotted) and t_{sea} (solid).

VITA

Adele Marie Babin received a Bachelor of Arts degree in mass communications from Louisiana State University in 1995. Afterward, she began a career in satellite remote sensing spanning 9 years and continuing. She enrolled in the Master of Natural Sciences program at LSU in August 2000 while continuing full time employment with the university. She also completed a broadcast meteorological internship during her graduate coursework. Her wish is to combine her communications and meteorological skills to work in broadcast meteorology. She is extremely interested in tropical cyclone satellite meteorology as evidenced by her thesis research "Characteristics of Hurricane Lili's Intensity Changes" completed in Fall 2004. She will be awarded the degree of Master of Natural Sciences at the December 2004 commencement.